

# ENVISAT-1

## GROUND SEGMENT

### MERIS

#### MEdium Resolution Imaging Spectrometer

*Specification of the Contents of the MERIS Radiative Transfer Tools  
used to Generate the Level-2 Auxiliary Data Products*

**Document Number:** PO-RS-PAR-GS-0003

**Issue:** 4

**Revision:** A

**Issue Date:** December 16, 2010

**Filenames:**

PO-RS-PAR-GS-0003 4A - Code\_Spec\_Part1-Theory.doc

PO-RS-PAR-GS-0003 4A - Code\_Spec\_Part2-Appendices.doc

|                     | <i>Function (Company)</i>   | <i>Name</i>      | <i>Signature</i> | <i>Date</i> |
|---------------------|-----------------------------|------------------|------------------|-------------|
| <i>Prepared by:</i> | Scientist (PARBLEU)         | Francis Zagolski |                  |             |
| <i>Checked by:</i>  | Scientist (LISE-Wimereux)   | Richard Santer   |                  |             |
| <i>Checked by:</i>  | Scientist (FUB-Berlin)      | Juergen Fischer  |                  |             |
| <i>Approved by:</i> | Project Manager (ESA/ESTEC) | Jean-Paul Huot   |                  |             |
| <i>Released by:</i> | Project Manager (ESA/ESRIN) | Philippe Goryl   |                  |             |

## TABLE OF CONTENTS

|   |           |
|---|-----------|
| <b>TABLE OF CONTENTS</b> .....  | <b>2</b>  |
| <b>LIST OF FIGURES</b> .....  | <b>5</b>  |
| <b>LIST OF TABLES</b> .....   | <b>6</b>  |
| <b>DOCUMENT CHANGE RECORD</b> .....   | <b>7</b>  |
| <b>1. INTRODUCTION</b> .....  | <b>8</b>  |
| 1.1 PURPOSE OF DOCUMENT .....   | 8         |
| 1.2 SCOPE .....   | 8         |
| 1.3 DOCUMENT OVERVIEW .....   | 8         |
| 1.4 REFERENCES.....   | 8         |
| 1.4.1 <i>Applicable documents</i> .....                                       | 8         |
| 1.4.2 <i>Reference documents</i> .....  | 9         |
| 1.5 ACRONYMS AND ABBREVIATIONS.....   | 13        |
| 1.5.1 <i>Acronyms</i> .....   | 13        |
| 1.5.2 <i>Scientific units</i> .....   | 14        |
| 1.6 DEFINITIONS.....  | 15        |
| 1.6.1 <i>Radiometry</i> .....   | 15        |
| 1.6.2 <i>Physical principles</i> .....  | 15        |
| 1.7 GLOSSARY .....  | 16        |
| 1.8 LIST OF SYMBOLS .....   | 17        |
| 1.8.1 <i>Operator symbols</i> .....   | 17        |
| 1.8.2 <i>Vector symbols</i> .....   | 17        |
| 1.8.3 <i>Matrix symbols</i> .....   | 18        |
| 1.8.4 <i>Other symbols</i> .....  | 18        |
| <b>2. PHYSICAL BASES</b> .....  | <b>22</b> |
| 2.1 EXTINCTION, SCATTERING AND ABSORPTION COEFFICIENTS.....                   | 22        |
| 2.2 SINGLE SCATTERING ALBEDO AND OPTICAL DEPTH .....                          | 23        |
| 2.3 SCATTERING PHASE FUNCTION .....   | 23        |
| 2.3.1 <i>Definition</i> .....   | 23        |
| 2.3.2 <i>Truncation of phase function</i> .....                               | 24        |
| 2.4 IRRADIANCE, RADIANCE AND REFLECTANCE .....                                | 26        |
| 2.5 STOKES PARAMETERS.....  | 28        |
| 2.6 PHASE MATRIX .....  | 30        |
| 2.7 RAYLEIGH SCATTERING .....   | 31        |
| 2.8 MIE SCATTERING.....   | 34        |
| 2.8.1 <i>Mie theory</i> .....   | 34        |
| 2.8.1.1 <i>Computation of complex functions (<math>a_n, b_n</math>)</i> ..... | 34        |
| 2.8.1.2 <i>Computation of the Ricatti-Bessel function</i> .....               | 35        |
| 2.8.1.3 <i>Computation of functions (<math>D_n, G_n</math>)</i> .....         | 38        |
| 2.8.1.4 <i>Computation of functions (<math>\pi_n, \tau_n</math>)</i> .....    | 38        |
| 2.8.2 <i>Optical properties</i> .....   | 40        |
| 2.8.3 <i>Phase matrix</i> .....   | 41        |
| 2.8.4 <i>Forward scattering proportion</i> .....                              | 41        |
| 2.9 GASEOUS ABSORPTION .....  | 42        |
| 2.10 FRESNEL LAWS .....   | 44        |

|           |   |           |
|-----------|---|-----------|
| <b>3.</b> | <b>ATMOSPHERIC OPTICAL PROPERTIES .....</b>           | <b>47</b> |
| 3.1       | DRY AIR (MOLECULAR ATMOSPHERE) .....                  | 47        |
| 3.1.1     | <i>Inherent optical properties</i> .....              | 47        |
| 3.1.1.1   | Scattering coefficient .....                          | 47        |
| 3.1.1.2   | Scattering phase function .....                       | 48        |
| 3.1.2     | <i>Vertical distribution</i> .....                    | 48        |
| 3.1.2.1   | Molecular scale height .....                          | 48        |
| 3.1.2.2   | Vertical profile .....                                | 50        |
| 3.2       | AEROSOLS .....  | 50        |
| 3.2.1     | <i>Inherent optical properties</i> .....              | 50        |
| 3.2.1.1   | Sample of identical particles .....                   | 50        |
| 3.2.1.2   | Mixing of different particles .....                   | 51        |
| 3.2.1.3   | Convergence criterion .....                           | 52        |
| 3.2.2     | <i>Particle size distribution</i> .....               | 53        |
| 3.2.3     | <i>Aerosol models</i> .....                           | 53        |
| 3.2.4     | <i>Vertical distribution</i> .....                    | 55        |
| 3.3       | CLOUDS .....  | 55        |
| 3.3.1     | <i>Inherent optical properties</i> .....              | 55        |
| 3.3.2     | <i>Particle size distribution</i> .....               | 55        |
| 3.3.3     | <i>Cloud models</i> .....                             | 55        |
| 3.3.4     | <i>Vertical distribution</i> .....                    | 55        |
| <b>4.</b> | <b>WATER OPTICAL PROPERTIES .....</b>                 | <b>57</b> |
| 4.1       | PURE SEA WATER .....                                  | 57        |
| 4.2       | PHYTOPLANKTON .....                                   | 58        |
| 4.2.1     | <i>Inherent optical properties</i> .....              | 58        |
| 4.2.2     | <i>Vertical distribution</i> .....                    | 60        |
| 4.3       | YELLOW SUBSTANCE .....                                | 60        |
| 4.3.1     | <i>Inherent optical properties</i> .....              | 60        |
| 4.3.2     | <i>Vertical distribution</i> .....                    | 60        |
| 4.4       | SUSPENDED PARTICULATE MATTER AND GELBSTOFF .....      | 60        |
| 4.4.1     | <i>Inherent optical properties</i> .....              | 60        |
| 4.4.2     | <i>Vertical distribution</i> .....                    | 61        |
| <b>5.</b> | <b>SEA SURFACE STATE .....</b>                        | <b>62</b> |
| <b>6.</b> | <b>RADIATIVE TRANSFER.....</b>                        | <b>63</b> |
| 6.1       | GEOMETRY .....  | 63        |
| 6.2       | GENERAL FORMULATION .....                             | 64        |
| 6.2.1     | <i>Radiative Transfer Equation (RTE)</i> .....        | 64        |
| 6.2.2     | <i>Solving the RTE</i> .....                          | 65        |
| 6.2.2.1   | Single and multiple scattering .....                  | 67        |
| 6.2.2.2   | Fourier series expansion of the radiation field ..... | 68        |
| <b>7.</b> | <b>DESCRIPTION OF RTC/UDL .....</b>                   | <b>72</b> |
| 7.1       | SCAMAT MODULE .....                                   | 72        |
| 7.1.1     | <i>Description</i> .....                              | 72        |
| 7.1.2     | <i>Tool</i> .....                                     | 72        |
| 7.1.3     | <i>Mie processing</i> .....                           | 73        |
| 7.2       | UPRAD MODULE .....                                    | 74        |
| 7.2.1     | <i>Description</i> .....                              | 74        |
| 7.2.2     | <i>Tools</i> .....                                    | 75        |
| 7.2.3     | <i>RTC/GAME</i> .....                                 | 75        |
| 7.2.4     | <i>RTC/SO</i> .....                                   | 76        |
| 7.2.5     | <i>RTC/SOAO</i> .....                                 | 80        |

|           |                                     |           |
|-----------|-------------------------------------|-----------|
| 7.3       | OTHER MODULE: RTC/MOS .....         | 86        |
| 7.3.1     | <i>Description</i> .....            | 86        |
| 7.3.2     | <i>Tools</i> .....                  | 86        |
| 7.3.3     | <i>RTC/lut_alb_gddv</i> .....       | 86        |
| 7.3.4     | <i>RTC/lut_rhob_agddv</i> .....     | 87        |
| 7.3.5     | <i>RTC/lut_rhob_Rgddv</i> .....     | 88        |
| 7.3.6     | <i>RTC/lut_rhob_aR</i> .....        | 88        |
| <b>8.</b> | <b>DESCRIPTION OF RTC/FUB .....</b> | <b>90</b> |
| 8.1       | MIE MODULE .....                    | 90        |
| 8.1.1     | <i>Description</i> .....            | 90        |
| 8.1.2     | <i>Tool</i> .....                   | 90        |
| 8.1.3     | <i>Mie processing</i> .....         | 91        |
| 8.2       | MOMO MODULE .....                   | 91        |
| 8.2.1     | <i>Description</i> .....            | 91        |
| 8.2.2     | <i>Tools</i> .....                  | 91        |
| 8.2.3     | <i>RTC/MOMO</i> .....               | 92        |
| 8.2.3.1   | Matrix-Operator Method .....        | 92        |
| 8.2.3.2   | Numerical method .....              | 96        |
| 8.2.3.3   | Air-sea interface .....             | 96        |

## LIST OF FIGURES

|   |    |
|---|----|
| <u>Figure 1:</u> Schematic representation of a radiant flux propagation within a scattering and absorbing medium. ....  | 22 |
| <u>Figure 2:</u> Schematic representation of scattered radiant flux within a particulate layer. ....  | 24 |
| <u>Figure 3:</u> Illustration of the phase function truncation technique which substitutes the forward scattering peak by a linear extrapolation. Area below the phase function $p(\theta)$ (solid line) is replaced by the hatched area (modified scattering function $p'(\theta)$ ). The amount $\alpha$ of forward scattered light is considered as not being scattered. ....  | 25 |
| <u>Figure 4:</u> Same legend as <u>Figure 3</u> but using a second order polynomial curve to substitute the forward scattering peak. ....   | 26 |
| <u>Figure 5:</u> Illumination configuration of an elementary ground surface $dS$ . ....   | 26 |
| <u>Figure 6:</u> Viewing and illumination configuration of an elementary ground surface $dS$ . ....   | 27 |
| <u>Figure 7:</u> Representation of the elliptic polarization of an electromagnetic wave describing the temporal variation of the amplitude $A(t)$ of the electric field in the perpendicular plane to the propagation direction. ....   | 29 |
| <u>Figure 8:</u> Illustration of Rayleigh scattering: (a) parallel ( $//$ ) and perpendicular ( $\perp$ ) components of the incident ( $\vec{E}_i, \vec{s}_0$ ) and emitted ( $\vec{E}_s, \vec{s}$ ) electric field, (b) molecule dipole emission. ....   | 32 |
| <u>Figure 9:</u> Samples of $a_n(\kappa, n)$ and $b_n(\kappa, n)$ curves computed for a refractive index $n = 1.33 - i 0.001$ with $\kappa = 10$ and $\kappa = 50$ . ....   | 36 |
| <u>Figure 10:</u> Samples of spherical Bessel functions, (a) $j_n(x)$ and (b) $n_n(x)$ , for $\kappa = 10$ and $\kappa = 50$ . ....   | 36 |
| <u>Figure 11:</u> Samples of $D_n(n\kappa \text{ or } \kappa)$ and $G_n(\kappa)$ curves computed for a refractive index $n = 1.33 - i 0.001$ with $\kappa = 10$ and $\kappa = 50$ . ....  | 39 |
| <u>Figure 12:</u> Samples of $\pi_n(\theta)$ and $\tau_n(\theta)$ functions for several $n$ values ( $n$ varying from 1 to 6). ....   | 39 |
| <u>Figure 13:</u> Reflexion and transmission of the incident electric field $\vec{E}_i$ through the air-water interface characterized by their refractive index, respectively $n_a$ and $n_w$ : (a) for the parallel component of the electric field ( $\vec{E}_{i, //}, \vec{E}_{r, //}, \vec{E}_{t, //}$ ), and (b) for the perpendicular component of the electric field ( $\vec{E}_{i, \perp}, \vec{E}_{r, \perp}, \vec{E}_{t, \perp}$ ). Subscripts $i$ , $r$ and $t$ stand for incidence, reflection and transmission. .... | 46 |
| <u>Figure 14:</u> Illumination and viewing configuration for MERIS sensor. ....   | 63 |
| <u>Figure 15:</u> Schematic representation of radiative transfer problem. ....  | 65 |
| <u>Figure 16:</u> Flowchart of the MIE processing. ....   | 73 |
| <u>Figure 17:</u> Schematic representation of the «3 aerosol-layers» atmosphere over ocean. ....  | 78 |
| <u>Figure 18:</u> Flowchart of the RTC/UdL. ....  | 83 |
| <u>Figure 19:</u> Flowchart of the RTC/SO. ....   | 84 |
| <u>Figure 20:</u> Description of the primary scattering for the atmospheric upwelling radiance: ....  | 85 |
| <u>Figure 21:</u> Description of the primary scattering for the in-water downwelling radiance: ....   | 85 |
| <u>Figure 22:</u> Interaction principle within an elementary layer $[\tau_0; \tau_1]$ . ....  | 93 |

## LIST OF TABLES

|   |    |
|---|----|
| <u>Table 1</u> : Definition of some physical quantities useful for remote sensing data. ....  | 15 |
| <u>Table 2</u> : Rayleigh optical thickness ( $\tau^R$ ) for a barometric pressure of 1013.25 hPa derived from [RD 13],<br>ozone optical thickness ( $\tau^{O_3}$ ) derived from line-by-line computations using HITRAN-2000 and an<br>amount of 1 cm-atm, and gaseous transmittivities in the 15 MERIS spectral bands computed with<br>GAME and 6S for a MLS profile, a solar zenith angle of 45 degrees and a nadir viewing (extracted<br>from [RD 17]). .... | 43 |
| <u>Table 3</u> : Microphysical characteristics of the aerosol types (dry particles) from WCRP-1986 [RD 34]. ....  | 52 |
| <u>Table 4</u> : Percentage density of particles from WCRP-1986 [RD 34]. ....   | 52 |
| <u>Table 5</u> : Complex refractive indices of the aerosol types (dry particles) from WCRP-1986 [RD 34]. ....   | 52 |
| <u>Table 6</u> : Aerosol components and their respective contributions (as percent of the volume (Vol.), or as percent of<br>the number of particles (Pcl.)) in the composition of the aerosol models. ....   | 54 |
| <u>Table 7</u> : Pure water absorption coefficient $\sigma_a^w$ for 10 MERIS spectral bands. ....   | 57 |
| <u>Table 8</u> : Values of $A_\lambda$ and $B_\lambda$ coefficients for 10 MERIS spectral bands useful to compute $\sigma_a^{chl}(\lambda)$ . ....  | 58 |
| <u>Table 9</u> : Petzold phase function $P_p(\theta)$ derived from [RD 44]. ....  | 59 |
| <u>Table 10</u> : Values of $C_\lambda$ coefficients in 10 MERIS spectral bands useful to compute $\sigma_s^{spm}(\lambda)$ . ....  | 61 |

## DOCUMENT CHANGE RECORD

| <i>Issue</i> | <i>Rev.</i> | <i>Date</i>   | <i>Chapter/Paragraph Number, Change Description (and Reasons)</i>  |
|--------------|-------------|---------------|--|
| Draft        | -           | Nov. 18, 1997 | - Draft release of the document  |
| 1            | -           | Feb. 20, 1998 | - Release of the first issue of the document   |
| 2            | -           | Apr. 28, 1998 | - Updated issue following the discussions and comments from the FUB and LISE institutes. The document was completely restructured and a new section was added.   |
| 2            | A           | Jan. 31, 2000 | - Updated issue for the latest revision of FUB and LISE  |
| 3            | -           | May 7, 2001   | - New version of the document with an attached data dictionary devoted to the use of the radiative transfer tools  |
| 3            | A           | Dec. 20, 2001 | - Reviewed version by the FUB and LISE institutes<br>- Update of the data dictionary<br>- Overview of the radiative transfer tools (RTC / FUB & RTC / UdL)<br>- ABB internal release only                  |
| 3            | B           | Sep. 16, 2002 | - Last reviewed version by the FUB and LISE institutes<br>- Correction of Travis / Hansen formula for <i>Rayleigh</i> optical depth<br>- Last update of the data dictionary<br>- ABB internal release only |
| 3            | C           | Dec. 15, 2002 | - Add Section 7.3 for generation of 4 MERIS LUTs at the level-2 relying on the DDV parameters for the bidirectionality correction.<br>- Insert Appendix-3 with specification of the RTC/MOS package        |
| 3            | D           | Oct. 31, 2003 | - Update of the Appendix-3 (I/O description for each tool in the RTC/MOS package)  |
| 4            | -           | July 21, 2009 | - Update of the Appendices   |
| 4            | A           | Dec. 16, 2010 | - Add a section to define the molecular (or <i>Rayleigh</i> ) scale height ( <a href="#">Section 3.1.2.1</a> )<br>- Update of the Appendix-3 (tools from the RTC/MOS package)                              |

## 1. INTRODUCTION

### 1.1 PURPOSE OF DOCUMENT

The purpose of this document is to describe the radiative transfer processes simulated within a coupled 'Atmosphere-Land/Ocean' system by two different codes developed by «Freie Universität Berlin» (FUB) in Germany and «Laboratoire Interdisciplinaire en Sciences de l'Environnement - Université du Littoral» (LISE/UdL) in France. In the framework of the MERIS project, these two radiative transfer codes (RTCs), referred as *MOMO* and *UPRAD* for the FUB and LISE institutes respectively, have been intervalidated for a set of representative test cases (see [AD-8] for more details) before to be used to generate MERIS look-up tables (LUTs) for the level-2 processing. A complete list of tools/modules used in each of the two RTCs (FUB & UdL) for providing these MERIS LUTs is given in [AD-5].

### 1.2 SCOPE

This work is essential for the level-2 processing of MERIS ground segment data. Some parts of this report have been written with the help of scientific documents provided by the two institutes (FUB & LISE).

### 1.3 DOCUMENT OVERVIEW

This document contains an overview of physical bases useful for the radiative transfer computations within a coupled 'Atmosphere-Land/Ocean' system, a complete description of the optical properties for the atmospheric and oceanic compounds as well as for the sea surface state, the radiative transfer equation within the coupled 'Atmosphere-Land/Ocean' system, and a detailed presentation of the two RTCs (FUB & UdL) used for the MERIS LUTs generation with an attached data dictionary in the appendices.

**Warning:** *The inherent optical properties (IOPs) of oceanic components presented in Section 4 of this document are only samples used for the RTC/Intervalidation [AD-8]. The formulations given in this section provide from [AD-4] (Issue3, Rev.1) and are not the reference model for the MERIS LUTs generation.*


### 1.4 REFERENCES

This section presents a list of applicable and reference documents. The reader must refer to the Software Transfer Document [AD-6] for obtaining the issue number of each reference pertinent to the current MERISAT (MERIS Auxiliary data Tool) software release.

#### 1.4.1 Applicable documents

| No     | Document          | Title   |
|--------|-------------------|---|
| [AD-1] | PO-TN-MEL-GS-0003 | "MERIS Input/Output Data Definition"                            |
| [AD-2] | PO-TN-MEL-GS-0005 | "MERIS Level-2 ATBD: Algorithm Theoretical Basis Document"      |
| [AD-3] | PO-TN-MEL-GS-0002 | "MERIS Level-2 Detailed Processing Model & Parameter Data List" |
| [AD-4] | PO-TN-MEL-GS-0026 | "Reference model for MERIS level-2 processing"                  |



|   |  |   |
|---|--|---|
|  | <b>MERIS/ ENVISAT-1</b><br>Medium Resolution Imaging<br>Spectrometer | <u>Ref.:</u> PO-RS-PAR-GS-0003<br><u>Issue:</u> 4 <u>Rev.:</u> A<br><u>Date:</u> 16-Dec-10 <u>Page:</u> 9 |
|---|--|---|

|        |                          |   |
|--------|--------------------------|---|
| [AD-5] | <i>PO-RS-PAR-GS-0002</i> | "Specification of the Scientific Contents of the MERIS Level-2 Auxiliary Data Products" |
| [AD-6] | <i>PO-MA-BOM-GS-0003</i> | "Software Transfer Document for MERIS Level-2 Auxiliary Data Tool S/W"                  |
| [AD-7] | <i>PO-MA-BOM-GS-0008</i> | "Software User's Manual for MERIS Level-2 Auxiliary Data Tool Software"                 |
| [AD-8] | <i>PO-RP-BOM-GS-0024</i> | "Radiative Transfer Code Intervalidation Report for MERIS level-2 processing"           |

## 1.4.2 Reference documents

| No      | Reference (authors, title, journal)   |
|---------|---|
| [RD-1]  | <b>Bohren, C.F., and D.R. Huffman, 1983.</b> "Absorption and scattering of light by small particles", <i>Academic Press, Wiley (NY)</i> .   |
| [RD-2]  | <b>Mie, G., 1908.</b> "Beitraege zur optik trüber medien, speziell kolloidaler metallösungen", <i>Annalen der Physik.:</i> <b>25</b> , 377-445.   |
| [RD-3]  | <b>Johnson, W.R., and F.D. Feiock, 1968.</b> "Rayleigh scattering and the electromagnetic susceptibility of atoms", <i>Physical Review:</i> <b>168</b> , 22-31.   |
| [RD-4]  | <b>Fell, F., and J. Fischer, 2001.</b> "Numerical simulation of the light field in the atmosphere-ocean system using the matrix-operator method", <i>Journal of Quantitative Spectroscopy &amp; Radiative Transfer:</i> <b>69</b> (3), 351-388. |
| [RD-5]  | <b>Chandrasekhar, S., 1950.</b> "Radiative transfer", <i>Oxford University Press, Oxford (England)</i> .  |
| [RD-6]  | <b>Lenoble, J., 1993.</b> "Atmospheric radiative transfer", <i>A. Deepak Publishing, Hampton (VA)</i> .   |
| [RD-7]  | <b>Van de Hulst, H.C., 1981.</b> "Light scattering by small particles", <i>Dover Publications, New York (NY)</i> .  |
| [RD-8]  | <b>Aden, A.L., 1951.</b> "Electromagnetic scattering from spheres with sizes comparable to the wavelength", <i>Journal of Applied Physics:</i> <b>22</b> (5), 601-605.  |
| [RD-9]  | <b>Deirmendjian, D., R. Clasen, and W. Viezee, 1961.</b> "Mie scattering with complex index of refraction", <i>Journal of Optical Society of America:</i> <b>51</b> (6), 620-633.   |
| [RD-10] | <b>Wyatt, P.J., 1962.</b> "Scattering of electromagnetic plane waves from inhomogeneous spherically symmetric objects", <i>Physical Review:</i> <b>127</b> (5), 1837-1843.  |
| [RD-11] | <b>Kattawar, G.W., and G.N. Plass, 1967.</b> "Electromagnetic scattering from absorbing spheres", <i>Applied Optics:</i> <b>6</b> (8), 1377-1382.   |
| [RD-12] | <b>Dave, J.V., 1969.</b> "Scattering of visible light by large water spheres", <i>Applied Optics:</i> <b>8</b> (1), 155-164.  |
| [RD-13] | <b>Hansen, J.E., and L. Travis, 1974.</b> "Light scattering in planetary atmospheres", <i>Space Science Reviews:</i> <b>16</b> , 527-610.   |
| [RD-14] | <b>Liou, K.N., 1980.</b> "An introduction to atmospheric radiation", <i>Academic Press, San Diego (CA)</i> .  |
| [RD-15] | <b>Corbato, F.J., and J.L. Uretsky, 1959.</b> "Generation of spherical Bessel functions in digital computers", <i>Journal of the Association for Computing Machinery:</i> <b>6</b> , 366-375.   |

- [RD-16] **McClatchey, R.A., R.W. Fenn, J.E.A. Selby, F.E. Voltz, and J.S. Garing, 1972.** "Optical properties of the atmosphere", *AFCRF-72-0497 report, Hanscom Air Force Base, Bedford (Mass.):* 98 p.
- [RD-17] **Santer, R., V. Carrère, P. Dubuisson, and J.C. Roger, 1999.** "Atmospheric correction over land for MERIS", *International Journal of Remote Sensing:* **20** (9), 1819-1840.
- [RD-18] **Lacis, A.A., and V. Oinas, 1991.** "A description of the correlated k-distribution method for modeling non-grey gaseous absorption, thermal emission, and multiple scattering in vertically inhomogeneous atmospheres", *Journal of Geophysical Research:* **96**, 9027-9074.
- [RD-19] **Malkmus, W., 1967.** "Random Lorentz band models with exponential tailed S<sup>-1</sup> line intensity distribution function", *Journal of Optical Society of America:* **21**, 323-329.
- [RD-20] **Rothman, L.S., K.V. Chance, J. Schroeder, and A. Goldman, 2001.** "A new edition of the HITRAN database", *Proceedings of 11<sup>th</sup> Atmospheric Research Modelling Science Team Meeting, Atlanta (GA).*
- [RD-21] **Dubuisson, P., J-C. Buriez, and Y. Fouquart, 1996.** "High spectral resolution solar radiative transfer in absorbing and scattering media: Application to the satellite simulation", *Journal of Quantitative Spectroscopy & Radiative Transfer:* **55** (1), 103-126.
- [RD-22] **Clough, S.A., F.X. Kneizys, and R. Davies, 1989.** "Line shape and the water vapor continuum", *Journal of Atmospheric Research:* **23**, 229-241.
- [RD-23] **Clough, S.A., M.J. Iacono, and J.L. Moncet, 1992.** "Line-by-line calculations of atmospheric fluxes and cooling rates: Application to water vapor", *Journal of Geophysical Research:* **97**, 15761-15785.
- [RD-24] **Kneizys, F.X., E.P. Shettle, W.O. Gallery, J.H. Chetwynd, Jr. L.W. Abreu, J.E.A. Selby, R.W. Fenn, and R.A. McClatchey, 1980.** "Atmospheric transmittance/radiance: Computer code LOWTRAN 5", *AFGL-TR-80-0067 report, Air Force Geophysics Laboratory, Bedford (Mass.).*
- [RD-25] **Peck and Reeder, 1972.** "Formulation of air refraction index", *Journal of Optical Society of America:* **62**.
- [RD-26] **Bucholtz, 1995.** "Formulation of the molecular depolarization factor", *Applied Optics:* **34** (15).
- [RD-27] **Young, A.T., 1980.** "Revised depolarization corrections for atmospheric extinction", *Applied Optics:* **19**, 3427-3428.
- [RD-28] **D'Almeida, G.A., P. Koepke, and E.P. Shettle, 1991.** "Atmospheric aerosols global climatology and radiative characteristics", *A. Deepak Publishing, Hampton (VA).*
- [RD-29] **Davies, C.N., 1974.** "Size distribution of atmospheric particles", *Journal of Aerosol Science:* **5**, 293-300.
- [RD-30] **Junge, C.E., 1952.** "Gesetzmäßigkeiten in der droßenverteilung atmosphärischer aerosole über dem kontinent", *Berd. Deirsch Wetterdienst U.S.-Zone:* **35**, 261-277.
- [RD-31] **Deirmendjian, D., 1964.** "Scattering and polarization properties of water clouds and hazes in the visible and infrared", *Applied Optics:* **3**, 187-196.
- [RD-32] **Deirmendjian, D., 1969.** "Electromagnetic scattering on spherical polydispersion", *Elsevier Eds., New-York (NY).*
- [RD-33] **Shettle, E.P., and R.W. Fenn, 1979.** "Models for the aerosols of the lower atmosphere and the effects of humidity variations on their optical properties", *Environmental Research Papers, AFGL-TR-79-0214, Hanscom (Mass.).*

- [RD-34] **World Climate Research Program, 1986.** "A preliminary cloudless standard atmosphere for radiation computation", *International Association for Meteorology & Atmospheric Physics, Radiation Commission, March 1986, WCP-112, WMO/TD-N° 24.*
- [RD-35] **Moulin, C., H.R. Gordon, V.F. Banzon, and R.H. Evans, 2001.** " Assessment of Saharan dust absorption in the visible from SeaWiFS imagery", *Geophysical Research Letters: 106D* (18), 239-249.
- [RD-36] **Brogniez, G., J-C Buriez, V. Giraud, F. Parol, and C. Vanbauce, 1995.** *Monthly Weather Review: 123*, 1025.
- [RD-37] **Stephen, G.L., 1979.** "Optical properties of eight water cloud types", *CSIRO Aust. Div. Atmospheric Physics, Technical Paper: (36)*, 1-35.
- [RD-38] **Pope, R.M., and E.S. Fry, 1997.** "Absorption spectrum (380-700nm) of pure water: II. Integrating cavity measurements", *Applied Optics: 36*, 8710-8723.
- [RD-39] **Hale, G.M., and M.R. Querry, 1973.** "Optical constants of water in the 200nm to 200µm wavelength region", *Applied Optics: 12*, 555-563.
- [RD-40] **Morel, A., 1974.** "Optical properties of pure water and sea water", *In: Optical Aspects of Oceanography, N.G. Jerlov and E. Steemann-Nielsen Eds, Academic Press: 1-24.*
- [RD-41] **Morel, A., 1966.** "Etude expérimentale de la diffusion de la lumière par l'eau, les solutions de chlorure de sodium et l'eau de mer optiquement pure", *Journal of Chemical Physics: 10*, 1359-1366.
- [RD-42] **Bricaud, A., A. Morel, M. Badin, K. Allali and H. Claustre, 1998.** "Variations of light absorption by suspended particles with chlorophyll-*a* concentration in oceanic waters: Analysis and implications for bio-optical models", *Journal of Geophysical Research: 103*, 31033-31044.
- [RD-43] **Loisel, H., and A. Morel, 1998.** "Light scattering and chlorophyll concentration in waters: A re-examination", *Limnology & Oceanography: 43* (5), 847-858.
- [RD-44] **Petzold, T.L., 1972.** "Volume scattering functions for selected ocean waters", *Scripps Institute of Oceanography, Ref. 72-78, San Diego (CA): 79 p.*
- [RD-45] **Platt, T., and S. Sathyendranath, 1988.** "Oceanic primary production: Estimation by remote sensing at local and regional scales", *American Journal of Science: 241*, 1613-1620.
- [RD-46] **Cox, C., and W. Munk, 1954.** "Measurements of roughness of the sea surface from photographs of the sun glitter", *Journal of Optical Society of America, 44* (11): 838-888.
- [RD-47] **Vermote, E., D. Tanré, J.L. Deuzé, M. Herman, and J.J. Morcrette, 1997.** "Second simulation of the satellite signal in the solar spectrum, 6S: An overview", *I.E.E.E. Transaction on Geoscience & Remote Sensing: 35* (3), 675-687.
- [RD-48] **Lenoble, J., 1985.** "Radiative transfer in scattering and absorbing atmospheres: Standard computational procedures", *A. Deepak Publishing, Hampton (Virginia).*
- [RD-49] **Preisendorfer, R.W., 1961.** "Application of radiative transfer theory to light measurements in the sea", *Monograph International Union of Geodynamics & Geophysics, Paris (France): 10*, 11-30.
- [RD-50] **Kattawar, G.W., and G.N. Plass, 1976.** "Assymptotic radiance and polarization in optically thick media: Ocean and clouds", *Applied Optics: 15* (12), 3166-3178.
- [RD-51] **Van de Hulst, H., 1980.** "Multiple light scattering: Tables, formulas and applications", *Academic Press, New-York (NY).*

- [RD-52] **Stamnes, K., S. Tsay, W. Wiscombe, and K. Jayaweera, 1988.** "Numerically stable algorithm for discrete ordinates method radiative transfer in multiple scattering and emitting layered media", *Applied Optics*: **27** (12).
- [RD-53] **Deuzé, J.L., M. Herman, and R. Santer, 1989.** "Fourier series expansions of the transfer equation in the atmosphere-ocean system", *Journal of Quantitative Spectroscopy & Radiative Transfer*: **41** (6), 483-494.
- [RD-54] **Lenoble, J., M. Herman, J.L. Deuzé, B. Lafrance, R. Santer and D. Tanré, 2007.** "A successive order of scattering code for solving the vector equation of transfer in the Earth's atmosphere with aerosols", *Journal of Quantitative Spectroscopy & Radiative Transfer*, 107, pp. 479-507 ([doi: 10.1016/j.jqsrt.2007.03.010](https://doi.org/10.1016/j.jqsrt.2007.03.010)).
- [RD-55] **Hapke, B., 1981.** "Bidirectional reflectance spectroscopy - 1: Theory", *Journal of Geophysical Research*: **86**, 3039-3054.
- [RD-56] **Plass, G., G. Kattawar, and F. Catchings, 1973.** "Matrix-operator theory of radiative transfer - 1: Rayleigh scattering", *Applied Optics*: **12** (2), 314-329.
- [RD-57] **Potter, J., 1970.** "The delta function approximation in radiative transfer theory", *Journal of the Atmospheric Sciences*: **27**, 943-949.
- [RD-58] **Kattawar, G., T. Humphreys, and G. Plass, 1978.** "Radiative transfer in an atmosphere-ocean system: A matrix-operator approach", *SPIE proceedings*: **160**, 123-131.
- [RD-59] **Nakajima, T., and M. Tanaka, 1983.** "Effect of wind-generated waves on the transfer of solar radiation in the atmosphere-ocean system", *Journal of Quantitative Spectroscopy & Radiative Transfer*: **29** (6), 521-537.
- [RD-60] **Fischer, J., and H. Grassl, 1991.** "Detection of cloud-top height from backscattered radiances within the oxygen-A band. Part 1: Theoretical study", *Journal of Applied Meteorology*: **30** (9), 1245-1259.
- [RD-61] **Fischer, J., and U. Kronfeld, 1990.** "Sun stimulated chlorophyll fluorescence. 1: Influence of oceanic properties", *International Journal of Remote Sensing*: **11** (12), 2125-2147.
- [RD-62] **Böttger, U., 1997.** "Zur ableitbarkeit von aerosoleigenschaften aus polarisation messungen", *Ph.D. Thesis*, Freie Universität Berlin, Fachbereich Geowissenschaften, Berlin (Germany).
- [RD-63] **Fell, F., and Preusker R., 1996.** "Effects of the wind direction on the light field reflected from a wind roughened sea surface", In *Ocean Optics XIII, SPIE proceedings*: 2963.
- [RD-64] **Fischer, J., and H. Grassl, 1984.** "Radiative transfer in an atmosphere-ocean system: An azimuthally dependent matrix-operator approach", *Applied Optics*: **23**, 1031-1039.
- [RD-65] **Scott, N.S., 1974.** "A direct method of computation of the transmission function of an homogeneous gaseous medium. I: Description of the method", *Journal of Quantitative Spectroscopy & Radiative Transfer*: **14**, 691.
- [RD-66] **Press, W.H., S.A. Teukolsky, W.T. Vetterling, and B.P. Flannery, 1992.** "Numerical recipes in C: The art of scientific computing", *Second Edition*, Cambridge University Press, Cambridge (Mass.): 994p.
- [RD-67] **Burden, R.L., and J.D. Faires, 1988.** "Numerical analysis", *Fourth Edition*, PWS-KENT Publishing Company, Boston (Mass.).
- [RD-68] **Caceci, M.S., and W.P. Cacheris, 1984.** "Fitting curves to data: The simplex algorithm is the answer", *BYTE Magazine*: 340-362.
- [RD-69] **Beer, R., 1994.** "Cross with your spectra? Cross-correlate instead!", *5<sup>th</sup> Workshop on Atmospheric Science from Space using Fourier Transform Spectroscopy, Proceedings of the ASSFTS, Nov 30-Dec 2, 1994*: 311-329.

- [RD-70] **Nelder, J.A., and R. Mead, 1965.** "A simple method for function minimization", *Computer Journal*: 7, 308-313.
- [RD-71] **Bevington, P.R., and D.K. Robinson, 1992.** "Data reduction and error analysis for the physical sciences", *Second Edition, McGraw-Hill Inc.*, New-York (NY): 328p.
- [RD-72] **Hair, J.F., Jr. R.E. Anderson, R.L. Tatham, 1987.** "Multivariate data analysis, with readings", *Second Edition, Macmillan Publishing Company*, London: 449p.
- [RD-73] **Kreyszig, E., 1993.** "Advanced Engineering Mathematics", *Seventh Edition, John Wiley & Sons Inc.*, New-York (NY): 1400p.

## 1.5 ACRONYMS AND ABBREVIATIONS

### 1.5.1 Acronyms

|          |  |
|----------|--|
| 6S       | Second Simulation of the Satellite Signal in Solar Spectrum  |
| AOT      | Aerosol Optical Thickness  |
| BOA      | Bottom Of the Atmosphere   |
| BRDF     | Bidirectional Reflectance Distribution Function  |
| CESBIO   | Centre d'Etudes Spatiales de la BIOSphere, (Toulouse - France)   |
| CDOM     | Coloured Dissolved Organic Matter  |
| DDV      | Dense Dark Vegetation  |
| DOM      | Discrete Ordinates Method  |
| ESFT     | Exponential Sum Fitting Technique (for computing gaseous transmittivity)                                   |
| FUB      | Freie Universität Berlin, Institute for Space Science, (Berlin - Germany)                                  |
| GAME     | Global Absorption ModEl  |
| I/O      | Inputs/Outputs   |
| IOP      | Inherent Optical Properties  |
| LBL      | Line By Line computation   |
| LISE/UdL | Laboratoire Interdisciplinaire en Sciences de l'Environnement, Université du Littoral, (Wimereux - France) |
| LUT      | Look-Up Table  |
| MERIS    | MEdium Resolution Imaging Spectrometer   |
| MERISAT  | MERIS Auxiliary data Tool software   |
| MLS      | Mid-Latitude Summer (atmospheric profile)  |
| MOMO     | Matrix-Operator MethOd   |
| OTC      | Optical Thickness Code   |
| RH       | Relative Humidity  |
| RTC      | Radiative Transfer Code  |
| RTE      | Radiative Transfer Equation  |
| SAM      | Standard Aerosol Model   |
| SO       | Successive Orders method for the <i>atmosphere</i>   |
| SOAO     | Successive Orders method for the coupled ' <i>Atmosphere-Ocean</i> ' system                                |
| SPM      | Suspended Particulate Matter   |
| STP      | Standard Temperature and Pressure ( $T_0=273.5K$ ; $P_0=1013.25hPa$ )                                      |
| TOA      | Top Of the Atmosphere  |
| WCRP     | World Climate Research Program   |

## 1.5.2 Scientific units

|                        |  |
|------------------------|--|
| <i>deg</i>             | degree ( <i>angle unit</i> )   |
| <i>DU</i>              | Dobson Unit ( $10^{-3}$ cm-atm)  |
| <i>Fm<sup>-1</sup></i> | Farad per meter ( <i>dielectric constant unit</i> )<br>( <i>Note: 1 Fm<sup>-1</sup> = 1 Cb<sup>2</sup>.N<sup>-1</sup>.m<sup>-2</sup> with Cb the Coulomb unit, and N the Newton unit</i> ) |
| <i>hPa</i>             | hecto Pascal or $10^2$ Pa ( <i>pressure unit</i> )<br>( <i>Note: 1 atm = 760.31 torr = 1013.25 hPa; 1 torr = 1mmHg = 1.333 mbar</i> )  |
| <i>J</i>               | Joule ( <i>energetic unit</i> )  |
| <i>μm</i>              | micrometer ( <i>wavelength unit</i> )  |
| <i>n.u.</i>            | non unit ( <i>unitless</i> )   |
| <i>sr</i>              | steradian ( <i>solid angle unit</i> )  |
| <i>W</i>               | watt ( <i>power unit</i> )   |

## 1.6 DEFINITIONS

Some definitions of energetic quantities and physical principles currently used in radiometry are given in this section to make more easier the comprehension of physical bases useful to compute radiative transfer within the coupled 'Atmosphere-Land/Ocean' system.

### 1.6.1 Radiometry

Analysis of remote sensing measurements requires the well knowledge of some physical quantities summarized in [Table 1](#). Note that the spectral irradiance and radiance will be expressed as  $\mu\text{m}^{-1}$ .

*Table 1: Definition of some physical quantities useful for remote sensing data.*

| Quantity                        | Symbol    | Units (SI)                         | Comments   |
|---------------------------------|-----------|------------------------------------|--|
| Wavelength                      | $\lambda$ | $[\mu\text{m}]$                    | Electromagnetic wave frequency   |
| Wavenumber                      | $k$       | $[\text{cm}^{-1}]$                 | Quantity defined as $2\pi/\lambda$   |
| Radiant energy                  | $W$       | $[\text{J}]$                       | Energy emitted, transmitted or received in electromagnetic wave form                         |
| Radiant flux or energetic power | $\Phi$    | $[\text{W}]$                       | Radiant energy emitted, transmitted or received per time unit $[\text{J}\cdot\text{s}^{-1}]$ |
| Radiant flux density            | $F$       | $[\text{W m}^{-2}]$                | Radiant flux crossing an area unit   |
| Irradiance                      | $E$       | $[\text{W m}^{-2}]$                | Radiant flux density incident on an area   |
| Radiant exitance                | $M$       | $[\text{W m}^{-2}]$                | Radiant flux density emerging from an area   |
| Radiant intensity               | $I$       | $[\text{W sr}^{-1}]$               | Radiant flux per solid angle unit  |
| Radiance                        | $L$       | $[\text{W m}^{-2} \text{sr}^{-1}]$ | Radiant flux density per unit solid angle  |

### 1.6.2 Physical principles

– *Geometrical optics:* Useful to describe the light scattering by a particle (approximated by a sphere) the size of which is large compared to the wavelength of the incident radiation. Reflexion, refraction and absorption of the light at the scatterer interface are well computed by this theory for a large *Mie's* parameter value ( $\kappa$ ) which is expressed as the ratio of the particle circumference to the incident wavelength ( $\kappa = 2\pi r / \lambda$ ).

*Typical values:*  $\kappa > 50$  for the cloud drops, drizzle and raindrops.

The interaction of the solar radiation with all the hydrometeor types falls in this regime. A wide variety of optical phenomena such as raindrops and halos can be explained by the geometrical optics.

– *Mie theory:* Analytical solutions using the *Maxwell's* equations for the light scattering by an isotropic sphere embedded in an homogeneous medium (see [\[RD-1\]](#) & [\[RD-2\]](#)). This theory is of particular interest for particles with an intermediate size which would be too large to be considered as being entirely comprised in an homogeneous periodic electric field, and too small to neglect the curvature

radius of a surface element in so far as such an element is also large enough to contain an optical ray.

*Typical values:*  $0.1 < \kappa < 50$  for the aerosols (*i.e.*, smoke, dust and haze).

– *Rayleigh scattering:* Process which describes the scattering of photons without changing their initial wavelength. This is opposed to the *Compton's* scattering where the wavelength of the scattered photons is shifted from its initial value. The *Rayleigh* dispersion occurs when the air molecules are small compared to the wavelength of the incoming sunlight, which makes the *Rayleigh* scattering insensitive to the particle shape [RD-3].

*Typical values:*  $0.001 < \kappa < 0.1$  for the molecules.

Molecular scattering varies as  $\lambda^{-4}$  (incident radiation wavelength), making it negligible for  $\kappa < 0.001$ .

## 1.7 GLOSSARY

*Absorbance:* The ratio of the absorbed radiant flux to the incident radiant flux.

*Aerosols:* Small suspended particles in the air (*e.g.*, smoke, dust and haze).

*Albedo:* The spectral albedo of a surface is expressed as the ratio of the upwelling spectral radiant flux ( $\Phi_{\lambda}^{\uparrow}$ ) to the downwelling spectral radiant flux ( $\Phi_{\lambda}^{\downarrow}$ ) within the upper and lower semi-hemisphere respectively:

$$A_{\lambda} = \frac{\Phi_{\lambda}^{\uparrow}}{\Phi_{\lambda}^{\downarrow}} \quad (n.u.)$$

Surface albedo can be also defined as the ratio of the radiant exitance  $M$  (due to reflection) to the irradiance  $E$  and is ranged within [0;1]. This quantity is independent of incoming and outgoing scattering angles.

*Single scattering albedo* ( $\omega_0$ ): This quantity represents the ratio of scattered radiant flux in all the directions to the extinct radiance flux (absorbed plus scattered radiant fluxes). It can be expressed as the ratio of the scattering coefficient ( $\sigma_s$ ) to the extinction coefficient ( $\sigma_e$ ).

*Clouds:* Clouds consist of water droplets or ice crystals with approximately  $10 \mu m$  radii. Droplet concentration in clouds is of the order of  $10^8 m^{-3}$  which means droplets stand around  $10^{-3} mm$  apart.

*Drizzle:* Drops characterized by  $100 \mu m$  radii with a significant fall speed.

*Irradiance:* Mean value of the radiant energy during some finite interval of time expressed as  $W.m^{-2}$ . This is proportional to the square of the amplitude of the electric field.

*Optical depth:* Integral of the scattering coefficient ( $\sigma_s$ ) within a layer defined by its depth  $dz$  :

$$\tau = \int_{z_2}^{z_1} \sigma_s(z) \cdot dz$$



*Optical thickness:* See optical depth.

Note that the *Rayleigh* optical thickness for the *Earth's* atmosphere is around 0.098 at 550nm wavelength, the aerosol optical thickness typically varies between 0.03 and 0.3 above oceans and between 0.04 and 0.8 above land surfaces. The clouds optical thickness is around 2 for the thin stratus and up to 300 for the cumulonimbus.

*Rain drops:* Drops with a radius size of 1 mm.

*Raman effect:* Scattering of the incident light by the molecules with a wavelength which differs to the incident frequency. This effect is not related to a characteristic frequency of the molecular scattering as for the fluorescence process or the resonance phenomenon.

*Reflectance:* The ratio of the reflected radiant flux to the incident radiant flux.

*Reflexion:* The *specular* reflexion corresponds to the part of the incident radiant flux reflected in the mirror direction. A reflective surface will be considered as smooth when the size of the irregularities at the surface level will be small compared to the incident wavelength.

By opposition, the *diffuse* reflexion will occur when the reflective surface presents irregularities the size of which is larger than the incident wavelength. This surface will be considered as *Lambertian* when radiances are uniformly distributed in all the upward directions (isotropic surface).

*Sun glint:* The solar radiation directly reflected by the water surface (*Fresnel* reflexion).

*Scattering:* Deflection of the trajectories of particles or energetic beams (*i.e.*, the light dispersion).

*Transmittance:* The ratio of the transmitted radiant flux to the incident radiant flux.

## 1.8 LIST OF SYMBOLS

### 1.8.1 Operator symbols

|     |  |
|-----|--|
| $I$ | unit operator ( <i>n.u.</i> )                              |
| $J$ | spectral source operator ( $W.m^{-2}.sr^{-1}.\mu m^{-1}$ ) |
| $R$ | reflection operator ( <i>n.u.</i> )                        |
| $F$ | transmission operator ( <i>n.u.</i> )                      |

### 1.8.2 Vector symbols

|               |  |
|---------------|--|
| $\tilde{E}_s$ | <i>Stokes</i> vector ( $E_o,0,0,0$ ) of solar radiation beam ( $W.m^{-2}.\mu m^{-1}$ ) |
| $\tilde{I}$   | <i>Stokes</i> vector ( $I,Q,U,V$ ) of radiation beam ( $W.m^{-2}.\mu m^{-1}$ )         |
| $\tilde{L}$   | <i>Stokes</i> vector ( $I,Q,U,V$ ) of radiance ( $W.m^{-2}.sr^{-1}.\mu m^{-1}$ )       |

### 1.8.3 Matrix symbols

|                                       |  |
|---------------------------------------|--|
| <b>0</b>                              | matrix for which all elements are equal to 0 ( <i>n.u.</i> )                         |
| <b>1</b>                              | matrix for which all elements are equal to 1 ( <i>n.u.</i> )                         |
| <b>C</b>                              | <i>Gaussian</i> atmospheric weights matrix ( <i>n.u.</i> )                           |
| <b>C*</b>                             | <i>Gaussian</i> oceanic weights matrix ( <i>n.u.</i> )                               |
| <b>F</b>                              | transmission matrix for direct solar radiation ( <i>n.u.</i> )                       |
| <b>F<sub>p</sub>(θ)</b>               | scattering matrix for one type of particles (or molecules) ( <i>n.u.</i> )           |
| <b>M</b>                              | scattering phase matrix ( <i>n.u.</i> )  |
| <b><math>\tilde{M}(\theta)</math></b> | phase matrix for a given scattering direction( <i>n.u.</i> )                         |
| <b>Mu</b>                             | incidence angles matrix ( <i>n.u.</i> )  |
| <b>P<sub>m</sub><sup>R</sup></b>      | scattering phase matrix for the reflection ( <i>n.u.</i> )                           |
| <b>P<sub>m</sub><sup>T</sup></b>      | scattering phase matrix for the transmission ( <i>n.u.</i> )                         |
| <b>R</b>                              | <i>Fresnel</i> reflection matrix on the sea water surface ( <i>n.u.</i> )            |
| <b>T</b>                              | <i>Fresnel</i> transmission matrix at the <i>air-water</i> interface ( <i>n.u.</i> ) |

### 1.8.4 Other symbols

|                       |  |
|-----------------------|--|
| <b>a, b</b>           | parameters of the particle size distribution ( <i>n.u.</i> )   |
| <b>a<sub>v</sub></b>  | weights associated with monochromatic absorption coefficients used in ESFT ( <i>n.u.</i> )                           |
| <b>dN(r)</b>          | number of particle per volume unit with a radius between <i>r</i> and <i>r + dr</i> ( <i>cm</i> <sup>-3</sup> )      |
| <b>E</b>              | spectral irradiance ( <i>W.m</i> <sup>-2</sup> . <i>μm</i> <sup>-1</sup> )   |
| <b>E<sub>o</sub></b>  | spectral solar irradiance at TOA ( <i>W.m</i> <sup>-2</sup> . <i>μm</i> <sup>-1</sup> )                              |
| <b>F<sub>o</sub></b>  | spectral solar radiance ( <i>W.m</i> <sup>-2</sup> . <i>sr</i> <sup>-1</sup> . <i>μm</i> <sup>-1</sup> )             |
| <b>f<sub>sp</sub></b> | forward scattering proportion ( <i>n.u.</i> )  |
| <b>H<sub>a</sub></b>  | aerosol scale height ( <i>km</i> )   |
| <b>H<sub>m</sub></b>  | <i>Rayleigh</i> (molecular) scale height ( <i>km</i> )   |
| <b>ind</b>            | index for selecting the type of particle size distribution ( <i>n.u.</i> )   |
| <b>I<sub>s</sub></b>  | maximum order of the <i>Legendre</i> polynomial decomposition of the phase function and the radiance ( <i>n.u.</i> ) |
| <b>k</b>              | either imaginary part of the refractive index ( <i>n.u.</i> )<br>or wavenumber ( <i>cm</i> <sup>-1</sup> )           |
| <b>k<sub>a</sub></b>  | absorption efficiency ( <i>n.u.</i> )  |
| <b>k<sub>e</sub></b>  | extinction efficiency ( <i>n.u.</i> )  |
| <b>k<sub>s</sub></b>  | scattering efficiency ( <i>n.u.</i> )  |
| <b>k<sub>v</sub></b>  | monochromatic absorption coefficients ( <i>cm</i> <sup>2</sup> . <i>g</i> <sup>-1</sup> )                            |

|                        |  |
|------------------------|--|
| $L$                    | spectral radiance ( $W.m^{-2}.sr^{-1}.\mu m^{-1}$ )  |
| $m$                    | real part of the refractive index ( <i>n.u.</i> )  |
| $M$                    | either the number of <i>Fourier</i> terms ( <i>n.u.</i> )<br>or the airmass (defined as $[1/\cos \mathcal{G}_s + 1/\cos \mathcal{G}_v]$ or $[1/\mu_s + 1/\mu_v]$ ) ( <i>n.u.</i> ) |
| $n$                    | index for selecting a MERIS spectral band ( <i>n.u.</i> )<br>or complex refractive index ( <i>n.u.</i> )   |
| $n_a$                  | refractive index of air ( <i>n.u.</i> )  |
| $n_w$                  | refractive index of pure water ( <i>n.u.</i> )   |
| $n(r)$                 | particle size distribution ( $cm^{-3}.\mu m^{-1}$ )  |
| $N$                    | either number of size distributions used in the <i>Mie's</i> computation ( <i>n.u.</i> )<br>or number of discrete atmospheric zenithal angles ( <i>n.u.</i> )                      |
| $N^*$                  | number of discrete oceanic zenithal angles ( <i>n.u.</i> )   |
| $n_2$                  | number of scattering angles in the <i>Mie's</i> computation ( <i>n.u.</i> )  |
| $n_i / n$              | component mixing ratio ( <i>i.e.</i> , volume percentage of particles characterized by the $i^{th}$ size distribution) ( <i>n.u.</i> )   |
| $p$                    | normalized scattering phase function ( $sr^{-1}$ )   |
| $P_s$                  | surface pressure ( <i>mbar</i> or <i>hPa</i> )   |
| $Q_a$                  | absorption cross section ( $m^{-2}$ )  |
| $Q_e$                  | extinction cross section ( $m^{-2}$ )  |
| $Q_s$                  | scattering cross section ( $m^{-2}$ )  |
| $r$                    | geometrical radius of a scatterer ( $\mu m$ )  |
| $r_{min}, r_{max}, dr$ | minimum and maximum radius ( $\mu m$ ), and radius increment ( $\mu m$ ) of the particles in a given size distribution   |
| $r_{//}, r_{\perp}$    | <i>Fresnel</i> reflection coefficients in the $//$ and $\perp$ direction to the incidence plane ( <i>n.u.</i> )  |
| $t_{//}, t_{\perp}$    | <i>Fresnel</i> transmission coefficients in the $//$ and $\perp$ direction to the incidence plane ( <i>n.u.</i> )  |
| $T(u)$                 | spectrally integrated transmission function for an absorber amount $u$ ( <i>n.u.</i> )   |
| $U_{H_2O}$             | total water vapor content ( $g.cm^{-2}$ )  |
| $U_{O_2}$              | total oxygen vapor content ( $g.cm^{-2}$ )   |
| $U_{O_3}$              | total ozone content ( <i>cm-atm</i> )  |
| $w_i$                  | <i>Gaussian</i> weigths ( <i>n.u.</i> )  |
| $w_s$                  | wind speed above sea level ( $m.s^{-1}$ )  |
| $\delta_{i,j}$         | <i>Dirac's</i> delta function ( <i>n.u.</i> )  |
| $\Delta\phi$           | relative azimuthal angle, noted also as $\Delta\phi$ ( <i>deg.</i> )   |

|                  |   |
|------------------|---|
| $\Delta\nu$      | spectral interval ( $s^{-1}$ or <i>hertz</i> )  |
| $\varphi_o$      | illumination azimuthal angle ( <i>deg.</i> )  |
| $\varphi_s$      | solar azimuthal angle ( <i>deg.</i> )   |
| $\varphi_v$      | viewing azimuthal angle ( <i>deg.</i> )   |
| $\lambda$        | wavelength ( $\mu m$ or <i>nm</i> )   |
| $\mu$            | cosine of zenithal angle ( <i>n.u.</i> )  |
| $\mu_i$          | <i>Gaussian</i> angles ( <i>n.u.</i> )  |
| $\sigma_a$       | absorption coefficient (aerosols / molecules) ( $m^{-1}$ )                                    |
| $\sigma_a^p$     | absorption coefficient for phytoplankton ( $m^{-1}$ )   |
| $\sigma_a^{spm}$ | absorption coefficient for SPM ( $m^{-1}$ )   |
| $\sigma_a^{ys}$  | absorption coefficient for yellow substance ( $m^{-1}$ )                                      |
| $\sigma_a^w$     | absorption coefficient for pure sea water ( $m^{-1}$ )  |
| $\sigma_e$       | extinction coefficient (aerosols / molecules) ( $m^{-1}$ )                                    |
| $\sigma_e^p$     | extinction coefficient for phytoplankton ( $m^{-1}$ )   |
| $\sigma_e^{spm}$ | extinction coefficient for SPM ( $m^{-1}$ )   |
| $\sigma_e^{ys}$  | extinction coefficient for yellow substance ( $\sigma_e^{ys} = \sigma_a^{ys}$ ) ( $m^{-1}$ )  |
| $\sigma_e^w$     | extinction coefficient for pure sea water ( $m^{-1}$ )  |
| $\sigma_s$       | scattering coefficient (aerosols / molecules) ( $m^{-1}$ )                                    |
| $\sigma_s^p$     | scattering coefficient for phytoplankton ( $m^{-1}$ )   |
| $\sigma_s^{spm}$ | scattering coefficient for SPM ( $m^{-1}$ )   |
| $\sigma_s^w$     | scattering coefficient for pure sea water ( $m^{-1}$ )  |
| $\theta$         | scattering angle ( <i>deg.</i> )  |
| $\theta_p$       | phase function truncation angle ( <i>deg.</i> )   |
| $\vartheta_c$    | critical zenithal angle for total internal reflection ( <i>deg.</i> )                         |
| $\vartheta_o$    | illumination zenithal angle ( <i>deg.</i> )   |
| $\vartheta_s$    | solar zenithal angle ( <i>deg.</i> )  |
| $\vartheta_v$    | viewing zenithal angle ( <i>deg.</i> )  |
| $\rho_s$         | reflectance of ground surface or ocean bottom assumed to be <i>Lambertian</i> ( <i>n.u.</i> ) |
| $\rho_G$         | specular reflection of sunlight over ocean waves ( <i>n.u.</i> )                              |
| $\rho_F$         | <i>Fresnel</i> reflectance at the <i>air-sea</i> interface ( <i>n.u.</i> )                    |

|                   |  |
|-------------------|--|
| $\rho_{DDV}$      | ground DDV albedo ( <i>n.u.</i> )  |
| $\bar{\rho}_{aG}$ | aerosol-ground DDV coupling bidirectionality term ( <i>n.u.</i> )          |
| $\bar{\rho}_{aR}$ | aerosol-molecule coupling bidirectionality term ( <i>n.u.</i> )            |
| $\bar{\rho}_{RG}$ | <i>Rayleigh</i> -ground DDV coupling bidirectionality term ( <i>n.u.</i> ) |
| $\tau$            | optical thickness ( <i>n.u.</i> )  |
| $\tau^a$          | aerosol optical thickness ( <i>n.u.</i> )                                  |
| $\tau^c$          | cloud optical thickness ( <i>n.u.</i> )                                    |
| $\tau^R$          | <i>Rayleigh</i> (molecular) optical thickness ( <i>n.u.</i> )              |
| $\tau^{O_3}$      | ozone optical thickness ( <i>n.u.</i> )                                    |
| $\omega_o$        | single scattering albedo ( <i>n.u.</i> )                                   |
| $\omega_o^p$      | single scattering albedo for phytoplankton( <i>n.u.</i> )                  |
| $\omega_o^{spm}$  | single scattering albedo for SPM( <i>n.u.</i> )                            |
| $\omega_o^w$      | single scattering albedo for pure sea water( <i>n.u.</i> )                 |
| $\Omega$          | solid angle ( <i>sr</i> )  |

## 2. PHYSICAL BASES

### 2.1 EXTINCTION, SCATTERING AND ABSORPTION COEFFICIENTS

Let us consider an elementary layer  $dz$  of homogeneously distributed absorbing and scattering spherical particles which receives a perpendicular monochromatic incident radiant flux  $\phi_0$  at the top of its interface (Figure 1). This radiant flux which propagates along  $z$  axis within the layer is then attenuated by the scatterers and absorbers encountered. The outgoing radiant flux ( $\phi_0 + d\phi_0$ ) at the bottom interface is then lower than the incoming radiant flux.

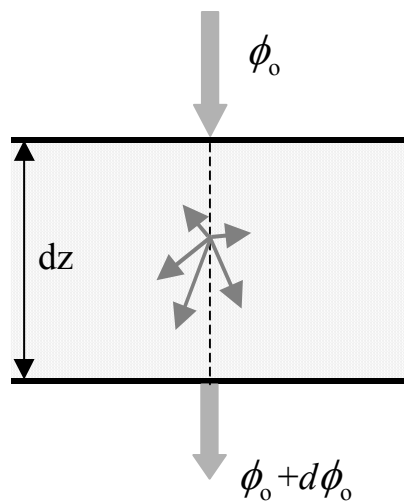


*Figure 1: Schematic representation of a radiant flux propagation within a scattering and absorbing medium.*

Assuming an isotropic medium, the variation of the radiant flux  $d\phi_0$  is directly proportional to the incoming radiant flux  $\phi_0$  and it can be expressed as:

$$d\phi_0 = -\sigma_e \cdot \phi_0 \cdot dz \quad (1)$$

or

$$\frac{d\phi_0}{\phi_0} = -\sigma_e \cdot dz \quad (2)$$

where  $dz$  is the geometrical thickness of the layer and  $\sigma_e$  ( $m^{-1}$ ) the extinction coefficient.

Note that all the quantities mentioned above and hereafter are monochromatic, and to simplify the notation the subscript  $\lambda$  corresponding to the wavelength is omitted.

The energy loss in the layer  $dz$  relies on two physical processes:

- *absorption*: photons are purely absorbed then re-emitted at a frequency which differs to the initial incident wavelength (e.g., in the thermal region of the solar spectrum),
- *scattering*: photons are scattered in all the directions of the space.

The propagation medium is then characterized by an absorption coefficient  $\sigma_a$  and a scattering coefficient  $\sigma_s$  expressed as  $m^{-1}$ . These two coefficients verify the following relationship:

$$\sigma_e = \sigma_a + \sigma_s \quad (3)$$

## 2.2 SINGLE SCATTERING ALBEDO AND OPTICAL DEPTH

The previous layer can be optically described by the two following parameters:

- the *single scattering albedo*  $\omega_0$  which is defined as:

$$\omega_0 = \frac{\sigma_s}{\sigma_e} \quad \text{with} \quad 0 \leq \omega_0 \leq 1 \quad (4)$$

- the layer *optical depth*  $\tau$  which represents the total extinction coefficient  $\sigma_e$  integrated between its upper ( $z_1$ ) and lower ( $z_2$ ) interfaces:

$$\tau = \int_{z_2}^{z_1} \sigma_e(z) \cdot dz \quad (5)$$

## 2.3 SCATTERING PHASE FUNCTION

### 2.3.1 Definition

Similarly to Equation (1) the radiant flux loss  $d^2\phi_0^s(\theta, \Omega)$  in the layer  $dz$ , due to the scattering process only, along a particular scattering direction  $\theta$  within a solid angle  $d\Omega$  (Figure 2), can be written as:

$$d^2\phi_0^s(\theta, d\Omega) = f(\theta) \cdot \phi_0 \cdot dz \cdot d\Omega \quad (6)$$

where  $f(\theta)$  represents the angular distribution function of the scattered photons in all the directions of the space, expressed as  $m^{-1}sr^{-1}$ .

Integration of Equation (6) over  $d\Omega$  for all the directions of the space yields to:

$$d\phi_0^s = -\sigma_s \cdot \phi_0 \cdot dz \quad (7)$$

where,

$$\sigma_s = 2\pi \cdot \int_0^\pi f(\theta) \cdot \sin\theta \cdot d\theta \quad (8)$$

It is more convenient to introduce a normalized phase function  $p(\theta)$  related to the scattering function as follows:

$$p(\theta) = \frac{4\pi}{\sigma_s} \cdot f(\theta) \quad (sr^{-1}) \quad (9)$$

where the normalization is given by:

$$\iint_{space} p(\theta) \cdot d\Omega = 4\pi \quad (10)$$

The scattering phase function depends on the physical characteristics of the scatterers (*i.e.*, the refractive index and the particle size distribution) and does not take into account their density number which reflects on  $\sigma_s$  only.

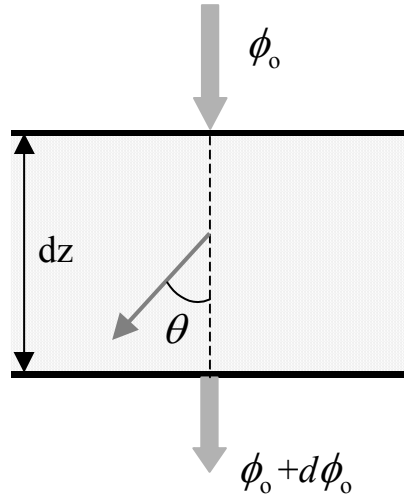


*Figure 2: Schematic representation of scattered radiant flux within a particulate layer.*

### 2.3.2 Truncation of phase function

Large particles present a strong forward scattering peak which makes very difficult the angular integration of their phase function. Several approaches have been developed to overcome this difficulty. The latter consist in substituting the phase function by a similar function more accessible to numerical treatment. These methods, referred as the phase function truncation techniques, rely on the assumption that the scattered light into the forward direction cannot be distinguished from unscattered light. Consequently, this phase function  $p(\theta)$  can be approximated by a linear combination of *Dirac's* delta function representing a certain amount  $\alpha$  of forward scattering and a modified phase function  $p'(\theta)$  with a reduced proportion of forward scattering for angles smaller than a certain threshold value  $\theta_p$  (Figure 3):

$$p(\theta) = \alpha \cdot \delta_{1, \cos \theta} + (1 - \alpha) \cdot p'(\theta) \quad (11)$$

with  $p'(\theta)$  defined as:

$$\begin{cases} p'(\theta) = a \cdot \theta + b & \text{for } \theta \in [0; \theta_p] \\ p'(\theta) = p(\theta) & \text{otherwise} \end{cases} \quad (12)$$

where  $a$  and  $b$  are determined by the following conditions:

$$\begin{cases} p'(\theta_p) = p(\theta_p) \\ \left(\frac{dp'}{d\theta}\right)_{\theta_p} = \left(\frac{dp}{d\theta}\right)_{\theta_p} \end{cases} \quad (13)$$

The fraction  $\alpha$  represents the amount of radiation considered as being scattered exactly into the forward direction. The modified phase function  $p'(\theta)$  is then normalized according to Equation (10).

Consequently, the extinction of the incident radiant flux  $\phi_0$  within the layer is smaller and the new scattering ( $\sigma_s'$ ) and extinction ( $\sigma_e'$ ) coefficients become:



$$\begin{cases} \sigma_s' = \sigma_s \cdot (1 - \alpha) \\ \sigma_e' = \sigma_e \cdot (1 - \omega_o \cdot \alpha) \end{cases} \quad (14)$$

Keeping a constant absorption coefficient, the modified single scattering albedo ( $\omega_o'$ ) can be deduced by including Equations (3) and (4) into Equation (12):

$$\omega_o' = \frac{\omega_o \cdot (1 - \alpha)}{1 - \omega_o \cdot \alpha} \quad (15)$$

Note that certain authors prefer to replace the forward scattering peak by a second order polynomial (Figure 4). In this case,  $p'(\theta)$  is expressed as follows [RD-4]:

$$\begin{cases} p'(\theta) = a \cdot \theta^2 + c & \text{for } \theta \in [0; \theta_p] \\ p'(\theta) = p(\theta) & \text{otherwise} \end{cases} \quad (16)$$

where  $a$  and  $c$  are derived from the following conditions:

$$\begin{cases} p'(\theta_p) = p(\theta_p) \\ \left(\frac{dp'}{d\theta}\right)_{\theta_p} = \left(\frac{dp}{d\theta}\right)_{\theta_p} \\ \left(\frac{dp'}{d\theta}\right)_0 = 0 \end{cases} \quad (17)$$

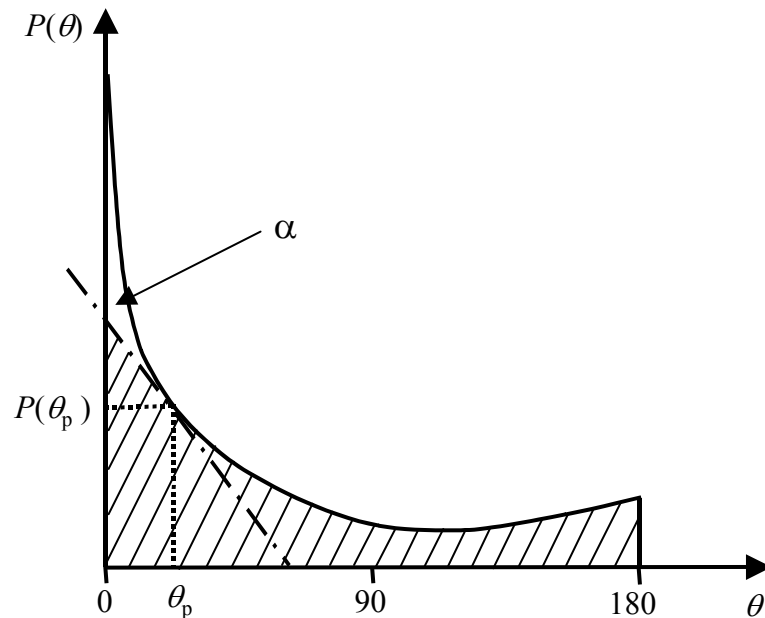


*Figure 3: Illustration of the phase function truncation technique which substitutes the forward scattering peak by a linear extrapolation. Area below the phase function  $p(\theta)$  (solid line) is replaced by the hatched area (modified scattering function  $p'(\theta)$ ). The amount  $\alpha$  of forward scattered light is considered as not being scattered.*

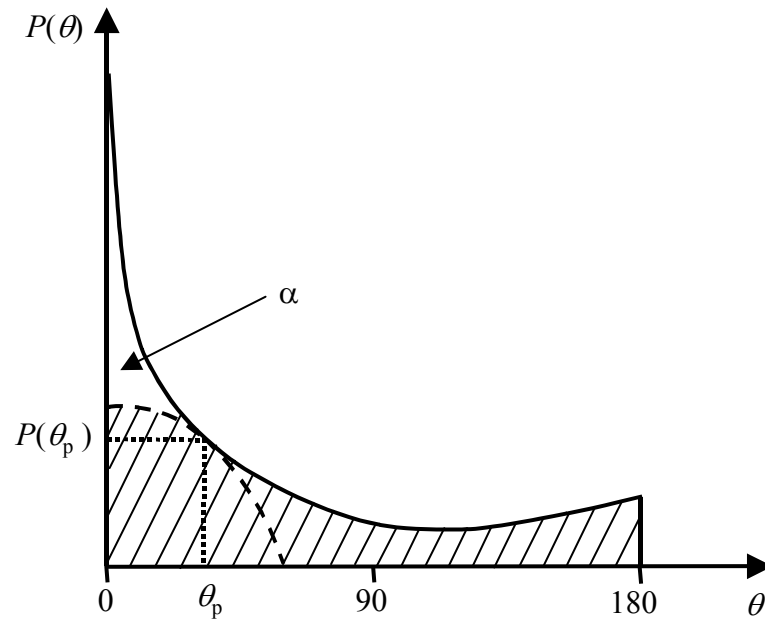


Figure 4: Same legend as Figure 3 but using a second order polynomial curve to substitute the forward scattering peak.

## 2.4 IRRADIANCE, RADIANCE AND REFLECTANCE

Let us consider an horizontal elementary ground surface  $dS$  enlightened by an incident parallel sun beam from direction  $\vartheta_0$  (Figure 5), the irradiance  $E_s$  received by  $dS$  is then expressed as:

$$E = E_0 \cdot \cos \vartheta_0 \quad (W m^{-2}) \quad (18)$$

where  $E_0$  is the radiant flux density on the elementary surface  $d\Sigma$  perpendicular to the incident beam and  $\vartheta_0$  the zenithal angle of the illumination source.

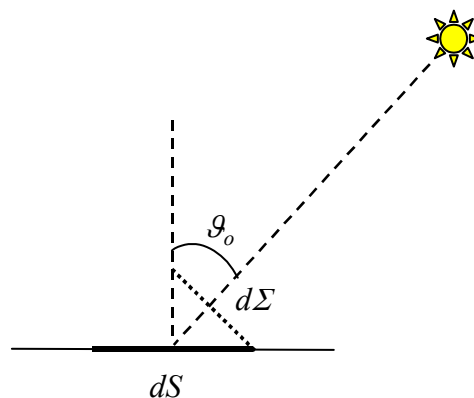


Figure 5: Illumination configuration of an elementary ground surface  $dS$ .

This relationship is currently used to define the solar irradiance  $E_s$  at the top of the atmosphere (TOA) for which the incident direction is determined by the solar zenithal angle  $\theta_s$  and the solar azimuthal angle  $\varphi_s$ . The geographic north direction refers to  $\varphi_s = 0$  and  $\theta_s$  is ranged within  $[0; \pi/2]$ .

The incident solar radiance  $L_s$  on the surface  $dS$  is defined as the incident radiant flux density  $E_s$  (or irradiance) per unit of solid angle  $d\Omega$  (Figure 6):

$$L_s = \frac{dE_s}{d\Omega} \quad (W \ m^{-2} \ sr^{-1}) \quad (19)$$

where  $d\Omega$  represents the solid angle ( $sr$ ) under which is viewed the surface  $dS$  from the solar illumination.

$$d\Omega = \sin \vartheta_s \cdot d\vartheta_s \cdot d\varphi_s \quad (20)$$

Similarly, the upwelling radiance  $L$  leaving the surface  $dS$  is defined as the reflected or emitted radiant flux density  $E$  per unit of solid angle  $d\omega$ :

$$L = \frac{dE}{d\omega} \quad (W \ m^{-2} \ sr^{-1}) \quad (21)$$

where  $d\omega$  is the solid angle under which is viewed the surface  $dS_d$  from the ground surface  $dS$ .

$$d\omega = \sin \vartheta_v \cdot d\vartheta_v \cdot d\varphi_v \quad (22)$$

or

$$d\omega = d\mu_v \cdot d\varphi_v \quad \text{with} \quad \mu_v = \cos \vartheta_v$$

where  $\vartheta_v$  and  $\varphi_v$  stand for the viewing zenithal and azimuthal angles, respectively.

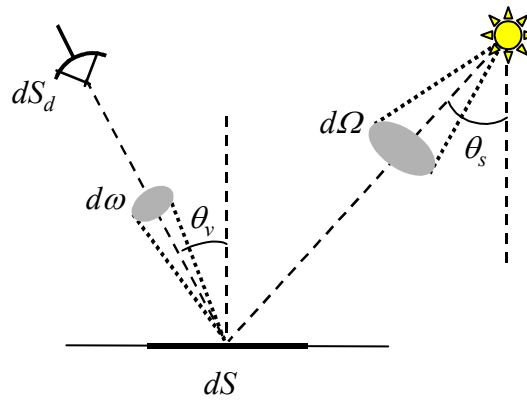


*Figure 6: Viewing and illumination configuration of an elementary ground surface  $dS$ .*

The elementary irradiance  $dE$  included within  $d\omega$  can be written as:

$$dE = L \cdot \mu_v \cdot d\mu_v \cdot d\varphi_v \quad (23)$$

where  $\mu_v$  corresponds to the cosine projection of the elementary surface  $dS$ .

The total upwelling radiance  $E^\uparrow$  in the upper semi-hemisphere over the ground surface  $dS$  is then computed as:

$$E^\uparrow = \int_0^{2\pi} \int_0^1 L(\mu_v, \varphi_v) \cdot \mu_v \cdot d\mu_v \cdot d\varphi_v \quad (24)$$

For a *Lambertian* surface (*i.e.*, an isotropic surface) the radiance  $L$  is independent of  $\vartheta_v$  and  $\varphi_v$ , and the total upwelling radiance above the surface is then:  $E^\uparrow = \pi L$

The surface reflectance  $\rho_s$  is then defined as the ratio between the total upwelling ( $E^\uparrow$ ) to downwelling ( $E^\downarrow$ ) radiances:

$$\rho_s = \frac{E^\uparrow}{E^\downarrow} \quad (25)$$

For a *Lambertian* reflector enlightened by the direct solar irradiance only, the surface reflectance is deduced from Equations (18) and (25):

$$\rho_s = \frac{\pi L}{\mu_s E_s} \quad (26)$$

## 2.5 STOKES PARAMETERS

Let a plane electromagnetic wave propagates along  $z$  axis with a wavenumber  $k$  ( $k = 2\pi/\lambda$ , with  $\lambda$  the wavelength) and an angular frequency  $\omega$  ( $\omega = k \cdot c$ , with  $c$  the light velocity). The electric field vector  $\vec{E}$  may be decomposed into two components  $E_{//}$  and  $E_{\perp}$  (complex and oscillating functions) which represent the electric field in the parallel ( $//$ ) and perpendicular ( $\perp$ ) directions in the plane ( $x, y$ ) through the propagation direction:

$$\begin{cases} E_{//} = A_{//} \cdot e^{-i\varphi_{//}} \cdot e^{-i(k \cdot z + \omega \cdot t)} \\ E_{\perp} = A_{\perp} \cdot e^{-i\varphi_{\perp}} \cdot e^{-i(k \cdot z + \omega \cdot t)} \end{cases} \quad (27)$$

where  $A_{//}$  and  $A_{\perp}$  are respectively the amplitudes of each of the two electric field components ( $E_{//}$  and  $E_{\perp}$ ), and  $\varphi_{//}$ ,  $\varphi_{\perp}$  the associated phases. Note that a plane electromagnetic wave is characterized by a constant phase.

Since the intensity of the electromagnetic wave is proportional to the square of the electric field, four *Stokes* parameters ( $I, Q, U, V$ ) are then introduced:

$$\begin{cases} I = E_{//} E_{//}^* + E_{\perp} E_{\perp}^* \\ Q = E_{//} E_{//}^* - E_{\perp} E_{\perp}^* \\ U = E_{//} E_{\perp}^* + E_{\perp} E_{//}^* \\ V = -i (E_{//} E_{\perp}^* - E_{\perp} E_{//}^*) \end{cases} \quad (28)$$

where the asterisk denotes the complex conjugate value of the electric field. These *Stokes* parameters define an elliptically polarized wave and verify the following relationship:

$$I^2 = Q^2 + U^2 + V^2 \quad (29)$$

Note that the ellipse, corresponding to the polarization form of the electromagnetic wave, describes the temporal variation of the wave amplitude in the perpendicular plane to the propagation direction.

Introducing Equation (27) into (28) yields to:

$$\begin{cases} I = (A_{//})^2 + (A_{\perp})^2 \\ Q = (A_{//})^2 - (A_{\perp})^2 \\ U = 2 A_{//} \cdot A_{\perp} \cdot \cos \delta \\ V = 2 A_{//} \cdot A_{\perp} \cdot \sin \delta \end{cases} \quad (30)$$

with  $\delta = \varphi_{//} - \varphi_{\perp}$ .

The intensities  $I_{//}$  and  $I_{\perp}$  observed respectively along the parallel and perpendicular directions are expressed as:

$$\begin{cases} I_{//} = (A_{//})^2 \\ I_{\perp} = (A_{\perp})^2 \end{cases} \quad (31)$$

Assuming that  $\alpha$  is the inclination of the principal axes of the ellipse with the directions of the polarization plane ( $A_{//}, A_{\perp}$ ) and  $\beta$  the angle corresponding to the excentricity (Figure 7), the *Stokes* parameters can be formulated with the intensities  $I, I_{//}, I_{\perp}$  and the angles  $\alpha$  and  $\beta$ :

$$\begin{cases} I = I_{//} + I_{\perp} \\ Q = I \cdot \cos 2\alpha \cdot \cos 2\beta \\ U = I \cdot \sin 2\alpha \cdot \cos 2\beta \\ V = I \cdot \sin 2\beta \end{cases} \Rightarrow \begin{cases} I = I_{//} + I_{\perp} \\ Q = I_{//} - I_{\perp} \\ U = (I_{//} - I_{\perp}) \cdot \tan 2\alpha \\ V = (I_{//} - I_{\perp}) \cdot \tan 2\beta / \cos 2\alpha \end{cases} \quad (32)$$

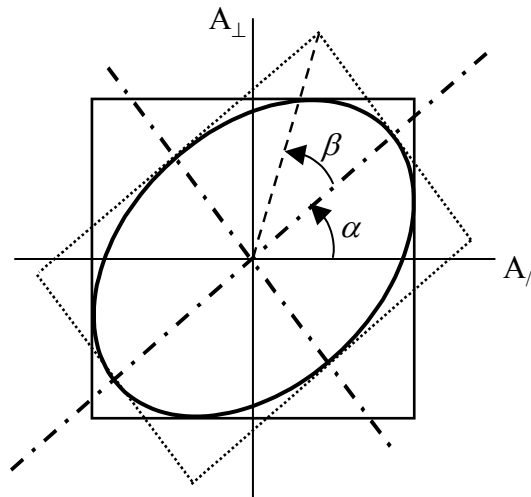


*Figure 7: Representation of the elliptic polarization of an electromagnetic wave describing the temporal variation of the amplitude  $A(t)$  of the electric field in the perpendicular plane to the propagation direction.*

Due to the high frequency of the light beam there exists millions of successive waves with independent phases within a very short time. Thus each measurement of the light integrates millions of wave intensities. Introducing a time average and the apparent intensities in the parallel and perpendicular directions, the *Stokes* parameters become:

$$\begin{cases} I = (\bar{A}_{//})^2 + (\bar{A}_{\perp})^2 \\ Q = (\bar{A}_{//})^2 - (\bar{A}_{\perp})^2 \\ U = 2 \bar{A}_{//} \bar{A}_{\perp} \cos \delta \\ V = 2 \bar{A}_{//} \bar{A}_{\perp} \sin \delta \end{cases} \quad (33)$$

Note that for a natural (or unpolarized) radiation, the light is unaffected by the different wave phases, and consequently  $\overline{\cos \delta}$  and  $\overline{\sin \delta}$  are equals to zero. Moreover, amplitudes are the same whatever the direction ( $A_{//} = A_{\perp}$ ). In fact, as mentioned by Chandrasekhar, *Natural light is equivalent to any two independent oppositely polarized streams*  $\{(\beta, \alpha) \text{ and } (-\beta, \alpha + \pi/2)\}$  of half the intensity [RD-5]. Thus, using Equations (33) it can be easily shown that:

$$\begin{cases} Q(\alpha) + Q(\alpha + \pi/2) = 0 \\ U(\alpha) + U(\alpha + \pi/2) = 0 \\ V(\beta) + V(-\beta) = 0 \end{cases} \quad (34)$$

Finally, for a *natural light* such as sunlight the *Stokes* parameters become:  $(I, Q, U, V) = (I_{\text{unpol}}, 0, 0, 0)$ .

Note that:

- For a *totally polarized light*, the parameter  $\delta$  is constant and Equation (29) remains right. The wave state is described by the following *Stokes* parameters:

$$(I, Q, U, V) = (I_{\text{pol}}, Q, U, V) \text{ with } I_{\text{pol}} \text{ the polarized intensity}$$

- For a *partially polarized light*, Equation (29) becomes:

$$I^2 \geq Q^2 + U^2 + V^2$$

and the wave state is described by the following *Stokes* parameters:

$$(I, Q, U, V) = (I_{\text{unpol}}, 0, 0, 0) + (I_{\text{pol}}, Q, U, V)$$

## 2.6 PHASE MATRIX

On the basis of *Stokes* parameters, the intensity of electromagnetic waves  $I$  at each point of a given propagation direction can be related to the natural incident wave  $(I_0, 0, 0, 0)$  by the following relationship:

$$\begin{bmatrix} I \\ Q \\ U \\ V \end{bmatrix} = \mathbf{M}(\theta) \cdot \begin{bmatrix} I_0 \\ 0 \\ 0 \\ 0 \end{bmatrix} \quad (35)$$

where  $\mathbf{M}(\theta)$  represents the phase matrix and  $\theta$  the scattering angle.

The scattering phase matrix is defined as:

$$\mathbf{M}(\theta) = \frac{\sigma_s}{4\pi r^2} \cdot \mathbf{F}_p(\theta) \quad (36)$$

where  $\mathbf{F}_p(\theta)$  is the scattering matrix for one type of particles (or molecules).

Each term of the matrix corresponds to the angular distribution of the scattered intensity by a sphere. For a single isotropic and homogeneous sphere, the phase matrix  $\mathbf{F}_p(\mu)$  is defined as:

$$\mathbf{F}_p(\mu) = \begin{bmatrix} P_{11}(\mu) & P_{12}(\mu) & 0 & 0 \\ P_{12}(\mu) & P_{11}(\mu) & 0 & 0 \\ 0 & 0 & P_{33}(\mu) & -P_{34}(\mu) \\ 0 & 0 & P_{34}(\mu) & P_{33}(\mu) \end{bmatrix}, \text{ with } \mu = \cos\theta \quad (37)$$

## 2.7 RAYLEIGH SCATTERING

The *Rayleigh* (or molecular) scattering theory presented below is extracted from [RD-6]. The latter is based on the assumption that the electric field ( $\vec{E}$ ) of the incident electromagnetic wave induces the presence of an electric dipole moment ( $\vec{P}$ ) within the molecule oscillating at the incident wave frequency. This oscillating dipole always emits at the same frequency according to the classical electromagnetic theory.

The *Rayleigh* theory is only applied to molecules and particles the size of which is much smaller than the radiation wavelength, *i.e.*, for which the electric field can be assumed to be constant around the particle. The induced moment  $\vec{P}$  and the incident electric field  $\vec{E}$  are related by the polarizability tensor which is reduced to a constant polarizability coefficient  $\alpha$  for an isotropic molecule:

$$\vec{P} = \alpha \cdot \vec{E} \quad (38)$$

From the electromagnetic theory, the total radiant energy ( $W$ ) emitted by the dipole is defined as:

$$W = \frac{c k^4}{12\pi\epsilon_0} \cdot (P P^*) \quad (39)$$

with  $\epsilon_0$  the dielectric constant in vacuum ( $\epsilon_0 = 8.85 \cdot 10^{-12} \text{ Fm}^{-1}$ ),  $c$  the light velocity in vacuum ( $c = 2.998 \cdot 10^8 \text{ m s}^{-1}$ ),  $k$  the wavenumber ( $k = 2\pi / \lambda$ , with  $\lambda$  the wavelength of the incident radiation), and  $P_0$  the amplitude of moment  $\vec{P}$ ; the asterisk denotes the complex conjugate value.

The incident radiant flux density  $F$  (irradiance) on the spherical particle (molecule) is expressed as:

$$F = \frac{c \epsilon_0}{2} \cdot (E E^*) \quad (40)$$

If  $W$  is interpreted as the radiant flux (or energetic power) scattered by the spherical particle (molecule) in all the directions, the scattering cross section  $Q_s^{mol}$  ( $\text{m}^{-2}$ ) of the particle is then written as:

$$Q_s^{mol} = \frac{W}{F} \quad (41)$$

or with Equations (38), (39) and (40):

$$Q_s^{mol} = \frac{k^4 \alpha^2}{6\pi\epsilon_0^2} \quad (42)$$

For a propagation medium with  $N$  molecules per unit volume ( $m^{-3}$ ), the resulting scattering coefficient  $\sigma_s$  is given by:

$$\sigma_s = N \cdot Q_s^{mol} \quad (43)$$

The electric field  $\vec{E}_s$  emitted at a distance  $d$  from the dipole (Figure 8a) which is much larger than the wavelength is defined as:

$$\vec{E}_s = \frac{k^2 \vec{P}}{4\pi\epsilon_0 d} \cdot \sin \gamma \cdot e^{-ik \cdot d} \quad (44)$$

where  $\gamma$  is the angle between the dipole moment  $\vec{P}$  and the viewing direction  $\vec{s}$ . The vibration of  $\vec{E}$  is in the plane  $(\vec{P}, \vec{s})$ .

Considering the scattering plane defined by  $\vec{s}_0$  and  $\vec{s}$ , the incident and scattering directions respectively, and the scattering angle  $\theta = (\vec{s}, \vec{s}_0)$ , the scattered electric field  $(\vec{E}_s, \vec{s})$  can be splitted up into its parallel  $(\vec{E}_{s, //})$  and perpendicular  $(\vec{E}_{s, \perp})$  components to the scattering plane (Figure 8b):

- the parallel component  $\vec{E}_{s, //}$  corresponds to a scattered field in the scattering plane with  $\gamma = \pi/2 - \theta$ ,

$$E_{s, //} = \frac{k^2 \alpha A_{//}}{4\pi\epsilon_0 d} \cdot \cos \theta \cdot e^{-ik \cdot d} \quad (45)$$

with  $A_{//}$  the amplitude of  $\vec{E}_{s, //}$ .

- the perpendicular component  $\vec{E}_{s, \perp}$  corresponds to a scattered field in a perpendicular direction to the scattering plane with  $\gamma = \pi/2$ ,

$$E_{s, \perp} = \frac{k^2 \alpha A_{\perp}}{4\pi\epsilon_0 d} \cdot e^{-ik \cdot d} \quad (46)$$

with  $A_{\perp}$  the amplitude of  $\vec{E}_{s, \perp}$ .

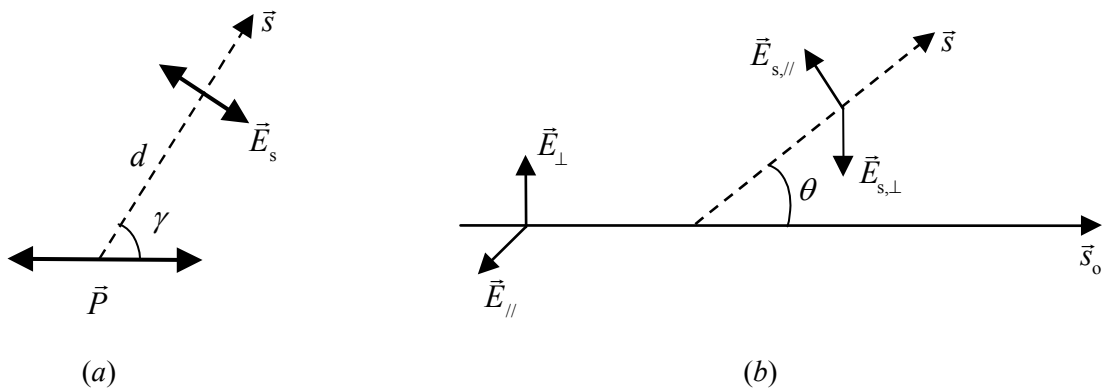


**Figure 8:** Illustration of Rayleigh scattering: (a) parallel (//) and perpendicular ( $\perp$ ) components of the incident  $(\vec{E}_0, \vec{s}_0)$  and emitted  $(\vec{E}_s, \vec{s})$  electric field, (b) molecule dipole emission.



The two components of the irradiance ( $F_{s,\parallel}, F_{s,\perp}$ ) at a distance  $d$  from the molecule in the plane perpendicular to  $\vec{s}$  can be expressed as:

$$\begin{cases} F_{s,\parallel} = \frac{c \varepsilon_0}{2} \cdot (E_{s,\parallel} E_{s,\parallel}^*) \\ F_{s,\perp} = \frac{c \varepsilon_0}{2} \cdot (E_{s,\perp} E_{s,\perp}^*) \end{cases} \quad (47)$$

This corresponds to the radiant flux density  $d^2\varphi_s(\theta, d\Omega)$  scattered within a solid angle  $d\Omega = 1/d^2$ .

Two scattering functions  $f_{\parallel}(\theta)$  and  $f_{\perp}(\theta)$  can then be deduced from Equations (6), (27), (40), (45), (46) and (47) for each of two polarization cases of the incident beam:

$$\begin{cases} f_{\parallel}(\theta) = \frac{k^4 \alpha^2}{16\pi^2 \varepsilon_0^2} \cdot \cos^2 \theta \\ f_{\perp}(\theta) = \frac{k^4 \alpha^2}{16\pi^2 \varepsilon_0^2} \end{cases} \quad (48)$$

For a natural (unpolarized) incident radiation the two components of  $\vec{E}$  are incoherent. Consequently the radiant amplitudes  $A_{\parallel}$  and  $A_{\perp}$  verify:

$$(A_{\parallel})^2 = (A_{\perp})^2 = \frac{A^2}{2} \quad (49)$$

According to Equation (48), the scattered radiation is then partially linearly polarized with a vibration perpendicular to the scattering plane. The radiant intensities (defined as  $d^2\phi(\theta, d\omega)/d\omega$ ) for each of the two polarization states ( $I_{\parallel}(\theta)$  and  $I_{\perp}(\theta)$ ) are expressed as:

$$\begin{cases} I_{\parallel}(\theta) = \frac{k^4 \alpha^2}{32\pi^2 \varepsilon_0^2} \cdot A^2 \cdot \cos^2 \theta \\ I_{\perp}(\theta) = \frac{k^4 \alpha^2}{32\pi^2 \varepsilon_0^2} \cdot A^2 \end{cases} \quad (50)$$

Thus, for the total radiant intensity (defined as  $I = I_{\parallel} + I_{\perp}$ ) the scattering function is expressed as:

$$f(\theta) = \frac{k^4 \alpha^2}{32\pi^2 \varepsilon_0^2} \cdot (1 + \cos^2 \theta) \quad (51)$$

The normalized molecular phase function  $p(\theta)$  can then be deduced from Eqs (8), (9), (10) and (51):

$$p(\theta) = \frac{3}{4} \cdot (1 + \cos^2 \theta) \quad (52)$$

## 2.8 MIE SCATTERING

The *Mie's* theory is based on the assumption that the aerosols and hydrosols can be considered as spherical particles. This allows one to compute the optical properties (extinction and scattering coefficients, and phase function) for a mixing of scattering particles using their physical characteristics (*i.e.*, their particle size distributions and their refractive indices).

The interaction of an electromagnetic wave with an absorbing sphere is fully described and expressed by the *Mie's* theory [RD-1]. The latter has been particularly detailed in [RD-7] and largely discussed by many other authors (*see* [RD-8], [RD-9], [RD-10], [RD-11], [RD-12], [RD-13] & [RD-14]). In this section, the basic equations used for the computation procedures of the *Mie's* scattering are outlined.

### 2.8.1 Mie theory

Let us consider  $\lambda$  the incident wavelength,  $r$  the radius of the scatterer (assumed to be a sphere),  $\kappa$  the *Mie's* parameter ( $\kappa = 2\pi r / \lambda$ ),  $n$  the complex refractive index ( $n = m - ik$ ), and  $\theta$  the scattering angle, two complex functions  $S_1(\kappa, n, \theta)$  and  $S_2(\kappa, n, \theta)$  related to the amplitude of the incident ( $E_{i,\parallel}, E_{i,\perp}$ ) and scattered ( $E_{s,\parallel}, E_{s,\perp}$ ) electric fields decomposed into parallel and perpendicular components are then derived from the *Maxwell's* equations as follows:

$$\begin{cases} S_1(\kappa, n, \theta) = \sum_{n=1}^{\infty} \frac{(2n+1)}{n(n+1)} \cdot [a_n(\kappa, n) \cdot \pi_n(\cos\theta) + b_n(\kappa, n) \cdot \tau_n(\cos\theta)] \\ S_2(\kappa, n, \theta) = \sum_{n=1}^{\infty} \frac{(2n+1)}{n(n+1)} \cdot [a_n(\kappa, n) \cdot \tau_n(\cos\theta) + b_n(\kappa, n) \cdot \pi_n(\cos\theta)] \end{cases} \quad (53)$$

where the complex functions  $a_n(\kappa, n)$  and  $b_n(\kappa, n)$ , which represent the contributions of oscillating electromagnetic dipoles to the scattered field, derive from the *Ricatti-Bessel* functions  $\psi_n(\kappa$  or  $n\kappa)$  and  $\xi_n(\kappa)$ . The functions  $\pi_n$  and  $\tau_n$ , which depend on the scattering angle  $\theta$  only, are related to the associated *Legendre* polynomials of the first kind  $P_n^1(\cos\theta)$ .

#### 2.8.1.1 Computation of complex functions ( $a_n, b_n$ )

The complex functions  $a_n(\kappa, n)$  and  $b_n(\kappa, n)$  are expressed as:

$$\begin{cases} a_n(\kappa, n) = \frac{\psi_n'(n\kappa) \cdot \psi_n(\kappa) - n \psi_n(n\kappa) \cdot \psi_n'(\kappa)}{\psi_n'(n\kappa) \cdot \xi_n(\kappa) - n \psi_n(n\kappa) \cdot \xi_n'(\kappa)} \\ b_n(\kappa, n) = \frac{n \psi_n'(n\kappa) \cdot \psi_n(\kappa) - \psi_n(n\kappa) \cdot \psi_n'(\kappa)}{n \psi_n'(n\kappa) \cdot \xi_n(\kappa) - \psi_n(n\kappa) \cdot \xi_n'(\kappa)} \end{cases} \quad (54)$$

where the prime denotes the derivative of the function with respect of the argument ( $\kappa$  or  $n\kappa$ ).

The *Ricatti-Bessel* functions  $\psi_n(z)$ ,  $\chi_n(z)$  and  $\xi_n(z)$  are given by:

$$\begin{cases} \psi_n(z) = \sqrt{(1/2) \cdot \pi z} \cdot J_{n+(1/2)}(z) = z \cdot j_n(z) \\ \chi_n(z) = -\sqrt{(1/2) \cdot \pi z} \cdot N_{n+(1/2)}(z) = -z \cdot n_n(z) \\ \xi_n(z) = \sqrt{(1/2) \cdot \pi z} \cdot H_{n+(1/2)}^{(2)}(z) = z \cdot h_n^{(2)}(z) = \psi_n(z) + i \chi_n(z) \end{cases} \quad (55)$$

where  $J_{n+(1/2)}(z)$ ,  $N_{n+(1/2)}(z)$  and  $H_{n+(1/2)}^{(2)}(z)$  are respectively the *Bessel* functions of first, second, and third kind, with the corresponding spherical *Bessel* functions  $j_n(z)$ ,  $n_n(z)$  and  $h_n^{(2)}(z)$ .  $N_{n+(1/2)}(z)$  is also called the *Neumann* functions and  $H_{n+(1/2)}^{(2)}(z)$  the half integral order *Hankel* function of the second kind.

In order to make the computational work more convenient, it is useful to introduce the logarithmic derivative of the *Ricatti-Bessel* functions ( [RD-8] and [RD-11]):

$$\begin{cases} D_n(z) = \frac{d}{dz} [\ln \psi_n(z)] \\ G_n(z) = \frac{d}{dz} [\ln \xi_n(z)] \end{cases} \quad (56)$$

The functions  $a_n(\kappa, n)$  and  $b_n(\kappa, n)$  can then be rewritten as:

$$\begin{cases} a_n(\kappa, n) = \frac{\psi_n(\kappa)}{\xi_n(\kappa)} \cdot \frac{D_n(n\kappa) - n D_n(\kappa)}{D_n(n\kappa) - n G_n(\kappa)} \\ b_n(\kappa, n) = \frac{\psi_n(\kappa)}{\xi_n(\kappa)} \cdot \frac{n D_n(n\kappa) - D_n(\kappa)}{n D_n(n\kappa) - G_n(\kappa)} \end{cases} \quad (57)$$

These expressions are now reduced to a ratio of *Ricatti-Bessel* functions involving real arguments and a ratio of  $D_n(\kappa$  or  $n\kappa)$  and  $G_n(\kappa)$  functions which are easily computable. Some examples of  $a_n(\kappa, n)$  and  $b_n(\kappa, n)$  values are depicted on [Figure 9](#) for  $n = 1.33 - i 0.001$  and two values of  $\kappa$ , 10 and 50 respectively which means  $r$  is around  $0.8 \mu m$  and  $4 \mu m$  respectively at the  $500 nm$  wavelength.

In order to save more computational time, the criterion defined by *Deirmendjian* (see [RD-9]) is then used:

"The computation of  $a_n(\kappa, n)$  and  $b_n(\kappa, n)$  is completed when  $(a_n a_n^* + b_n b_n^*) / n < 10^{-14}$  "

### 2.8.1.2 Computation of the Ricatti-Bessel function

The ratio of *Ricatti-Bessel* functions can be reduced to a ratio of spherical *Bessel* functions with a real argument  $x$  as follows:

$$\frac{\psi_n(\kappa)}{\xi_n(\kappa)} = \frac{j_n(x)}{h_n^{(2)}(x)} = \frac{j_n(x)}{j_n(x) - i n_n(x)} \quad (58)$$

The spherical *Bessel* functions  $j_n(x)$ ,  $n_n(x)$  and  $h_n^{(2)}(x)$  have different behaviors following they are below or above the transition line defined by  $x^2 = n(n+1)$ . Below the transition line ( $n(n+1) < x^2$ ), they behave as oscillating functions of both order and argument, whereas the behavior becomes monotonic above the transition line (*i.e.*, for  $n(n+1) > x^2$ ).

It has been shown by many authors that  $n_n(x)$  and  $h_n^{(2)}(x)$  can be processed using an upward recurrence whatever the values of  $n$  and  $x$ . Functions  $n_n(x)$  and  $j_n(x)$  are computed using the following relationship (see [Figure 10](#)):

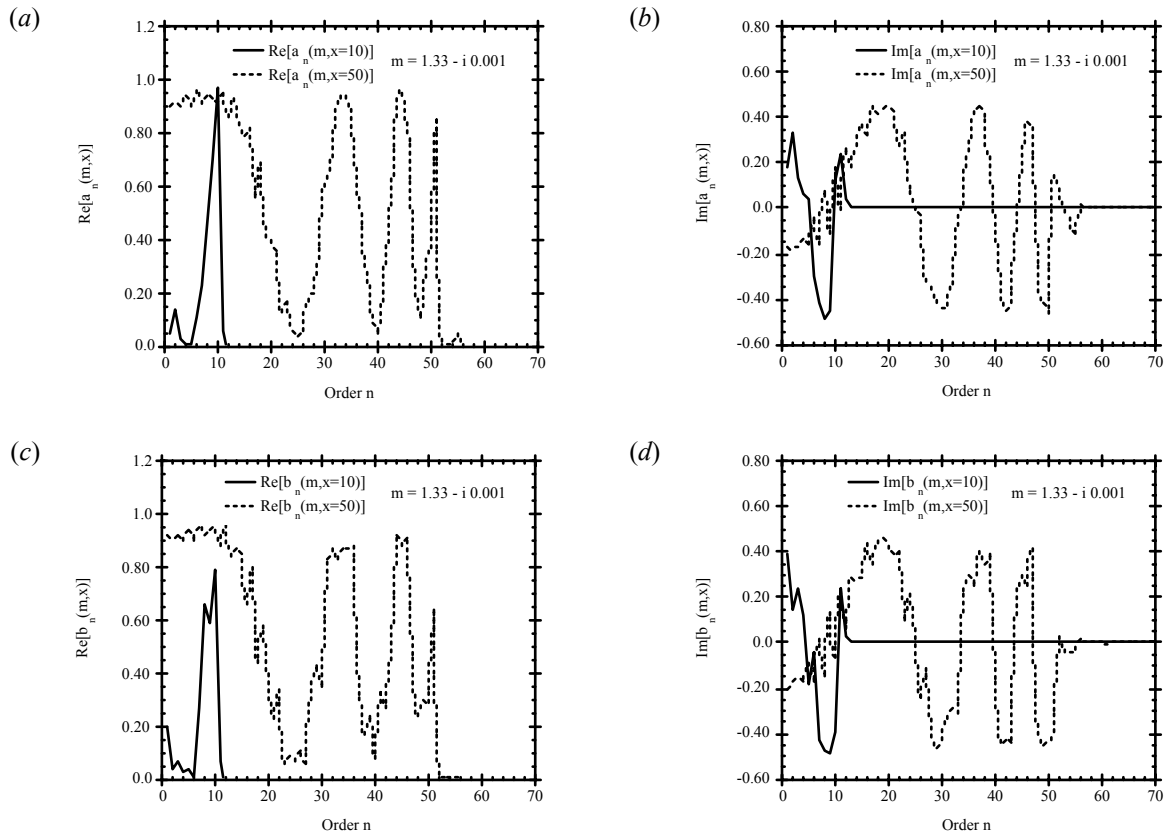


Figure 9: Samples of  $a_n(\kappa, n)$  and  $b_n(\kappa, n)$  curves computed for a refractive index  $n = 1.33 - i 0.001$  with  $\kappa = 10$  and  $\kappa = 50$ .

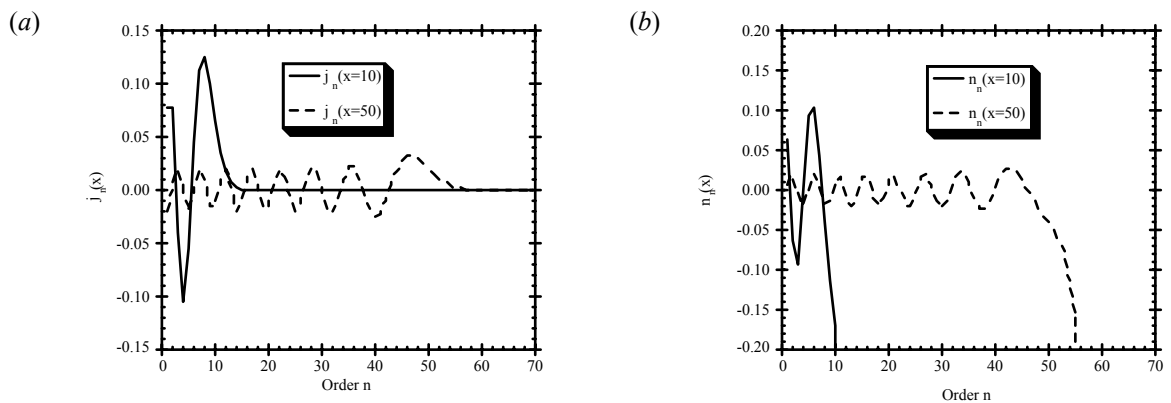


Figure 10: Samples of spherical Bessel functions, (a)  $j_n(x)$  and (b)  $n_n(x)$ , for  $\kappa = 10$  and  $\kappa = 50$ .

$$\begin{cases} n_{n+1}(x) = \frac{2n+1}{x} \cdot n_n(x) + n_{n-1}(x) \\ j_{n+1}(x) = \frac{2n+1}{x} \cdot j_n(x) + j_{n-1}(x) \end{cases} \quad (59)$$

with

$$\begin{cases} n_0(x) = -\frac{\cos x}{x} & \text{and} & n_1(x) = -\frac{\cos x}{x^2} - \frac{\sin x}{x} \\ j_0(x) = -\frac{\cos x}{x} & \text{and} & j_1(x) = -\frac{\cos x}{x^2} - \frac{\sin x}{x} \end{cases}$$

but as it is explained [RD-15], the function  $j_n(x)$  cannot be computed by an upward recurrence "since an upward recursion (except in the region of the  $x-n$  plane where  $j_n(x)$  oscillates) would bring about a rapid loss of accuracy". Then a downward recurrence is called for, but we have to define the starting value of  $n$ , and for that purpose we use the work of Corbato and Uretsky (see [RD-15]) which is summarized hereafter.

Let  $N$  be the starting order of the recursion with  $N(N+1) > x^2$ , they show in their paper that "rather than accurately evaluate  $j_N(x)$  and  $j_{N-1}(x)$  to start the process, a very approximately starting the recursion at a higher order will give a set of numbers which are accurately proportional to the  $j_n$  over the desired range of  $n$  from 0 to  $N$ ". Let  $\bar{j}_n$  be one of these numbers.

They propose to define the higher order  $\nu$  as follows:

$$\nu = N' - \frac{\ln \varepsilon_N}{\ln 2} \cdot \left[ A + \frac{B u' (2 - u'^2)}{2(1 - u'^2)} \right] \quad (60)$$

with  $A = 0.10$ ,  $B = 0.35$ ,  $\varepsilon_N = 2^{-30}$  (this value comes from the fact that generally computers can store floating numbers with a 30 binary digit mantissa), and  $u'$  defined as:

$$u' = \frac{2x}{(2N'+1)} \quad \text{with} \quad N' = N \text{ or } N' = x - \frac{1}{2} + \sqrt{-\frac{\ln \varepsilon_N}{\ln 2} \cdot B \cdot x}$$

such as  $\nu$  be the lower with however  $N' \geq N$ .

Note that in the SCAMAT module from RTC/UdL package,  $u'$  is defined as  $2n\kappa/(2N'+1)$  in order to better take the highest radii and the particular absorption into account.

To avoid computational difficulties above the transition line, Corbato and Uretsky worked with the ratio  $\bar{r}_n = \bar{j}_{n+1}/\bar{j}_n$  using the recurrence relation:

$$\bar{r}_{n-1}(x) = \frac{x}{2n+1-x\bar{r}_n(x)} \quad (61)$$

with the starting point  $\bar{r}_\nu = 0$ . The recurrence continues downward until a ratio  $\bar{r}_n$  which exceeds 1 is reached. Then, they set  $\bar{j}_{n+1} = \bar{r}_n$  and  $\bar{j}_n = 1$  and continue downward using the following recurrence relationship:

$$\bar{j}_{n-1}(x) = \frac{2n+1}{x} \cdot \bar{j}_n(x) + \bar{j}_{n+1}(x) \quad (62)$$

The positive number  $\bar{j}_n$  is defined as  $\bar{j}_n(x) = \alpha \cdot j_n(x)$  with  $\alpha$  a constant of proportionality derived from:

$$\alpha = [\bar{j}_0(x) - x \cdot \bar{j}_1(x)] \cdot \cos x + x \cdot \bar{j}_0(x) \cdot \sin x \quad (63)$$

### 2.8.1.3 Computation of functions ( $D_n, G_n$ )

As pointed out by *Kattawar and Plass* [RD-11], the computation of  $D_n(z)$  with an upward recurrence is unstable. A downward process is then needed and  $D_n(z)$  is defined as:

$$D_{n-1}(z) = \frac{n}{z} - \frac{1}{D_n(z) + (n/z)} \quad (64)$$

Calculations have to be started at an order  $n = v' \gg |z|$  with a starting point value of which is not crucial due to the fast convergence of the series towards the exact value. Consequently  $D_v(z) = 0$  is a convenient starting value. For  $n < |z|$ ,  $D_n(z)$  becomes oscillatory and there is then no problem for the computation in using the recurrence relation. For practical reasons,  $v' = v$  is selected as defined for  $j_n$ . The authors have also shown that  $G_n(x)$  can always be calculated using an upward process with a starting value  $G_0(x) = -i$  as follows:

$$G_n(x) = -\frac{n}{x} - \frac{1}{G_{n-1}(x) + (n/x)} \quad (65)$$

Some samples of  $D_n(n\kappa \text{ or } \kappa)$  and  $G_n(\kappa)$  are depicted on [Figure 11](#) for  $n = 1.33 - i 0.001$  and two values of  $\kappa$ , 10 and 50 respectively.

### 2.8.1.4 Computation of functions ( $\pi_n, \tau_n$ )

Functions  $\pi_n$  and  $\tau_n$  are related to the associated *Legendre* polynomials of the first kind  $P_n^1(\cos \theta)$ :

$$\begin{cases} \pi_n(\cos \theta) = \frac{1}{\sin \theta} \cdot P_n^1(\cos \theta) \\ \tau_n(\cos \theta) = \frac{d}{d\theta} [P_n^1(\cos \theta)] \end{cases} \quad (66)$$

and they are computed from the following upward recurrence relations:

$$\begin{cases} n \cdot \pi_{n+1}(\cos \theta) = (2n+1) \cdot \cos \theta \cdot \pi_n(\cos \theta) - (n+1) \cdot \pi_{n-1}(\cos \theta) \\ \tau_{n+1}(\cos \theta) = (n+1) \cdot \cos \theta \cdot \pi_{n+1}(\cos \theta) - (n+2) \cdot \pi_n(\cos \theta) \end{cases} \quad (67)$$

with the starting values  $\pi_0(\cos \theta) = 0$  and  $\pi_1(\cos \theta) = 1$ .

In [Figure 12](#) are displayed some examples of  $\pi_n(\cos \theta)$  and  $\tau_n(\cos \theta)$  for several  $n$  values (*i.e.*,  $n \in [1; 6]$ ) and a scattering angle  $\theta$  within  $[0^\circ; 90^\circ]$ .

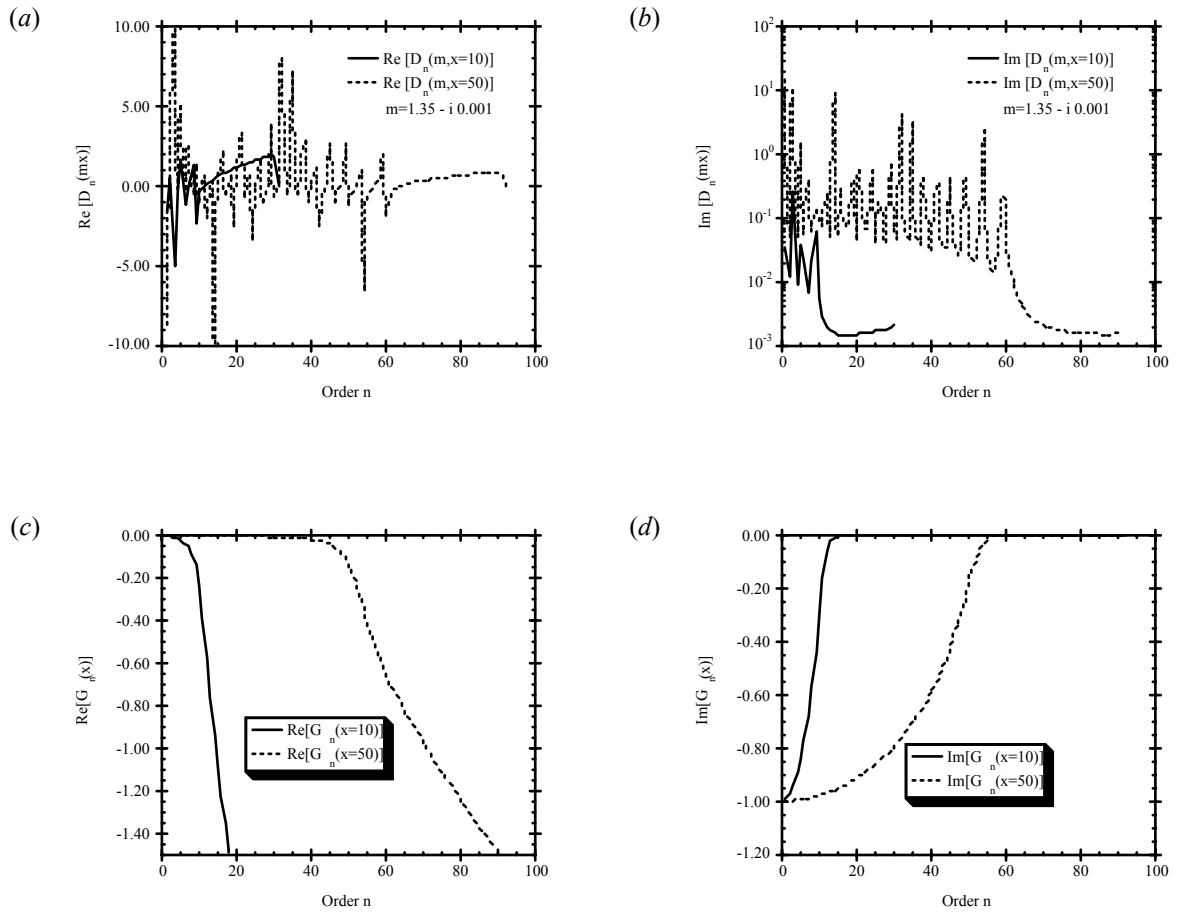


Figure 11: Samples of  $D_n(n\kappa \text{ or } \kappa)$  and  $G_n(\kappa)$  curves computed for a refractive index  $n = 1.33 - i 0.001$  with  $\kappa = 10$  and  $\kappa = 50$ .

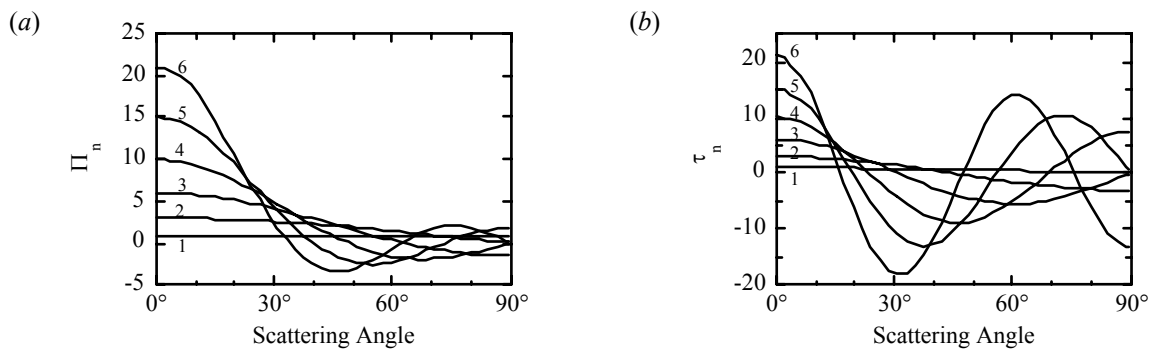


Figure 12: Samples of  $\pi_n(\theta)$  and  $\tau_n(\theta)$  functions for several  $n$  values ( $n$  varying from 1 to 6).

## 2.8.2 Optical properties

The continuity equations of the electric fields at the interface of the spherical particle allow one to compute the extinction, absorption and scattering efficiencies as well as the phase function of the sphere. The latter are expressed as infinite series which slowly converge.

- *Extinction cross section*  $Q_e$  : this parameter represents the amount of energy removed (scattered and absorbed) from the incident beam by the particle, and it can be computed by considering a point in the forward direction ( $\theta = 0$ ) in the far field. With the assumption of an isotropic homogeneous sphere the extinction cross section is expressed as,

$$Q_e(\lambda, r, n) = \frac{4\pi}{(2\pi/\lambda)^2} \cdot \Re_e[S(\kappa, n, \theta = 0)] \quad (68)$$

- *Extinction efficiency*  $k_e$  : this is defined as the ratio of the extinction cross section to the geometrical section of the spherical particle,

$$k_e(\lambda, r, n) = \frac{Q_e(\lambda, r, n)}{\pi r^2} = \frac{2}{\kappa^2} \cdot \sum_{n=1}^{\infty} (2n+1) \cdot \Re_e[a_n(\kappa, n) + b_n(\kappa, n)] \quad (69)$$

- *Scattering cross section*  $Q_s$  : similarly to the extinction cross section definition, but by considering only the scattered light in an arbitrary direction, this parameter is defined as,

$$Q_s(\lambda, r, n) = \frac{\pi}{(\kappa/r)^2} \cdot \int_0^{\pi} [S_1(\kappa, n, \theta) S_1^*(\kappa, n, \theta) + S_2(\kappa, n, \theta) S_2^*(\kappa, n, \theta)] \cdot \sin\theta \cdot d\theta \quad (70)$$

Owing of  $\pi_n$  and  $\tau_n$  functions, products of the associated *Legendre* polynomials must be integrated. Using the orthogonal and recurrence properties of these polynomials, the scattering cross section can be written as:

$$Q_s(\lambda, r, n) = \frac{2\pi}{(\kappa/r)^2} \cdot \sum_{n=1}^{\infty} (2n+1) \cdot [a_n(\kappa, n) a_n^*(\kappa, n) + b_n(\kappa, n) b_n^*(\kappa, n)] \quad (71)$$

where the asterisk denotes the complex conjugate value.

- *Scattering efficiency*  $k_s$  : this is determined by the scattering cross section to the geometrical section of the spherical particle ratio as follows,

$$k_s(\lambda, r, n) = \frac{Q_s(\lambda, r, n)}{\pi r^2} = \frac{2}{\kappa^2} \cdot \sum_{n=1}^{\infty} (2n+1) \cdot [a_n(\kappa, n) a_n^*(\kappa, n) + b_n(\kappa, n) b_n^*(\kappa, n)] \quad (72)$$

- *Absorption cross section*  $Q_a$  and *absorption efficiency*  $k_a$  : these two quantities can be directly deduced from  $Q_e$ ,  $Q_s$ ,  $k_e$  and  $k_s$  as follows,

$$Q_a(\lambda, r, n) = Q_e(\lambda, r, n) - Q_s(\lambda, r, n) \quad (73)$$

$$k_a(\lambda, r, n) = k_e(\lambda, r, n) - k_s(\lambda, r, n)$$

- Another useful quantity is the *asymmetry factor*  $g$  which is also the first moment of the phase function:



$$g = \int_{4\pi} P_{11}(\lambda, r, n, \theta) \cdot \sin\theta \cdot d\Omega$$

The asymmetry factor describes the shape of the phase function:  $g > 1$  indicates that forward scattering is favoured while  $g < 1$  means that the backscattering is favoured. It is a useful parameter for characterizing the phase function independent of the scattering angle. The *Mie's* asymmetry factor can be expressed as:

$$g = 2 \cdot \sum_{n=1}^{\infty} \frac{n(n+2)}{(n+1)} \cdot \Re_e[a_n(\kappa, n) \cdot a_{n+1}^*(\kappa, n) + b_n(\kappa, n) \cdot b_{n+1}^*(\kappa, n)] + \frac{2n+1}{n(n+1)} \cdot \Re_e[a_n(\kappa, n) + b_n^*(\kappa, n)]$$

### 2.8.3 Phase matrix

*Phase matrix*  $\mathbf{F}_p(\lambda, r, n, \theta)$ : for a scatterer (aerosol or droplet of cloud) assuming as an isotropic homogeneous sphere, the four independent elements of the phase matrix are computed as follows,

$$\left\{ \begin{array}{l} P_{11}(\lambda, r, n, \theta) = \frac{2\pi}{(\kappa/r)^2 \cdot Q_s(\lambda, r, n)} \cdot [S_1(\kappa, n, \theta) S_1^*(\kappa, n, \theta) + S_2(\kappa, n, \theta) S_2^*(\kappa, n, \theta)] \\ P_{12}(\lambda, r, n, \theta) = \frac{2\pi}{(\kappa/r)^2 \cdot Q_s(\lambda, r, n)} \cdot [S_2(\kappa, n, \theta) S_2^*(\kappa, n, \theta) - S_1(\kappa, n, \theta) S_1^*(\kappa, n, \theta)] \\ P_{33}(\lambda, r, n, \theta) = \frac{2\pi}{(\kappa/r)^2 \cdot Q_s(\lambda, r, n)} \cdot [S_2(\kappa, n, \theta) S_1^*(\kappa, n, \theta) + S_1(\kappa, n, \theta) S_2^*(\kappa, n, \theta)] \\ P_{34}(\lambda, r, n, \theta) = \frac{2\pi}{(\kappa/r)^2 \cdot Q_s(\lambda, r, n)} \cdot [S_2(\kappa, n, \theta) S_1^*(\kappa, n, \theta) - S_1(\kappa, n, \theta) S_2^*(\kappa, n, \theta)] \end{array} \right. \quad (74)$$

where  $S_1(\kappa, n, \theta)$  and  $S_2(\kappa, n, \theta)$  are the scattering functions described above.

Of course, each element of the phase matrix  $P_{ij}(\lambda, r, n, \theta)$  must verify:

$$\int_0^{2\pi} \int_0^\pi P_{ij}(\lambda, r, n, \theta) \cdot \sin\theta \cdot d\theta \cdot d\varphi = 4\pi \quad (75)$$

### 2.8.4 Forward scattering proportion

The forward scattering proportion ( $f_{sp}$ ) of a scatterer is computed using its phase function  $p(\theta)$ . The latter corresponds to the upper left element  $P_{11}(\theta)$  of the phase matrix  $\mathbf{F}_p(\theta)$ , and can be developed into a series of *Legendre* polynomials  $p_l(\mu = \cos\theta)$  as follows:

$$p(\theta) = \sum_{l=0}^L \beta_l p_l(\mu)$$

where the normalization of the phase function imposes  $\beta_0 = 1$  ( $\beta_l$  being the coefficients of the *Legendre* polynomials expansion). The order  $L$  of the development depends on the *Mie's* parameter ( $\kappa = 2\pi r / \lambda$ ). For large particles,  $L$  increases very fast mainly to represent the strong forward peak. A delta truncature is then applied on  $p(\theta)$  (see Section 2.3.2) and  $L$  is usually limited to 80.

Using the *Legendre* polynomials expansion of the phase function, the forward scattering proportion  $f_{sp}(\mu=0)$  is then computed as:

$$f_{sp}(\mu=0) = \frac{1}{2} \cdot \sum_{l=0}^L \left( \beta_l p_l(\mu=0) \cdot \sum_{i=1}^N w_i \cdot p_l(\mu_i) \right)$$

where  $N$  represents the total number of directions used in the *Gauss* quadrature to describe the angular variation of the phase function,  $\mu_i$  the cosine of *Gaussian* angle and  $w_i$  the associated weight.

## 2.9 GASEOUS ABSORPTION

The main absorbers in the MERIS spectral range are defined in [Table 2](#) and the transmittivity values are given for a *Mid-Latitude Summer* (MLS) atmospheric profile [\[RD-16\]](#). We have to account for the line absorption ( $H_2O$  and  $O_2$ ) with strong spectral variations as well as the continuum absorption ( $H_2O$  and  $O_3$ ) which have smooth spectral variations.

The absorption effects are accurately treated from the *correlated k-distribution* method [\[RD-18\]](#) to account for the interactions between the scattering and molecular absorption. The spectrally integrated transmission function  $T(u)$  for an homogeneous path, over the spectral interval  $\Delta\nu$  between  $\nu_1$  and  $\nu_2$ , can be written as:

$$T(u) = \frac{1}{\Delta\nu} \cdot \int_{\nu_1}^{\nu_2} e^{-k_\nu \cdot u} \cdot d\nu \quad (76)$$

with  $u$  the absorber amount and  $k_\nu$  the absorption coefficient. This transmission function becomes a transmission integral over the density distribution of absorption coefficient strengths:

$$T(u) = \int_0^{\infty} f(k) \cdot e^{-k \cdot u} \cdot dk \quad (77)$$

The function  $f(k)$  defines the fraction of the spectral interval  $\Delta\nu$  for which the absorption coefficient  $k_\nu$  is between  $k$  and  $k+dk$ . Likewise, the transmission integral over the inverse cumulative density distribution yields to:

$$T(u) = \int_0^1 e^{-k \cdot u} \cdot dg(k) \quad (78)$$

with  $g(k)$  the cumulative frequency distribution.  $T(u)$  can then be approximated by an exponential sum fitting technique (ESFT):

$$T(u) = \sum_{l=1}^N a_l \cdot e^{-k_l \cdot u} \quad \text{with } a_l = \int_{k_{l-1}}^{k_l} f(k) \cdot dk \quad (79)$$

The transmission formula in Equation (76) has the standard form of a *Laplace* transform. The probability density distribution of the absorption coefficient strengths  $f(k)$  can be formally identified as the *inverse Laplace* transform of the transmission function  $T(u)$ :

$$f(k) = L^{-1}(T(u)) \quad (80)$$

*Table 2: Rayleigh optical thickness ( $\tau^R$ ) for a barometric pressure of 1013.25hPa derived from [RD-13], ozone optical thickness ( $\tau^{O_3}$ ) derived from line-by-line computations using HITRAN-2000 and an amount of 1 cm-atm, and gaseous transmittivities in the 15 MERIS spectral bands computed with GAME and 6S for a MLS profile, a solar zenith angle of 45 degrees and a nadir viewing (extracted from [RD-17]).*

| Band | $\lambda(\text{nm})$ | $\Delta\lambda(\text{nm})$ | $\tau^{O_3}$           | $\tau^R$               | Absorbers  | $T_{H_2O}^{(\text{line})}$ | $T_{H_2O}^{(\text{line+cont.})}$ | $T_{O_2}$ | $T_{O_3}$ |
|------|----------------------|----------------------------|------------------------|------------------------|--|----------------------------|----------------------------------|-----------|-----------|
| 1    | 412.50               | 10                         | $2.1785 \cdot 10^{-4}$ | $3.1528 \cdot 10^{-1}$ | -  | 1.000                      | 1.000                            | 1.000     | 0.99983   |
| 2    | 442.50               | 10                         | $2.8136 \cdot 10^{-3}$ | $2.3591 \cdot 10^{-1}$ | O <sub>3</sub>                                   | 1.000                      | 1.000                            | 1.000     | 0.99783   |
| 3    | 490.00               | 10                         | $2.0057 \cdot 10^{-2}$ | $1.5516 \cdot 10^{-1}$ | O <sub>3</sub>                                   | 1.000                      | 1.000                            | 1.000     | 0.98462   |
| 4    | 510.00               | 10                         | $4.0809 \cdot 10^{-2}$ | $1.3171 \cdot 10^{-1}$ | H <sub>2</sub> O+O <sub>3</sub>                  | 0.993                      | 0.987                            | 1.000     | 0.96897   |
| 5    | 560.00               | 10                         | $1.0399 \cdot 10^{-1}$ | $8.9912 \cdot 10^{-2}$ | H <sub>2</sub> O*+O <sub>3</sub>                 | 1.000                      | 0.992                            | 1.000     | 0.92281   |
| 6    | 620.00               | 10                         | $1.0903 \cdot 10^{-1}$ | $5.9433 \cdot 10^{-2}$ | H <sub>2</sub> O*+O <sub>3</sub>                 | 1.000                      | 0.988                            | 1.000     | 0.91922   |
| 7    | 665.00               | 10                         | $5.0504 \cdot 10^{-2}$ | $4.4730 \cdot 10^{-2}$ | H <sub>2</sub> O+O <sub>3</sub>                  | 0.995                      | 0.981                            | 1.000     | 0.96173   |
| 8    | 681.25               | 7.5                        | $3.5258 \cdot 10^{-2}$ | $4.0562 \cdot 10^{-2}$ | H <sub>2</sub> O+O <sub>3</sub>                  | 0.998                      | 0.982                            | 1.000     | 0.97313   |
| 9    | 708.75               | 10                         | $1.8808 \cdot 10^{-2}$ | $3.4558 \cdot 10^{-2}$ | H <sub>2</sub> O+O <sub>3</sub>                  | 0.906                      | 0.888                            | 1.000     | 0.98558   |
| 10   | 753.75               | 7.5                        | $8.8966 \cdot 10^{-3}$ | $2.6944 \cdot 10^{-2}$ | H <sub>2</sub> O*+O <sub>3</sub>                 | 1.000                      | 0.978                            | 1.000     | 0.99315   |
| 11   | 761.875              | 3.75                       | $6.6342 \cdot 10^{-3}$ | $2.5802 \cdot 10^{-2}$ | H <sub>2</sub> O*+O <sub>2</sub> +O <sub>3</sub> | 1.000                      | 0.978                            | 0.380     | 0.99489   |
| 12   | 778.75               | 15                         | $7.6933 \cdot 10^{-3}$ | $2.3617 \cdot 10^{-2}$ | H <sub>2</sub> O*+O <sub>2</sub>                 | 1.000                      | 0.977                            | 0.994     | 0.99407   |
| 13   | 865.00               | 20                         | $2.1922 \cdot 10^{-3}$ | $1.5459 \cdot 10^{-2}$ | H <sub>2</sub> O*                                | 1.000                      | 0.970                            | 1.000     | 0.99831   |
| 14   | 885.00               | 10                         | $1.2107 \cdot 10^{-3}$ | $1.4099 \cdot 10^{-2}$ | H <sub>2</sub> O                                 | 0.945                      | 0.911                            | 1.000     | 0.99907   |
| 15   | 900.00               | 10                         | $1.5167 \cdot 10^{-3}$ | $1.3176 \cdot 10^{-2}$ | H <sub>2</sub> O                                 | 0.647                      | 0.601                            | 1.000     | 0.99883   |

*H<sub>2</sub>O\* denotes the water vapor continuum absorption only.*

*O<sub>3</sub> transmittivity ( $T_{O_3}$ ) is computed with an ozone amount of 0.32 cm-atm.*

Band models provide convenient analytical expressions for computing the transmission function. In so far as the *Malkmus* band model [RD-19] uses an inverse *Laplace* transform, this is particularly well mathematically suited for the computation of this transmission function:

$$T(u) = \exp \left[ -\frac{B}{2} \cdot \left( \sqrt{1 + \frac{4Su}{B}} - 1 \right) \right] \quad (81)$$

which depends on the two parameters  $B$  and  $S$  defined as:

$$B = \frac{4}{\Delta\nu} \cdot \frac{\left( \sum_{j=1}^{N_0} \sqrt{S_j(T) \cdot \alpha_j(P, T)} \right)^2}{\sum_{j=1}^{N_0} S_j(T)} ; S = \frac{1}{\Delta\nu} \cdot \sum_{j=1}^{N_0} S_j(T) \quad (82)$$

where  $N_0$  is the total line number in the frequency interval  $\Delta\nu$ , and  $\alpha_j$  and  $S_j$  respectively the *Lorentz* half width ( $\text{cm}^{-1}$ ) and the strength ( $\text{cm}^{-1} / (\text{molec. cm}^{-2})$ ) of the  $j^{\text{th}}$  spectral line. These values can be directly retrieved from a spectroscopic database with the reference conditions.

$B$  and  $S$  depend on temperature  $T$  and pressure  $P$ . In practice, these parameters are computed using a spectroscopic database for a limited set of temperatures and a standard pressure  $P_0$ . The determination of  $S$  is performed through interpolations according to the temperature of the atmospheric model used for calculations. Assuming that  $B(P)$  varies with the pressure according to a *Lorentz* dependence, it can then be accounted for the half width  $\alpha_j$  of the line as follows:

$$B(P) = B(P_0) \cdot \frac{P}{P_0} \cdot \left( \frac{T_0}{T} \right)^n \quad (83)$$

where  $B(P_0)$  is the reference value for the standard pressure  $P_0$ , and  $T_0$  the standard temperature.

For the case of the stratosphere, this approximation can certainly lead to some errors due to the fact that the shape of absorption lines follows a *Voigt* profile (*i.e.*, the width of a spectral line corresponds to the convolution product of the *Lorentz* and *Doppler* shapes).

Note that both for the two radiative transfer codes (RTCs) used to generate the MERIS LUTs for the level-2 processing [AD-3], the parameters  $B$  and  $S$  are derived from the HITRAN-2000 spectroscopic database [RD-20]. Moreover, in the troposphere typical errors are in the order of 10-20% using the *Malkmus* band model with the line data [RD-18]. These errors are only due to the use of the spectroscopic database, and can be minimized by using line-by-line (LBL) calculations. The LBL model allows one to perform accurate computations of absorption with a very high spectral resolution ( $\sim 10^{-7} \mu m$ ), accounting for the line shape from the spectroscopic database. Thus,  $B$  and  $S$  are estimated by least-squares fitting the MERIS band model with a LBL model [RD-21] and the HITRAN-2000 database. Water vapor absorption is included in the calculations from the parameterization developed in [RD-22].

In practice, transmittivities are computed for a standard pressure with a limited set of temperatures and realistic absorber amounts. From these results, the parameters  $B$  and  $S$  are estimated by least-squares fitting the band model. Pressure and temperature variations are taken into account through interpolations for which the line shape is assumed to be *Lorentzian*.

The continuum for  $O_3$  absorption is also considered in the transmittivity computations. Data derive from the *correlated k-distribution* algorithm (see [RD-23] for more details) including continuum for all the major atmospheric gases. By considering that the maximum of  $O_3$  absorption occurs in the stratosphere, interactions between  $O_3$  and other atmospheric constituents can be neglected in the computations. This assumption leads to the following satellite reflectance ( $\rho^*$ ):

$$\rho^* \approx \rho_{na} \cdot T_{O_3} \quad (84)$$

where  $\rho_{na}$  is the satellite signal without any gaseous absorption and  $T_{O_3}$  the ozone transmittivity. The latter is expressed as a function of the total ozone content  $U_{O_3}$  ( $cm - atm$ ) and the airmass ( $M$ ):

$$T_{O_3} = \exp(-U_{O_3} \cdot M \cdot \tau^{O_3}) \quad (85)$$

with pre-computed values of  $\tau^{O_3}$  coefficients for the ozone absorption [RD-24].

## 2.10 FRESNEL LAWS

The *Snellius-Fresnel* laws are used to describe the interaction of the incident electric field at the boundary conditions through the *air-water* interface (Figure 13). Assuming a flat surface, the reflection and

transmission coefficients of the amplitude of the incident electric field in the parallel ( $r_{//}, t_{//}$ ) and perpendicular ( $r_{\perp}, t_{\perp}$ ) directions to the incidence plane are given by *Fresnel* formulas:

$$\left\{ \begin{array}{l} r_{\perp} = -\frac{\sin(\vartheta_a - \vartheta_w)}{\sin(\vartheta_a + \vartheta_w)} ; t_{\perp} = \frac{2 \cos \vartheta_a \cdot \sin \vartheta_w}{\sin(\vartheta_a + \vartheta_w)} \\ r_{//} = -\frac{\tan(\vartheta_a - \vartheta_w)}{\tan(\vartheta_a + \vartheta_w)} ; t_{//} = \frac{2 \cos \vartheta_a \cdot \sin \vartheta_w}{\sin(\vartheta_a + \vartheta_w) \cdot \cos(\vartheta_a - \vartheta_w)} \end{array} \right. \quad (86)$$

where  $\vartheta_a$  and  $\vartheta_w$  are the zenithal angles in the air and the water respectively.

The *Snellius* law of the refraction relates the directions of light propagation at both sides of the dielectric interface:

$$n_a \cdot \sin(\vartheta_a) = n_w \cdot \sin(\vartheta_w) \quad (87)$$

where  $n_a$  and  $n_w$  are respectively the refractive index of the air and the water.

The radiation which propagates into the direction of an optically less dense medium (*i.e.*, from water to air) will be totally reflected at the interface for the incident angles larger than the critical angle  $\vartheta_c$  defined as:

$$\vartheta_c = \arcsin(n_a / n_w)$$

The reflection matrix ( $R$ ) on the water surface and the transmission matrix ( $T$ ) from air to water are derived from Equations (86) and (87):

$$\left\{ \begin{array}{l} R = \frac{1}{2} \cdot \begin{pmatrix} r_{//}^2 + r_{\perp}^2 & r_{//}^2 - r_{\perp}^2 & 0 \\ r_{//}^2 - r_{\perp}^2 & r_{//}^2 + r_{\perp}^2 & 0 \\ 0 & 0 & 2 r_{\perp} \cdot r_{//} \end{pmatrix} \\ T = \frac{1}{2} \cdot \frac{n_w \cdot \cos \theta_w}{\cos \theta_a} \cdot \begin{pmatrix} t_{//}^2 + t_{\perp}^2 & t_{//}^2 - t_{\perp}^2 & 0 \\ t_{//}^2 - t_{\perp}^2 & t_{//}^2 + t_{\perp}^2 & 0 \\ 0 & 0 & 2 t_{\perp} \cdot t_{//} \end{pmatrix} \end{array} \right. \quad (88)$$

Thus, a part of the incident atmospheric (*resp.*, oceanic) radiance  $L_a(\mu_a, \varphi)$  (*resp.*,  $L_w(\mu_w, \varphi)$ ) will be reflected at the *air-sea* interface, and the other transmitted through this interface. The refracted radiance in the water (optically more denser) will be increased due to the fact that photons are concentrated into a smaller solid angle. Using the energetic conservation considerations, these boundary conditions for an incident atmospheric radiance on the *air-sea* interface will be expressed as:

$$\left\{ \begin{array}{l} L_a(-\mu_a, \varphi) = R(\mu_a, n_w / n_a) \cdot L_a(\mu_a, \varphi) \\ L_w(\mu_w, \varphi) = \left(\frac{n_w}{n_a}\right)^2 \cdot T(\mu_a, n_w / n_a) \cdot L_a(\mu_a, \varphi) \end{array} \right. \quad (89)$$

with  $\mu_a$  and  $\mu_w$  the cosine of zenithal angles in the air and the water respectively, and  $-\mu_a$  denotes the upwelling atmospheric radiance.

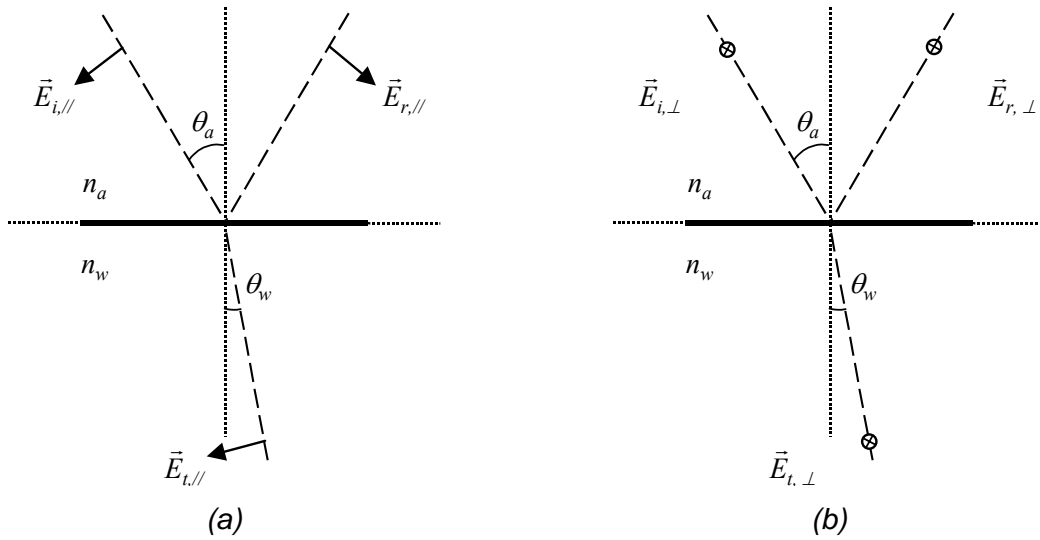


*Figure 13: Reflexion and transmission of the incident electric field  $\vec{E}_i$  through the air-water interface characterized by their refractive index, respectively  $n_a$  and  $n_w$ : (a) for the parallel component of the electric field ( $\vec{E}_{i,||}, \vec{E}_{r,||}, \vec{E}_{t,||}$ ), and (b) for the perpendicular component of the electric field ( $\vec{E}_{i,\perp}, \vec{E}_{r,\perp}, \vec{E}_{t,\perp}$ ). Subscripts  $i$ ,  $r$  and  $t$  stand for incidence, reflection and transmission.*

### 3. ATMOSPHERIC OPTICAL PROPERTIES

The atmosphere is considered as composed of air (molecular scattering:  $N_2$ ,  $O_2$ ,  $Ar$ ), gases (mainly  $H_2O$ ,  $O_2$  and  $O_3$  absorption), aerosols and clouds (scattering and absorption). All other atmospheric constituents are neglected.

#### 3.1 DRY AIR (MOLECULAR ATMOSPHERE)

##### 3.1.1 Inherent optical properties

###### 3.1.1.1 Scattering coefficient

The scattering coefficient  $\sigma_s$  of the dry air medium is given by (see Section 2.7):

$$\sigma_s = N \cdot Q_s^{mol} = N \cdot \frac{k^4 \alpha^2}{6\pi \epsilon_0^2} \quad (90)$$

According to the *Lorentz* model, the general expression relying the total polarisability  $\alpha$  and the dielectric constant for the medium is expressed as,

$$\alpha \cdot N = 3 \epsilon_0 \cdot \frac{n^2 - 1}{n^2 + 2} \quad (91)$$

with  $n$  the refractive index of the gas which contains  $N$  molecules per volume unit.

By substituting Equation (91) into (90) with  $k = 2\pi/\lambda$ , the scattering coefficient of the dry air medium becomes:

$$\sigma_s = \frac{24 \pi^3}{\lambda^4} \cdot \left( \frac{n^2 - 1}{n^2 + 2} \right)^2 \cdot \frac{1}{N} \quad (92)$$

It is more convenient to introduce the refractive index in standard temperature and pressure (STP) conditions. This yields to:

$$\sigma_s = \frac{24 \pi^3}{\lambda^4} \cdot \left( \frac{n_a^2 - 1}{n_a^2 + 2} \right)^2 \cdot \frac{N}{N_0} \quad (93)$$

where  $n_a$  is the air refractive index and  $N_0$  the molecular density in STP conditions (*i.e.*,  $N_0 = 2.54143 \cdot 10^{19}$ ).

Now, the consideration of the molecular anisotropy needs to introduce a molecular depolarization factor  $\delta$  in Equation (93) to correct the expression of the scattering coefficient of the dry air medium:

$$\sigma_s = \frac{24 \pi^3}{\lambda^{4.05}} \cdot \left( \frac{n_a^2 - 1}{n_a^2 + 2} \right)^2 \cdot \left( \frac{6 + 3 \delta}{6 - 7 \delta} \right) \cdot \frac{N}{N_0} \quad (94)$$

Because of small variations of  $n_a$  with  $\lambda$ ,  $\sigma_s$  varies as  $\lambda^{-4.05}$ .

In fact, the spectral dependence of the air refractive index ( $n_a$ ) is given by [RD-25]:

$$n_a = 1 + \left( \frac{5791817}{238.0185 - \frac{1}{\lambda^2}} + \frac{167909}{57.362 - \frac{1}{\lambda^2}} \right) \cdot 10^{-8} \quad (95)$$

where the wavelength  $\lambda$  is expressed as  $nm$ .

The molecular depolarization factor  $\delta$  can be estimated as a polynomial function of  $\lambda$  ( $nm$ ) according to [RD-26]:

$$\delta = 0.033133 - 1.215 \cdot 10^{-5} \lambda + 6.3069 \cdot 10^{-9} \lambda^2 \quad (96)$$

In practice, the molecular density is computed with a pressure ( $P$ ) and temperature ( $T$ ) profile as:

$$N = \frac{N_A}{R} \cdot \frac{P}{T} \quad (97)$$

where  $N_A$  is the *Avogadro* number ( $6.022 \cdot 10^{23} \text{ mole}^{-1}$ ) and  $R_g$  the gas constant ( $8.31 \text{ J K}^{-1} \text{ mole}^{-1}$ ).

Thus, the scattering coefficient  $\sigma_s$  of the dry air medium is computed as:

$$\sigma_s = \frac{24 \pi^3}{\lambda^{4.05}} \cdot \left( \frac{n_a^2 - 1}{n_a^2 + 2} \right)^2 \cdot \left( \frac{6 + 3\delta}{6 - 7\delta} \right) \cdot \frac{R_g}{N_A} \cdot \frac{T_0^2}{P_0^2} \cdot \frac{P}{T} \quad (98)$$

### 3.1.1.2 Scattering phase function

By taking the molecular anisotropy into account, the *Rayleigh* scattering phase function  $P(\theta)$  is expressed as:

$$P(\theta) = \frac{3}{2(2+\delta)} \cdot \left[ (1-\delta) \cdot \cos^2 \theta + (1+\delta) \right] \quad (99)$$

or

$$P(\theta) = \frac{3}{4(1+2\gamma)} \cdot \left[ (1-\gamma) \cdot \cos^2 \theta + (1+3\gamma) \right] \quad \text{with} \quad \gamma = \frac{\delta}{2-\delta} \quad (100)$$

with  $\delta$  the molecular depolarization factor.

Note that both in the two RTCs (FUB & LISE/UdL),  $\delta$  is taken to be equal to 0.0279 (see [RD-27]) in the atmosphere and 0.0906 in the water ocean whatever the wavelength.

## 3.1.2 Vertical distribution

### 3.1.2.1 Molecular scale height

The molecular scale height ( $H_m$ ) represents the vertical distance upwards, over which the atmospheric pressure decreases by a factor of  $e$ . The latter remains constant for a particular temperature and can be computed as:



$$H_m = \frac{k \cdot T}{M \cdot g},$$

with:

$k$  the *Boltzmann's* constant ( $1.38 \cdot 10^{-23} \text{ J.K}^{-1}$ )

$T$  the mean surface temperature (K),

$M$  the mean molecular mass of dry air (kg),

$g$  the acceleration due to the gravity on the *Earth's* surface ( $\text{m/s}^2$ )

In the atmosphere the pressure is the force per unit area exerted against a surface by the weight of air above that surface. In most circumstances, this is closely approximated by the hydrostatic pressure caused by the weight of air above the measurement point. Low pressure areas have less atmospheric mass above their location, whereas high pressure areas have more atmospheric mass above their location. Similarly, as elevation increases there is less overlying atmospheric mass, so that pressure decreases with increasing elevation. Consequently, if at a given altitude ( $z$ ) the atmosphere has an air density ( $\rho$ ) and a pressure ( $P$ ), then moving upwards at an infinitesimally small height  $dz$  will decrease the pressure by an amount of  $dP$ , equal to the weight of a layer of atmosphere of thickness  $dz$ :

$$\frac{dP}{dz} = -g \cdot \rho.$$

For small  $dz$  it is possible to assume  $g$  to be constant. Therefore, by using the equation of state for an ideal gas of mean molecular mass  $M$  at temperature  $T$ , the density can be expressed as:

$$\rho = \frac{M \cdot P}{k \cdot T}.$$

This yields to:

$$\frac{dP}{P} = -\frac{M \cdot g}{k \cdot T} \cdot dz,$$

which can then be expressed as function of the molecular scale height ( $H_m$ ) as follows:

$$\frac{dP}{P} = -\frac{dz}{H_m}.$$

This will not change unless the temperature does. By assuming that  $P_0$  corresponds to the surface pressure at the sea level ( $z=0$ ), then the pressure  $P(z)$  at any altitude  $z$  can be determined with a decreasing exponential as:

$$P(z) = P_0 \cdot \exp(-z / H_m).$$

In the *Earth's* atmosphere, the surface pressure at the sea level ( $P_0$ ) averages about 1013.25 hPa, with a mean mass of dry air ( $M$ ) of  $4.808 \cdot 10^{-26} \text{ kg}$  and  $g=9.81 \text{ m/s}^2$ . As a function of temperature the molecular scale height ( $H_m$ ) is therefore around 29.26 m/K, yielding to these tabulated  $H_m$  values for representative air temperatures ( $T$ ) at surface level.

| $T$ (K) | $H_m$ (m) |
|---------|-----------|
| 290     | 8500      |
| 273     | 8000      |
| 260     | 7610      |
| 210     | 6000      |

- Notes:** 1. The air density is related to the pressure by the law of ideal gases. Therefore, with some departures caused by varying temperature density will also decrease exponentially with height from a sea level value of  $\rho_0$  roughly equal to  $1.2 \text{ kg/m}^3$ .
2. At altitudes over  $100 \text{ km}$ , the atmospheric scattering means that each molecular atomic species has its own scale height.

### 3.1.2.2 Vertical profile

About 80-85% of the atmospheric mass is located in the troposphere. The three major constituents are the nitrogen ( $N_2=75\%$ ), the oxygen ( $O_2=23\%$ ) and the argon ( $Ar=1.3\%$ ). Assuming the average vertical equilibrium of the atmosphere as hydrostatic, the vertical distribution follows an exponential law with a molecular scale height  $H_m$  of about  $8 \text{ km}$  :

$$\sigma_s(z) = \sigma_s(0) \cdot e^{-z/H_m} \quad (101)$$

The *Rayleigh* (or molecular) optical thickness  $\tau^R$  is then expressed as:

$$\tau^R = \int_0^{\infty} \sigma_s(z) \cdot dz \quad (102)$$

For the MERIS LUTs generation,  $\tau^R$  is estimated with the formula from [RD-13]:

$$\tau^R = \frac{P_s}{P_0} \cdot \left[ 8.524 \cdot 10^{-3} \cdot \lambda^{-4} + 9.63 \cdot 10^{-5} \cdot \lambda^{-6} + 1.1 \cdot 10^{-6} \cdot \lambda^{-8} \right] \quad (103)$$

where  $P_s$  is the surface pressure ( $hPa$ ),  $P_0$  the pressure in the STP conditions, and  $\lambda$  the wavelength expressed as  $\mu m$ .

## 3.2 AEROSOLS

### 3.2.1 Inherent optical properties

The *Mie's* theory presented in Section 2.8 allows one to compute the inherent optical properties (IOPs) of a spherical particle characterized by its complex refractive index  $n$  (*i.e.*,  $n = m - ik$ ) and its geometrical radius  $r$ .

#### 3.2.1.1 Sample of identical particles

Let us consider in the atmosphere a simple aerosol model composed of a uniuquetype of particles for which the particle size distribution is characterized by  $n(r)$  expressed as  $cm^{-3} \mu m^{-1}$  such as:

$$\int_0^{\infty} n(r) \cdot dr = \int_0^{\infty} \frac{dN(r)}{dr} \cdot dr = 1 \quad (104)$$

where  $dN(r)$  represents the number of particles per volume unit with a radius between  $r$  and  $r + dr$ .

Assuming the particles are sufficiently far from each other compared with the wavelength of the incident electromagnetic wave in order to consider only one scattering, it is then possible to add scattered

intensities independently of the wave phase. Thus, the radiative characteristics upon the particle size distribution can be defined:

- *Extinction, scattering and absorption coefficients*

The extinction ( $e$ ), scattering ( $s$ ) and absorption ( $a$ ) coefficients of this simple aerosol model are then defined as:

$$\sigma_{e,s,a}(\lambda, m) = \int_{r_{\min}}^{r_{\max}} k_{e,s,a}(\lambda, r, m) \cdot \pi r^2 \cdot \frac{dN(r)}{dr} \cdot dr \quad (105)$$

with the single scattering albedo:  $\omega_0(\lambda, m) = \frac{\sigma_s(\lambda, m)}{\sigma_e(\lambda, m)}$

- *Scattering phase function*

By including Equation (105) into (36) the normalized scattering phase function  $P(\lambda, m, \theta)$  for the sample of identical particles characterized by its size distribution  $n(r)$  is given by:

$$P(\lambda, m, \theta) = \frac{1}{\sigma_s(\lambda, m)} \cdot \int_{r_{\min}}^{r_{\max}} P_{11}(\lambda, r, m, \theta) \cdot 4\pi r^2 \cdot \frac{dN(r)}{dr} \cdot dr \quad (106)$$

Computationally,  $\sigma_{e,s,a}(\lambda, m)$  and  $P(\lambda, m, \theta)$  are integrated step by step as follows:

$$\sigma_{e,s,a}(\lambda, m) = \sum_{r_{\min}}^{r_{\max}} k_{e,s,a}(\lambda, r, m) \cdot \pi r^2 \cdot \frac{dN(r)}{dr} \cdot \Delta r \quad (107)$$

and

$$P(\lambda, m, \theta) = \frac{1}{k_s(\lambda, m)} \cdot \sum_{r_{\min}}^{r_{\max}} P_{11}(\lambda, r, m, \theta) \cdot 4\pi r^2 \cdot \frac{dN(r)}{dr} \cdot \Delta r \quad (108)$$

where  $\Delta r$  is the particle size increment.

The  $\Delta r$  value of 0.001 is recommended in order to preserve a good accuracy with a reasonable computational time. For example *D'Almeida* used a very small step width 0.011 for the computations (see [RD-28]).

### 3.2.1.2 Mixing of different particles

For an atmosphere with a mixing of aerosols originating from  $N$  different sources, IOPs are computed as previously (*i.e.*, for a simple aerosol model) by introducing the percentage density of particles ( $n_i/n$ ) for each type  $i$  of aerosols. The mixing of individual components (or type) of an aerosol is then characterized by its own size distribution  $n_i(r)$  (then by its microphysical identity:  $r_{M_i}$  and  $\sigma_i$  see Table 3 and Table 4 for some examples) and its own complex refractive index  $m_i$  (Table 5). For the size distribution the *Log-Normal* is well adapted to emphasize the individual components of a mixture (see [RD-28] & [RD-29]).

The scattering phase matrix  $P(\lambda, \theta)$  of a typical aerosol mixing is computed as the sum of each independant phase matrix  $P(\lambda, m_i, \theta)$  for each constituent  $i$  weighted by its volume percentage  $n_i/n$  (or component mixing ratio) and its scattering coefficient  $\sigma_s(\lambda, m_i)$  :

$$P(\lambda, \theta) = \frac{N_p}{\sigma_s(\lambda, m)} \cdot \sum_{i=1}^N \frac{n_i}{n} \cdot P(\lambda, m_i, \theta) \cdot \sigma_s(\lambda, m_i) \quad (109)$$

with

$$N_p = \frac{1}{\sum_{i=1}^N \frac{n_i}{n} \cdot \sigma_e(550, m_i)} \quad \text{and} \quad \sigma_s(\lambda, m) = \sum_{i=1}^N \frac{n_i}{n} \cdot \sigma_s(\lambda, m_i) \quad (110)$$

where  $N_p$  is the equivalent number of particles,  $\sigma_s(\lambda, m)$  the scattering coefficient of the mixing, and  $\sigma_e(550, m_i)$  the extinction coefficient of the constituent  $i$  at 550 nm wavelength.

### 3.2.1.3 Convergence criterion

In order to save computational time the following criterion on the summation is commonly used:

$$\frac{n_i}{n} \cdot \pi r^2 \cdot \frac{dN(r)}{dr} \cdot \Delta r < \sqrt{\lambda} \cdot 10^{-8} \quad (111)$$

where  $n_i/n$  is the percentage density of particles.

*Table 3: Microphysical characteristics of the aerosol types (dry particles) from WCRP-1986 [RD-34].*

| Parameters            | Oceanic (RH=90%) | Water soluble | Dust-Like | Soot-like |
|-----------------------|------------------|---------------|-----------|-----------|
| $r_{M_i}$ ( $\mu m$ ) | 0.3803           | 0.0050        | 0.5000    | 0.0118    |
| $\sigma_i$            | 2.5119           | 2.9900        | 2.9900    | 2.0000    |

*Table 4: Percentage density of particles from WCRP-1986 [RD-34].*

| Aer. Model  | Oceanic (RH=90%)  | Water soluble | Dust-Like         | Soot-like |
|-------------|-------------------|---------------|-------------------|-----------|
| Continental | -                 | 0.938299      | 2.26490 $10^{-6}$ | 0.0616987 |
| Maritime    | 4.20823 $10^{-4}$ | 0.999579      | -                 | -         |
| Urban       | -                 | 0.592507      | 1.65125 $10^{-7}$ | 0.4074920 |

*Table 5: Complex refractive indices of the aerosol types (dry particles) from WCRP-1986 [RD-34].*

| $\lambda$ ( $\mu m$ ) | Oceanic (RH=90%) |                | Water soluble |                | Dust-Like |                | Soot-like |       |
|-----------------------|------------------|----------------|---------------|----------------|-----------|----------------|-----------|-------|
|                       | $m$              | $k$            | $m$           | $k$            | $m$       | $k$            | $m$       | $k$   |
| 0.400                 | 1.385            | 9.90 $10^{-9}$ | 1.530         | 5.00 $10^{-3}$ | 1.530     | 8.00 $10^{-3}$ | 1.750     | 0.460 |
| 0.488                 | 1.382            | 6.41 $10^{-9}$ | 1.530         | 5.00 $10^{-3}$ | 1.530     | 8.00 $10^{-3}$ | 1.750     | 0.450 |
| 0.515                 | 1.381            | 3.70 $10^{-9}$ | 1.530         | 5.00 $10^{-3}$ | 1.530     | 8.00 $10^{-3}$ | 1.750     | 0.450 |
| 0.550                 | 1.381            | 4.26 $10^{-9}$ | 1.530         | 6.00 $10^{-3}$ | 1.530     | 8.00 $10^{-3}$ | 1.750     | 0.440 |
| 0.633                 | 1.377            | 1.62 $10^{-8}$ | 1.530         | 6.00 $10^{-3}$ | 1.530     | 8.00 $10^{-3}$ | 1.750     | 0.430 |
| 0.694                 | 1.376            | 5.04 $10^{-8}$ | 1.530         | 7.00 $10^{-3}$ | 1.530     | 8.00 $10^{-3}$ | 1.750     | 0.430 |

| $\lambda$ ( $\mu\text{m}$ ) | Oceanic (RH=90%) |                      | Water soluble |                      | Dust-Like |                      | Soot-like |       |
|-----------------------------|------------------|----------------------|---------------|----------------------|-----------|----------------------|-----------|-------|
|                             | $m$              | $k$                  | $m$           | $k$                  | $m$       | $k$                  | $m$       | $k$   |
| 0.860                       | 1.372            | $1.09 \cdot 10^{-6}$ | 1.520         | $1.20 \cdot 10^{-2}$ | 1.520     | $8.00 \cdot 10^{-3}$ | 1.750     | 0.430 |
| 1.536                       | 1.359            | $2.43 \cdot 10^{-4}$ | 1.510         | $2.30 \cdot 10^{-2}$ | 1.400     | $8.00 \cdot 10^{-3}$ | 1.770     | 0.460 |
| 2.250                       | 1.334            | $8.50 \cdot 10^{-4}$ | 1.420         | $1.00 \cdot 10^{-2}$ | 1.220     | $9.00 \cdot 10^{-3}$ | 1.810     | 0.500 |
| 3.750                       | 1.398            | $2.90 \cdot 10^{-3}$ | 1.452         | $4.00 \cdot 10^{-3}$ | 1.270     | $1.10 \cdot 10^{-2}$ | 1.900     | 0.570 |

### 3.2.2 Particle size distribution

Three models of aerosol size distribution are proposed hereafter:

- a *Junge power-law* function (see [RD-30]) for the size distributions the radii ( $r$ ) of which are larger than  $0.1 \mu\text{m}$  described by,

$$\frac{dN(r)}{d \log r} = \ln(10) \cdot c \cdot r_0^\alpha \cdot \left(\frac{1}{r}\right)^{\alpha-1} \quad \text{or} \quad \frac{dN(r)}{dr} = c \cdot r_0^\alpha \cdot \left(\frac{1}{r}\right)^\alpha \quad (112)$$

with  $\alpha$  an exponent varying between 3 and 5, and  $c$  the number density of particles with an arbitrary radius  $r_0$ . The *Model C* defined by [RD-32] is commonly used as the size distribution function:  $c \cdot r_0^\alpha = 1$  and  $\alpha = 4$ .

- a *Modified Gamma* distribution function (see [RD-31]) to compute the scattering properties of water haze and to fit the aerosol measurements,

$$\frac{dN(r)}{dr} = A \cdot \left(\frac{r}{r_0}\right)^\alpha \cdot \exp\left[-b \cdot \left(\frac{r}{r_0}\right)^\gamma\right] \quad \text{with } r_0 = 1 \mu\text{m} \quad (113)$$

where  $A, b, \alpha, \gamma$  represents the four parameters of the distribution.  $A$  and  $\gamma$  are generally taken to be equal to 1 (see [RD-32]).

- a *Log-Normal* distribution function (see [RD-29]) based on the *Junge power-law* function introduced to take the large particles into account,

$$\frac{dN(r)}{d \log r} = \frac{N}{\sqrt{2\pi} \log \sigma} \cdot \exp\left[-\left(\frac{\log r - \log r_m}{\sqrt{2} \log \sigma}\right)^2\right] \quad (114)$$

where  $r_m$  is the mean radius of the particle, and  $\sigma$  the standard deviation of  $r$ . This distribution is particularly well adapted to emphasize the individual components of the aerosol mixture (see [RD-28] and [RD-29]).

### 3.2.3 Aerosol models

The aerosol models are defined as an homogeneous mixing of the basic constituents which are assumed to be spherical particles characterized by their complex refractive index at all the wavelengths and their particle size distribution with the microphysical characteristics (see Section 3.2.2 for more details). Numerous samples of refractive indices for various aerosol components in all the MERIS spectral bands and several examples of particle size distributions for various aerosol models are given in [AD-4].

For atmospheric corrections of MERIS data, two sets of aerosol models have been defined:

- Over land, *the aerosol models* are considered as homogeneous in terms of composition and the particles size distribution follows a *Junge's* power law function.
- Over ocean, *basic constituents* are homogeneously mixed to build-up *models*. The particle size distribution is usually defined as a sum of *Log-Normal* distributions associated with these constituents. Note that the combination of aerosol models in 3 major layers (boundary, troposphere and stratosphere) defines an aerosol assemblage.

6 basic components are distinguished in the atmosphere over ocean:


- *desert dust* aerosols,
- *dust-like* particles,
- *oceanic* particles (*sea-salt solution* in water),
- *water-soluble* particles,
- *soot-like* particles,
- *rural aerosol mixture* (70% of water soluble particles and 30% of dust-like particles),

In the stratosphere, the *sulphuric acid solution* in water is built by combining two basic constituents excepted the rural aerosol mixture. A *Modified-Gamma* distribution function is used to describe the particle size distribution.

From these 7 basics components (including H<sub>2</sub>SO<sub>4</sub>), 6 aerosol models (4 boundary models, 1 tropospheric model and 1 stratospheric model) have been defined and summarized in [Table 6](#).

*Table 6: Aerosol components and their respective contributions (as percent of the volume (Vol.), or as percent of the number of particles (Pcl.)) in the composition of the aerosol models.*

| <i>Aerosol model</i>                                | <i>Components</i>  | <i>Vol. (%)</i> | <i>Pcl. (%)</i>                                  | <i>Atmosph. Layer</i>  |
|---|--|-----------------|--|--|
| <b>Maritime</b><br>(Shettle and Fenn, 1979) [RD-33] | - rural aerosol mixtures<br>- oceanic (sea-salt solution in water) | -<br>-          | 99.0<br>1.0                                      | <i>Boundary layer</i><br><i>[0-2 km]</i>                         |
| <b>Coastal</b><br>(Shettle and Fenn, 1979) [RD-33]  | - rural aerosol mixtures<br>- oceanic (sea-salt solution in water) | -<br>-          | 99.5<br>0.5                                      | <i>Boundary layer</i><br><i>[0-2 km]</i>                         |
| <b>Rural</b><br>(Shettle and Fenn, 1979) [RD-33]    | - water soluble + dust-like  | 100             | 100  | <i>Boundary layer</i><br><i>[0-2 km]</i>                         |
| <b>Desert dusts</b>                                 |  |                 |  |  |
| • DBS1 & DBW1<br>(Moulin at al., 2001) [RD-35]      | - large particles<br>- medium particles<br>- small particles       | -<br>-<br>-     | 3.861 10 <sup>-5</sup><br>45.785735<br>54.214226 | <i>Boundary layer +</i><br><i>Troposphere</i><br><i>[0-7 km]</i> |
| • DBS2 & DBW2<br>(Moulin at al., 2001) [RD-35]      | - large particles<br>- medium particles<br>- small particles       | -<br>-<br>-     | 3.861 10 <sup>-4</sup><br>45.785562<br>54.214052 | <i>Boundary layer +</i><br><i>Troposphere</i><br><i>[0-7 km]</i> |
| • DBS1 & DBW1<br>(Moulin at al., 2001) [RD-35]      | - large particles<br>- medium particles<br>- small particles       | -<br>-<br>-     | 7.722 10 <sup>-4</sup><br>45.785369<br>54.213859 | <i>Boundary layer +</i><br><i>Troposphere</i><br><i>[0-7 km]</i> |
| <b>Continental</b><br>(WCRP, 1986) [RD-34]          | - water soluble<br>- dust-like<br>- soot-like                      | 29<br>70<br>1   | 93.876773<br>2.27 10 <sup>-4</sup><br>6.123      | <i>Troposphere</i><br><i>[2-12 km]</i>                           |

|   |  |  |
|---|--|--|
|  | <b>MERIS/ ENVISAT-1</b><br>Medium Resolution Imaging<br>Spectrometer | <u>Ref.:</u> PO-RS-PAR-GS-0003         |
|   |  | <u>Issue:</u> 4 <u>Rev.:</u> A         |
|   |  | <u>Date:</u> 16-Dec-10 <u>Page:</u> 55 |

| <i>Aerosol model</i>                                       | <i>Components</i>   | <i>Vol. (%)</i> | <i>Pcl. (%)</i> | <i>Atmosph. Layer</i>             |
|--|---|-----------------|-----------------|-----------------------------------|
| <b>H<sub>2</sub>SO<sub>4</sub></b><br>(WCRP, 1986) [RD-34] | - 75 % solution of sulphuric acid<br>(H <sub>2</sub> SO <sub>4</sub> ) in water | 100             | 100             | <i>Stratosphere</i><br>[12-50 km] |

### 3.2.4 Vertical distribution

Depending on the number of aerosol layers defined in the atmosphere two vertical distributions of the particles are commonly used:

- 1 aerosol layer (case over land): The aerosol optical thickness  $\tau_a(z)$  at the altitude  $z$  follows an exponential law as,

$$\tau_a(z) = \tau_a(0) e^{-z/H_a} \quad (115)$$

where  $\tau_a(0)$  is the AOT of the whole atmosphere at ground level, and  $H_a$  the aerosol scale height. Over land,  $H_a$  is usually taken to be equal to  $2\text{ km}$ .

- 3 aerosol layers (case over ocean): The aerosol optical thickness can be either homogeneously (RTC/UdL & FUB) or heterogeneously (RTC/FUB only) distributed in each of these 3 layers,
  - *a boundary layer*: model, optical thickness at  $550\text{ nm}$ , between  $0$  and  $2\text{ km}$  altitude,
  - *a tropospheric layer*: model, optical thickness at  $550\text{ nm}$ , between  $2$  and  $12\text{ km}$  altitude,
  - *a stratospheric layer*: model, optical thickness at  $550\text{ nm}$ , above  $12\text{ km}$  altitude.

## 3.3 CLOUDS

### 3.3.1 Inherent optical properties

Except for the cirrus, cloud IOPs are computed according to the *Mie* theory (see Section 2.8). Similarly to the aerosols, the water droplet is assumed to be a spherical particle characterized by its complex refractive index  $n$  and its effective geometrical radius  $r$ . The cloud extinction, scattering and absorption coefficients as well as the phase function are expressed as identical to the IOPs of the aerosol particles (see Section 3.2.1). For a cirrus cloud layer IOPs could be derived from [RD-36] but are not considered in the two RTCs for the MERIS project.

### 3.3.2 Particle size distribution

The drop size distributions are usually described by the *Modified Gamma* distribution function presented in Section 3.2.2.

### 3.3.3 Cloud models

The standard cloud types are fully described by [RD-37] for the *Mie*'s calculations.

### 3.3.4 Vertical distribution

The cloud profile is specified by a type and an extinction coefficient ( $m^{-1}$ ) in each of atmospheric layer. Three major cloud layers is predefined in the atmosphere. The cloud optical thickness can be either homogeneously or heterogeneously (RTC/UdL & FUB) distributed in each of these 3 layers:

- a 1<sup>st</sup> cloud layer:    model, optical thickness at 550 *nm*, between 0 and 2 *km* altitude,
- a 2<sup>nd</sup> cloud layer:    model, optical thickness at 550 *nm*, between 2 and 9 *km* altitude,
- a 3<sup>rd</sup> cloud layer:    model, optical thickness at 550 *nm*, between 7 and 12 *km* altitude,.



## 4. WATER OPTICAL PROPERTIES

Two ocean water cases are distinguished (see [AD-4] for more details):

- *Case 1:* the oceanic waters (*i.e.*, open oceans) for which the apparent optical properties only depend on the IOPs of *phytoplankton* (such as living alga cells, heterotrophic bacteria and organisms, various debris) and the associated *yellow substances* (coloured dissolved organic material CDOM generated through excretion, organism decay, *etc.*)
- *Case 2:* the coastal waters which are seen as *case 1 waters* but with additional other optically active substances such as the inorganic particulate matter so-called *Gelbstoff* (exogenous particles, mainly sediments, either transported by rivers or re-suspended from the bottom in shallow waters).

The total extinction ( $e$ ), scattering ( $s$ ), absorption ( $a$ ) coefficients for these ocean water cases result from the sum of the contributions of each oceanic component.

$$\sigma_{e,s,a} = \sigma_{e,s,a}^w + \sigma_{e,s,a}^p + \sigma_{e,s,a}^{ys} + \sigma_{e,s,a}^{spm} \quad (116)$$

with  $w$  for the pure sea water,  $p$  for the phytoplankton,  $ys$  for the yellow substance (or *Gelbstoff*) and  $spm$  for the inorganic particles (suspended particulate matter).

### 4.1 PURE SEA WATER

The absorption coefficient  $\sigma_a^w$  of the pure sea water is tabulated in [RD-38] for wavelengths up to 709 nm and in [RD-39] above 709 nm. These values are resampled for 10 MERIS spectral bands (Table 7). As expected this absorption spectrum stresses an increase with the wavelength.

*Table 7: Pure water absorption coefficient  $\sigma_a^w$  for 10 MERIS spectral bands.*

| $\lambda$ (nm) | $\sigma_a^w$ ( $nm^{-1}$ ) |
|----------------|----------------------------|
| 412.50         | 0.00452                    |
| 442.50         | 0.00696                    |
| 490.00         | 0.01500                    |
| 510.00         | 0.03250                    |
| 560.00         | 0.06190                    |
| 620.00         | 0.27550                    |
| 665.00         | 0.42900                    |
| 708.75         | 0.79150                    |
| 778.75         | 2.34000                    |
| 865.00         | 4.93790                    |

The scattering coefficient  $\sigma_s^w$  of the pure sea water strongly decreases with the wavelength. The *Morel*'s formulation [RD-40] expresses this wavelength dependence as:

$$\sigma_s^w(\lambda) = 0.00288 \cdot \left(\frac{\lambda}{500}\right)^{-4.32} \quad (117)$$

The scattering phase function of the pure sea water is defined as [RD-41]:

$$P_w(\theta) = \frac{3}{3+p} \cdot (1 + p \cdot \cos^2 \theta) \quad (118)$$

with  $p$  the polarization factor at  $90^\circ$  ( $p = 0.84$ ). However, the anisotropy of the molecular scattering for the pure sea water is often taken into account using a depolarization factor ( $\delta$ ) of 0.0906 in the molecular scattering phase function (Equation 99).

## 4.2 PHYTOPLANKTON

### 4.2.1 Inherent optical properties

- *Absorption and scattering coefficients:*

The absorption coefficient  $\sigma_a^p$  ( $m^{-1}$ ) of phytoplankton is taken from [RD-42]:

$$\sigma_a^p(\lambda, [chl]) = A_\lambda \cdot [chl]^{B_\lambda} \quad (119)$$

with  $[chl]$  the chlorophyll- $a$  concentration (in  $mg \cdot m^{-3}$ ), and  $A_\lambda$ ,  $B_\lambda$  two spectral coefficients tabulated for which the values are reproduced at 10 MERIS wavelengths in Table 8.

*Table 8: Values of  $A_\lambda$  and  $B_\lambda$  coefficients for 10 MERIS spectral bands useful to compute  $\sigma_a^{chl}(\lambda)$ .*

| $\lambda$ (nm) | $A_\lambda$ | $B_\lambda$ |
|----------------|-------------|-------------|
| 412.50         | 0.0474995   | 0.6840705   |
| 442.50         | 0.0511810   | 0.6266249   |
| 490.00         | 0.0341240   | 0.6200260   |
| 510.00         | 0.0231810   | 0.7060040   |
| 560.00         | 0.0100310   | 0.8412540   |
| 620.00         | 0.0089570   | 0.8438080   |
| 665.00         | 0.0167630   | 0.8207835   |
| 708.75         | 0.0010000   | 1.0000000   |
| 778.75         | 0           | 1.0000000   |
| 865.00         | 0           | 1.0000000   |

The scattering coefficient  $\sigma_s^p$  of phytoplankton is expressed according to [RD-43]:

$$\sigma_s^p(\lambda) = A_{chl} \cdot [chl]^{B_{chl}} \cdot \left(\frac{\lambda}{550}\right)^{-1} \quad (120)$$

where  $A_{chl}$ ,  $B_{chl}$  are respectively equal to 0.416 and 0.766.

• *Scattering phase function:*

The *Petzold* phase function is often used to define the scattering phase function of the phytoplankton (Table 9). The latter can be also computed by the *Mie's* theory (see Section 2.8). The real part of the refractive index  $m$  is ranged within [1.01;1.09] and the imaginary part  $k$  is often equal to 0. The particle size distribution  $n(r)$  is described by a *Junge power-law* function (see Section 3.2.2) with a standard  $\alpha$  of -3.2. The particle size values are ranged from  $0.01\mu\text{m}$  to  $200\mu\text{m}$ .

*Table 9: Petzold phase function  $P_p(\theta)$  derived from [RD-44].*

| $\theta$ | $P_p(\theta)$ | $\theta$  | $P_p(\theta)$ |
|----------|---------------|-----------|---------------|
| 0.00000  | 1.00000E+04   | 40.00000  | 4.20985E-02   |
| 0.05000  | 8.63700E+03   | 45.00000  | 3.06722E-02   |
| 0.10000  | 1.76661E+03   | 50.00000  | 2.27533E-02   |
| 0.12589  | 1.29564E+03   | 55.00000  | 1.69904E-02   |
| 0.15849  | 9.50172E+02   | 60.00000  | 1.31254E-02   |
| 0.19953  | 6.99092E+02   | 65.00000  | 1.04625E-02   |
| 0.25119  | 5.13687E+02   | 70.00000  | 8.48826E-03   |
| 0.31623  | 3.76373E+02   | 75.00000  | 6.97601E-03   |
| 0.39811  | 2.76318E+02   | 80.00000  | 5.84232E-03   |
| 0.50119  | 2.18839E+02   | 85.00000  | 4.95306E-03   |
| 0.63096  | 1.44369E+02   | 90.00000  | 4.29232E-03   |
| 0.79433  | 1.02241E+02   | 95.00000  | 3.78161E-03   |
| 1.00000  | 7.16082E+01   | 100.00000 | 3.40405E-03   |
| 1.25890  | 4.95803E+01   | 105.00000 | 3.11591E-03   |
| 1.58490  | 3.39511E+01   | 110.00000 | 2.91222E-03   |
| 1.99530  | 2.28129E+01   | 115.00000 | 2.79696E-03   |
| 2.51190  | 1.51622E+01   | 120.00000 | 2.68568E-03   |
| 3.16230  | 1.00154E+01   | 125.00000 | 2.57142E-03   |
| 3.98110  | 6.57957E+00   | 130.00000 | 2.47603E-03   |
| 5.01190  | 4.29530E+00   | 135.00000 | 2.37667E-03   |
| 6.30960  | 2.80690E+00   | 140.00000 | 2.32898E-03   |
| 7.94330  | 1.81927E+00   | 145.00000 | 2.31308E-03   |
| 10.00000 | 1.15257E+00   | 150.00000 | 2.36475E-03   |
| 15.00000 | 4.89344E-01   | 155.00000 | 2.50584E-03   |
| 20.00000 | 2.44424E-01   | 160.00000 | 2.66183E-03   |
| 25.00000 | 1.47151E-01   | 165.00000 | 2.83472E-03   |
| 30.00000 | 8.60848E-02   | 170.00000 | 3.03046E-03   |
| 35.00000 | 5.93075E-02   | 175.00000 | 3.09206E-03   |
|          |               | 180.00000 | 3.15366E-03   |

## 4.2.2 Vertical distribution

Whatever the ocean water case, the phytoplankton is assumed to be homogeneously distributed in the water column. This is especially true for the coastal waters due to a strong hydrodynamic. In the case of the open sea waters, certain authors prefer rather to use a shifted *Gaussian* curve from [RD-45] to modelize the vertical distribution of the phytoplankton which seems to be more adapted.

## 4.3 YELLOW SUBSTANCE

### 4.3.1 Inherent optical properties

The yellow substance is a purely absorbing component. Its absorption coefficient  $\sigma_a^{ys}$  is expressed as (see [RD-42]):

$$\sigma_a^{ys}(\lambda) = \sigma_a^{ys}(443) \cdot \exp[-S_{ys} \cdot (\lambda - 443)] \quad (121)$$

with  $S_{ys}$  a yellow substance coefficient equal to  $0.014 \text{ nm}^{-1}$  (*resp.*,  $0.0176 \text{ nm}^{-1}$ ) for the oceanic waters from case 1 (*resp.*, from case 2 with the CDOM absorption), and  $\sigma_a^{ys}(443)$  the absorption coefficient of the yellow substance at the  $443 \text{ nm}$  wavelength which is given by:

$$\sigma_a^{ys}(443) = \frac{1}{2} \cdot [\sigma_a^w(443) + \sigma_a^p(443, [chl])] \quad (122)$$

where  $\sigma_a^w(443)$  and  $\sigma_a^p(443, [chl])$  represent respectively the absorption coefficient of the pure sea water and the phytoplankton at the  $443 \text{ nm}$  wavelength.

### 4.3.2 Vertical distribution

The yellow substance is assumed homogeneously distributed in the water column. For many coastal waters this is a realistic assumption, but of course this is not true for the river plumes where very strong vertical gradients are observed.

## 4.4 SUSPENDED PARTICULATE MATTER AND GELBSTOFF

### 4.4.1 Inherent optical properties

• *Absorption and scattering coefficients:*

The non-chlorophyll suspended particulate matter (SPM) strongly differs in composition with very large range of concentrations in the coastal waters which makes very difficult the modelling of its bio-optical properties.

The absorption coefficient of SPM  $\sigma_a^{spm}$  is expressed as for the yellow substance:

$$\sigma_a^{spm}(\lambda) = \sigma_a^{spm}(443) \cdot \exp[-S_{spm} \cdot (\lambda - 443)] \quad (123)$$

with  $S_{spm}$  a SPM coefficient equal to  $0.0122 \text{ nm}^{-1}$  for the oceanic waters from case 2, and  $\sigma_a^{spm}(443)$  the absorption coefficient of SPM at the  $443 \text{ nm}$  wavelength which is given by:

$$\sigma_a^{spm}(443) = A_{spm} \cdot SPM^{B_{spm}} \quad (124)$$

where  $A_{spm}$ ,  $B_{spm}$  are respectively equal to 0.0216 and 1.0247.

The scattering coefficient  $\sigma_s^{spm}$  of SPM is expressed as:

$$\sigma_s^{spm}(\lambda) = C_\lambda \cdot C_{555} \cdot SPM \quad (125)$$

with  $SPM$  the SPM concentration (in  $g\ m^{-3}$ ), and  $C_\lambda$  a spectral coefficient tabulated for which the values are reproduced at MERIS wavelengths in [Table 10](#), and  $C_{555}$  the value of  $C_\lambda$  at the 555 nm wavelength.

*Table 10: Values of  $C_\lambda$  coefficients in 10 MERIS spectral bands useful to compute  $\sigma_s^{spm}(\lambda)$ .*

| $\lambda$ (nm) | $C_\lambda$ |
|----------------|-------------|
| 412.50         | 1.016       |
| 442.50         | 1.002       |
| 490.00         | 1.003       |
| 510.00         | 1.007       |
| 560.00         | 0.996       |
| 620.00         | 0.951       |
| 665.00         | 0.914       |
| 708.75         | 0.928       |
| 778.75         | 0.931       |
| 865.00         | 0.931       |

• **Scattering phase function:**

The *Petzold* phase function is often used to define the scattering phase function of SPM ([Table 9](#)). The latter can be also computed by the *Mie's* theory (see [Section 2.8](#)). The real part of the refractive index  $m$  is ranged from 1.15 to 1.20 and the imaginary part  $k$  from -0.008 to 0. The particle size distribution  $n(r)$  is represented by the *Junge power-law* function (see [Section 3.2.2](#)) with a standard  $\alpha$  of -4. The particle size values are ranged from  $0.01\ \mu m$  to  $50\ \mu m$ .

**4.4.2 Vertical distribution**

SPM are assumed homogeneously distributed in the water column.

## 5. SEA SURFACE STATE

The effect of the *air-sea* interface shape (*i.e.*, the water surface roughness) on the *Fresnel* reflection and refraction is usually modelled according to the statistical description of the wave facet distribution derived by *Cox and Munk* [RD-46]. This surface model assumes an isotropic distribution of the facet slopes independently of the wind orientation, and the reflectance above sea surface level depends on the wind speed. Shadowing effects are not accounted for in the total upwelling radiances.

In this surface model, the probability density function of facet slopes  $p(\theta_s, \theta_v, \Delta\phi)$  for the illumination and viewing configurations  $(\theta_s, \theta_v, \Delta\phi)$  is expressed as:

$$p(\theta_s, \theta_v, \Delta\phi) = \frac{1}{\pi \sigma^2} \cdot \exp\left(-\frac{\tan^2 \beta}{\sigma^2}\right) \quad (126)$$

where  $\beta$  the angle between the local normal and the normal to the facet, and  $\sigma$  the root mean square of facet slopes are defined by:

$$\cos \beta = \frac{\cos \theta_v + \cos \theta_s}{2 \cos \omega} \quad (127)$$

with,

$$\cos 2\omega = \cos \theta_s \cdot \cos \theta_v - \sin \theta_s \cdot \sin \theta_v \cdot \cos \Delta\phi$$

and

$$\sigma^2 = 0.003 + 5.12 \cdot 10^{-3} \cdot w_s \quad (128)$$

with  $w_s$  the wind speed ( $m s^{-1}$ ) at 0.5 m height above sea level.

The sun glint  $\rho_G$  (*i.e.*, the specular reflection of the sunlight over the ocean waves) just above sea level is then defined as:

$$\rho_G = \rho_F(\omega) \cdot \frac{\pi p(\theta_s, \theta_v, \Delta\phi)}{4 \cos \theta_s \cos \theta_v \cos^4 \beta} \quad (129)$$

where  $\rho_F(\omega)$  is the *Fresnel* reflectance at the *air-sea* interface for the angle  $\omega$  given by (*see Section 2.10*):

$$\left\{ \begin{array}{l} \rho_F(\omega) = \frac{1}{2} \cdot \left[ \left( \frac{\sin(\omega - \mathcal{G}_t)}{\sin(\omega + \mathcal{G}_t)} \right)^2 + \left( \frac{\tan(\omega - \mathcal{G}_t)}{\tan(\omega + \mathcal{G}_t)} \right)^2 \right] \quad \text{for } \omega \neq \mathcal{G}_t \\ \rho_F(\omega) = \left( \frac{n_w - 1}{n_w + 1} \right)^2 \quad \text{for } \omega = \mathcal{G}_t \end{array} \right.$$

with  $\mathcal{G}_t = \arcsin(\sin \omega / n_w)$ .

## 6. RADIATIVE TRANSFER

The theory of the radiative transfer is based on the assumption of an infinite plane-parallel dielectric medium (atmosphere or ocean) where the optical properties only depend on the vertical coordinate.

### 6.1 GEOMETRY

The geometry conventions are depicted in [Figure 14](#). The sun illumination and viewing configurations are given by the solar zenithal angle  $\vartheta_s$  (also noted  $\vartheta_o$ ), the viewing zenithal angle  $\vartheta_v$ , and the relative azimuthal angle  $\Delta\phi$  between the solar incidence and viewing planes ( $\Delta\phi = \phi_s - \phi_v$ ). The azimuthal angle  $\Delta\phi$  in [Figure 14](#) corresponds to the azimuth angle difference for the 6S geometry conventions [RD-47].

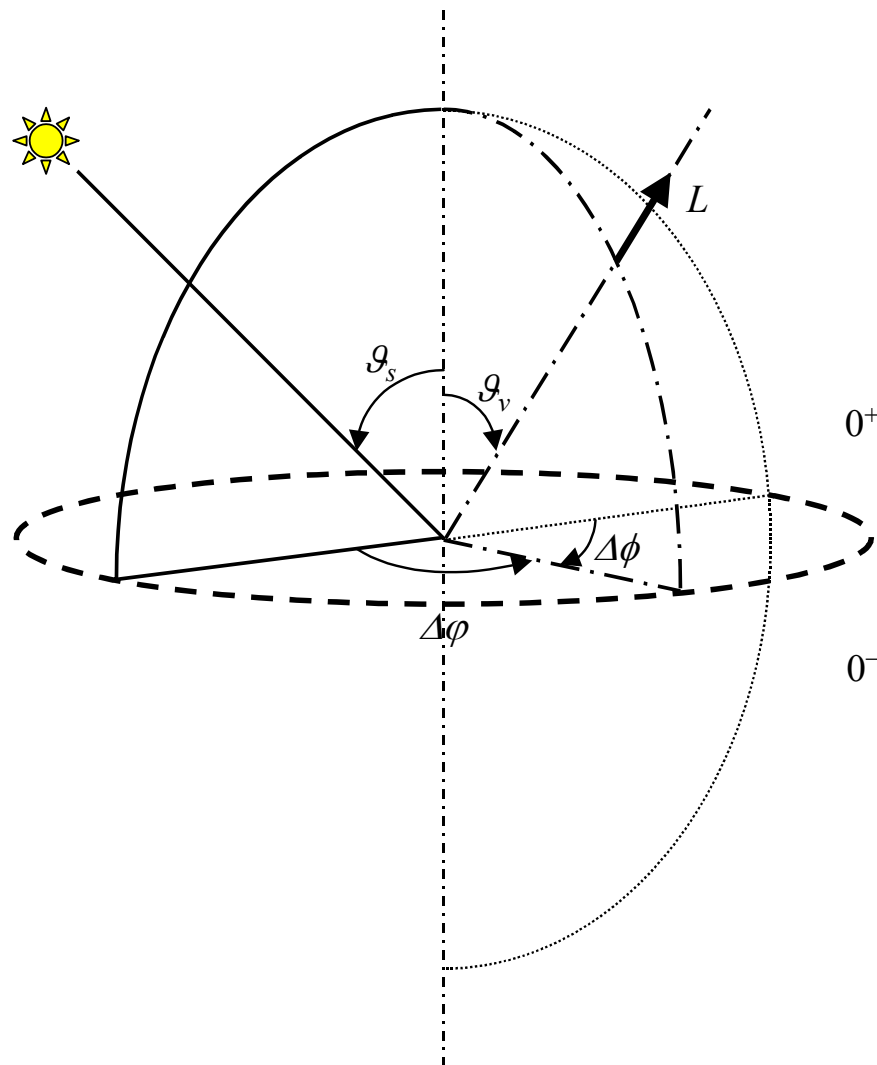


*Figure 14: Illumination and viewing configuration for MERIS sensor.*

The scattering angle  $\theta$  is defined as:

$$\cos \theta = \mp \cos \vartheta_s \cdot \cos \vartheta_v \pm \sin \vartheta_s \cdot \sin \vartheta_v \cdot \cos \Delta\phi \quad (130)$$

The first configuration ( - cos + sin ) corresponds to an upward signal (namely an observation towards the surface) and the second one ( + cos – sin ) to a downward signal (namely a skyward observation).

## 6.2 GENERAL FORMULATION

### 6.2.1 Radiative Transfer Equation (RTE)

Generally speaking, the light propagating within a dielectric medium may be attenuated by the absorption or the scattering of photons out of the light propagation direction but may be also intensified by the scattering and the emission of photons into the light propagation direction.

For a passive medium (*i.e.*, without any internal source of radiation), the radiative transfer equation (RTE) accounts for the loss of radiance due to the scattering and absorption in the propagation direction, and for the gain of radiance due to the scattering from other directions. Thus, the two parameters of this equation are the attenuation coefficient and the phase function. The radiative balance for an elementary layer with an infinitesimal optical thickness  $d\tau$  enlightened by an incident light  $(\mu_0, \varphi_0)$  and viewed under the direction  $(\mu, \varphi)$  is expressed as (*see* [RD-48] & [RD-49] for more details):

$$\mu \cdot \frac{dL(\tau, \mu, \varphi)}{d\tau} = L(\tau, \mu, \varphi) - \frac{\omega_0(\tau)}{4\pi} \cdot P(\tau, \mu, \mu_0, \Delta\varphi) \cdot E_0 \cdot e^{\tau/\mu_0} - \frac{\omega_0(\tau)}{4\pi} \cdot \int_0^{2\pi} \int_{-1}^1 P(\tau, \mu, \mu', \Delta\varphi) \cdot L(\tau, \mu', \varphi') \cdot d\mu' \cdot d\varphi' \quad (131)$$

with  $\mu d\tau < 0$  and where,

$\mu_0, \mu$  : cosine of zenithal angle  $\theta_0$  (incident light,  $\mu_0 \leq 0$ ) and  $\theta$  (viewing angle) respectively,

$\varphi, \Delta\varphi$  : azimuthal viewing angle and relative azimuthal angle ( $\varphi_0 - \varphi$ ) respectively,

$\omega_0(\tau)$  : single scattering albedo located at  $\tau$  within the elementary layer,

$P(\tau, \mu, \mu_0, \Delta\varphi), P(\tau, \mu, \mu', \Delta\varphi)$  : scattering phase functions located at  $\tau$  within the layer,

$L(\tau, \mu', \varphi'), L(\tau, \mu, \varphi)$  : incident and scattered radiances located at  $\tau$  within the elementary layer,

$E_0 \cdot e^{\tau/\mu_0}$  : irradiance not yet intercepted at  $\tau$  within the elementary layer ( $E_0$  corresponds usually to the solar constant).

The first term in the right part of the RTE represents the radiance attenuated (scattering + absorption) along  $(\mu, \varphi)$  direction within the layer  $d\tau$ , the second term the radiance along  $(\mu, \varphi)$  direction due to the scattering of the incident radiation  $(\mu_0, \varphi_0)$  not yet intercepted within the layer  $d\tau$ , and the third term the radiance along  $(\mu, \varphi)$  direction due to the scattering of radiations already scattered within the layer  $d\tau$ .

Note that, the prime notation used here and in following sections, denotes the incident field light. Moreover, all energetic quantities mentioned above and hereafter are mono-chromatic, and to simplify notation the subscript  $\lambda$  corresponding to the wavelength is omitted.

By considering  $\tau_1$  as the total optical thickness of the elementary layer (Figure 15) the RTE can then be written as the following standard integral forms [RD-47]:



$$\left\{ \begin{array}{l} I(\tau, \mu, \varphi) = I(\tau_1, \mu, \varphi) \cdot e^{-(\tau_1-\tau)/\mu} + \int_{\tau_1}^{\tau} J(\tau', \mu, \varphi) \cdot e^{-(\tau'-\tau)/\mu} \cdot \frac{d\tau'}{\mu} \\ I(\tau, -\mu, \varphi) = I(0, -\mu, \varphi) \cdot e^{-\tau/\mu} + \int_0^{\tau} J(\tau', -\mu, \varphi) \cdot e^{-(\tau'-\tau)/\mu} \cdot \frac{d\tau'}{\mu} \end{array} \right. \quad \text{with } (0 < \mu \leq 1) \quad (132)$$

where  $I(\tau, \mu, \varphi)$  and  $I(\tau, -\mu, \varphi)$  are respectively the upwelling and downwelling radiance located at  $\tau$  within the layer, and  $J(\tau, \mu, \varphi)$  the source function which accounts for the interaction of the present radiation field with the particles of the layer located at  $\tau$ . This source function is expressed as:

$$J(\tau, \mu, \varphi) = \frac{\omega_0(\tau)}{4} \cdot F_0 \cdot P(\tau, \mu, \varphi, \mu_0, \varphi_0) \cdot e^{\tau/\mu_0} + \frac{\omega_0(\tau)}{4\pi} \cdot \int_0^{2\pi} \int_{-1}^1 I(\tau, \mu', \varphi') \cdot P(\tau, \mu, \varphi, \mu', \varphi') \cdot d\mu' \cdot d\varphi' \quad (133)$$

The first term represents the illumination source  $E_0 = \pi F_0$  (*i.e.*, the direct solar radiation) which propagates across the elementary layer along  $(\mu_0, \varphi_0)$  directly up to the level  $\tau$  and being scattered in the  $(\mu, \varphi)$  direction (*primary scattering*), and the second term is related to the *multiple scattering* and quantifies the redistribution of diffuse light into the considered direction of light propagation.

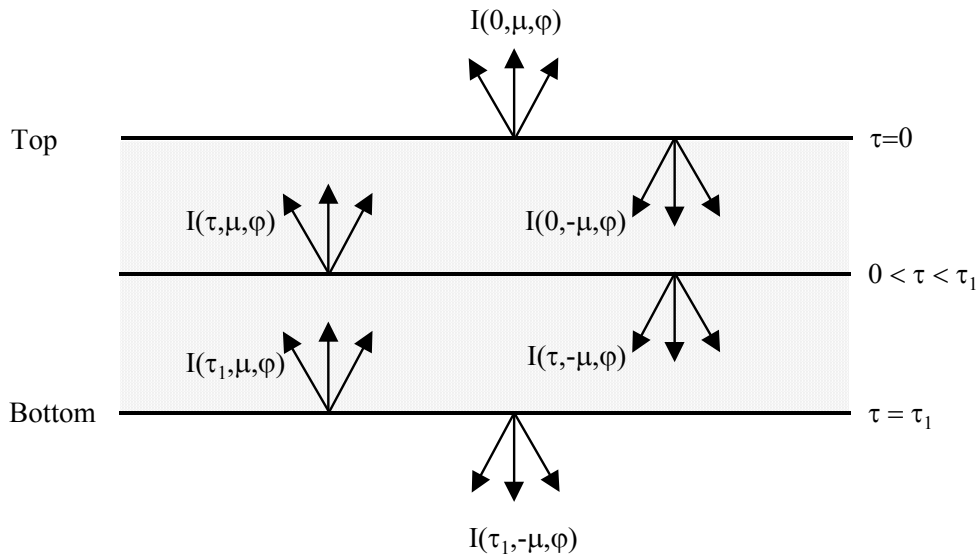


*Figure 15: Schematic representation of radiative transfer problem.*

## 6.2.2 Solving the RTE

Analytical solutions of the RTE exist for a number of simple source functions such as for the isotropic or *Rayleigh* scattering (*see* [RD-5] & [RD-50]). However, in most cases the source function presents a complex dependence with the optical properties of the medium and the angular distribution of the incident light, and the RTE needs to be solved numerically. Numerous developed methods to solve the RTE in a scattering and absorbing medium all have in common to start with some analytical treatment followed by numerical computations. The computer time requirement strongly depends on the complexity of the physical problem (phase function, vertical inhomogeneity) and on the expected accuracy.

Hereafter are briefly described four numerical approaches commonly used to solved the RTE:

• *Monte Carlo method:*

This method is potentially the most exact in theory, in particular for media with a complex geometry and anisotropic scattering phase functions. However it is more computer time-consuming. Classically, this method begins with an illumination phase of the medium simulated by the tracking of the trajectories of photons. An angular scattering and absorption probability is then associated with each eventual interaction. The trajectory of each photon is tracked up to its absorption or its outgoing from the medium. This process iterates until to reach statistically stable results for all the scattering directions.

• *Double Adding method:*

This numerical approach is commonly used to solve the RTE in the stellar and planetary atmospheres. This method developed by *Van de Hulst [RD-51]* needs relatively few computational times and is particularly useful for the case of anisotropic scattering phase functions. In this method, the optical properties of the particles with a layer are characterized by two matrices **R** and **T**, respectively the directional reflectance and transmittance, the size of which is equal to the number of selected propagation directions. The superimposition of two layers yields to the following optical properties **R'** and **T'**:

$$\begin{cases} \mathbf{R}' = \mathbf{R} + \mathbf{T} \cdot \mathbf{R} \cdot [\mathbf{1} - \mathbf{R} \cdot \mathbf{R}]^{-1} \cdot \mathbf{T} \\ \mathbf{T}' = \mathbf{T} \cdot [\mathbf{1} - \mathbf{R} \cdot \mathbf{R}]^{-1} \cdot \mathbf{T} \end{cases} \quad (134)$$

The first phase of the method consists in the use of an infinitely thin layer, *e.g.*, a layer with an optical thickness of  $2^{-25}$ . This layer is then doubled and the optical characteristics of this resulting layer are recomputed. This double adding of layers is repeated until to reach the desired optical depth. It can be note that only 50 iterations are needed for obtaining an optical depth of  $2^{25}$ . This method can be easily adapted to consider layers with different optical properties (*see Section 8.2.3.1*).

- *Discrete Ordinates Method (DOM):*

This DOM approach relies on the discretization of all the space for incident and scattered directions [RD-52]. Thus photons can be only propagated along a finite number of directions. This approximation may lead to some artefacts inherent to this method. Of course the number of selected directions  $N$  must be sufficiently large to obtain accurate results, but not too much for an acceptable computational time. Moreover the solution derived from this technique needs to be checked to be realistic (or positive).

Thus, by using this approach the RTE becomes a system of  $N$  differential integral equations. For a plane parallel medium and by considering the mean value for each selected direction, this set of equations is written as:

$$\begin{aligned} \frac{1}{\Delta\Omega_j} \cdot \int_{\Delta\Omega_j} \mu \cdot \frac{dL(\tau, \Omega)}{d\tau} \cdot d\Omega = \frac{1}{\Delta\Omega_j} \cdot \int_{\Delta\Omega_j} L(\tau, \Omega) \cdot d\Omega - \frac{\omega_o(\tau)}{4\pi} \cdot E_o \cdot e^{\tau/\mu_o} \cdot \frac{1}{\Delta\Omega_j} \cdot \int_{\Delta\Omega_j} \int_{\Delta\Omega_j, 4\pi} P(\tau, \Omega, \Omega_o) \cdot d\Omega \\ - \frac{\omega_o(\tau)}{4\pi} \cdot \frac{1}{\Delta\Omega_j} \cdot \int_{\Delta\Omega_j} \int_{\Delta\Omega_j, 4\pi} P(\tau, \Omega, \Omega') \cdot L(\tau, \Omega') \cdot d\Omega' \cdot d\Omega \end{aligned} \quad (135)$$

where,

$\Omega_o, \Omega$ : solid angles for the incident and scattered direction respectively,

$\Delta\Omega_j$ : increment of solid angle for the  $j^{th}$  discrete angular sector in the space,

Using the following quantities,

$$L_j(\tau) = \frac{1}{\Delta\Omega_j} \cdot \int_{\Delta\Omega_j} L(\tau, \Omega) \cdot d\Omega$$

$$\mu_j = \frac{1}{\Delta\Omega_j} \cdot \int_{\Delta\Omega_j} \mu \cdot d\Omega$$

$$P_{k,j} = \frac{1}{\Delta\Omega_k} \cdot \frac{1}{\Delta\Omega_j} \cdot \int_{\Delta\Omega_k} \int_{\Delta\Omega_j} P(\tau, \Omega, \Omega') \cdot d\Omega' \cdot d\Omega$$

the  $N$  differential integral equations can be substituted by the  $N$  following linear equations at first order,

$$\mu_j \cdot \frac{dL_j(\tau)}{d\tau} = L_j(\tau) - \frac{\omega_o(\tau)}{4\pi} \cdot P_{o,j}(\tau) \cdot E_o \cdot e^{\tau/\mu_o} - \frac{\omega_o(\tau)}{4\pi} \cdot \sum_{k=1}^N P_{k,j}(\tau) \cdot L_k(\tau) \cdot \Delta\Omega_k$$

which can be analytically or numerically solved for a small value of  $N$ .

A classical approach consists in the use of the *Gauss* quadrature with an even number of directions (pivots) which optimizes the representation of energetic propagation within the space. The latter are the roots of *Legendre* polynomials at the  $N^{th}$  order (see [RD-53] for more details). Note that for strongly anisotropic media, an assymetric quadrature such as *Gauss-Lobatto* quadrature would be more appropriate to describe the energetic propagation within the anisotropic angular region.

- *Successive Orders (SO) method:*

By combining the left term and the first right term of the RTE (Equation 130), we can write:

$$\mu \cdot \frac{dL(\tau, \mu, \varphi)}{d\tau} - L(\tau, \mu, \varphi) = \mu \cdot e^{\tau/\mu} \cdot \frac{d}{d\tau} [L(\tau, \mu, \varphi) \cdot e^{-\tau/\mu}] \quad (136)$$

which yields to,

$$\frac{d}{d\tau} [L(\tau, \mu, \varphi) \cdot e^{-\tau/\mu}] = -\frac{\omega_o(\tau)}{2\mu} \cdot e^{-\tau/\mu} \left[ \frac{1}{2\pi} \cdot P(\tau, \mu, \mu_o, \Delta\varphi) \cdot E_o \cdot e^{\tau/\mu_o} + \int_{-1}^1 P(\tau, \mu, \mu', \Delta\varphi) \cdot L(\tau, \mu', \varphi') \cdot d\mu' \right] \quad (137)$$

or then,

$$\frac{d}{d\tau} [L(\tau, \mu, \varphi) \cdot e^{-\tau/\mu}] = -\frac{\omega_o(\tau)}{4\pi\mu} \cdot e^{-\tau/\mu} \cdot \int_0^{2\pi} \int_{-1}^1 P(\tau, \mu, \varphi, \mu', \varphi') \cdot L(\tau, \mu', \varphi') \cdot d\mu' \cdot d\varphi' \quad (138)$$

The SO method consists in an iterative processus with an approximate solution which will be inserted within the double integral form. A new analytical or numerical solution is then computed, and the process continues while the needed accuracy is not reached. The following section outlines this method.

### 6.2.2.1 Single and multiple scattering

The RTE is numerically solved by iteration. First the solution is computed for the primary scattering radiation for each layer of the stratified propagation medium then for the scattering at successive orders.

- *Single scattering:*

The light which propagates within an optically very thin layer ( $\Delta\tau/\mu \leq 10^{-3}$ ) is unlikely to undergo more than one scattering process inside the layer [RD-5]. Multiple scattering can then be neglected and by

using the RTE in its integral form (*see* Equation 131), the primary scattering radiation for the upward and downward directions (respectively,  $I^{(1)}(\tau, \mu, \varphi)$  and  $I^{(1)}(\tau, -\mu, \varphi)$ ) is given by:

$$\begin{cases} I^{(1)}(\tau, \mu, \varphi) = \frac{\omega_0(\tau)}{4\mu} \cdot F_0 \cdot P(\tau, \mu, \varphi, \mu_0, \varphi_0) \cdot e^{\tau/\mu_0} \cdot \Delta\tau \\ I^{(1)}(\tau, -\mu, \varphi) = \frac{\omega_0(\tau)}{4\mu} \cdot F_0 \cdot P(\tau, -\mu, \varphi, \mu_0, \varphi_0) \cdot e^{\tau/\mu_0} \cdot \Delta\tau \end{cases} \quad (139)$$

• *Multiple scattering:*

Thus, for higher order of scattering the  $n$ -times scattered light in the upward and downward directions (respectively,  $I^{(n)}(\tau, \mu, \varphi)$  and  $I^{(n)}(\tau, -\mu, \varphi)$ ) can then be estimated from the  $(n-1)$  times scattered light knowing the primary scattering radiations from the direct sun beam:

$$\begin{cases} I^{(n)}(\tau, \mu, \varphi) = \frac{1}{\mu} \cdot \sum_{j=i}^N J^{(n)}(\tau_j, \mu, \varphi) \cdot e^{-(\tau_j - \tau)/\mu} \cdot \Delta\tau \\ I^{(n)}(\tau, -\mu, \varphi) = \frac{1}{\mu} \cdot \sum_{j=1}^i J^{(n)}(\tau_j, -\mu, \varphi) \cdot e^{-(\tau - \tau_j)/\mu} \cdot \Delta\tau \end{cases} \quad \text{with } (0 < \mu \leq 1) \quad (140)$$

where  $N$  represents the number of layers used in the stratification of the propagation medium,  $\tau$  and  $\tau_j$  respectively the optical thickness at level  $i$  and  $j$ , and  $\Delta\tau$  the optical thickness increment between the two layer interfaces.

The source function  $J^{(n)}$  is computed from  $I^{(n-1)}$  as follows:

$$J^{(n)}(\tau, \mu, \varphi) = \frac{\omega_0(\tau)}{4\pi} \cdot \int_0^1 \int_{-1}^1 I^{(n-1)}(\tau, \mu', \varphi') \cdot P(\tau, \mu, \varphi, \mu', \varphi') \cdot d\mu' \cdot d\varphi' \quad (141)$$

The numerical integration of this equation is performed considering a *Fourier* series expansion in azimuth for the radiance.

Note that here, only the contribution of the elastic scattering to the source function is considered. Moreover, assuming that the atmosphere and the ocean are isotropic media where the scattering probability only depends on the scattering angle  $\theta$ , the volume scattering phase function  $P$  can be expressed as the product of scattering coefficient  $\sigma_s$  by the normalized phase function  $p$ :

$$P(\tau, \mu, \varphi, \mu', \varphi') = \sigma_s(\tau) \cdot p(\tau, \cos\theta) \quad (142)$$

with  $\cos\theta = \mu \cdot \mu' + \sqrt{1 - \mu^2} \cdot \sqrt{1 - \mu'^2} \cdot \cos(\varphi - \varphi')$

### 6.2.2.2 Fourier series expansion of the radiation field

An usual procedure for numerically solving the RTE consists in a *Fourier* series decomposition of the radiation field as a function of the azimuth [RD-53] & [RD-54]. The *Fourier* analysis allows one to separate the zenithal ( $\vartheta$ ) and azimuthal ( $\varphi$ ) angular dependence, and the RTE splits up into a set of independent equations with the zenithal angle as the unique coordinate. Each equation can then be solved independently in the *Fourier* space before to be recombined to yield to the solution in the Euclidian space.

In fact, taking the radiation field polarization into account the RTE in a plane-parallel finite medium is written as:

$$\mu \cdot \frac{d\tilde{I}(\tau, \mu, \varphi)}{d\tau} = \tilde{I}(\tau, \mu, \varphi) - \frac{\omega_0(\tau)}{4\pi} \cdot \tilde{M}(\tau, \mu, \mu_0, \Delta\varphi) \cdot \tilde{E}_s \cdot e^{\tau/\mu_0} - \frac{\omega_0(\tau)}{4\pi} \cdot \int_{-1}^1 \int_{-1}^1 \tilde{M}(\tau, \mu, \mu', \Delta\varphi) \cdot \tilde{I}(\tau, \mu', \varphi') \cdot d\mu' \cdot d\varphi' \quad (143)$$

with  $\tilde{I}$  the *Stokes* vector located in the meridian plane, the components of which are the four *Stokes* parameters ( $I, Q, U, V$ ) defined in [Section 2.5](#), and  $\tilde{M}$  the phase matrix for a given scattering direction.

Two additional matrices  $\tilde{L}(-\chi)$  and  $\tilde{L}(\chi')$  are required to rotate the meridian planes before and after scattering onto the scattering plane. In fact for an incident radiation, ( $I', Q', U', V'$ ) refers to the directions  $l'$  and  $r'$  which describe a perpendicular plane to the incident plane. Let  $\tilde{I}(\mu', \varphi')$  be the vector ( $I', Q', U', V'$ ), then to compute the scattered intensities ( $I, Q, U, V$ ) (or  $\tilde{I}(\mu, \varphi)$ ) we need to use the phase matrix  $\tilde{M}(\theta)$ . However the latter refers to the scattering plane which can differ from the incident plane. So  $\tilde{I}(\mu, \varphi)$  has to be projected in the scattering plane by applying the rotation matrix  $\tilde{L}(-\chi)$  where  $\chi$  is the angle between the incident and scattering planes. Thus the product  $\tilde{L}(-\chi) \cdot \tilde{I}(\mu, \varphi)$  defines the new *Stokes* matrix referring to the scattering plane. After scattering, we need to come back in the plane ( $l, r$ ) by applying a rotation matrix  $\tilde{L}(\pi - \chi')$  with  $\chi'$  the angle between the scattering plane and the plane of the scattered radiation.

Finally, the phase matrix for a scattering direction is:

$$\tilde{M}(\tau, \mu, \varphi, \mu', \varphi') = \tilde{L}(-\chi) \cdot \tilde{M}(\cos\theta) \cdot \tilde{L}(\chi') \quad (144)$$

where  $\tilde{M}(\cos\theta)$  represents the phase matrix in the scattering plane and  $\theta$  the scattering angle.

The rotation matrix is expressed as:

$$\tilde{L}(\chi) = \begin{bmatrix} 1 & 0 & 0 \\ 0 & \cos 2\chi & \sin 2\chi \\ 0 & -\sin 2\chi & \cos 2\chi \end{bmatrix} \quad (145)$$

Considering an isotropic medium illuminated by an unpolarized radiation beam, *i.e.*, with the *Stokes* parameters ( $E_0, 0, 0, 0$ ) and with symmetrical boundary conditions with respect to the incident plane, the *Stokes* vector components can then be developed in azimuth using a *Fourier* series expansion as follows (see [\[RD-53\]](#) & [\[RD-54\]](#) for more details):

$$\left\{ \begin{array}{l} I(\tau, \mu, \varphi) = \sum_{m=0}^M (2 - \delta_{0,m}) \cdot I_m(\tau, \mu) \cdot \cos [m \cdot (\varphi - \varphi')] + R(M) \\ Q(\tau, \mu, \varphi) = \sum_{m=0}^M (2 - \delta_{0,m}) \cdot Q_m(\tau, \mu) \cdot \cos [m \cdot (\varphi - \varphi')] + R(M) \\ U(\tau, \mu, \varphi) = \sum_{m=0}^M (2 - \delta_{0,m}) \cdot U_m(\tau, \mu) \cdot \sin [m \cdot (\varphi - \varphi')] + R(M) \\ V(\tau, \mu, \varphi) = \sum_{m=0}^M (2 - \delta_{0,m}) \cdot V_m(\tau, \mu) \cdot \sin [m \cdot (\varphi - \varphi')] + R(M) \end{array} \right. \quad (146)$$

where  $M$  is the number of terms used in the *Fourier* series expansion,  $R(M)$  the tail of the series expansion (so-called the error term), and  $\delta_{0,m}$  the Dirac's delta function which is equal to 1 for  $m = 0$  and 0 otherwise.

If the phase matrix terms are expanded in the same manner in a *Fourier* series, the RTE is then completely transformed into the following set of  $(M + 1)$  independent differential equations due to the orthogonality of the trigonometric functions:

$$\mu \cdot \frac{d\tilde{I}_m(\tau, \mu)}{d\tau} = \tilde{I}_m(\tau, \mu) - \frac{\omega_o(\tau)}{4\pi} \cdot \tilde{M}_m(\tau, \mu, \mu_o) \cdot \tilde{E}_s \cdot e^{\tau/\mu_o} - \frac{\omega_o(\tau)}{2} \cdot \int_{-1}^1 \tilde{M}_m(\tau, \mu, \mu') \cdot \tilde{I}_m(\tau, \mu') \cdot d\mu' \quad (147)$$

Thus for a black background, the resulting equations for each term  $m$  of the *Fourier* series expansion of  $\tilde{I}(\tau, \mu, \varphi)$  are expressed as:

- For the *primary scattering* ( $n=1$ ):

$$\begin{cases} \tilde{I}_m^{(1)}(\tau, \mu > 0) = \frac{1}{4\pi\mu} \cdot \int_{\tau_1}^{\tau} \omega_o(\tau') \cdot e^{-(\tau'-\tau)/\mu} \cdot \tilde{M}_m(\tau', \mu, \mu_o) \cdot E_o \cdot e^{\tau'/\mu_o} \cdot d\tau' \\ \tilde{I}_m^{(1)}(\tau, \mu < 0) = \frac{1}{4\pi\mu} \cdot \int_0^{\tau} \omega_o(\tau') \cdot e^{-(\tau-\tau')/\mu} \cdot \tilde{M}_m(\tau', -\mu, \mu_o) \cdot E_o \cdot e^{\tau'/\mu_o} \cdot d\tau' \end{cases} \quad (148)$$

- For the *multiple scattering* ( $n > 1$ ):

$$\begin{cases} \tilde{I}_m^{(n)}(\tau, \mu > 0) = \frac{1}{2\mu} \cdot \int_{\tau_1}^{\tau} \omega_o(\tau') \cdot e^{-(\tau'-\tau)/\mu} \cdot \left[ \int_{-1}^1 \tilde{M}_m(\tau', \mu, \mu') \cdot \tilde{I}_m^{(n-1)}(\tau', \mu') \cdot d\mu' \right] \cdot d\tau' \\ \tilde{I}_m^{(n)}(\tau, \mu < 0) = \frac{1}{2\mu} \cdot \int_0^{\tau} \omega_o(\tau') \cdot e^{-(\tau-\tau')/\mu} \cdot \left[ \int_{-1}^1 \tilde{M}_m(\tau', -\mu, \mu') \cdot \tilde{I}_m^{(n-1)}(\tau', \mu') \cdot d\mu' \right] \cdot d\tau' \end{cases} \quad (149)$$

The number  $(M + 1)$  of independent equations depends on the length of the scattering matrix development (*i.e.*, the number of terms used in the *Legendre* polynomial expansion). The major advantage of the *Fourier* series expansion is to reduce the angular integration to  $\mu$ . Moreover, only the zeroth terms are of interest for the flux or radiance estimates in the nadir viewing direction. According to the reciprocity principle, the nadir radiance for any solar zenithal angle  $\vartheta_s$  can be derived from the radiance at the viewing zenithal angle  $\vartheta_v$  for null solar zenith angle, which requires only one computation of the zeroth terms of the *Fourier* series. Despite the number of equations to be solved, this numerical approach allows one to save much computer times.

For each term  $m$  of the *Fourier* series expansion, the scattering phase matrix elements of  $\tilde{M}_m(\tau, \mu, \mu')$  are developed in *Legendre* polynomials as follows (see [RD-53] & [RD-54] for more details):

$$\tilde{M}_m(\tau, \mu, \mu') = \begin{pmatrix} \sum_{l=m}^L \beta_l p_l^m p_l^{m'} & \sum_{l=m}^L \gamma_l p_l^m r_l^{m'} & -\sum_{l=m}^L \gamma_l p_l^m(\mu) t_l^m(\mu') & 0 \\ \sum_{l=m}^L \gamma_l r_l^m p_l^{m'} & \sum_{l=m}^L (\alpha_l r_l^m r_l^{m'} + \zeta_l t_l^m t_l^{m'}) & -\sum_{l=m}^L (\alpha_l r_l^m t_l^{m'} + \zeta_l t_l^m r_l^{m'}) & \sum_{l=m}^L \varepsilon_l t_l^m p_l^{m'} \\ -\sum_{l=m}^L \gamma_l t_l^m p_l^{m'} & -\sum_{l=m}^L (\alpha_l t_l^m r_l^{m'} + \zeta_l r_l^m t_l^{m'}) & -\sum_{l=m}^L (\alpha_l t_l^m t_l^{m'} + \zeta_l r_l^m r_l^{m'}) & -\sum_{l=m}^L \varepsilon_l r_l^m p_l^{m'} \\ 0 & -\sum_{l=m}^L \varepsilon_l p_l^m t_l^{m'} & \sum_{l=m}^L \varepsilon_l p_l^m r_l^{m'} & \sum_{l=m}^L \delta_l p_l^m p_l^{m'} \end{pmatrix}$$

with  $\alpha_l, \beta_l, \gamma_l, \zeta_l, \varepsilon_l, \delta_l$  the sets of  $L+1$  coefficients,  $L$  a number which has to be large enough to ensure the required accuracy, and  $p_l^m, r_l^m, t_l^m$  and  $p_l^{m'}, r_l^{m'}, t_l^{m'}$  respectively expressed as  $(\tau, \mu)$  and  $(\tau, \mu')$  which are the linear combinations of the generalized *Legendre* functions. The  $\beta_l$  coefficients are used for the expansion of the phase matrix element  $P_m(\tau, \mu, \mu')$ , and coefficients  $\alpha_l, \gamma_l, \zeta_l, \varepsilon_l, \delta_l$  are used to take the atmospheric polarization into account.

## 7. DESCRIPTION OF RTC/UDL

In the framework of the MERIS project, the RTC/UdL package was initially devoted to the pixel identification algorithm used at the level-2 processing for improving some basic classifications available at level-1b (see [AD-2] for more details). This tool package allows one to simulate the optical properties of the atmospheric and oceanic constituents and to compute the reflectance LUTs over several surface states (e.g., land, sea surface, oceanic composition) for a wide range of viewing and illumination configurations and atmospheric conditions (e.g., aerosols, clouds, water vapor). These simulations are of a particular interest to generate the thresholds and the coefficients useful for the discrimination between the different targets such as land-water surfaces, bright over ocean (e.g., sun glint, sea-ice), bright over land (e.g., sand, ice-snow), DDV (dense dark vegetation), and cloud heterogeneities. A main objective in the MERIS project is a better discrimination between the remotely sensed targets in order to correctly apply the atmospheric correction scheme or to better retrieve the atmospheric optical characteristics (e.g., aerosol optical depth) and ground surface properties.

RTC/UdL package is composed of two principal modules:

- *SCAMAT* module: This allows one to compute the optical properties (i.e., scattering phase function, extinction and scattering coefficients, and forward scattering proportion) for a mixture of  $N$  particle size distributions of atmospheric or oceanic constituents at a selected wavelength according to the *Mie's* theory.
- *UPRAD* module: This simulates the radiative transfer within a multi-layered '*Atmosphere-Land/Ocean*' system both using the DOM and SO techniques. All physical processes (single and multiple scattering, gaseous absorption, etc.) are accounted for in the computation of upwelling radiances at TOA.

These two modules are detailed in the following sections.

### 7.1 SCAMAT MODULE

#### 7.1.1 Description

This module allows one to compute the scattering phase matrix  $P(\lambda, r, n, \theta)$  and optical properties (i.e., the single scattering albedo  $\omega_0(\lambda, r, n)$  and the extinction coefficient  $\sigma_e(\lambda, r, n)$ ) for a mixture of  $N$  particle size distributions at a given wavelength  $\lambda$ . Each particle size distribution  $n_i(r)$  is characterized by a complex refractive index ( $n_{i,\lambda} = m_{i,\lambda} - i k_{i,\lambda}$ ), which is assumed to be identical for all the scatterers within the same distribution, and a component mixing ratio ( $n_i / n$ ). This computation is performed with the *Mie's* theory, assuming particles as homogeneous isotropic spheres the sizes of which are comparable to or larger than the incident wavelength.

Moreover, it allows to calculate as well the forward scattering proportion  $f_{sp}(\mu = 0)$  of a mixture of aerosols by using its computed scattering phase matrix  $P(\lambda, r, n, \theta)$ .

#### 7.1.2 Tool

The latest version of Mie/UdL package (available since July 27, 1999 – last release in March 31, 2009) is composed of:

- '*scamat.f*': for the *Mie's* computations,



- **'compute\_FSP.f'**: for the computation of the forward scattering proportion  $f_{sp}(\mu = 0)$  of a given scattering phase matrix  $P(\lambda, r, n, \theta)$ .

Only the scamat sub-module is detailed in the following section. A full I/O description for each of these two codes is given in Appendix 1 (Sections 9.1).

### 7.1.3 Mie processing

The *Mie's* processing is depicted in Figure 16. A complete description of the input / output data is provided in Appendix 1.

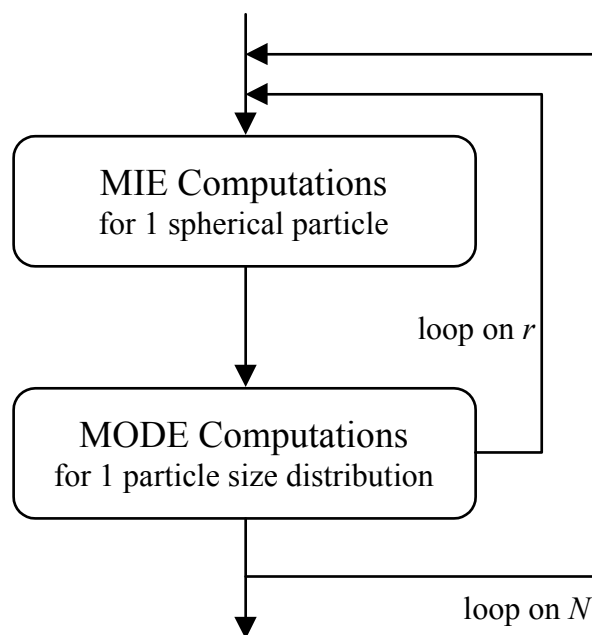


*Figure 16: Flowchart of the Mie processing*

#### • Sub-module MIE:


The *Mie's* theory fully describes the interaction of an incident electromagnetic wave with an homogeneous isotropic and absorbing sphere, the size of which is comparable to or larger than the incident wavelength.

Assuming the atmospheric or oceanic scatterer (*i.e.*, aerosol, cloud droplet, or sediment and phytoplankton) as an homogeneous isotropic sphere, its optical properties  $(\omega_{o,\lambda}, \sigma_{e,\lambda}, P_{\lambda}(\theta))$  can then be computed using this theory (*see* Section 2.8 for more details).

#### • Sub-module MODE:

Let us consider now a sample of identical particles, the sizes of which are described by a size distribution. Several size distributions are proposed to the operator (*see* Section 3.2.2):

- the *Junge power-law* function (for the simple tropospheric aerosols),
- the *Modified Gamma* distribution function (for the stratospheric aerosols and clouds),
- the *Log-Normal* distribution function (for the tropospheric aerosols including several modes).

|   |  |  |
|---|--|--|
|  | <b>MERIS/ ENVISAT-1</b><br>Medium Resolution Imaging<br>Spectrometer | <u>Ref.:</u> PO-RS-PAR-GS-0003<br><u>Issue:</u> 4 <u>Rev.:</u> A<br><u>Date:</u> 16-Dec-10 <u>Page:</u> 74 |
|---|--|--|

Once the size distribution selected, a loop on the particle sizes  $r$  is then performed to compute the optical scattering parameters of the sample: single scattering albedo, extinction coefficient and normalized phase function (see Section 3.1.1.1 for more details).

• *Loop on  $N$  (the number of components):*

For a mixture of several particles (or components) originating from different sources ( $N_{max} = 3$ ), a second loop on the number of components  $N$  allows then to compute the resulting optical properties of the mixture using a mixing ratio (see Section 3.2.1.2 for more details):

From the basic atmospheric constituents (desert dust, dust-like, oceanic, water soluble, soot-like), aerosol models can be built up by homogeneously mixing. Six typical aerosol models are already set up in this module, *i.e.*, maritime, coastal, rural, dust, continental and stratospheric models (see Section 3.2.3). The operator can also build up his own aerosol model using up to 3 components.

## 7.2 UPRAD MODULE

### 7.2.1 Description

The RTC/UPRAD allows one to simulate the upwelling normalized radiances ( $sr^{-1}$ ) at TOA over several surface states (land, sea surface, oceanic composition) for various atmospheric conditions (aerosols, clouds, water vapor) and viewing and illumination configurations. The spectral irradiance at TOA is fixed to  $1 \text{ W m}^{-2} \mu\text{m}^{-1}$  in the code, and a flag was included to activate or not the computation of polarization processes.

According to the selected input value for the  $i\_branch$  parameter, this module calls one of the three following specific sub-modules (Figure 18):

- **GAME:** the *Global Absorption Model* used to account for coupling between scattering and gaseous absorption,
- **SO:** the *Successive Orders* method used to compute the single and multiple scattering within the atmosphere,
- **SOAO:** the *Successive Orders* method for a coupled 'Atmosphere-Ocean' system based on the same approach as the SO technique.

Upwelling radiances over ocean under a clear-sky condition ( $i\_branch=2$ ) is computed either with the SO or SOAO code depending on the total extinction coefficient value of the oceanic medium. In the case where this total oceanic extinction is null, the SO sub-module is then selected to simulate upwelling radiances over a wind-roughened sea surface including or not the sun glint water reflectance (see Section 5; Note that a sun glint flag has to be raised in the SO code to include the direct-direct contribution in the TOA normalized radiances). Otherwise, the oceanic components are taking into account and radiative transfer within a coupled 'Atmosphere-Ocean' system is then computed with the SOAO code. Over land with a clear-sky condition ( $i\_branch=1$ ) the SO code is used to simulate upwelling radiances for a purely scattering atmosphere (*i.e.*, without gaseous absorption), whereas the GAME code is selected for an absorbing atmosphere ( $H_2O$ ,  $O_2$  and  $O_3$ ). GAME is also the unique sub-module for the treatment of the cloud ( $i\_branch=3$ ) or water vapor ( $i\_branch=4$ ) conditions. Moreover the atmospheric transmittances (diffuse, direct and total) over land/ocean and the primary scattering radiances over land ( $i\_branch=11$ ) can be computed for clear-sky conditions with RTC/SO.

## 7.2.2 Tools

The latest version of the RTC/UdL package (available since July 27, 1999 – last release in March 31, 2009) is composed of:

- **'rtc\_uprad.f'**: the main code for the radiative transfer computations,
- **'rtc\_game.f'**: for the GAME computations,
- **'rtc\_so.f'**: for the SO computations within the *atmosphère*,
- **'rtc\_soao.f'**: for the SO computations within the coupled '*Atmosphère-Océan*' system,
- **'rtc\_gauss.f'**: for the computation of the *Gauss* quadrature (angles and weights),
- **'step1.f', 'step2.f', 'step3.f', 'step4.f'** (RTC/Wind package):  
for the computation of the *Fourier* series expansion of the *Fresnel* reflexion matrix for a *Cox-Munk* surface model (wind-roughened sea surface),
- **'rtc\_po2.f'**: for the computation of the transmittance integrated over the oxygen band (only used with MERISAT for the LUTs generation)
- **'otc\_rayleigh.f'**: for the total *Rayleigh* optical thickness computation,
- **'otc\_ozone.f'**: for the total ozone optical thickness computation,
- **'iop\_water.f'**: for the computation of the optical properties of the oceanic components,

Only the first four sub-modules are detailed in the following sections. A full I/O description for all these sub-modules is given in Appendix 1 ([Sections 9.2 & 9.4](#)).

## 7.2.3 RTC/GAME

The *correlated k-distribution* method allows an accurate treatment of the overlapping atmospheric gaseous absorption and of the non-grey absorption for multiple scattering media. Transmission function can be approximated by the following ESFT (see [Section 2.9](#)):

$$T(u) = \sum_{l=1}^N a_l \cdot e^{-k_l \cdot u} \quad (150)$$

For each term of this exponential sum, the RTE is solved using the absorption coefficient  $k_l$  which yields to the optical thickness of the corresponding atmospheric gas. Numerous tests stressed that seven exponential terms ( $N = 7$ ) gives a good compromise between accuracy and computer time.

The RTE resolution in an horizontally homogeneous scattering atmosphere is achieved in the plane-parallel approximation using the DOM (see [Section 6.2.2](#) and [\[RD-52\]](#)) which employs a *Legendre* polynomial decomposition for the phase function and the radiance. Selection of sixty terms ( $I_s = 60$ ) in the *Legendre* expansion and a *Diraç's* delta truncature (see [Section 2.3.2](#)) are used to approximate the exact scattering phase function of clouds and aerosols and to compute the upwelling radiances.

Vertical profile (*i.e.*, 33 atmospheric layers according to the MLS atmosphere) of the extinction optical thickness, single scattering albedo and terms of the *Legendre* polynomial decomposition are derived from the optical properties of atmospheric constituents (aerosols, clouds and molecules) and gaseous absorption coefficients ( $H_2O, O_2$  and  $O_3$ ). These data are then used as input to the DOM. The mixture of absorbing and scattering components is defined as:

$$\tau_s = \tau_s^a + \tau_s^c + \tau_s^m \quad (151)$$

$$\tau_a = \tau_a^a + \tau_a^c + \tau_a^g \quad (152)$$

$$\omega_0 = \frac{\tau_s}{\tau_a + \tau_s} \quad (153)$$

$$m_l = \frac{1}{\tau_s} \cdot [m_l^a \cdot \tau_s^a + m_l^c \cdot \tau_s^c + m_l^m \cdot \tau_s^m] \quad (154)$$

with  $\tau$  the optical thickness,  $\omega_0$  the single scattering albedo and  $m_l$  the term at the order  $l$  in the *Legendre* polynomial decomposition. The exponents  $a$ ,  $c$ ,  $m$  and  $g$  refer to aerosol, cloud, molecule and gas component respectively, and subscript  $a$  and  $s$  to the absorbing and scattering processes. Of course, these parameters are defined in each layer of the atmospheric profile.

Note that this code is specially devoted to the radiative transfer computations within the clouds and the absorbing atmospheres. Although a depolarization factor  $\delta$  of 0.0279 is included in the *Rayleigh* phase function, the RTC/GAME does not take the polarization processes into account. Consequently, only the  $\beta$  coefficient is used for the *Legendre* polynomial decomposition of the phase function and the radiance.

## 7.2.4 RTC/SO

The RTC/SO solves the RTE (Equation 142) within an atmospheric medium. The *Fourier* series expansion of this equation allows one to separate the angular variables ( $\vartheta, \varphi$ ) for the integral computation (see Section 6.2.2.2 for more details). This yields to a set of  $(M+1)$  independent equations which only depends on the zenithal angle ( $\vartheta$ ). The upwelling and downwelling radiances are then computed for each term  $m$  of the *Fourier* series. A great advantage of this method is that the first term ( $m=0$ ) of the series directly provides the scattered flux. The length of the *Fourier* series depends on the number of *Legendre* terms ( $I_s = 79$  in the SO code) used to describe the scattering phase matrix.

### • Primary scattering

The upwelling  $L_m^{\uparrow(1)}$  and downwelling  $L_m^{\downarrow(1)}$  radiances arising from primary scattering ( $n=1$ ) are computed for each term  $m$  of the *Fourier* series as follows (see Section 6.2.2.2):

$$\begin{cases} L_m^{\uparrow(1)}(\tau, \mu > 0) = \frac{\omega_0}{4\pi\mu} \cdot \tilde{E}_s \cdot \int_{\tau_1}^{\tau} e^{\tau'/\mu_0} \cdot e^{-(\tau-\tau')/\mu} \cdot \tilde{M}_m(\tau', \mu, \mu_0) \cdot d\tau' \\ L_m^{\downarrow(1)}(\tau, \mu > 0) = \frac{\omega_0}{4\pi\mu} \cdot \tilde{E}_s \cdot \int_0^{\tau} e^{\tau'/\mu_0} \cdot e^{-(\tau-\tau')/\mu} \cdot \tilde{M}_m(\tau', -\mu, \mu_0) \cdot d\tau' \end{cases} \quad (155)$$

where  $\tau_1$  is the total optical depth of the medium,  $\omega_0$  the single scattering albedo. The *Stokes* vector  $\tilde{E}_s = (E_0, 0, 0)$  of the incident solar beam is unpolarized and  $E_0$  represents the extraterrestrial solar irradiance.

### • Multiple scattering

For the multiple scattering ( $n > 1$ ), the upwelling  $L_m^{\uparrow(n)}$  and downwelling  $L_m^{\downarrow(n)}$  radiances at the order  $n$  provide from the signal contributions at the order  $(n-1)$ . Thus for a given order  $n$  the signal is integrated over  $\mu'$  and  $\tau$  as follows (see Section 6.2.2.2):

$$\left\{ \begin{array}{l} L_m^{\uparrow(n)}(\tau, \mu > 0) = \frac{\omega_0}{2\mu} \cdot \int_{\tau_1}^{\tau} e^{-(\tau'-\tau)/\mu} \cdot \left[ \int_{-1}^1 \tilde{M}_m(\tau', \mu, \mu') \cdot L_m^{(n-1)}(\tau', \mu') \cdot d\mu' \right] \cdot d\tau' \\ L_m^{\downarrow(n)}(\tau, \mu > 0) = \frac{\omega_0}{2\mu} \cdot \int_0^{\tau} e^{-(\tau-\tau')/\mu} \cdot \left[ \int_{-1}^1 \tilde{M}_m(\tau', -\mu, \mu') \cdot L_m^{(n-1)}(\tau', \mu') \cdot d\mu' \right] \cdot d\tau' \end{array} \right. \quad (156)$$

The integration with respect to  $\mu'$  is performed using a *Gaussian* quadrature with 24 angles for each of two semi-hemispheres (lower and upper) and the computation with respect to  $\tau$  is accomplished by dividing the atmosphere into  $N$  optically homogeneous layers. Due to the fact aerosols and molecules in the atmosphere present different vertical distributions, these  $N$  layers are non-homogeneous. Of course higher is the  $N$  value more accurate will be the results of the numerical integration on  $\tau$  but more time-consuming is the computation. Sensitivity studies stressed the discretization of the atmosphere into 26 layers is the best compromise [RD-53][RD-54].

### • Vertical discretization of the atmosphere

In the current RTC/SO version, the atmosphere is deliberately layered into 33 levels. The Rayleigh optical depth  $\tau_R(z)$  is vertically distributed along  $z$  according to an exponential law:

$$\tau_R(z) = \tau_R(0) \cdot e^{-z/H_R}$$

where  $H_R$ , the molecular scale height, varies with the altitude. The standard  $H_R$  value in the troposphere is taken to be equal to  $7.9 \text{ km}$ .  $\tau_R(0)$  is the total *Rayleigh* optical thickness at ground level. The same formulation applies to the molecular extinction coefficient,  $\sigma_R(z)$ :

$$\sigma_R(z) = \frac{\tau_R(0)}{H_R} \cdot e^{-z/H_R}$$

As for the aerosols, these scatterers are distributed either within a unique layer for the whole atmosphere or in 3 major layers (boundary, troposphere and stratosphere). Two vertical distributions of scatterers are then defined according to the number of aerosol layers selected:

#### - Case of 1 aerosol layer:

As for the molecules, the aerosols are exponentially distributed along  $z$  with a scale height ( $H_a$ ) of  $2 \text{ km}$  over land (*resp.*,  $3 \text{ km}$  over ocean) following Equation (114). The *Rayleigh* ( $\alpha_R(z)$ ) and aerosol ( $\alpha_a(z)$ ) mixing rates at level  $z$  are then computed as:

$$\left\{ \begin{array}{l} \alpha_a(z) = 1 - \alpha_R(z) \\ \alpha_R(z) = \frac{\sigma_R(z)}{\sigma_R(z) + \sigma_a(z)}, \text{ with } \sigma_a = \frac{\tau_a(0)}{H_a} \cdot e^{-z/H_a} \end{array} \right.$$

and  $\tau_a(0)$  is the total aerosol optical thickness at ground level.

#### - Case of 3 aerosol layers:

The aerosols are assumed to be homogeneously distributed within the 3 majors layers. A schematic representation of this atmosphere is displayed in [Figure 17](#):

- *the stratosphere (Layer#1)* above the troposphere, located around  $z_2$ ,
- *the troposphere (Layer#2)* above the boundary layer,
- *the boundary layer (or the mixing layer, layer#3)*, between the surface level ( $z_0$ ) and the altitude  $z_1$  where the inversion of temperature occurs.

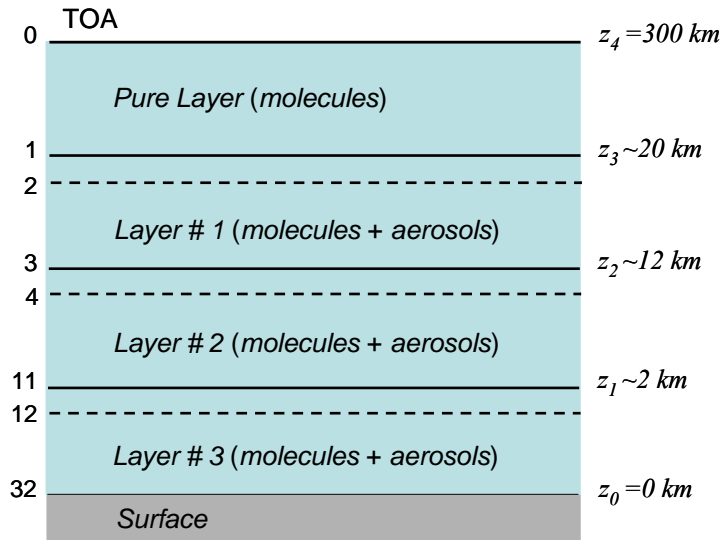


*Figure 17: Schematic representation of the «3 aerosol-layers» atmosphere over ocean*

In the RTC/SO, the surface is at sea level ( $z_0=0 \text{ km}$ ) and the tropospheric layer is bounded by the lower surface at  $z_1=1.902 \text{ km}$  and the upper surface at  $z_2=12.927 \text{ km}$ . These values remain acceptable considering that the altitudes of the mixing layer and the troposphere vary. More the atmosphere above  $z_3=20 \text{ km}$  is assumed to be a free-stratospheric aerosol layer. The TOA is located at  $z_4=300 \text{ km}$ . This atmosphere is then discretized into 32 elementary sub-layers. In order to assure a continuity of the extinction coefficient ( $\sigma$ ) of the light propagated between two consecutive major aerosol layers, an infinitesimal sub-layer has been introduced at the transition. The schematic distribution of the atmosphere is proposed as follows:

- a pure molecular atmosphere (1 sub-layer) between ( $z_3+10^{-7}$ ) and  $z_4$ ,
- a transition layer (1 optically thin sub-layer) between  $z_3$  and ( $z_3+10^{-7}$ ), with  $\sigma(z_3+10^{-7})=\sigma_R(z_3)$  and  $\sigma(z_3)=\sigma_R(z_3)+\sigma_3$ (1 sub-layer),
- a stratospheric layer (1 sub-layer) between  $z_3$  and ( $z_2+10^{-7}$ ),
- a transition layer (1 optically thin sub-layer) between  $z_2$  and ( $z_2+10^{-7}$ ) km, with  $\sigma(z_2+10^{-7})=\sigma_R(z_2)+\sigma_3$  and  $\sigma(z_2)=\sigma_R(z_2)+\sigma_2$ (1 sub-layer),
- a tropospheric layer (8 sub-layers) between  $z_2$  and ( $z_1+10^{-7}$ ) km,
- a transition layer (1 optically thin sub-layer) between  $z_1$  and ( $z_1+10^{-7}$ ) km, with  $\sigma(z_1+10^{-7})=\sigma_R(z_1)+\sigma_2$  and  $\sigma(z_1)=\sigma_R(z_1)+\sigma_1$ (1 sub-layer),
- a boundary layer (19 sub-layers) between  $z_1$  and  $z_0$ .

with  $\sigma_1$ (1 sub-layer),  $\sigma_2$ (1 sub-layer) and  $\sigma_3$ (1 sub-layer) the extinction coefficient for an elementary sub-layer within the aerosol layer #1 (boundary), #2 (troposphere) and #3 (stratosphere) respectively. The Rayleigh ( $\alpha_R(z)$ ) and aerosol ( $\alpha_a^i(z)$ ) mixing rates for an elementary sub-layer from the aerosol layer  $i$  ( $i=1, 2$  and  $3$ ) are then computed as: ( $\alpha_a^i(z)$ )  $\alpha_R(z)$

$$\begin{cases} \alpha_a^i(z) = \frac{\omega_o^i \cdot \sigma_a^i(z)}{\sigma_R(z) + \sigma_a^i(z)} \\ \alpha_R(z) = \frac{\sigma_R(z)}{\sigma_R(z) + \sigma_a^i(z)} \end{cases}, \text{ with } \sigma_a^i(z) = \tau_a(0) \cdot \frac{z}{z_i - z_{i+1}}$$

Figure 19 displays the flowchart of the RTC/SO. Using the inputs described in Appendix 1 (Section 9.1), the mixing rates (defined as the ratio of the scattering coefficient of an atmospheric component to the sum on the extinction coefficients of all the atmospheric components) of aerosol and molecular optical properties are then computed for each atmospheric layer to generate the corresponding primary scattering source functions at each *Gauss* angle ( $\mu'$ ). Then the computation of the upwelling  $L_m^{\uparrow(1)}$  and downwelling  $L_m^{\downarrow(1)}$  primary scattering radiances ( $n = 1$ ) within the layer is performed for each term  $m$  of the *Fourier* series. At this step starts the iterative process to determine the contribution of multiple scatterings ( $n > 1$ ) to the upwelling  $L_m^{\uparrow(n)}$  and downwelling  $L_m^{\downarrow(n)}$  radiances.

### • Convergence tests

For a given term  $m$  of the *Fourier* series, the iterative process over the successive orders of scattering ( $n > 1$ ) is broken as soon as one of the two following criteria applied to the first *Stokes* parameter is verified:

- *Test 1:* This test (namely '*weakness of signal*' in Figure 19) compares the radiance contribution at the order  $n$  with the sum of the contributions from all the previous orders as follows,

$$\left| \frac{L_m^{(n)}(\tau, \mu_v)}{\sum_{i=0}^{n-1} L_m^{(i)}(\tau, \mu_v)} \right| < 10^{-5} \quad (157)$$

- *Test 2:* This test (namely '*convergence*' in Figure 19) examines if the radiance contribution from the successive orders of scattering converge into a geometrical series. If this is the case, the iterations are then stopped and the tail of the geometrical series is added to the contribution of the scattering order for which the convergence was detected. Generally, this test is often firstly checked and greatly reduces the computational time. Convergence is reached at the order  $n$  if the ratio of the current to the previous order contributions verifies,

$$\left| \frac{L_m^{(n)}(\tau, \mu_v)}{L_{m-1}^{(n)}(\tau, \mu_v)} - \frac{L_{m-1}^{(n)}(\tau, \mu_v)}{L_{m-2}^{(n)}(\tau, \mu_v)} \right| < 10^{-2} \quad (158)$$

Note that the order of scattering is very dependent on the solar zenithal angle. In fact, lower is the sun in the sky (*i.e.*, for the largest solar zenithal angles), higher is the maximum order of scattering ( $n_{max}$ ). Tests stressed the iterative process could be broken for a  $n_{max}$  value of 200.

The following step consists in a recombination of the solution (*i.e.*, a sum on the *Fourier* series) for the lower and upper hemispheres, which is resampled to input viewing angles using a spline interpolation scheme. A last test of convergence is then added to determine the truncation of the *Fourier* series expansion. This test is applied to the upwelling radiance simulated in the specular direction ( $\Delta\phi = 180^\circ$ ) expressed as:

$$L(\mu, \mu_0, 180) = \sum_{m=0}^{\infty} (2 - \delta_{0,m}) \cdot L_m(\mu, \mu_0) \quad (159)$$

Convergence is achieved if the contribution of a given term  $m$  verifies:

$$\frac{L_m}{L} < 10^{-4} \quad (160)$$

For a land case the ground surface is assumed to be *Lambertian* and is characterized by its reflectance. Over black ocean, the wind-roughened sea surface is described by the *Cox & Munk* wave slope distribution (see Section 5). A sophisticated *Fourier* series expansion of the reflection matrix combined with the wave slope distribution function is then achieved using the wind speed (see [RD-53] & [RD-54] for more details).

## 7.2.5 RTC/SOAO

The RTC/SOAO solves the RTE within a coupled '*Atmosphere-Ocean*' system for which the interface is assumed to be plane. The boundary conditions through the *air-water* interface are modeled according to the *Snellius-Fresnel* laws described in Section 2.10. The refractive index ( $n_w$ ) of the sea water is assumed to be constant whatever the wavelength and equal to 1.34, whereas for the air this index ( $n_a$ ) is taken to be equal to 1. For a flat surface, the reflection ( $r_{//}, r_{\perp}$ ) and transmission ( $t_{//}, t_{\perp}$ ) coefficients are given by the *Fresnel* formulas (see Equations 86 and 87).

The polarization of the signal due to the specular reflection at the *air-water* interface is accounted for in the RTC/SOAO by treating radiance as a vector ( $\tilde{L}$ ). So the *Fresnel* reflection matrix ( $R$ ) on the sea water surface and transmission matrix ( $T$ ) from *air* to *water* are computed according to Equations (88). These matrices are expressed in the reflection plane (*i.e.*, the meridian plane). More, due to the fact that for a specular reflexion the terms of the *Fourier* series expansion are constant, these matrices then correspond to the *Fourier* series terms.

Thus for an horizontal sea surface, an incident atmospheric beam will be partly reflected in the specular direction and the other part will be refracted in the water. These boundary conditions at sea level becomes:

$$\begin{cases} \tilde{L}^{\uparrow}(\tau_1, -\mu_0, \varphi) = R(\mu_0, n_w) \cdot \tilde{L}^{\downarrow}(\tau_1, \mu_0, \varphi) \\ \tilde{L}^{\downarrow}(\tau_1^w, \mu_0^w, \varphi) = n_w^2 \cdot T(\mu_0, n_w) \cdot \tilde{L}^{\downarrow}(\tau_1, \mu_0, \varphi) \end{cases} \quad (161)$$

where  $\tau_1$  and  $\tau_1^w$  are the optical depths of the atmosphere and the ocean respectively,  $\mu_0$  and  $\mu_0^w$  the cosine of incident and refracted (in the water) zenithal angles respectively ( $\mu_0 < 0$  and  $\mu_0^w < 0$ ).

The terms describing the specular reflection at the plane *air-water* interface, which are the second source for the primary scattering, are defined as:

$$\begin{cases} L_m^{(1)\uparrow}(\tau, \mu > 0) = \frac{\omega_0}{4\pi\mu} \cdot R(\mu_0, n_w) \cdot \tilde{E}_s \cdot e^{\tau_1/\mu_0} \cdot \int_{\tau_1}^{\tau} e^{(\tau_1-\tau')/\mu_0} \cdot e^{-(\tau-\tau')/\mu} \cdot \tilde{M}_m(\tau', \mu, \mu_0) \cdot d\tau' \\ L_m^{(1)\downarrow}(\tau, \mu > 0) = \frac{\omega_0}{4\pi\mu} \cdot R(\mu_0, n_w) \cdot \tilde{E}_s \cdot e^{\tau_1/\mu_0} \cdot \int_0^{\tau} e^{(\tau_1-\tau')/\mu_0} \cdot e^{-(\tau-\tau')/\mu} \cdot \tilde{M}_m^w(\tau', -\mu, \mu_0) \cdot d\tau' \end{cases} \quad (161)$$

The incident in-water source is the solar irradiance attenuated by the two media (atmosphere + water) and transmitted into the water. The upwelling and downwelling radiances in the water are expressed as follows:



$$\left\{ \begin{array}{l} L_m^{(1)\uparrow}(\tau, \mu^w > 0) = \frac{\omega_o}{4\pi\mu^w} \cdot T(\mu_o, n_w) \cdot \tilde{E}_s \cdot e^{\tau_1/\mu_o} \cdot \int_{\tau_1+\tau_w}^{\tau} e^{(\tau'-\tau_1)/\mu_o^w} \cdot e^{-(\tau'-\tau)/\mu^w} \cdot \tilde{M}_m^w(\tau', \mu^w, \mu_o^w) \cdot d\tau' \\ L_m^{(1)\downarrow}(\tau, \mu^w > 0) = \frac{\omega_o}{4\pi\mu^w} \cdot T(\mu_o, n_w) \cdot \tilde{E}_s \cdot e^{\tau_1/\mu_o} \cdot \int_{\tau_1}^{\tau} e^{(\tau'-\tau_1)/\mu_o^w} \cdot e^{-(\tau-\tau')/\mu^w} \cdot \tilde{M}_m^w(\tau', -\mu^w, \mu_o^w) \cdot d\tau' \end{array} \right. \quad (162)$$

where  $\tilde{M}^w$  is the scattering phase matrix of the oceanic particles.

Thus for the primary scattering, the total upwelling radiance at TOA is then the sum of the atmospheric scattering radiances (Equations 154 and 160) and the water leaving radiance (Equation 161) for which the refraction law is applied. This total upwelling radiance is then attenuated in the atmospheric path:

$$L_m^{(1)\uparrow}(\tau, \mu) = T(\mu^w) \cdot L_m^{(1)\uparrow}(\tau, \mu^w) / n_w^2 \quad (163)$$

As concerns the downwelling radiance in the water, the latter is computed using the downwelling atmospheric radiance (sources of which comes from the direct solar beam and the specular reflection at the *air-sea* interface) at the sea level (Equations 154 and 160). Conversely this downwelling radiance increases by a factor  $n_w^2$  in the direction *air* to *water* before being attenuated in the water.

$$L_m^{(1)\downarrow}(\tau, \mu^w) = n_w^2 \cdot T(\mu) \cdot L_m^{(1)\downarrow}(\tau, \mu) \quad (164)$$

The boundary conditions at the bottom of the atmosphere (BOA) depend on the presence of the foam (*i.e.*, white caps) which is considered as a *Lambertian* reflector, whereas for the ocean these rely on the bottom also assumed to be *Lambertian*. Strictly speaking, the primary scattering should include the first interaction of the reflected solar beam by the foam in the atmosphere as well as for the reflection by the sea bottom. Because of the isotropic nature of the reflected radiance, Equations (160) and (161) are not directly applied. For a numerical convenience these terms will be computed in the multiple scattering module.


The different contributions to the primary scattering for the upward atmospheric path radiance are depicted in [Figure 20](#). In this case, the direct solar beam being the unique source of the downwelling atmospheric radiance, each of these contributions can be computed using Equations (154) and (160).

In [Figure 21](#) are summarized the different contributions for the downward water path radiance. For the leaving water radiance (not shown), only the direct solar beam is considered in the computation.

The relevant equations for the multiple scattering are similar to Equations (155) for which the source function is the scattering radiance at the  $(n-1)$  order. As an example, the second scattering in the air will have as the source function, (*i*) the primary scattering for the atmospheric upwelling ([Figure 20](#)) and downwelling radiances and (*ii*) the isotropic radiance reflected by the foam and the sea bottom. This last term is unpolarized and just introduced for  $m=0$  (isotropy).

For the coupled '*Atmosphere-Ocean*' system, there are boundary conditions at the *air-water* interface as well as in each medium. Numerically, the interface can be considered as an infinitely thin layer (*i.e.*, with an optical depth of  $10^{-7}$ ). This permits then the application of the *Fresnel's* equations from a medium to another. Due to the fact that the refractive indices of the air and water differ, the refracted angles in the ocean do not correspond to the atmospheric *Gaussian* angles. Consequently, these angles need to be adjusted using a polynomial interpolation (spline method) in order to use the *Gauss* quadrature below the *air-water* interface.

As for the atmosphere (*see* [Section 7.2.4](#) for more details), the ocean is discretized into a finite number of layers with an identical optical thickness but not necessarily homogeneous depending on the vertical profile of the oceanic constituents (phytoplankton, sediment, *etc.*). Because the ocean is optically denser

|   |  |  |
|---|--|--|
|  | <b>MERIS/ ENVISAT-1</b><br>Medium Resolution Imaging<br>Spectrometer | <u>Ref.:</u> PO-RS-PAR-GS-0003<br><u>Issue:</u> 4 <u>Rev.:</u> A<br><u>Date:</u> 16-Dec-10 <u>Page:</u> 82 |
|---|--|--|

than the atmosphere (the optical depth in the water could exceed 10), the number of layers required for accurate computations of the oceanic radiative transfer is then greater than the number of atmospheric layers. Tests carried out over a purely scattering ocean (which is admittedly unrealistic) stressed the need of around 80 oceanic layers for accurate computations.

In order to reduce the computational time, the convergence criteria from the RTC/SO (Equations 156, 157 and 159) are employed in the RTC/SOAO, but with a threshold of  $10^{-6}$  for *Test 1* and a maximum order of scattering ( $n_{max} = 10^4$ ).

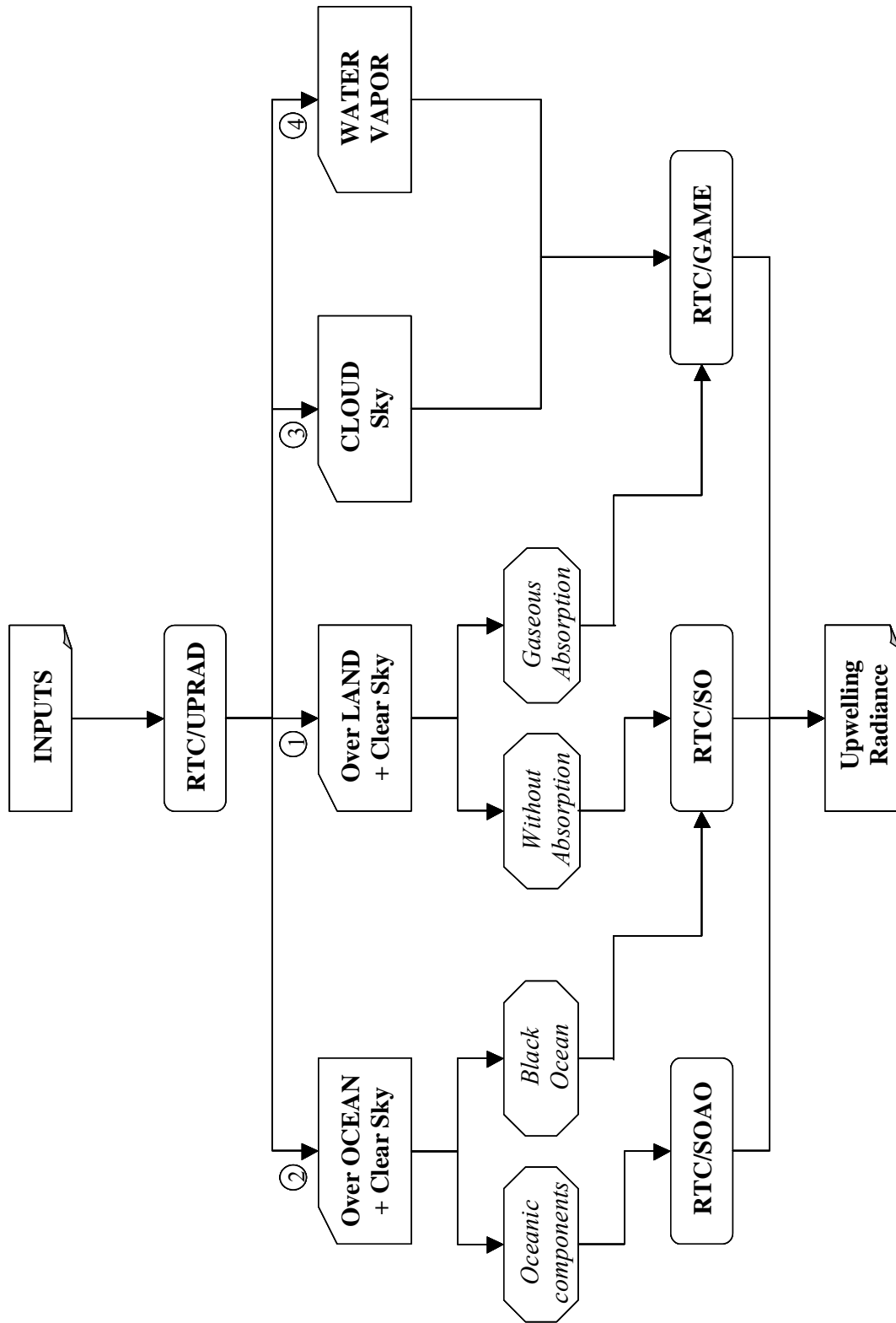


Figure 18: Flowchart of the RTC/UdL.

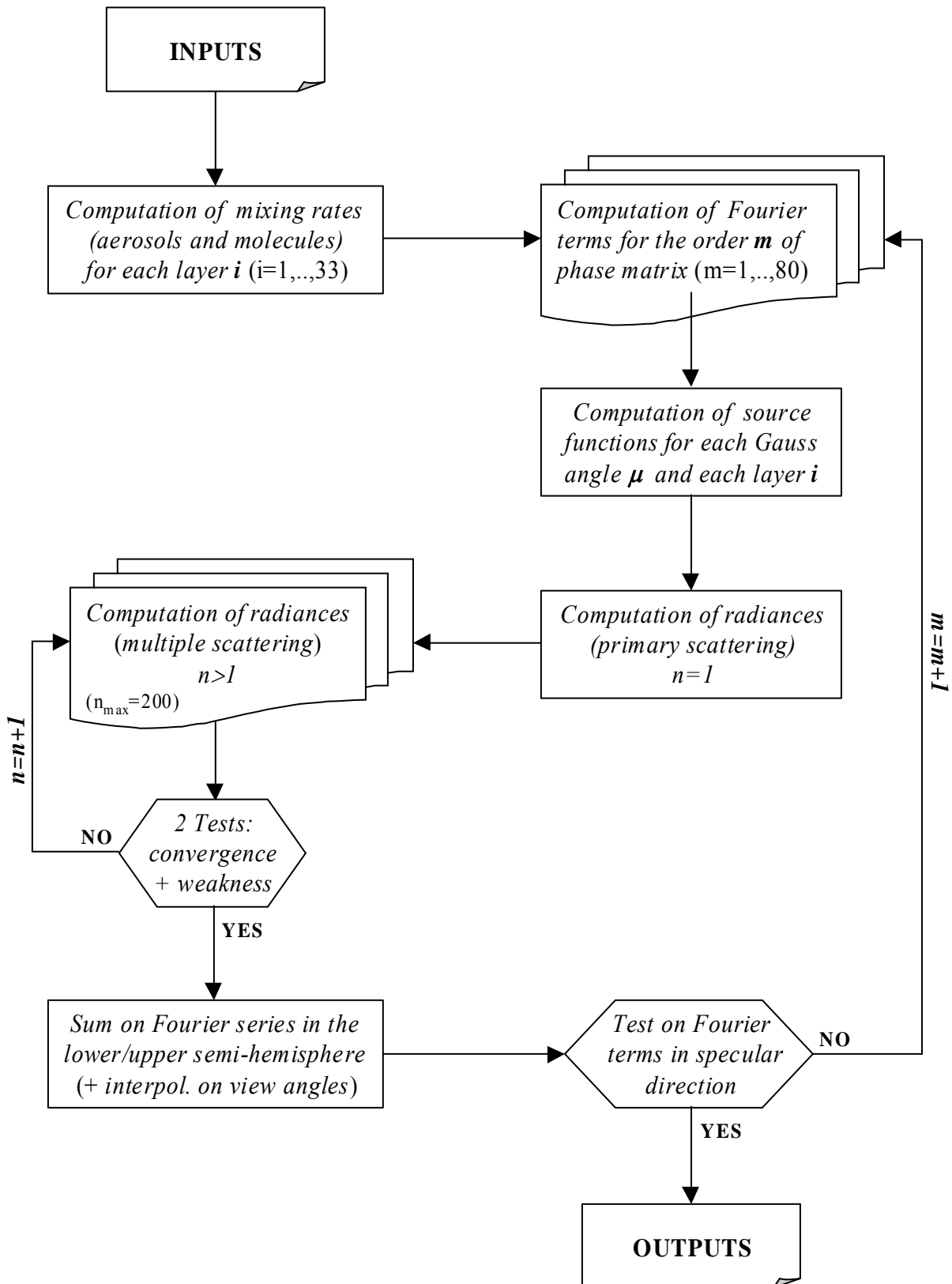
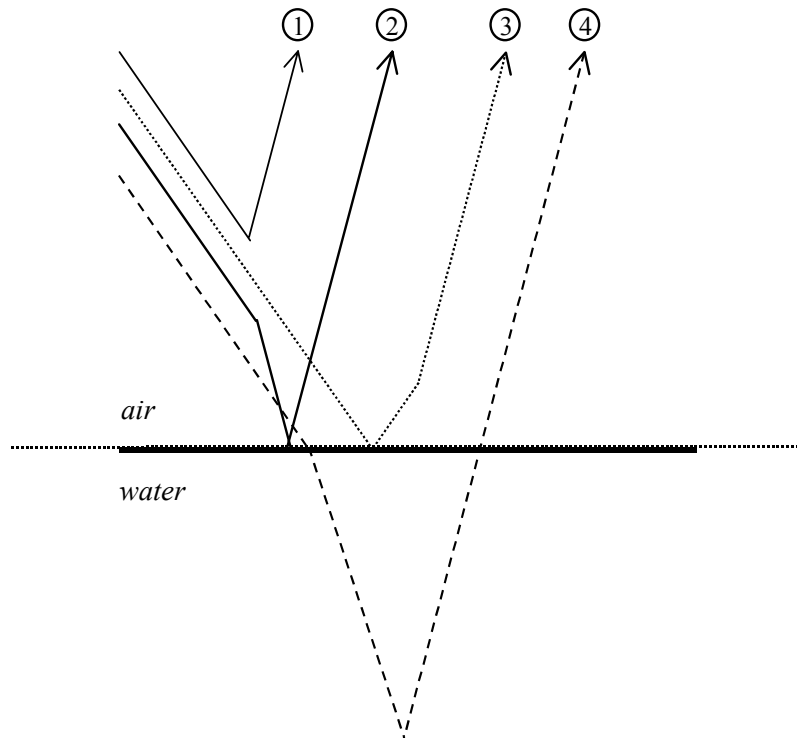
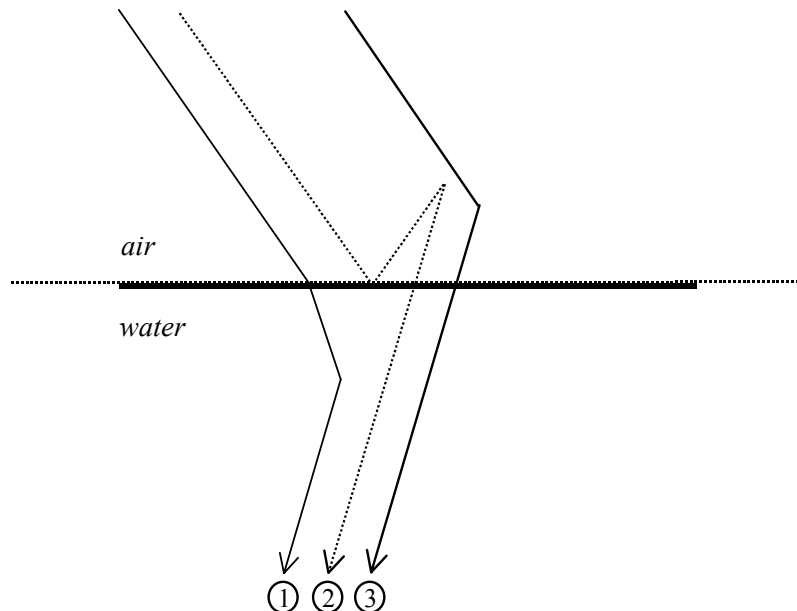


Figure 19: Flowchart of the RTC/SO



*Figure 20: Description of the primary scattering for the atmospheric upwelling radiance:*

- ① primary scattering of the intrinsic atmospheric radiance,
- ② reflection of the primary scattering of atmospheric radiance at the air-water interface,
- ③ forward scattering of the direct solar beam reflected at the air-water interface,
- ④ water leaving radiance.



*Figure 21: Description of the primary scattering for the in-water downwelling radiance:*

- ① primary scattering of the in-water radiance,
- ② transmission of the backward atmospheric radiance at the air-water interface,
- ③ transmission of the primary scattering of atmospheric radiance at the air-water interface.

## 7.3 OTHER MODULE: RTC/MOS

### 7.3.1 Description

The RTC/MOS module allows one to generate 4 MERIS LUTs at the level-2 relying on the dense dark vegetation (DDV) parameters for the bidirectionality correction. The latter used in the over land atmospheric correction algorithm are:

- *LUT-320*: the *Rayleigh-ground DDV* coupling bidirectionality term ( $\bar{\rho}_{RG}$ ),
- *LUT-321*: the *aerosol-ground DDV* coupling bidirectionality term ( $\bar{\rho}_{aG}$ ),
- *LUT-322*: the ground DDV albedos at 3 MERIS wavelengths ( $\rho_{DDV}$ ),
- *LUT-324*: the *aerosol-molecule* coupling bidirectionality term ( $\bar{\rho}_{aR}$ ).

### 7.3.2 Tools

The latest version of the RTC/MOS package (available since October 28<sup>th</sup>, 2002 – last release on December 14<sup>th</sup>, 2010) is composed of:

- *'lut\_alb\_gddv.f'*: for the generation of MERIS LUT-322,
- *'lut\_rhob\_agddv.f'*: for the generation of MERIS LUT-321,
- *'lut\_rhob\_Rgddv.f'*: for the generation of MERIS LUT-320,
- *'lut\_rhob\_aR.f'*: for the generation of MERIS LUT-324,
- *'lut\_library.f'*: library which contains routines for the generation of the 4 MERIS LUTs mentioned above.

Only the first four sub-modules are detailed in the following sections. A complete input/output description for all these sub-modules is given in Appendix 3 ([Section 11](#)).

### 7.3.3 RTC/lut\_alb\_gddv

The ground DDV albedos ( $\rho_{DDV}$ ) are determined at 4 MERIS wavelengths (412.5nm, 442.5nm, 490nm and 665nm) for 20 DDV reflectance models defined by the CESBIO (Centre d'Etudes Spatiales de la BIOSphere, Toulouse - FRANCE) institute. These models are built using the *Hapke's* representation:

The *Hapke's* bidirectional reflectance distribution function (BRDF)  $R$  is defined as [\[RD-55\]](#):

$$R(\mu_s, \mu_v, \theta, \omega) = \frac{\omega}{4} \cdot \frac{1}{\mu_s + \mu_v} \cdot [p(\theta) \cdot (1 + B(\theta)) + H(\omega, \mu_s) \cdot H(\omega, \mu_v) - 1] \quad (165)$$

where  $\mu_s$  and  $\mu_v$  are respectively the cosine of solar and viewing zenithal angle,  $\theta$  the phase (scattering) angle,  $\omega$  the single scattering albedo,  $p(\theta)$  the scattering phase function,  $B(\theta)$  the backscattering function (referred also as the opposition effect function), and  $H(\omega, x)$  a function which accounts for multiple scattering.

The scattering angle  $\theta$  is defined as:

$$\cos \theta = \mu_s \cdot \mu_v + \sqrt{1 - \mu_s^2} \cdot \sqrt{1 - \mu_v^2} \cdot \cos \Delta\phi$$

where  $\Delta\phi$  is the relative azimuthal angle between solar and viewing directions.

The backscattering function  $B(\theta)$  which ranges from  $-1$  to  $+1$  is expressed as:

$$B(\theta) = \frac{B_0}{1 + \frac{\tan(\theta/2)}{h}}$$

where  $h$  and  $B_0$  are respectively the width and the amplitude of the hot-spot. The latter which is given by,

$$B_0 = \frac{S}{\omega \cdot p(0)}$$

is controlled by the relative value of the parameter  $S$ .

The phase function  $p(\theta)$  employed here is the *Henye-Greenstein* function:

$$p(\theta) = \frac{1 - g^2}{(1 + g^2 + 2g \cdot \cos \theta)^{3/2}}$$

with  $g$  the asymmetry factor ranging from  $-1$  to  $1$ . Note that  $g = 0$  for isotropic scattering particles,  $g > 0$  for forward scattering particles and  $g < 0$  for backward scattering particles.

Finally, the multiple scattering functions  $H(\omega, x)$  derive from the *Hapke's* approximation:

$$H(\omega, x) = \frac{1 + 2x}{1 + 2x \cdot \sqrt{1 - \omega}}$$

In summary, the *Hapke's* reflectance model is defined by the 4 following parameters:  $\omega$ ,  $g$ ,  $S$  and  $h$ .

The ground DDV albedo ( $\rho_{DDV}(\lambda)$ ) at each MERIS wavelength ( $\lambda$ ) is then computed by the angular integration of the DDV BRDF ( $R_{DDV}(\lambda, \vartheta', \vartheta_v, \Delta\phi')$ ) as follows:

$$\rho_{DDV}(\lambda) = \frac{1}{2\pi} \cdot \int_0^{2\pi} \int_0^1 \int_0^1 R_{DDV}(\lambda, \vartheta', \vartheta_v, \Delta\phi') \cdot d\mu' \cdot d\mu_v \cdot d\Delta\phi' \quad (166)$$

These angular integrations on  $\mu'$ ,  $\mu_v$  and  $d\Delta\phi'$  are performed using the *Gauss* quadrature.

### 7.3.4 RTC/lut\_rhob\_agddv

The aerosol-ground DDV coupling bidirectionality term ( $\bar{\rho}_{aG}$ ) is computed by the double angular integration of the DDV BRDF ( $R_{DDV}(\lambda, \vartheta', \vartheta_v, \Delta\phi')$ ) weighted by the downward normalized aerosol phase function ( $P(\vartheta_s, \vartheta', \Delta\phi, \Delta\phi')$ ):

$$\bar{\rho}_{aG}(\lambda, \vartheta_s, \vartheta_v, \Delta\phi) = \frac{\int_0^{2\pi} \int_0^1 R_{DDV}(\lambda, \vartheta', \vartheta_v, \Delta\phi') \cdot P(\vartheta_s, \vartheta', \Delta\phi, \Delta\phi') \cdot d\mu' \cdot d\Delta\phi'}{\int_0^{2\pi} \int_0^1 P(\vartheta_s, \vartheta', \Delta\phi, \Delta\phi') \cdot d\mu' \cdot d\Delta\phi'} \quad (167)$$

The integration on  $\mu'$  is performed using the *Gauss* quadrature, and the integration on  $d\Delta\phi'$  using the *Newton-Cotes* method.

In order to remove the  $\Delta\phi$  dependence,  $\bar{\rho}_{aG}$  is expanded into *Fourier* series of 4<sup>th</sup> order:

$$\bar{\rho}_{aG}(\lambda, \vartheta_s, \vartheta_v) = \sum_{s=0}^4 (\bar{\rho}_{aG})^{(s)}(\lambda, \vartheta_s, \vartheta_v, \Delta\phi) \cdot \cos(s \cdot \Delta\phi) \quad (168)$$

Note that this computation is completed at 4 MERIS wavelengths (412.5 nm, 442.5 nm, 490 nm and 665 nm), for each of the 20 DDV BRDF models defined by the CESBIO institute and for each of 78 SAMs (*Junge's* models) over Land.

### 7.3.5 RTC/lut\_rhob\_Rgddv

The *Rayleigh*-ground DDV coupling bidirectionality term ( $\bar{\rho}_{RG}$ ) is computed as the mean of a double integration of the DDV BRDF ( $R_{DDV}(\lambda, \vartheta_s, \vartheta_v, \Delta\phi')$ ) on the solar zenithal angle ( $\vartheta_s$ ) and relative azimuthal angle ( $\Delta\phi$ ):

$$\bar{\rho}_{RG}(\lambda, \vartheta_v) = \frac{1}{2\pi} \cdot \int_0^{2\pi} \int_0^{\pi} R_{DDV}(\lambda, \vartheta_s, \vartheta_v, \Delta\phi) \cdot d\mu_s \cdot d\Delta\phi \quad (169)$$

Note that this computation is completed at 4 MERIS wavelengths (412.5 nm, 442.5 nm, 490 nm and 665 nm) and for each of the 20 DDV BRDF models defined by the CESBIO institute.

### 7.3.6 RTC/lut\_rhob\_aR

The aerosol-molecule coupling bidirectionality term ( $\bar{\rho}_{aR}$ ) is defined as the integration of the intrinsic aerosol TOA radiance at the first *Fourier* series term ( $L^{(0)}$ ) over  $\mu_v$  using a *Gauss* quadrature:


$$\bar{\rho}_{aR}(\tau^a, \vartheta_s) = \int_0^1 L^{(0)}(\tau^a, \vartheta_s, \vartheta_v) \cdot d\mu_v \quad (170)$$

In the framework of the MOS ground segment,  $\bar{\rho}_{aR}$  have been completed with a MLS profile, for 78 SAMs (*Junge's* models) over land and with several aerosol optical thicknesses at 550 nm (*i.e.*,  $\tau^a$  in [0.1;1.5] by step of 0.1). A *Gauss* quadrature with 24 angles was used for the angular integration of  $\bar{\rho}_{aR}$ . For each *Fourier* series term  $s$  ( $s = [1; 6]$ ), a third order polynomial fit has then been determined as function of  $\tau^a$ , and the derived coefficients have been tabulated for each of the first 6 *Fourier* orders.

Using results derived from the MOS experiment, once interpolated to the *Gauss* quadrature for MERIS ground segment (12 angles) the polynomial coefficients fits at the first 6 *Fourier* orders are recombined to yield the aerosol-molecule coupling bidirectionality term ( $\bar{\rho}_{aR}$ ) for the MERIS ground segment. A third order polynomial fit as function of aerosol optical thickness ( $\tau^a$ ) is then applied on the  $\bar{\rho}_{aR}$  values in order to remove the explicit dependence on  $\tau^a$ :

$$\bar{\rho}_{aR}(\tau^a, \vartheta_s) = \sum_{i=0}^3 k_i(\vartheta_s) \cdot (\tau^a)^i \quad (171)$$



|   |  |  |
|---|--|--|
|  | <b>MERIS/ ENVISAT-1</b><br>MEdium Resolution Imaging<br>Spectrometer | <u>Ref.:</u> PO-RS-PAR-GS-0003<br><u>Issue:</u> 4 <u>Rev.:</u> A<br><u>Date:</u> 16-Dec-10 <u>Page:</u> 89 |
|---|--|--|

with  $k_i$  the polynomial coefficients.

Note that the simulations are completed with a MLS profile for 78 SAMs over land with several  $\tau^a$  values in  $[0.1;1.5]$  by step of 0.1. Moreover, the polynomial coefficients for each of the 78 SAMs have been retrieved by adding the point  $(0;0)$  into the set of  $(\tau^a; \bar{\rho}^{aR})$  points and by using a constraint on the polynomial fit in order to get a value close to 0 for the first polynomial coefficient (*i.e.*, for the constant term).

## 8. DESCRIPTION OF RTC/FUB

The RTC/FUB is the second simulation tool used to generate the MERIS LUTs for the level-2 processing. This package allows one to determine the optical properties of the complex absorbing and scattering media such as the atmosphere and the ocean, and to compute the upwelling and downwelling radiances for a discrete number of propagation directions at predefined depth levels. This code is particularly appropriate for the light propagation in optically dense media such as clouds and oceans, and therefore well suited for the development of the MERIS algorithms regarding the retrieval of cloud properties (albedo, optical thickness, droplets) for the global energy budget studies or specific optical properties of water constituents for the ocean colour studies.

RTC/FUB package is composed of two principal modules:

- *MIE* module: This allows one to compute the optical properties (*i.e.*, scattering phase function, extinction and scattering coefficients) for a mixture of  $N$  particle size distributions of atmospheric or oceanic constituents at a selected wavelength according to the *Mie's* theory,
- *MOMO* module: This computes the radiative transfer in the coupled '*Atmosphere-Ocean*' system. The approach is based on the matrix-operator method (also known as doubling-adding method) which solves the RTE for the diffuse radiation within a multi-layered medium. Direct sun propagation through atmosphere and ocean is independently computed using *Beer-Lambert's* law. All physical processes (single and multiple scattering, gaseous absorption, *etc.*) are accounted for in the computation of upwelling radiances at TOA.

These two modules are presented in the following sections.

### 8.1 MIE MODULE

#### 8.1.1 Description


This module allows one to compute the scattering phase matrix  $P(\lambda, r, n, \theta)$  and the optical properties (*i.e.*, the single scattering albedo  $\omega_0(\lambda, r, n)$  and the extinction coefficient  $\sigma_e(\lambda, r, n)$ ) for a mixture of  $N$  particle size distributions at a given wavelength  $\lambda$ . Each particle size distribution  $n_i(r)$  is characterized by a complex refractive index  $(n_{i,\lambda} = m_{i,\lambda} - i k_{i,\lambda})$ , which is assumed to be identical for all the scatterers within the same distribution, and a component mixing ratio  $(n_i/n)$ . This computation is performed with the *Mie's* theory, assuming particles as homogeneous isotropic spheres the sizes of which are comparable to or larger than the incident wavelength.

Moreover, it allows to calculate as well the forward scattering proportion  $f_{sp}(\mu = 0)$  of a mixture of aerosols by using its computed scattering phase matrix  $P(\lambda, r, n, \theta)$ .

#### 8.1.2 Tool

The latest version of the *Mie*/FUB package (available since July 27, 1999 – last release in March 31, 2009) is composed of:

- '*mie36.f*': for the *Mie's* computations,
- '*scfp\_2.f*': for the computation of the forward scattering proportion  $f_{sp}(\mu = 0)$  of a given list of selected aerosol models (*i.e.*, scattering phase matrices  $P(\lambda, r, n, \theta)$ ).

|   |  |  |
|---|--|--|
|  | <b>MERIS/ ENVISAT-1</b><br>Medium Resolution Imaging<br>Spectrometer | <u>Ref.:</u> PO-RS-PAR-GS-0003<br><u>Issue:</u> 4 <u>Rev.:</u> A<br><u>Date:</u> 16-Dec-10 <u>Page:</u> 91 |
|---|--|--|

Only the Mie sub-module is detailed in the following section. A full I/O description for each of these two codes is given in Appendix 1 ([Sections 10.1](#)).

### 8.1.3 Mie processing

The *Mie* processing is fully described in [Section 7.1.3](#) and a complete list of I/O data is given in Appendix 2 ([Section 10.1](#)). Compared with the 'SCAMAT' module from RTC/UdL, this *Mie* code allows one to compute the optical properties of a mixture composed with up to 5 different sources of particles (or components), and one additional particle size distribution is available: the *Gamma-Hansen* distribution [[RD-13](#)].

$$\frac{dN(r)}{dr} = r^{(1-3r_b)/r_b} \cdot \exp[-r / (r_i \cdot r_b)]$$

where  $r_i$  and  $r_b$  are respectively the effective radius of the particle and its standard deviation expressed as  $\mu\text{m}$ . The  $r_i$  values usually varies between 4 and 30  $\mu\text{m}$ . However the lack of information about  $r_i$  makes the *Modified Gamma* distribution (see [Section 3.2.2](#)) is often chosen as the droplet size distribution.

## 8.2 MOMO MODULE

### 8.2.1 Description

The purpose of the MOMO (Matrix-Operator Method) code is to simulate MERIS radiances by computing the radiative transfer processes within a coupled '*Atmosphere-Ocean*' system [[RD-4](#)]. The approach is based on the matrix-operator method (also known as the *doubling-adding* method) which solves the RTE for the diffuse radiation. The propagation of the direct solar flux through the atmosphere and ocean is independently calculated using the *Beer-Lambert's* law.

With respect to the radiative transfer processes, the coupled '*Atmosphere-Ocean*' system can be divided into four distinct sub-systems: atmosphere, interface between atmosphere and ocean, ocean, and ocean ground. Each sub-system requires a special treatment adapted to its particularities. The sub-system '*Atmosphere-Ocean*' and '*Ocean-Ground*' interface are each represented by one layer, whereas the ocean and the atmosphere are defined as a multi-layered medium the number of layers of which depends on the precision to describe the vertical structure of the medium. For each layer, reflection and transmission matrices and source functions are derived to describe how diffuse radiation is transmitted through, reflected and emitted from the layer.

The primary model output consists of azimuthally and zenithally resolved diffuse radiances at the layer boundaries. Secondary output consists in quantities that can be derived from radiances such as fluxes, reflectances, etc.

### 8.2.2 Tools

The latest version of the RTC/FUB package (available since July 27, 1999 – last release in March 31, 2009) is composed of:

- '*mom39.f*': the main code for the radiative transfer computations,
- '*vtp.f*': for generating the vertical atmospheric / oceanic profile with respect to the defined model layers, the *US Standard62* atmospheric profile and the vertical distribution of the constituents,

|   |  |  |
|---|--|--|
|  | <b>MERIS/ ENVISAT-1</b><br>Medium Resolution Imaging<br>Spectrometer | <u>Ref.:</u> PO-RS-PAR-GS-0003<br><u>Issue:</u> 4 <u>Rev.:</u> A<br><u>Date:</u> 16-Dec-10 <u>Page:</u> 92 |
|---|--|--|

- **'cox\_munk.f':** for the computation of the reflection and transmission functions of a *Cox-Munk* wave slope distribution at the *air-sea* interface (code not available).

Only the first sub-module is detailed in the following sections. A full I/O description for all these sub-modules is given in Appendix 2 ([Sections 10.2 & 10.3](#)).

## 8.2.3 RTC/MOMO

The development of the RTC/MOMO benefits from many previous research works. In fact, the implementation of the matrix-operator method mainly derived from [\[RD-56\]](#), the analytical treatment of strongly peak phase functions is based on [\[RD-57\]](#), the effects of the refraction at the *air-sea* interface on the *Gaussian-Lobatto* quadrature scheme are outlined in [\[RD-58\]](#). The reflection at the rough sea surface modeled by the statistical description of the wave facet distribution derived by *Cox and Munk* [\[RD-46\]](#) is incorporated as described by [\[RD-59\]](#). The atmospheric gas absorption [\[RD-60\]](#), the chlorophyll-*a* fluorescence [\[RD-61\]](#) and the *Raman* scattering have also been included in the code. Polarization as well as wind direction dependent effects at the rough sea surface have been recently incorporated into a new version of this code ([\[RD-62\]](#) & [\[RD-63\]](#)). A detailed description of the matrix-operator method for the '*Atmosphere-Ocean*' system including the numerical treatment and the effects at the rough sea surface is given in [\[RD-4\]](#). Here we outline the principal bases of the method which have been implemented in the RTC/MOMO the structure of which was developed by [\[RD-64\]](#).

### 8.2.3.1 Matrix-Operator Method

The application of the matrix-operator method is based on the assumption that the vertical structure of the medium can be approximated by an appropriate number of homogeneous layers. Reflection, transmission and source operators for each layer are then obtained by repeated application of the *doubling* algorithm to an optically very thin sub-layer for which the single scattering approximation can be applied. The individual layers are then combined using the *adding* algorithm. The final output consists of the diffuse light field at the layer boundaries for all selected solar incident angles. The efficiency of this method for the treatment of optically thick media relies on the *doubling* algorithm.

#### • Single scattering approximation

Using the *Fourier* analysis to separate zenith and azimuth dependence (*see* [Section 6.2.2.2](#)), the upwelling and downwelling diffuse radiance  $L_m$  produced by elastic scattering of a solar beam  $E_0$  within an optically thin layer ( $\Delta\tau / \mu \leq 10^{-3}$ ) can be approximated using Equations (138) by:

$$L_m(\Delta\tau, \mu) = \omega_0 \cdot P_m(\mu, \mu_0) \cdot E_0 \cdot \frac{\Delta\tau}{|\mu|} \quad (172)$$

with  $P_m(\mu, \mu_0)$  the normalized phase function. This single scattering approximation is of fundamental importance for the development of the matrix-operator method.

#### • Interaction principle

The interaction principle within an absorbing, scattering and emitting medium can be expressed by reflexion, transmission and source operators. By considering  $\tau_0$  and  $\tau_1$  the upper and lower boundaries of an elementary layer, the upward directed radiance ( $L_0^+$ ) at  $\tau_0$  can be expressed as ([Figure 22](#)):

$$L_0^+ = R_{01} \cdot L_0^- + T_{10} \cdot L_1^+ + J_{10}^+ \quad (173)$$

where  $R_{01}$  quantifies the reflexion of downward radiation,  $T_{10}$  the transmission of the upward radiance, and  $J_{10}^+$  the contribution of the internal radiation sources to the upward radiance at the layer boundary  $\tau_0$ . The prime denotes the incident radiation on the layer.

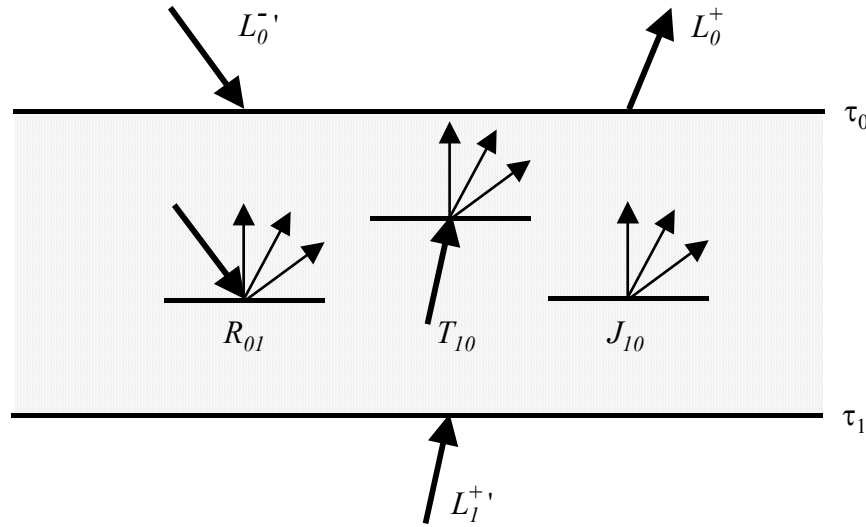


*Figure 22: Interaction principle within an elementary layer  $[\tau_0; \tau_1]$*

#### • Radiance at internal layer boundaries

A formalism to compute the radiance at the internal boundary between two layers can be derived from the interaction principle (see [RD-56] for more details). Thus, the radiance distribution at the internal boundary  $\tau_1$  can then be determined from Equation (172) using the optical properties of the adjacent layers and the inward directed radiance on the external boundaries  $\tau_0$  and  $\tau_2$ :

$$\begin{cases} L_1^+ = (I - R_{12} \cdot R_{10})^{-1} \cdot (R_{12} \cdot T_{01} \cdot L_0^- + T_{21} \cdot L_2^+ + R_{12} \cdot J_{01}^- + J_{21}^+) \\ L_1^- = (I - R_{10} \cdot R_{12})^{-1} \cdot (R_{10} \cdot T_{21} \cdot L_2^+ + T_{01} \cdot L_0^- + R_{10} \cdot J_{21}^+ + J_{01}^-) \end{cases} \quad (174)$$

with  $I$  the unity operator. Multiple internal reflexions between the layers are included in Equations (173). This appears as an expansion of the term  $(I - R_{10} \cdot R_{12})^{-1}$  for example into a geometrical series.

Since there is no downwelling diffuse radiation at TOA, the diffuse radiation transfer within the coupled 'Atmosphere-Ocean' system can be written as:

$$\begin{cases} L_1^+ = (I - R_{12} \cdot R_{10})^{-1} \cdot (T_{21} \cdot L_2^+ + R_{12} \cdot J_{01}^- + J_{21}^+) \\ L_1^- = (I - R_{10} \cdot R_{12})^{-1} \cdot (R_{10} \cdot T_{21} \cdot L_2^+ + R_{10} \cdot J_{21}^+ + J_{01}^-) \end{cases} \quad (175)$$

As seen just above, the computation of the radiance at level  $\tau_1$  requires the radiance  $L_2^+$  entering the system at the lower boundary  $\tau_1$ . Consequently, the radiances will be calculated from the bottom to the top. Considering the ocean bottom or the land surface as a *Lambertian* reflector, then the radiance just above the surface can be deduced from Equations (174) as follows:

$$\begin{cases} L_1^+ = (I - R_B \cdot R_{10})^{-1} \cdot (R_B \cdot J_{01}^- + J_B^+) \\ L_1^- = (I - R_{10} \cdot R_B)^{-1} \cdot (R_{10} \cdot J_B^+ + J_{01}^-) \end{cases} \quad (176)$$

where the subscript  $B$  denotes the background (*i.e.*, ocean bottom or land surface).

### • Adding and doubling

Layers are combined by the so-called *adding* algorithm which derives from the interaction principle. The resulting reflection, transmission and source operators from two consecutive layers are expressed as:

$$\begin{cases} R_{02} = R_{01} + T_{10} \cdot (I - R_{12} \cdot R_{10})^{-1} \cdot R_{12} \cdot T_{01} \\ R_{20} = R_{21} + T_{12} \cdot (I - R_{10} \cdot R_{12})^{-1} \cdot R_{10} \cdot T_{21} \\ T_{02} = T_{10} \cdot (I - R_{12} \cdot R_{10})^{-1} \cdot T_{21} \\ T_{20} = T_{12} \cdot (I - R_{10} \cdot R_{12})^{-1} \cdot T_{01} \\ J_{20}^+ = J_{10}^+ + T_{10} \cdot (I - R_{12} \cdot R_{10})^{-1} \cdot (R_{12} \cdot J_{01}^- + J_{21}^+) \\ J_{02}^- = J_{12}^- + T_{12} \cdot (I - R_{10} \cdot R_{12})^{-1} \cdot (R_{10} \cdot J_{21}^+ + J_{01}^-) \end{cases} \quad (177)$$

By considering two identical and homogeneous layers ( $[\tau_0; \tau_1]$  and  $[\tau_1; \tau_2]$ ),

$$\begin{cases} R_{01} = R_{10} = R_{12} = R_{21} = R \\ T_{01} = T_{10} = T_{12} = T_{21} = T \end{cases} \quad (178)$$

Equations (176) and (177) yield to the following *doubling* algorithm:

$$\begin{cases} R_{02} = R_{20} = R + T \cdot (I - R \cdot R)^{-1} \cdot R \cdot T \\ T_{02} = T_{20} = T \cdot (I - R \cdot R)^{-1} \cdot T \\ J_{20}^+ = J_{10}^+ + T \cdot (I - R \cdot R)^{-1} \cdot (R \cdot J_{01}^- + J_{21}^+) \\ J_{02}^- = J_{12}^- + T \cdot (I - R \cdot R)^{-1} \cdot (R \cdot J_{21}^+ + J_{01}^-) \end{cases} \quad (179)$$

### • Reflexion, transmission and source operators

For applying the matrix-operator method, reflexion, transmission and source operators have to be determined from the optical properties of the propagation medium. Let consider as an example the reflection of downwelling diffuse radiation  $L_m^-$  (after expanded in *Fourier* series) by an homogeneous thin layer  $\Delta\tau$ , and the transmitted diffuse radiation at the lower boundary of  $\Delta\tau$ , we can then write using the operator notations:

$$\begin{cases} L_m^+(\Delta\tau) = R_m(\Delta\tau) \cdot L_m^- \\ L_m^-(\Delta\tau) = T_m(\Delta\tau) \cdot L_m^- \end{cases} \quad (180)$$

Because of the homogeneity of the thin layer  $\Delta\tau$ , the reflection  $R_m(\Delta\tau)$  and transmission  $T_m(\Delta\tau)$  operators are identical both for the two paths. By introducing a quadrature scheme for the discretization of zenithal angular directions,  $L_m$  is expressed as a vector each element of which represents the radiance for a couple of incident and viewing discrete directions and the phase normalized function  $P_m$  as a matrix the elements of which indicate the probability density of photon redistribution between two discrete directions.

Using a quadrature scheme  $(N, \mu_i, w_i)$ , with  $N$  the number of discrete zenithal angles,  $\mu_i$  and  $w_i$  respectively the cosine of *Gaussian* angles and associated weights, the matrix representations of  $R_m(\Delta\tau)$  and  $T_m(\Delta\tau)$  are expressed as follows (see [RD-4] for more details):

$$\begin{cases} R_m(\Delta\tau) = [1 + \delta_{0,m}] \cdot \pi\omega_0 \cdot \Delta\tau \cdot \mathbf{Mu}^{-1} \cdot \mathbf{P}_m^R \cdot \mathbf{C} \\ T_m(\Delta\tau) = \mathbf{F}(\Delta\tau) + [1 + \delta_{0,m}] \cdot \pi\omega_0 \cdot \Delta\tau \cdot \mathbf{Mu}^{-1} \cdot \mathbf{P}_m^T \cdot \mathbf{C} \end{cases} \quad (181)$$

with,

$$\begin{cases} \mathbf{Mu}^{-1} = [(\mu_i)^{-1} \cdot \delta_{i,j}] \\ \mathbf{C} = [w_i \cdot \delta_{i,j}] \end{cases} \quad \text{with } i, j \in \{1, \dots, N\}$$

$$\mathbf{F}(\tau) = [\exp(-\tau / \mu_i) \cdot \delta_{i,j}]$$

where  $\mathbf{P}_m^R$  and  $\mathbf{P}_m^T$  are the scattering phase matrices for the reflection and transmission respectively,  $\mathbf{Mu}$  the incidence angles matrix,  $\mathbf{C}$  the *Gaussian* weights matrix, and  $\mathbf{F}$  the transmission matrix for direct solar radiation.  $\delta_{i,j}$  represents the *Dirac's* delta function which is equal to 1 for  $(i = j)$  and 0 otherwise.

In the same way, the source operators for upwelling and downwelling diffuse radiations within the optically thin layer located at  $\tau_0$  are given by:

$$\begin{cases} J_m^+(\Delta\tau) = \omega_0 \cdot \Delta\tau \cdot E_0 \cdot \mathbf{Mu}^{-1} \cdot \mathbf{P}_m^T \cdot \mathbf{F}(\tau_0) \\ J_m^-(\Delta\tau) = \omega_0 \cdot \Delta\tau \cdot E_0 \cdot \mathbf{Mu}^{-1} \cdot \mathbf{P}_m^R \cdot \mathbf{F}(\tau_0) \end{cases} \quad (182)$$

### • Lambertian surfaces

In the matrix-operator method, the lower boundary of the system is often considered as a non-transmitting *Lambertian* reflector which makes easier the computation of the upwelling input radiation into the system by the below interface. As the first term of the *Fourier* series expansion of the reflected isotropic radiance is not null, it will be then the same for the corresponding *Fourier* expansion terms of the reflection function. The operator  $R_m^B$  describing the reflection of diffuse radiation at the *Lambertian* surface level is then derived from the surface albedo  $\rho_s$  as (see [RD-56] for more details):

$$\begin{cases} R_{m=0}^B = 2 \cdot \rho_s \cdot \mathbf{1} \cdot \mathbf{Mu} \cdot \mathbf{C} \\ R_{m>0}^B = \mathbf{0} \end{cases} \quad (183)$$

where,

$$\begin{cases} \mathbf{Mu} = [\mu_i \cdot \delta_{i,j}] \\ \mathbf{1} = [1_{i,j} = 1] \end{cases} \quad \text{with } i, j \in \{1, \dots, N\}$$

Since the direct solar radiation is scattered by the *Lambertian* surface, the latter also acts as a source of diffuse radiation, and the corresponding source term  $J_m^B$  is derived from  $\rho_s$  as follows:

$$\begin{cases} J_{m=0}^B = (\rho_s \cdot E_0 / \pi) \cdot \mathbf{1} \cdot \mathbf{Mu} \cdot \mathbf{F}(\tau_B) \\ J_{m>0}^B = \mathbf{0} \end{cases} \quad (184)$$

### 8.2.3.2 Numerical method

The integral computation with respect to the zenithal angles in the RTC/MOMO are evaluated with the *Gauss-Lobatto* quadrature scheme (see Section 12.6). Consequently, radiances are computed for a finite number  $N$  of discrete zenithal angles. Of course, the values of these angles depend on the number of points used for the quadrature.

To allow the incorporation of strongly peaked phase functions for which the *Fourier* expansion requires a large number of terms (e.g., 400 terms for cloud particles), the phase function truncation technique which substitutes the forward scattering peak by a second order polynomial (see Section 2.3.2) is used: the radiance scattered into a certain small solid angle around a scattering angle of  $0^\circ$  is removed from the diffuse radiation field and treated as being not scattered at all. In order to ensure the desired accuracy  $\varepsilon$  in the computations with the matrix-operator method, two successive tests are implemented:

- *Test 1:* It is firstly tested whether the quadrature of the normalized phase function  $P$  can be completed with the level of required accuracy for the selected value of  $N$  :

$$\left| 1 - \sum_{i=1}^N w_i \cdot [P(\tau, \mu_i) + P(\tau, -\mu_i)] \right| < \varepsilon \quad (185)$$

While this condition is not fulfilled, the forward peak of  $P$  will be truncated for an increasing angle of  $\mathcal{G}_p$ . Once this accuracy reached,  $N$  will then be increased if necessary, and  $\mathbf{P}_m^R$  and  $\mathbf{P}_m^T$  computed using the modified phase function  $P'$ .

- *Test 2:* The *Fourier* expansion for a given combination of angles  $(\mu'_j, \mu_i)$  will be stopped as soon as the following test is verified:

$$\left| P'_m(\tau, \mu'_j, \mu_i) \right| < \varepsilon_F \cdot P'_0(\tau, \mu'_j, \mu_i) \quad (186)$$

with  $\varepsilon_F$  the level of required accuracy in the *Fourier* expansion.

Numerous tests stressed the maximum number of *Fourier* series term ( $I_s = 70$ ) was sufficient for a good compromise between the accuracy and the computational time.

Moreover radiances for angles which differ to the quadrature have to be gathered by interpolation or introduction of ancillary zenithal angles with the corresponding weights set to zero. The latter is implemented in the RTC/MOMO.

Note that the atmospheric gaseous transmittivity is estimated (using the *correlated k-distribution* method) by an ESFT with the HITRAN-2000 database (see Sections 2.9 & 7.2.3).

### 8.2.3.3 Air-sea interface

The computation of reflection and transmission matrices for the '*Atmosphere-Ocean*' interface is based on the assumption that the orientation of the sea surface slopes follows a two-dimensional *Gaussian* probability density distribution (see Section 5). Effects due to the wind direction are not taken into account and the multiple reflections between the ocean facets and internal shading effects are not simulated. This *air-sea* interface is modeled as an infinitely thin layer whereas its real vertical profile depends on the wave height. This may lead errors if the in-water radiance near the ocean surface is computed. This section briefly describes the radiative processes in term of matrix representations of reflection, transmission and source operators included in the RTC/MOMO for flat and rough sea surfaces.

#### • Flat sea surface



Reflection and transmission of the light through the *air-water* interface are described by the *Fresnel* formulas and *Snellius* law of refraction (see [Section 2.10](#)) for which the refractive indice of air ( $n_a$ ) and water ( $n_w$ ) are fixed to 1 and 1.34 respectively whatever the wavelength.

Because of the non-linearity of the mapping of atmospheric *Gaussian* angles ( $N_a, \mu_i^a, w_i^a$ ) on the refraction angles in the water, a new *Gauss-Lobatto-like* quadrature scheme ( $N_w, \mu_i^w, w_i^w$ ) based on the energetic conservation considerations is then implemented for the acceptance angular cone of the atmospheric radiation into the water (see [\[RD-58\]](#) for more details). Moreover, since the angular domain of total internal reflection is not directly accessible to atmospheric radiation, a modified *Gauss-Lobatto* quadrature scheme is then added in the RTC/MOMO for the angular domain  $[0, \mu_c^w]$  with  $\mu_c^w$  the cosine of the critical angle in the water for which the reflection just below the *air-sea* interface is total.

In the case of a flat sea surface, there is no exchange of energy between the different zenith angles, which means only the diagonal elements of the reflection and transmission matrices are not null. More, the terms of the *Fourier* series expansion ( $m \in [0, M]$ ) for the reflection and transmission operators are constant. These flat sea operators are then defined as:

$$N_a \times N_a : R_m^{aa} = \begin{cases} \rho_F(\mu_i, n_w/n_a) & \text{for } i = j \\ 0 & \text{otherwise} \end{cases} \quad (187)$$

$$N_w \times N_w : R_m^{ww} = \begin{cases} \rho_F(\mu_i^*, n_a/n_w) & \text{for } i = j \text{ and } i, j \leq N_a \\ 1 & \text{for } i = j \text{ and } N_a < i, j \leq N_w \\ 0 & \text{otherwise} \end{cases} \quad (188)$$

$$N_a \times N_w : T_m^{aw} = \begin{cases} (n_w/n_a)^2 \cdot \tau_F(\mu_i, n_w/n_a) & \text{for } i = j \text{ and } i, j \leq N_a \\ 0 & \text{otherwise} \end{cases} \quad (189)$$

$$N_w \times N_a : T_m^{wa} = \begin{cases} (n_a/n_w)^2 \cdot \tau_F(\mu_i^*, n_a/n_w) & \text{for } i = j \text{ and } i, j \leq N_a \\ 0 & \text{otherwise} \end{cases} \quad (190)$$

where  $\rho_F$  and  $\tau_F$  represents the *Fresnel* reflection and transmission respectively (see [Section 2.10](#)) defined as,

$$\begin{cases} \rho_F = \frac{1}{2} \cdot (r_{//}^2 + r_{\perp}^2) \\ \tau_F = \frac{1}{2} \cdot \frac{n_w \cdot \cos \theta_w}{\cos \theta_a} \cdot (t_{//}^2 + t_{\perp}^2) \end{cases} \quad (184)$$

and  $R_m^{aa}$  the reflexion of diffuse atmospheric radiance,  $T_m^{wa}$  the transmission of oceanic radiance into the atmosphere, etc.

Moreover the flat sea surface does not generate any diffuse radiation, consequently the source operators are represented by the zero matrix for all the *Fourier* terms:

$$N_a \times N_w : J_m^+ = \mathbf{0} \quad (185)$$

$$N_a \times N_a : J_m^- = \mathbf{0} \quad (186)$$

Note that in the matrix-operator method the portion of the direct solar radiation reflected at the flat *air-sea* interface and scattered on its way back through the atmosphere is not considered.

### • Rough sea surface

Contrary to the the flat sea surface, the wind-roughened sea surface acts as a source of diffuse radiation due to the angular redistribution of the incident direct solar radiation.

The reflection operators for upwelling and downwelling radiances at the *air-sea* interface are expressed as (see [RD-4]):

$$N_a \times N_a : \tilde{R}_m^{aa} = [1 + \delta_{0,m}] \cdot \pi \cdot \tilde{\mathbf{R}}_m^{aa} \cdot \mathbf{C} \quad (191)$$

$$N_w \times N_w : \tilde{R}_m^{ww} = [1 + \delta_{0,m}] \cdot \pi \cdot \tilde{\mathbf{R}}_m^{ww} \cdot \mathbf{C}^* \quad (192)$$

where tilde is only used to denote the parameters of the rough sea surface described in Section 5. The matrices  $\mathbf{C}$  and  $\mathbf{C}^*$  for the atmospheric and oceanic weights are given in Equations (180), and the matrices  $\tilde{\mathbf{R}}_m^{aa}$  and  $\tilde{\mathbf{R}}_m^{ww}$  are defined by:

$$\begin{cases} \tilde{\mathbf{R}}_m^{aa} = \tilde{R}_m(+\mu_j, -\mu_i) & \text{with } i, j = 1, \dots, N \\ \tilde{\mathbf{R}}_m^{ww} = \tilde{R}_m(+\mu_j^*, -\mu_i^*) & \text{with } i, j = 1, \dots, N^* \end{cases}$$

The source operator which describes the production of upwelling diffuse radiance at the rough sea interface is then:

$$\tilde{J}_m^+ = \tilde{\mathbf{R}}_m^{aa} \cdot \mathbf{F}(\tau) \cdot E_o \quad (193)$$

with  $\tau$  the atmospheric optical depth and  $\mathbf{F}(\tau)$  defined in Equations (180).

The transmission operators for the rough sea surface used in the RTC/MOMO are formally identical to the transmission operator for a flat sea surface:

$$N_a \times N_w : \tilde{T}_m^{aw} = \tilde{\mathbf{T}}_m^{aw} = \begin{cases} (n_w/n_a)^2 \cdot \tilde{\tau}_F(\mu_i, n_w/n_a) & \text{for } i = j \text{ and } i, j \leq N_a \\ 0 & \text{otherwise} \end{cases} \quad (194)$$

$$N_w \times N_a : \tilde{T}_m^{wa} = \tilde{\mathbf{T}}_m^{wa} = \begin{cases} (n_a/n_w)^2 \cdot \tilde{\tau}_F(\mu_i^*, n_a/n_w) & \text{for } i = j \text{ and } i, j \leq N_a \\ 0 & \text{otherwise} \end{cases} \quad (195)$$

# APPENDICES

**Document Number:** PO-RS-PAR-GS-0003 (Appendices)

**Issue:** 4

**Revision:** A

**Issue Date:** December 16, 2010

**Filenames:**

PO-RS-PAR-GS-0003 4A - Code\_Spec\_Part1-Theory.doc

PO-RS-PAR-GS-0003 4A - Code\_Spec\_Part2-Appendices.doc

|                     | <i>Function (Company)</i>   | <i>Name</i>      | <i>Signature</i> | <i>Date</i> |
|---------------------|-----------------------------|------------------|------------------|-------------|
| <i>Prepared by:</i> | Scientist (PARBLEU)         | Francis Zagolski |                  |             |
| <i>Checked by:</i>  | Scientist (LISE-Wimereux)   | Richard Santer   |                  |             |
| <i>Checked by:</i>  | Scientist (FUB-Berlin)      | Juergen Fischer  |                  |             |
| <i>Approved by:</i> | Project Manager (ESA/ESTEC) | Jean-Paul Huot   |                  |             |
| <i>Released by:</i> | Project Manager (ESA/ESRIN) | Philippe Goryl   |                  |             |

## TABLE OF CONTENTS

|   |            |
|---|------------|
| <b>TABLE OF CONTENTS.....</b>                                   | <b>100</b> |
| <b>9. APPENDIX-1: SPECIFICATION OF RTC/UDL PACKAGE.....</b>     | <b>101</b> |
| 9.1 SCAMAT INPUT / OUTPUT DESCRIPTION .....                     | 101        |
| 9.1.1 <i>Input / Output description</i> .....                   | 101        |
| 9.1.2 <i>Input / Output sample</i> .....                        | 102        |
| 9.2 UPRAD INPUT/OUTPUT DESCRIPTION .....                        | 105        |
| 9.3 AUXILIARY FILE: 'UPRAD_DEF' .....                           | 108        |
| 9.4 ADDITIONAL TOOLS.....                                       | 110        |
| 9.4.1 <i>OTC/COMPUTE_FSP</i> .....                              | 110        |
| 9.4.2 <i>RTC/GAUSS</i> .....                                    | 111        |
| 9.4.3 <i>RTC/PO2</i> .....                                      | 112        |
| 9.4.4 <i>RTC/WIND</i> .....                                     | 113        |
| 9.4.5 <i>OTC/RAYLEIGH</i> .....                                 | 115        |
| 9.4.6 <i>OTC/OZONE</i> .....                                    | 116        |
| 9.4.7 <i>IOP/WATER</i> .....                                    | 117        |
| <b>10. APPENDIX-2: SPECIFICATION OF RTC/FUB PACKAGE .....</b>   | <b>119</b> |
| 10.1 MIE INPUT / OUTPUT DESCRIPTION .....                       | 119        |
| 10.1.1 <i>Input / Output description</i> .....                  | 119        |
| 10.1.2 <i>Input / Output sample</i> .....                       | 120        |
| 10.2 MOMO INPUT / OUTPUT DESCRIPTION.....                       | 125        |
| 10.3 SOFTWARE TECHNICAL DESCRIPTION .....                       | 128        |
| 10.3.1 <i>Include file: 'param'</i> .....                       | 128        |
| 10.3.2 <i>Auxiliary file: 'mom_def'</i> .....                   | 129        |
| 10.3.3 <i>Input files to RTC / MOMO</i> .....                   | 132        |
| 10.3.4 <i>Tree directories</i> .....                            | 132        |
| 10.3.5 <i>Vertical profile</i> .....                            | 134        |
| 10.3.6 <i>Forward scattering proportion computation</i> .....   | 137        |
| <b>11. APPENDIX-3: SPECIFICATION OF RTC/MOS PACKAGE.....</b>    | <b>139</b> |
| 11.1 RTC/LUT_ALB_GDDV.....                                      | 139        |
| 11.2 RTC/LUT_RHOB_AGDDV .....                                   | 140        |
| 11.3 RTC/LUT_RHOB_RGDDV.....                                    | 143        |
| 11.4 RTC/LUT_RHOB_AR .....                                      | 144        |
| <b>12. APPENDIX-4: SPECIFICATION OF TOOLS FOR MERISAT .....</b> | <b>147</b> |
| 12.1 LINEAR FITTING .....                                       | 147        |
| 12.2 POLYNOMIAL FITTING.....                                    | 149        |
| 12.3 LINEAR INTERPOLATION IN ONE DIMENSION .....                | 150        |
| 12.4 PARABOLIC INTERPOLATION IN ONE DIMENSION.....              | 152        |
| 12.5 INTERPOLATION IN MULTI-DIMENSIONS .....                    | 154        |
| 12.6 NUMERICAL INTEGRATION .....                                | 154        |
| 12.7 SIMPLEX MINIMIZATION .....                                 | 156        |
| 12.8 DETERMINATION OF THE GOODNESS OF FIT .....                 | 159        |

## 9. APPENDIX-1: SPECIFICATION OF RTC/UDL PACKAGE

An overview of the RTC/UdL package is displayed on [Figure 1](#).

### 9.1 SCAMAT INPUT/OUTPUT DESCRIPTION

#### 9.1.1 Input/Output description

#### SCAMAT Inputs

| <i>Input</i>                        | <i>Descriptive name</i>  | <i>Source</i> | <i>Format</i> | <i>Unit</i>                   | <i>Range</i>                                   | <i>Remarks</i>  |
|-------------------------------------|--|---------------|---------------|-------------------------------|--|---|
| <i>scamat_out</i>                   | Output filename  | -             | string        | <i>n.u.</i>                   | -  | <i>Scattering phase matrix</i>  |
| $\lambda$                           | Wavelength   | -             | float         | <i>nm</i>                     | [250;4000]                                     | <i>15 MERIS wavelengths in [400;900]</i>  |
| $\lambda_{ref}$                     | Reference wavelength   | -             | float         | <i>nm</i>                     | [250;4000]                                     | <i>15 MERIS wavelengths in [400;900]</i>  |
| $n_2$                               | Number of scattering angles  | -             | int           | <i>n.u.</i>                   | 83   | <i>Not used (fixed value in the code)</i>   |
| $N$                                 | Number of particle size distributions  | -             | int           | <i>n.u.</i>                   | [1;3]  | <i>Maximum of 3 particle size distributions</i>   |
| $m_\lambda(i), k_\lambda(i)$        | Real and imaginary parts of refractive index at wavelength $\lambda$ for size distribution $i$                 | -             | float         | <i>n.u. / n.u.</i>            | $m_\lambda > 0$<br>$k_\lambda \geq 0$          | $2 \times N$ values   |
| $m_{ref}(i), k_{ref}(i)$            | Real and imaginary parts of refractive index at reference wavelength $\lambda_{ref}$ for size distribution $i$ | -             | float         | <i>n.u. / n.u.</i>            | $m_{ref} > 0$<br>$k_{ref} \geq 0$              | $2 \times N$ values   |
| $r_{min}(i), r_{max}(i)$<br>$dr(i)$ | Minimum, maximum radii and size increment for size distribution $i$  | -             | float         | $\mu m / \mu m$<br>$\mu m$    | $r_{min}, r_{max} \geq 0$<br>$dr \geq 10^{-4}$ | $3 \times N$ values<br><i>Note: if <math>r_{min} \leq 0 \Rightarrow r_{min} = 10^{-4}</math></i>  |
| $ind(i)$<br>$a(i), b(i)$            | Index of selected particle size distribution and its 2 parameters for size distribution $i$                    | -             | float         | <i>n.u.</i><br>$\mu m / n.u.$ | $ind: [1;4]$<br>$(a,b) > 0$                    | $2 \times N$ values<br>$ind=1$ (Junge power-law): $a=r_o, b=\alpha$<br>$ind=2$ (Log normal): $a=r_m, b=\sigma$<br>$ind=3$ (Modified Gamma): $a=\alpha, b=b$<br>$ind=4$ (Gamma-Hansen): $a=r_i, b=r_b$ |
| $n(i) / n$                          | Component mixing ratio for distribution $i$  | -             | float         | <i>n.u.</i>                   | ]0;1]  | $N$ values  |

*Loop on the inputs #6, 7, 8, 9 & 10 for the size distributions (i+1) and (i+2) if necessary !*

Nb: (1) The 'Particle ratio' (see [Section 10.1.1](#)) is the default option included in the Mie's code.

(2) The size increment of  $10^{-4}$  is a critical value acceptable as the limit of Mie's theory. Better acceptable limit would be a value of  $10^{-3}$ .

**SCAMAT Outputs**

| Output   | Descriptive name  | Source | Format | Unit                          | Range    | Remarks   |
|--|---|--------|--------|-------------------------------|----------|---|
| <i>Inputs</i>                                      | Input data card   | -      | string | <i>n.u.</i>                   | -        | -   |
| $\theta$   | Scattering angles   | -      | float  | <i>deg.</i>                   | -        | $n_2$ values                                    |
| $P(\theta)$  | First <i>Stokes</i> parameter   | -      | float  | <i>n.u.</i>                   | -        | $n_2$ values                                    |
| $Q(\theta)$  | Second <i>Stokes</i> parameter  | -      | float  | <i>n.u.</i>                   | -        | $n_2$ values                                    |
| $U(\theta)$  | Third <i>Stokes</i> parameter   | -      | float  | <i>n.u.</i>                   | -        | $n_2$ values                                    |
| $\omega_{o,\lambda}, \omega_{o,\lambda_{ref}}$     | Single scattering albedos at wavelengths $\lambda$ and $\lambda_{ref}$              | -      | float  | <i>n.u.</i>                   | [0;1]    | -   |
| $\sigma_{e,\lambda}^*, \sigma_{e,\lambda_{ref}}^*$ | Normalized extinction coefficients at the wavelengths $\lambda$ and $\lambda_{ref}$ | -      | float  | <i>n.u.</i>                   | $\geq 0$ | Values normalized to $\sigma_{e,\lambda_{ref}}$ |
| $\sigma_{e,\lambda_{ref}}$                         | Extinction coefficient at the wavelength $\lambda_{ref}$                            | -      | float  | $\mu m^{-1} \cdot p c t^{-1}$ | $\geq 0$ | Values normalized to $\sigma_{e,\lambda_{ref}}$ |

*Nb:* Stokes parameters are not normalized to  $4\pi$ , and extinction coefficients are computed for 1 particle (pct) per  $cm^3$ .

**9.1.2 Input / Output sample**

**UDL SCAMAT INPUT CARD**

|               |          |       |  |                                 |
|---------------|----------|-------|--|---------------------------------|
| scamat_test12 |          |       |  | <i>scamat_out</i>               |
| 443.00        |          |       |  | $\lambda$                       |
| 865.00        |          |       |  | $\lambda_{ref}$                 |
| 83            |          |       |  | $n_2$                           |
| 3             |          |       |  | $N$                             |
| 1.530         | 0.500E-2 |       |  | $m_\lambda(1), k_\lambda(1)$    |
| 1.520         | 1.210E-2 |       |  | $m_{ref}(1), k_{ref}(1)$        |
| 0.001         | 20.000   | 0.001 |  | $r_{min}(1), r_{max}(1), dr(1)$ |
| 2             | 0.0050   | 2.99  |  | $ind(1), a(1), b(1)$            |
| 0.93877       |          |       |  | $n(1) / n$                      |
| 1.530         | 0.800E-2 |       |  | $m_\lambda(2), k_\lambda(2)$    |
| 1.530         | 0.800E-2 |       |  | $m_{ref}(2), k_{ref}(2)$        |
| 0.010         | 40.000   | 0.010 |  | $r_{min}(2), r_{max}(2), dr(2)$ |
| 2             | 0.5000   | 2.99  |  | $ind(2), a(2), b(2)$            |
| 2.27E-6       |          |       |  | $n(2) / n$                      |
| 1.750         | 4.550E-1 |       |  | $m_\lambda(3), k_\lambda(3)$    |
| 1.750         | 4.300E-1 |       |  | $m_{ref}(3), k_{ref}(3)$        |
| 0.001         | 20.000   | 0.001 |  | $r_{min}(3), r_{max}(3), dr(3)$ |
| 2             | 0.0118   | 2.00  |  | $ind(3), a(3), b(3)$            |
| 0.06123       |          |       |  | $n(3) / n$                      |

**UDL SCAMAT OUTPUT FILE**

```
'Wavelength (nm):' 443.00
'Reference wavelength (nm):' 865.00
'Number of scattering angles:' 83
'Number of particle size distributions:' 3
'Refractive index (Re,Im) 1:' 1.530 .500E-02
'                          2:' 1.530 .800E-02
'                          3:' 1.750 .455E+00
'Reference refractive index (Re,Im): 1:' 1.520 .121E-01
'                                   2:' 1.520 .800E-02
'                                   3:' 1.750 .430E+00
'Min,max,step of particle size (mic.) 1:' .0010 20.0000 .0010
'                                       2:' .0100 40.0000 .0100
'                                       3:' .0010 20.0000 .0010
'Size distrib. (ind) & param. (a,b) 1:' 2 .0050 2.9900
'                                       2:' 2 .5000 2.9900
'                                       3:' 2 .0118 2.0000
'Volume percentage 1:' .93877E+00
'                  2:' .22700E-05
'                  3:' .61230E-01

180.000 .3965297226511E+00 -.3033973745760E-18 -.3965297226511E+00
178.288 .3906987727427E+00 .3280904645194E-02 -.3870382071630E+00
176.071 .3713085613266E+00 .1299520252989E-01 -.3562193949808E+00
173.841 .3433655622993E+00 .2541934054221E-01 -.3176056777347E+00
171.607 .3155120644732E+00 .3849359643447E-01 -.2768608999339E+00
169.373 .2925413658440E+00 .5076203116121E-01 -.2385790292804E+00
167.138 .2761213689805E+00 .6137258006346E-01 -.2052855707270E+00
164.903 .2655951241019E+00 .6970987689505E-01 -.1772529859866E+00
162.667 .2586895005878E+00 .7502320979339E-01 -.1532783059357E+00
160.432 .2528095241508E+00 .7676175479982E-01 -.1325739325694E+00
158.196 .2466372353446E+00 .7523171336793E-01 -.1149637861313E+00
155.960 .2398535852267E+00 .7122990039459E-01 -.1001090365695E+00
153.724 .2325659609299E+00 .6559698870371E-01 -.8758926734734E-01
151.489 .2250455822688E+00 .5902456427466E-01 -.7698691525106E-01
149.253 .2175895262341E+00 .5201312901615E-01 -.6791749415455E-01
147.017 .2104523764868E+00 .4489674220163E-01 -.6003558561711E-01
144.781 .2038200399457E+00 .3788384348926E-01 -.5304275209904E-01
142.545 .1978108018673E+00 .3109302210777E-01 -.4669372027431E-01
140.309 .1924903934246E+00 .2458230215383E-01 -.4079335952967E-01
138.073 .1878895347772E+00 .1837191197609E-01 -.3518701959584E-01
135.837 .1840182111084E+00 .1245958164559E-01 -.2975007900509E-01
133.601 .1808757773289E+00 .6830317174896E-02 -.2437957273285E-01
131.365 .1784576788034E+00 .1463033470890E-02 -.1898772655123E-01
129.130 .1767595138042E+00 -.3665464958339E-02 -.1349719898464E-01
126.894 .1757795193519E+00 -.8578448587751E-02 -.7837665607403E-02
124.658 .1755203807095E+00 -.1329802754152E-01 -.1943121465736E-02
122.422 .1759904854018E+00 -.1784441743886E-01 .4250255561485E-02
120.186 .1772046894223E+00 -.2223565964570E-01 .1080573319270E-01
117.950 .1791850037403E+00 -.2648742809936E-01 .1778746678285E-01
115.714 .1819611286176E+00 -.3061302269933E-01 .2526182910894E-01
113.478 .1855708545548E+00 -.3462354832480E-01 .3329863351813E-01
111.242 .1900605895835E+00 -.3852804029184E-01 .4197235667038E-01
109.006 .1954860556603E+00 -.4233349406273E-01 .5136338727238E-01
106.770 .2019130171233E+00 -.4604494424065E-01 .6155925708358E-01
104.534 .2094181143805E+00 -.4966553852924E-01 .7265591323205E-01
102.298 .2180898579919E+00 -.5319656614699E-01 .8475909244826E-01
100.062 .2280297443749E+00 -.5663749643045E-01 .9798580242638E-01
97.826 .2393535466815E+00 -.5998599644858E-01 .1124659470415E+00
95.590 .2521928446245E+00 -.6323788887794E-01 .1283441366009E+00
93.354 .2666967989591E+00 -.6638707013675E-01 .1457816987864E+00
91.118 .2830341830591E+00 -.6942540902700E-01 .1649589085686E+00
90.000 .2919490839640E+00 -.7089988663745E-01 .1752620028366E+00
88.882 .3013957209052E+00 -.7234262178188E-01 .1860774662258E+00
86.646 .3219967863924E+00 -.7512614514356E-01 .2093632209823E+00
84.410 .3450805256102E+00 -.7776106337274E-01 .2350691604358E+00
```

|        |                    |                     |                    |
|--------|--------------------|---------------------|--------------------|
| 82.174 | .3709214772119E+00 | -.8023016270063E-01 | .2634787922518E+00 |
| 79.938 | .3998297784497E+00 | -.8251415304212E-01 | .2949100505564E+00 |
| 77.702 | .4321560206200E+00 | -.8459203530305E-01 | .3297198318375E+00 |
| 75.466 | .4682967419413E+00 | -.8644152340648E-01 | .3683093248970E+00 |
| 73.230 | .5087005086792E+00 | -.8803936491282E-01 | .4111302751507E+00 |
| 70.994 | .5538745831095E+00 | -.8936144838235E-01 | .4586921776910E+00 |
| 68.758 | .6043923279499E+00 | -.9038276052376E-01 | .5115700976860E+00 |
| 66.522 | .6609015550975E+00 | -.9107740399308E-01 | .5704132761754E+00 |
| 64.286 | .7241339363339E+00 | -.9141876002574E-01 | .6359551207304E+00 |
| 62.050 | .7949155235325E+00 | -.9137975833053E-01 | .7090240646960E+00 |
| 59.814 | .8741784387790E+00 | -.9093330211686E-01 | .7905551131647E+00 |
| 57.578 | .9629740012076E+00 | -.9005297052942E-01 | .8816028292046E+00 |
| 55.342 | .1062487336325E+01 | -.8871394928398E-01 | .9833561604056E+00 |
| 53.106 | .1174052643104E+01 | -.8689363126441E-01 | .1097154064357E+01 |
| 50.870 | .1299169689623E+01 | -.8457231204493E-01 | .1224502336334E+01 |
| 48.635 | .1439522682481E+01 | -.8173446166930E-01 | .1367093601552E+01 |
| 46.399 | .1597000177114E+01 | -.7837061470665E-01 | .1526826665302E+01 |
| 44.163 | .1773715816448E+01 | -.7447922496096E-01 | .1705825766275E+01 |
| 41.927 | .1972031591718E+01 | -.7006805385296E-01 | .1906463380878E+01 |
| 39.691 | .2194585738845E+01 | -.6515714180905E-01 | .2131385815751E+01 |
| 37.455 | .2444322938628E+01 | -.5978016793599E-01 | .2383539687270E+01 |
| 35.219 | .2724529706553E+01 | -.5398046675896E-01 | .2666205761382E+01 |
| 32.983 | .3038884222146E+01 | -.4781157539085E-01 | .2983041751257E+01 |
| 30.747 | .3391523191867E+01 | -.4134131095969E-01 | .3338141932163E+01 |
| 28.511 | .3787133636302E+01 | -.3465242342122E-01 | .3736137924503E+01 |
| 26.276 | .4231085409726E+01 | -.2784667275319E-01 | .4182360680465E+01 |
| 24.040 | .4729626940862E+01 | -.2105541361668E-01 | .4683084093184E+01 |
| 21.804 | .5290180612787E+01 | -.1445154963310E-01 | .5245882861391E+01 |
| 19.568 | .5921841958965E+01 | -.8287759103643E-02 | .5880187116887E+01 |
| 17.333 | .6636308013014E+01 | -.2959470447050E-02 | .6598206538319E+01 |
| 15.097 | .7449721688224E+01 | .9972953574741E-03  | .7416563762588E+01 |
| 12.862 | .8386539411706E+01 | .3127496904159E-02  | .8359627411350E+01 |
| 10.627 | .9488243096452E+01 | .3239096547501E-02  | .9468099476853E+01 |
| 8.393  | .1083929274598E+02 | .1285316601959E-02  | .1082545080801E+02 |
| 6.159  | .1267750140123E+02 | -.2563732325216E-02 | .1266852699469E+02 |
| 3.929  | .1612905922843E+02 | -.6998121219444E-02 | .1612278172232E+02 |
| 1.712  | .3473475333535E+02 | -.3941495664279E-02 | .3472943575538E+02 |
| .000   | .7369529881157E+03 | -.2867455687269E-15 | .7369529881157E+03 |

.901901846E+00 .843478122E+00  
.220750513E+01 .100000000E+01  
.340984554E-04

**Note:** Inputs used to generate the scattering phase function are given in the header. The output is formatted into 4 columns, respectively Theta, P(Theta), Q(Theta), U(Theta)

with Theta : scattering angle  
(P,Q,U): 3 Stokes parameters  
not normalized to 4 PI.

The last 5 values stand for, respectively:  
wo(l) ; wo(l\_ref) => single scatt. albedo  
Qext(l)/Qext(l\_ref) ; 1 => extinction coefficient  
Qext(l\_ref) => extinction coefficient at l\_ref  
[mic^-1]

*Nb: Columns are for  $\theta$ ,  $P(\theta)$ ,  $Q(\theta)$ ,  $U(\theta)$ . Last 5 values at the end of output file stand for  $\omega_{0,\lambda}$ ,  $\omega_{0,\lambda_{ref}}$ ,  $\sigma_{e,\lambda}^*$ ,  $\sigma_{e,\lambda_{ref}}^*$ ,  $\sigma_{e,\lambda_{ref}}$ .*



## 9.2 UPRAD INPUT/OUTPUT DESCRIPTION

### RTC/UdL-UPRAD Inputs

| Input             | Descriptive name  | Source   | Format | Unit        | Range             | Remarks  |
|-------------------|---|--|--------|-------------|-------------------|--|
| <i>out_file</i>   | Output filename   | -  | string | <i>n.u.</i> | -                 | MERIS radiances at TOA   |
| <i>i_branch</i>   | Index to select the type of test case   | -  | int    | <i>n.u.</i> | [1;4]<br>or<br>11 | 1-Land + Clear sky [SO/GAME]<br>2-Ocean + Clear sky [SO/SOAO]<br>3-Land + Cloud sky [GAME]<br>4-Land + Water vapor [GAME]<br>11-Primary scattering only [SO] |
| <i>n</i>          | MERIS band #  | -  | int    | <i>n.u.</i> | [1;15]            | 15 MERIS spectral bands (not used)   |
| $U_{H_2O}$        | Total water vapor amount  | -  | float  | $g/cm^2$    | $\geq 0$          | - GAME: $U_{H_2O} > 0$<br>- SO/SOAO: $U_{H_2O} = 0$  |
| $U_{O_2}$         | Total oxygen vapor amount   | -  | float  | $g/cm^2$    | $\geq 0$          | - GAME: $U_{O_2} > 0$ (See note 1)<br>- SO/SOAO: $U_{O_2} = 0$   |
| <i>ESFT</i>       | Auxiliary data file (number of ESFT terms and ESFT coefficients $[a_i, k_i]$ for $H_2O$ and $O_2$ transmittivities in the 15 MERIS bands) | File provided by UdL/LISE institute            | string | <i>n.u.</i> | -                 | Coefficients $(a_i, k_i)$ for computing $H_2O$ & $O_2$ transm. above layer <i>i</i><br>- used in GAME branch only<br>- filename: ' <i>input/RKLM_AL</i> '    |
| $P_s$             | Surface pressure  | -  | float  | <i>hPa</i>  | $\geq 194$        | - GAME:<br>if ( $P_s < 1013.25$ ) $\Rightarrow$ set $P_s$ with MLS<br>- SO/SOAO:<br>if ( $P_s < 1013.25$ ) $\Rightarrow$ call <i>otc_rayleigh</i>            |
| $\tau_\lambda^R$  | Rayleigh optical thickness (for $P_s \geq 1013.25$ <i>hPa</i> )   | Input value or output from <i>otc_rayleigh</i> | float  | <i>n.u.</i> | [0;1[             | - GAME: input value<br>- SO / SOAO: if ( $P_s < 1013.25$ )<br>$\Rightarrow \tau_\lambda^R$ recomputed<br>else input value                                    |
| <i>aerosol1</i>   | Scattering phase matrix for aerosol layer #1  | Output file from <i>scamat</i>                 | string | <i>n.u.</i> | -                 | $\theta, P(\lambda, r, m, \theta), \omega_{o,\lambda}, \sigma_{e,\lambda}$<br>for the legendre polynomial development of scatt. phase matrix                 |
| $\tau_{550}^a(1)$ | Aerosol optical thickness at 550nm for layer #1   | -  | float  | <i>n.u.</i> | [0;10]            | Realistic values in [0;0.8]  |
| <i>aerosol2</i>   | Scattering phase matrix for aerosol layer #2  | Output file from <i>scamat</i>                 | string | <i>n.u.</i> | -                 | $\theta, P(\lambda, r, m, \theta), \omega_{o,\lambda}, \sigma_{e,\lambda}$<br>for the Legendre polyn. development of scatt. phase matrix (See note 3)        |
| $\tau_{550}^a(2)$ | Aerosol optical depth at 550 nm for layer #2  | -  | float  | <i>n.u.</i> | [0;10]            | Realistic values in [0;0.8]  |
| <i>aerosol3</i>   | Scattering phase matrix for aerosol layer #3  | Output file from <i>scamat</i>                 | string | <i>n.u.</i> | -                 | $\theta, P(\lambda, r, m, \theta), \omega_{o,\lambda}, \sigma_{e,\lambda}$<br>for the Legendre polyn. development of scatt. phase matrix (See note 3)        |

| <i>Input</i>               | <i>Descriptive name</i>  | <i>Source</i>                               | <i>Format</i> | <i>Unit</i>   | <i>Range</i>                  | <i>Remarks</i>  |
|----------------------------|--|---|---------------|---------------|-------------------------------|---|
| $\tau_{550}^a(3)$          | Aerosol optical depth at 550 nm for layer 3  | -   | float         | n.u.          | [0;10]                        | Realistic values in [0;0.8]   |
| <i>cloud1</i>              | Scattering phase matrix for cloud layer 1  | Output file from <i>scamat</i>              | string        | n.u.          | -                             | GAME: $\theta, P(\lambda, r, m, \theta), \omega_{o,\lambda}, \sigma_{e,\lambda}$ for the Legendre polyn. development of scatt. phase matrix (See note 2)            |
| <i>cloud2</i>              | Scattering phase matrix for cloud layer 2  | Output file from <i>scamat</i>              | string        | n.u.          | -                             | GAME: $\theta, P(\lambda, r, m, \theta), \omega_{o,\lambda}, \sigma_{e,\lambda}$ for the Legendre polyn. development of scatt. phase matrix (See note 2)            |
| <i>cloud3</i>              | Scattering phase matrix for cloud layer 3  | Output file from <i>scamat</i>              | string        | n.u.          | -                             | GAME: $\theta, P(\lambda, r, m, \theta), \omega_{o,\lambda}, \sigma_{e,\lambda}$ for the Legendre polyn. development of scatt. phase matrix (See note 2)            |
| <i>phyto</i>               | Scattering phase matrix for phytoplankton  | File provided by UdL/LISE (Petzold)         | string        | n.u.          | -                             | SOAO: $\theta, P(\lambda, r, m, \theta), \omega_{o,\lambda}, \sigma_{e,\lambda}$ for the Legendre polyn. development of scatt. phase matrix                         |
| $\sigma_{e,\lambda}^p$     | Extinction coefficient for phytoplankton   | Input value or output from <i>iop_water</i> | float         | $m^{-1}$      | $\geq 0$                      | Only used in SOAO to compute the contribution of oceanic layers to upwelling radiances at TOA   |
| $\omega_{o,\lambda}^p$     | Single scattering albedo for phytoplankton   | Input value or output from <i>iop_water</i> | float         | n.u.          | [0;1]                         | Only used in SOAO to compute the contribution of oceanic layers to upwelling radiances at TOA   |
| <i>spm</i>                 | Scattering phase matrix for SPM  | File provided by UdL/LISE (Petzold)         | string        | n.u.          | -                             | SOAO: $\theta, P(\lambda, r, m, \theta), \omega_{o,\lambda}, \sigma_{e,\lambda}$ for the Legendre polyn. development of scatt. phase matrix                         |
| $\sigma_{e,\lambda}^{spm}$ | Extinction coefficient for SPM   | Input value or output from <i>iop_water</i> | float         | $m^{-1}$      | $\geq 0$                      | Only used in SOAO to compute the contribution of oceanic layers to upwelling radiances at TOA   |
| $\omega_{o,\lambda}^{spm}$ | Single scattering albedo for SPM   | Input value or output from <i>iop_water</i> | float         | n.u.          | [0;1]                         | Only used in SOAO to compute the contribution of oceanic layers to upwelling radiances at TOA   |
| $\sigma_{e,\lambda}^{ys}$  | Extinction coefficient for yellow substance  | Input value or output from <i>iop_water</i> | float         | $m^{-1}$      | $\geq 0$                      | Only used in SOAO to compute the contribution of oceanic layers to upwelling radiances at TOA   |
| <i>vertical</i>            | Vertical distribution of aerosol and cloud optical depths at ref. wavelength (550nm) | File provided by UdL/LISE                   | string        | n.u.          | -                             | Altitudes from sea level to TOA.<br><u>Note:</u> Cloud 1: Layer 0 to 5<br>Cloud 2: Layer 6 to 15<br>Cloud 3: Layer 16 +   |
| $I_s$                      | Maximum order of the Legendre polynomial decomposition (Fourier)                     | Optimal values after tests                  | int           | n.u.          | GAME [4;60]<br>SO/SOAO [0;80] | - GAME: $I_s = 60$ (optimal value)<br>- SO/SOAO: $I_s = 80$ (optimal value)<br>- for total atm. transm. computation, select $I_s = 0, \mathcal{G}_v = -1$ (with SO) |
| $\rho_s$                   | Surface reflectance  | -   | float         | n.u.          | [0;1]                         | -GAME/SO: Lambertian surface<br>-SOAO: $\rho_s$ fixed to 0 for sea bottom   |
| $E_o$                      | Solar constant at TOA  | -   | float         | $W/m^2/\mu m$ | 1                             | Not used (fixed value in the code)  |

| Input                  | Descriptive name                                      | Source                                      | Format | Unit     | Range        | Remarks   |
|------------------------|---|---|--------|----------|--------------|---|
| $\sigma_{e,\lambda}^w$ | Extinction coefficient for pure oceanic water         | Input value or output from <i>iop_water</i> | float  | $m^{-1}$ | $\geq 0$     | Only used in SOAO to compute the contribution of oceanic layers to upwelling radiances at TOA   |
| $\omega_{o,\lambda}^w$ | Single scattering albedo for pure oceanic water       | Input value or output from <i>iop_water</i> | float  | n.u.     | [0;1]        | Only used in SOAO to compute the contribution of oceanic layers to upwelling radiances at TOA   |
| $w_s$                  | Wind speed at 0.5 m above sea level                   | -   | float  | m/s      | $\geq 0$     | Only used in SO to compute multiple reflexions (sun glint) on the wind-roughened sea surface (See note 4)   |
| $n_s$                  | Nb of SZAs  | -   | int    | n.u.     | [1;60]       | For example (3, 16, 25) respectively as used in a RTC intervalvalidation  |
| $n_v$                  | Nb of VZAs  | -   | int    | n.u.     | [1;60]       |   |
| $n_{\Delta\phi}$       | Nb of RAAs  | -   | int    | n.u.     | [1;25]       |   |
| $\mathcal{G}_s$        | Solar zenith angles                                   | -   | float  | deg.     | [0;90[       | List of SZA values given in an increasing order. For example: 6.97; 29.96 or 69.99  |
| $\mathcal{G}_v$        | View zenith angles                                    | -   | float  | deg.     | -1 or [0;90[ | List of VZA values given in a decreasing order. For example: 87.14; 81.43; 75.71; 69.99; 64.28; 58.56; 52.84; 47.12; 41.40; 35.68; 29.96; 24.24; 18.51; 12.76; 6.97; 0  |
| $\Delta\phi$           | Relative azimuth angles between sun / view directions | -   | float  | deg.     | [0;180]      | List of RAA values given in an increasing order. For example: 0; 7.50; 15.00; 22.50; 30.00; 37.50; 45.00; 52.50; 60.00; 67.50; 75.00; 82.50; 90.00; 97.50; 105.00; 112.50; 120.00; 127.50; 135.00; 142.50; 150.00; 157.50; 165.00; 172.50; 180.00 |
| <i>pol</i>             | Flag for polarization                                 | -   | int    | n.u.     | 0 or 1       | - GAME: not used<br>- SO/SOAO:<br>0 - no polarization<br>1 - with polarization  |

Notes: (1) For  $U_{O_2} > 0$ , a vertical distribution of the oxygen vapor content is computed in RTC/GAME using a pressure profile derived from the MLS (33 layers). Thus the input  $U_{O_2}$  represents a fraction of an oxygen vapor amount of  $238.2 \text{ g cm}^{-2}$ . As an example,  $U_{O_2} = 1$  yields to a total oxygen vapor content of  $238.2 \text{ g cm}^{-2}$ .

(2) For cloudy-sky conditions, only one aerosol layer can be defined to be run with RTC/GAME.

(3) For clear-sky conditions, if the aerosol scattering is simulated for a unique aerosol layer (i.e., aerosol layer #1) then the aerosol scattering phase matrix of this layer has to be used as input for the two other aerosol layers.

(4) For a wind-roughened sea surface ( $w_s > 0$ ), RTC/SO needs a Cox-Munk binary file which contains the Fourier series terms of the Fresnel reflection matrix at the 'air-sea' interface generated with RTC/Wind. Note that 2 current versions of RTC/SO are available to be run with 2 different sets of 3 Cox-Munk files:

(a) Cox-Munk file for a wind-speed of 1.5 m/s ( $w_s < 2$ ), 3 m/s ( $2 \leq w_s < 5$ ), and 7.2 m/s ( $w_s \geq 5$ ).

(b) Cox-Munk file for a wind-speed of 1.5 m/s ( $w_s < 3.25$ ), 5 m/s ( $3.25 \leq w_s < 7.5$ ), and 10 m/s ( $w_s \geq 7.5$ ).

### RTC/UdL-UPRAD Outputs

| Input                         | Descriptive name  | Source | Format | Unit      | Range              | Remarks   |
|-------------------------------|---|--------|--------|-----------|--------------------|---|
| Inputs                        | Input data card   | -      | string | n.u.      | -                  | if 'OutputFlag'=1 in 'uprad_def'  |
| $\vartheta_s$                 | Solar zenith angles   | -      | float  | deg.      | [0;90[             | List of input SZAs. For example:<br>6.97; 29.96; 69.99  |
| $\vartheta_v$                 | Viewing zenith angles                                       | -      | float  | deg.      | -1<br>or<br>[0;90[ | List of input VZAs. For example:<br>0; 6.97; 12.76; 18.51; 24.24; 29.96;<br>35.68; 41.40; 47.12; 52.84; 58.56; 64.28;<br>69.99; 75.71; 81.43; 87.14   |
| $\Delta\phi$                  | Relative azimuth angles<br>between sun / view<br>directions | -      | float  | deg.      | [0;180]            | List of input RAAs. For example:<br>0; 7.50; 15.00; 22.50; 30.00; 37.50;<br>45.00; 52.50; 60.00; 67.50; 75.00; 82.50;<br>90.00; 97.50; 105.00; 112.50; 120.00;<br>127.50; 135.00; 142.50; 150.00; 157.50;<br>165.00; 172.50; 180.00 |
| $L_{\lambda}^{\uparrow(TOA)}$ | MERIS normalized<br>radiances (TOA)                         | -      | float  | $sr^{-1}$ | $\geq 0$           | $(n_s \times n_v \times n_{\Delta\phi})$ values<br>(solar irradiance = $1 W \cdot m^{-2} \cdot \mu m^{-1}$ )  |
| $T_{\lambda}^{(Total)}$       | MERIS total atmospheric<br>transmittance                    | -      | float  | n.u.      | [0;1]              | Total atmospheric transmittance<br>for inputs $I_s = 0$ , $\vartheta_v = -1$  |

### 9.3 AUXILIARY FILE: 'UPRAD\_DEF'

The *Mie's* code ('scamat.f') and RTC/UdL ('rtc\_uprad.f') are controlled by a common auxiliary file (namely, 'uprad\_def') which is read during the execution. This file contains input filenames, flags for additional output data and the definition of the 15 MERIS spectral bands.

#### 'uprad\_def' file

| Input       | Descriptive name  | Format | Unit | Value      | Code                     |
|-------------|---|--------|------|------------|--------------------------|
| RunOption   | Structure of the input card: [0] with full description of input data (used for MERISAT), [1] without comment (used for RTC/Intervalidation) | int    | n.u. | [0] or [1] | scamat<br>rtc_uprad      |
| Gauss_File1 | GAUSS quadrature data $(\mu_i, w_i)$ using 41 directions  | string | n.u. | -          | scamat<br>rtc_soao       |
| Gauss_File2 | GAUSS quadrature data $(\mu_i, w_i)$ using 24 directions  | string | n.u. | -          | step1                    |
| Gauss_File3 | GAUSS quadrature data $(\mu_i, w_i)$ using 25 directions (including nadir)  | string | n.u. | -          | step2<br>step3<br>rtc_so |
| Wind_File1  | Fourier series expansion of the Fresnel reflexion matrix for a wind-roughened sea surface (1 <sup>st</sup> wind-speed)                      | string | n.u. | -          | rtc_so                   |

| <i>Input</i>            | <i>Descriptive name</i>  | <i>Format</i> | <i>Unit</i> | <i>Value</i> | <i>Code</i>            |
|-------------------------|--|---------------|-------------|--------------|------------------------|
| <i>Wind_File2</i>       | <i>Fourier series expansion of the Fresnel reflexion matrix for a wind-roughened sea surface (2<sup>nd</sup> wind-speed)</i> | string        | <i>n.u.</i> | -            | rtc_so                 |
| <i>Wind_File3</i>       | <i>Fourier series expansion of the Fresnel reflexion matrix for a wind-roughened sea surface (3<sup>rd</sup> wind-speed)</i> | string        | <i>n.u.</i> | -            | rtc_so                 |
| <i>Beta_File</i>        | <i><math>\beta_l</math> coefficients derived from Legendre decomposition of Petzold's phase function</i>                     | string        | <i>n.u.</i> | -            | rtc_soao               |
| <i>Nb of bands</i>      | Number of MERIS spectral bands   | int           | <i>n.u.</i> | -            | rtc_uprad              |
| <i>MERIS band X</i>     | Nominal wavelength and FWMH for MERIS band X   | float         | <i>nm</i>   | -            | iop_water<br>rtc_uprad |
| <i>Output_structure</i> | Structure of the output file: [0] without header, [1] with header (list of inputs)   | int           | <i>n.u.</i> | [0] or [1]   | rtc_uprad              |

Note: This 'uprad\_def' file has to be created with an header of 4 lines. The last column indicates which codes from the RTC / UdL package use the inputs of 'uprad\_def'.

**Sample of 'uprad\_def' file**

```

*****
***  RTC/LISE - I/O files - Flags - MERIS Bands  ***
*****

'RunOption      = '      1
'Gauss_File1    = '      'input/gauss41'
'Gauss_File2    = '      'input/gauss24'
'Gauss_File3    = '      'input/gauss25'
'Wind_File1     = '      'input/wind01'
'Wind_File2     = '      'input/wind05'
'Wind_File3     = '      'input/wind10'
'Beta_File      = '      'input/beta_petzold'
'Nb of bands    = '      15
'MERIS band 01 = '      412.5    10.0
'band 02       = '      442.5    10.0
'band 03       = '      490.0    10.0
'band 04       = '      510.0    10.0
'band 05       = '      560.0    10.0
'band 06       = '      620.0    10.0
'band 07       = '      665.0    10.0
'band 08       = '      681.25   7.5
'band 09       = '      708.75   10.0
'band 10       = '      753.75   7.5
'band 11       = '      761.875  3.75
'band 12       = '      778.75   15.0
'band 13       = '      865.0    20.0
'band 14       = '      885.0    10.0
'band 15       = '      900.0    10.0
'OutputFlag    = '      0

```

## 9.4 ADDITIONAL TOOLS

The following tools are useful to generate some inputs to the RTC/UdL, except for the RTC/PO2 module which is used in the MERISAT to generate some MERIS LUTs [AD-7]. Each tool is briefly described and the local variables are listed in an associated table.

### 9.4.1 OTC/COMPUTE\_FSP

Description:

This module allows one to compute the forward scattering proportion  $f_{sp}(\mu=0)$  of a scattering phase matrix  $P(\lambda, r, n, \theta)$  using the polynomial  $P_n^1(\cos\theta)$  derived from its Legendre expansion (see Section 2.8.4).

Processing:

Using the Legendre polynomials expansion of the phase function, the forward scattering proportion  $f_{sp}(\mu=0)$  is computed as:

$$f_{sp}(\mu=0) = \frac{1}{2} \cdot \sum_{l=0}^L \left( \beta_l p_l(\mu=0) \cdot \sum_{i=1}^N w_i \cdot p_l(\mu_i) \right)$$

With  $L$  the number of Legendre polynomials,  $N$  the number of directions used in the Gauss quadrature to describe the angular variation of  $P(\lambda, r, n, \theta)$ ,  $\mu_i$  the cosine of Gaussian angle and  $w_i$  the associated weight.

Tool:

**'compute\_FSP.f'**

Input / Output description:

**OTC/COMPUTE\_FSP – Input/Output**

| <i>Input/Output</i><br><i>t</i>   | <i>Descriptive name</i>                      | <i>Source</i> | <i>Format</i> | <i>Unit</i> | <i>I/O</i> | <i>Remarks</i>   |
|-----------------------------------|--|---------------|---------------|-------------|------------|--|
| <i>Pa_file</i>                    | Input filename                               | -             | string        | <i>n.u.</i> | I          | <i>Phase function file with <math>P_a(\Theta, \lambda)</math></i>    |
| <i>Fa_file</i>                    | Output filename                              | -             | float         | <i>n.u.</i> | I          | <i>Phase function file with <math>f_{sp}(\theta, \lambda)</math></i> |
| $\theta, f_{sp, \lambda}(\theta)$ | Zenith angle & forward scattering proportion | -             | float         | <i>n.u.</i> | O          | -  |

## 9.4.2 RTC/GAUSS

### Description:

This module allows one to generate the *Gaussian* angles ( $\mu$ ) and associated weights ( $w$ ) using the *Gauss-Legendre* quadrature (see [Section 12.6](#)). This is used to numerically solve the RTE within the 'Atmosphere-Land / Ocean' system (see [Section 6.2.2](#)).

### Processing:

The *Gauss-Legendre* quadrature is fully described in [Section 12.6](#).

### Tool:

'rtc\_gauss.f'

### Input description:

#### RTC/GAUSS – Inputs

| Input                  | Descriptive name              | Source | Format | Unit        | Range   | Remarks  |
|------------------------|-------------------------------|--------|--------|-------------|---------|--|
| $n_g$                  | Number of <i>Gauss</i> angles | -      | int    | <i>n.u.</i> | [2;80]  | - <i>GAME, SO</i> : $n_g = 48$<br>- <i>SOAO</i> : $n_g = 80$ |
| $\varphi_i, \varphi_f$ | Azimuth angular interval      | -      | float  | <i>deg.</i> | [0;180] | Selected in [ 0 ; 180° ]                                     |

### Output description:

#### RTC/GAUSS – Outputs

| Output  | Descriptive name          | Source | Format | Unit        | Range | Remarks            |
|---------|---------------------------|--------|--------|-------------|-------|--------------------|
| $\mu_i$ | <i>Gauss</i> angle values | -      | float  | <i>n.u.</i> | [0;1] | $(n_g / 2)$ values |
| $w_i$   | Associated weights        | -      | float  | <i>n.u.</i> | [0;1] | -                  |

Nb: For *RTC/SO* and *RTC/SOAO* the exact nadir angle ( $\mu_o=1, w_o=0$ ) is added in the *Gauss* quadrature output file for a better estimate of the upwelling nadir radiance.

### 9.4.3 RTC/PO2

#### Description:

This module allows one to compute the transmittance integrated over each of the 21 shifted MERIS  $O_2$  filters (*i.e.*, each of the 21 lines corresponding to the 21 spectral shifts of  $\pm 0.1\text{ nm}$  applied on the MERIS  $O_2$  filter centred at  $761.75\text{ nm}$ ), as a function of the product of the air mass ( $M$ ) by the square of the surface pressure ( $P_s$ ). Each of the 21 output files will then be used in the MERISAT tool for retrieving the ESFT coefficients ( $a_l, k_l$ ) which rely the product ( $M.P_s^2$ ) to the  $O_2$  transmittance (see Section 2.9).

Note that this code is not used in the current generation of MERIS- $O_2$  LUTs (*i.e.*, transmittances and corrective factors for the surface pressure) for the 3<sup>rd</sup> MERIS data reprocessing.

#### Processing:

From the pre-computed monochromatic absorption coefficients, calculated with the LBL model and the HITRAN-2000 database ([RD-21], [RD-64]) for a standard atmospheric profile [RD-16], monochromatic transmittances  $T_v$  (for the total atmosphere) can be expressed as a function of the airmass ( $M$ ) and the surface pressure ( $P_s$ ). These monochromatic transmittances are defined as the product of intrinsic transmittances within the atmospheric layers:

$$T_v(M, P_s) = \prod_{P=P_s}^0 \exp[-k_v(P) \cdot U_{O_2}(P) \cdot M]$$

where  $k_v(P)$  and  $P$  are respectively the monochromatic absorption coefficients and the pressure at each altitude level.

A set of transmittances is generated for different ( $M, P$ ) values. Transmittance  $T$  integrated over the MERIS spectral band (from  $\nu_1$  to  $\nu_2$ ) can then be computed as a function of the filter spectral response  $f_v$  as follows:

$$T(M, P_s) = \frac{\int_{\nu_1}^{\nu_2} f_v \cdot T_v(M, P_s) \cdot d\nu}{\int_{\nu_1}^{\nu_2} f_v \cdot d\nu}$$

#### Tool:

'rtc\_po2.f'

#### Input description:

Three input files are required for running the RTC/PO2 module:

- *data\_O2*: atmospheric parameters description,
- *data\_LBL\_O2*: monochromatic absorption coefficients computed with the LBL code,
- *MERIS-O2*: filter at  $761.75\text{ nm}$  with the same spectral resolution as data from '*data\_LBL\_O2*'.

The number of altitude levels is fixed to 49 in the RTC/PO2 module.



**RTC/PO2 [data\_O2 input file]**

| Input     | Descriptive name         | Source | Format | Unit                  | Range    | Remarks  |
|-----------|--------------------------|--------|--------|-----------------------|----------|----------|
| $h$       | Altitude above sea level | -      | float  | km                    | $\geq 0$ | Not used |
| $P_s$     | Surface pressure         | -      | float  | hPa                   | $\geq 0$ | -        |
| $T$       | Temperature              | -      | float  | K                     | $\geq 0$ | Not used |
| $U_{O_2}$ | Absorber amount          | -      | float  | mol. cm <sup>-2</sup> | $\geq 0$ | -        |

**RTC/PO2 [data\_LBL\_O2 input file]**

| Input   | Descriptive name   | Source | Format | Unit                            | Range    | Remarks                            |
|---------|--|--------|--------|---------------------------------|----------|------------------------------------|
| $\nu$   | Wavenumber   | -      | float  | cm <sup>-1</sup>                | $\geq 0$ | [ 12800 – 13400 cm <sup>-1</sup> ] |
| $k_\nu$ | Monochromatic absorption coefficient values at each altitude level | -      | float  | cm <sup>2</sup> g <sup>-1</sup> | $\geq 0$ | -                                  |

Output description:

Twenty-one output files (namely resmp2-xx) are generated by PO2 module. Each file contains 80 transmittance values as a function of the airmass and the pressure.

**RTC/PO2 Outputs [resmp2-xx file]**

| Output    | Descriptive name                  | Source | Format | Unit             | Range    | Remarks |
|-----------|-----------------------------------|--------|--------|------------------|----------|---------|
| $M.P_s^2$ | Airmass by the square of pressure | -      | float  | hPa <sup>2</sup> | $\geq 0$ | -       |
| $T_{O_2}$ | Oxygen transmittivity             | -      | float  | n.u.             | [0;1]    | -       |

#### 9.4.4 RTC/WIND

Description:

This module generates the *Fourier* series expansion of the *Fresnel* reflexion matrix for a *Cox-Munk* surface model. This is used to simulate the sun glint over a wind-roughened sea surface characterized by a *Cox-Munk* wave slope distribution (see [Section 5](#)).

Processing:

The *Fourier* series expansion of the *Fresnel* reflexion matrix is performed with the following steps:

- *Step1:* Computation of the *Legendre* polynomial representation of the *Fresnel* matrix (i.e., the sets of  $L+1$  coefficients:  $\alpha_l, \beta_l, \gamma_l, \zeta_l$ ; see [Section 6.2.2.2](#)).
- *Step2:* Expansion of the *Cox-Munk* wave slope distribution into a *Fourier* series
  - The probability function is computed for each set of *Gaussian* angles.
  - The number of terms required for the integration step (which determines the *Fourier* components) is tested against a limiting contribution since the series monotonically decreases.
  - The integration to determine *Fourier* coefficients is carried out. This involves a bisection technique which subdivides the integration region into successively double the number of cell until convergence is reached.
- *Step3:* Computation of the *Fourier* serie components associated with the *Legendre* representation of the reflection matrix.  
  
Results are then combined with *Fourier* representation of the *Cox-Munk* wave slope distribution. Final result does not match with the input data form to the RTC/SO due to the angular decomposition mis-matches.
- *Step4:* Re-write the combined results from step3 in order to be used as input to the RTC/SO.

Tools:

The four steps of the methodology presented above are completed with the following tools: '*step1.f*', '*step2.f*', '*step3.f*' and '*step4.f*' (which make up the **RTC/WIND** package).

Input / Output description:

**RTC/WIND [step1] – Input/Output**

| In/Output    | Descriptive name                 | Source                | Format     | Unit | I/O | Remarks   |
|--------------|----------------------------------|-----------------------|------------|------|-----|---|
| $\mu_i, w_i$ | Gauss-Legendre quadrature        | Output from RTC/GAUSS | ASCII file | n.u. | I   | Internal file to 'step1.f', built with $n_g = 48$ |
| step1.out    | Legendre polynomial coefficients | -                     | ASCII file | n.u. | O   | $\alpha_l, \beta_l, \gamma_l, \zeta_l$            |

**RTC/WIND [step2] – Input/Output**

| Input/Output | Descriptive name                                | Source                | Format      | Unit       | I/O | Remarks  |
|--------------|---|-----------------------|-------------|------------|-----|--|
| $\mu_i, w_i$ | Gauss-Legendre quadrature                       | Output from RTC/GAUSS | ASCII file  | n.u.       | I   | Internal file to 'step1.f', built with $n_g = 48 + (\mu_0=1, w_0=0)$ |
| $w_s$        | Wind speed                                      | -                     | float       | $m s^{-1}$ | I   | -  |
| step2.out    | Fourier series expansion of Cox-Munk reflection | -                     | Binary file | n.u.       | O   | $\alpha_l, \beta_l, \gamma_l, \zeta_l$                               |

**RTC/WIND [step3] – Input/Output**

| <i>Input/Output</i> | <i>Descriptive name</i>  | <i>Source</i>                | <i>Format</i> | <i>Unit</i> | <i>I/O</i> | <i>Remarks</i>  |
|---------------------|--|------------------------------|---------------|-------------|------------|---|
| $\mu_i, w_i$        | <i>Gauss-Legendre quadrature</i>   | Output from RTC/GAUSS        | ASCII file    | <i>n.u.</i> | I          | <i>Internal file to 'step1.f', built with <math>n_g = 48</math></i> |
| $w_s$               | Wind speed   | -                            | float         | $m\ s^{-1}$ | I          | -   |
| <i>step1.out</i>    | <i>Legendre polynomial coefficients</i>  | Output from RTC/Wind [step1] | ASCII file    | <i>n.u.</i> | I          | $\alpha_1, \beta_1, \gamma_1, \zeta_1$                              |
| <i>step2.out</i>    | <i>Fourier series expansion of Cox-Munk reflection</i>                                     | Output from RTC/Wind [step2] | Binary file   | <i>n.u.</i> | I          | -   |
| <i>step3.out</i>    | <i>Fourier series component associated with Legendre polynomial of Cox-Munk reflection</i> | -                            | Binary file   | <i>n.u.</i> | O          | -   |

**RTC/WIND [step4] – Input/Output**

| <i>Input/Output</i> | <i>Descriptive name</i>  | <i>Source</i>                | <i>Format</i> | <i>Unit</i> | <i>I/O</i> | <i>Remarks</i>                                       |
|---------------------|--|------------------------------|---------------|-------------|------------|--|
| <i>windfile</i>     | Output filename  | -                            | string        | <i>n.u.</i> | I          | <i>windxx , xx digits for <math>w_s</math> value</i> |
| <i>step3.out</i>    | <i>Fourier series component associated with Legendre polynomial of Cox-Munk reflection</i> | Output from RTC/Wind [step3] | Binary file   | <i>n.u.</i> | I          | -  |
| <i>windxx</i>       | <i>Fourier series expansion of the Fresnel reflexion</i>                                   | -                            | Binary file   | <i>n.u.</i> | O          | -  |

### 9.4.5 OTC/RAYLEIGH

Description:

This module computes the total *Rayleigh* optical thickness ( $\tau_\lambda^R$ ) for a purely molecular atmosphere (dry air).

Processing:

$\tau_\lambda^R$  is estimated with the formula from [RD-13] (see Section 3.1.2, Equation 103)

Tool:

'otc\_rayleigh.f'

Input / Output description:

**OTC/RAYLEIGH – Input/Output**

| Input/Output | Descriptive name       | Source | Format | Unit    | I/O | Remarks |
|--------------|------------------------|--------|--------|---------|-----|---------|
| $\lambda$    | MERIS wavelength       | -      | float  | $\mu m$ | I   | -       |
| $P_s$        | Surface pressure       | -      | float  | hPa     | I   | -       |
| $\tau^R$     | Rayleigh optical depth | -      | float  | n.u.    | O   | -       |

### 9.4.6 OTC/OZONE

Description:

This module computes the total *Ozone* optical thickness ( $\tau^{O_3}$ ). This module is not used for the MERIS LUTs generation for the level-2 processing.

Processing:

$\tau^{O_3}$  are pre-computed values for each of all the 15 MERIS bands [RD-24].

Tool:

'otc\_ozone.f'

Input / Output description:

**OTC/OZONE – Input/Output**

| Input/Output | Descriptive name    | Source | Format | Unit    | I/O | Remarks |
|--------------|---------------------|--------|--------|---------|-----|---------|
| $n$          | MERIS band          | -      | int    | n.u.    | I   | -       |
| $U_{O_3}$    | Ozone amount        | -      | float  | cm-atm. | I   | -       |
| $\tau^{O_3}$ | Ozone optical depth | -      | float  | n.u.    | O   | -       |

## 9.4.7 IOP/WATER

### Description:

This module computes the IOPs of each oceanic component according to its concentration in each of all the 15 MERIS spectral bands. These IOPs are the extinction coefficients ( $\sigma_{e,\lambda}^w, \sigma_{e,\lambda}^p, \sigma_{e,\lambda}^{ys}, \sigma_{e,\lambda}^{spm}$ ) and the single scattering albedos ( $\omega_{0,\lambda}^w, \omega_{0,\lambda}^p, \omega_{0,\lambda}^{spm}$ ) for pure sea water, phytoplankton, yellow substance (or Gelbstoff) and SPM (inorganic particles). The latter allow one to determine the optical properties of the oceanic water used for the radiative transfer computation (RTC/SOAO).

Note that this code is not used in the current generation of MERIS-O2 LUTs (i.e., transmittances and corrective factors for the surface pressure) for the 3<sup>rd</sup> MERIS data reprocessing.

### Processing:

IOPs for each of all the oceanic components are fully described in [Section 4](#).

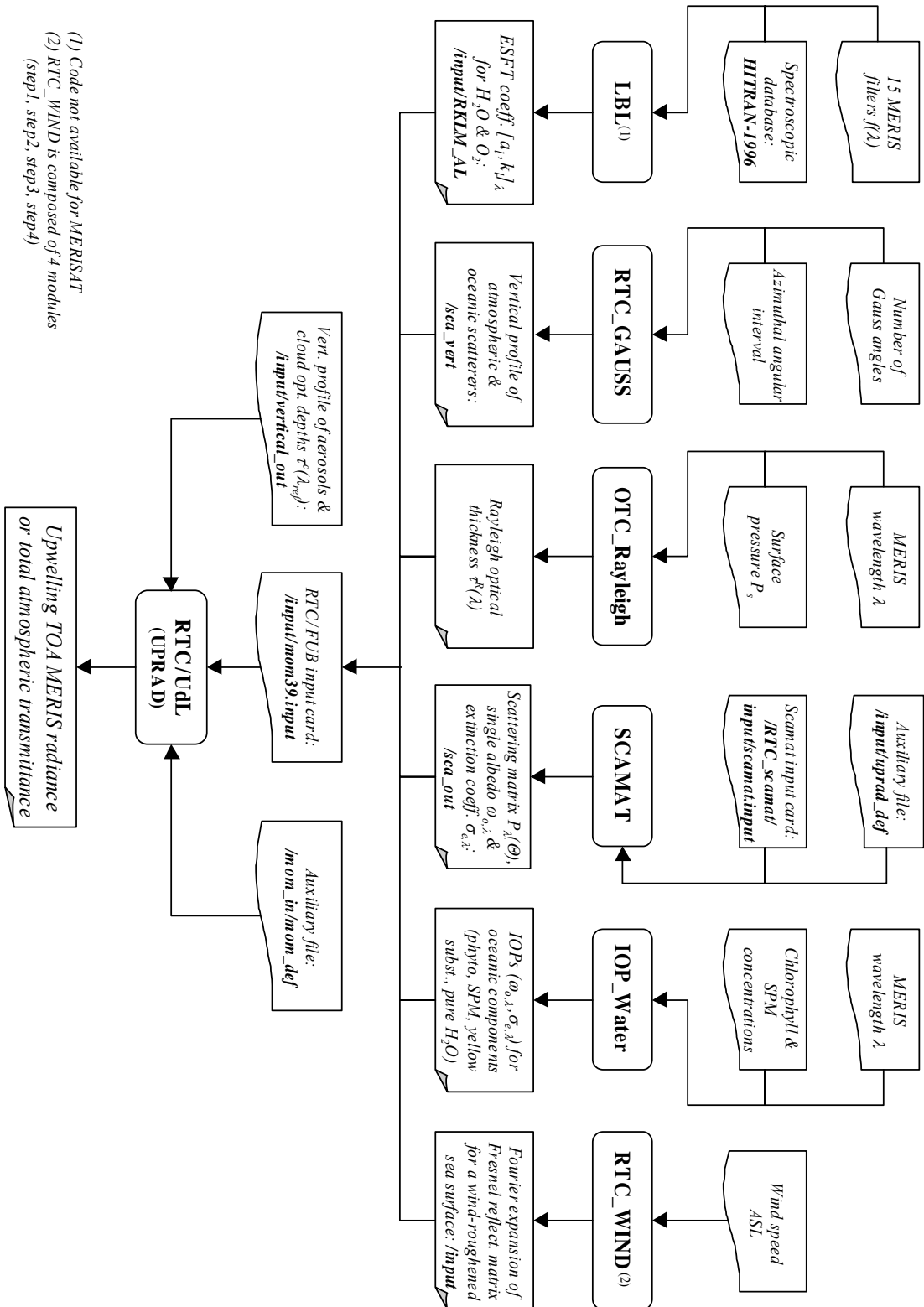
### Tool:

**'iop\_water.f'**

### Input / Output description:

#### **IOP/WATER – Input/Output**

| <i>Input/Output</i> | <i>Descriptive name</i>  | <i>Source</i> | <i>Format</i> | <i>Unit</i>     | <i>I/O</i> | <i>Remarks</i>  |
|---------------------|--|---------------|---------------|-----------------|------------|---|
| <i>IOP_file</i>     | Output filename  | -             | string        | <i>n.u.</i>     | I          | -   |
| <i>chl</i>          | Chlorophyll concentration  | -             | float         | $mg\ m^{-3}$    | I          | -   |
| <i>spm</i>          | SPM concentration  | -             | float         | $g\ m^{-3}$     | I          | -   |
| <i>IOPs</i>         | Single scattering albedo and extinction coefficient for all the oceanic compounds and all the 15 MERIS bands | -             | ASCII file    | $n.u.,\ m^{-1}$ | O          | $15 \times \begin{pmatrix} \omega_{0,\lambda}^w, \sigma_{e,\lambda}^w \\ \omega_{0,\lambda}^{spm}, \sigma_{e,\lambda}^{spm} \\ \omega_{0,\lambda}^p, \sigma_{e,\lambda}^p \\ \sigma_{e,\lambda}^{ys} \end{pmatrix}$ |



(1) Code not available for MERISAT  
 (2) RTC\_WIND is composed of 4 modules  
 (step1, step2, step3, step4)

Figure 1: Overview of the RTC/UdL package

## 10. APPENDIX-2: SPECIFICATION OF RTC/FUB PACKAGE

An overview of the RTC / FUB package is displayed on [Figure 2](#).

### 10.1 MIE INPUT/OUTPUT DESCRIPTION

#### 10.1.1 Input/Output description

| <b>MIE Inputs</b>  |  |               |               |                            |   |   |
|--|--|---------------|---------------|----------------------------|---|---|
| <i>Input</i>   | <i>Descriptive name</i>  | <i>Source</i> | <i>Format</i> | <i>Unit</i>                | <i>Range</i>                                    | <i>Remarks</i>  |
| <i>scamat_out</i>  | Output filename  | -             | string        | <i>n.u.</i>                | -   | Scattering phase matrix   |
| $\lambda$  | Wavelength   | -             | float         | <i>nm</i>                  | [250;4000]                                      | 15 MERIS wavelengths in [400; 900]  |
| $\lambda_{ref}$  | Reference wavelength   | -             | float         | <i>nm</i>                  | [250;4000]                                      | 15 MERIS wavelengths in [400; 900]  |
| $n_2$  | Number of scattering angles  | -             | int           | <i>n.u.</i>                | 171   | Not used (fixed value in the code)  |
| $N$  | Number of particle size distributions  | -             | int           | <i>n.u.</i>                | [1;5]   | Maximum of 5 particle size distributions  |
| $m_\lambda(i), k_\lambda(i)$   | Real and imaginary parts of refractive index at wavelength $\lambda$ for size distribution $i$                 | -             | float         | <i>n.u. / n.u.</i>         | $m_\lambda > 0$<br>$k_\lambda \geq 0$           | $2 \times N$ values   |
| $m_{ref}(i), k_{ref}(i)$   | Real and imaginary parts of refractive index at reference wavelength $\lambda_{ref}$ for size distribution $i$ | -             | float         | <i>n.u. / n.u.</i>         | $m_{ref} > 0$<br>$k_{ref} \geq 0$               | $2 \times N$ values   |
| $r_{min}(i), r_{max}(i)$<br>$dr(i)$  | Minimum, maximum radii and size increment for size distribution $i$  | -             | float         | $\mu m / \mu m$<br>$\mu m$ | $r_{min} > r_{max} \geq 0$<br>$dr \geq 10^{-4}$ | $3 \times N$ values<br><i>Note: if <math>r_{min} \leq 0 \Rightarrow r_{min} = 10^{-4}</math></i>  |
| $ind(i)$<br>$a(i), b(i)$   | Index of selected particle size distribution and its 2 parameters for size distribution $i$                    | -             | float         | $\mu m / n.u.$             | $ind: [1;5]$<br>$(a,b) > 0$                     | $2 \times N$ values<br>$ind=1$ (Junge power-law): $a=r_o, b=\alpha$<br>$ind=2$ (Log normal): $a=r_m, b=\sigma$<br>$ind=3$ (Modified Gamma): $a=\alpha, b=b$<br>$ind=4$ (Gamma-Hansen): $a=r_i, b=r_b$<br>$ind=5$ (Real size distribution) |
| $n(i) / n$   | Component mixing ratio for each size distribution $i$  | -             | float         | <i>n.u.</i>                | ]0;1]   | $N$ values  |
| <i>Loop on the inputs #6, 7, 8, 9 &amp; 10 for the size distributions (i+1), (i+2), (i+3) and (i+4) if necessary !</i> |  |               |               |                            |   |   |
| <i>Ratio</i>   | Volume or particle ratio   | -             | float         | <i>n.u.</i>                | 1 or 2  | 1- Volume ratio<br>2- Particle ratio  |

**Nb:** The size increment of  $10^{-4}$  is a critical value acceptable as the limit of Mie's theory. Better acceptable limit would be a value of  $10^{-3}$ .

### MIE Outputs

| Output   | Descriptive name  | Source | Format | Unit                  | Range    | Remarks   |
|--|---|--------|--------|-----------------------|----------|---|
| Inputs   | Input Mie data  | -      | string | n.u.                  | -        | -   |
| $\theta$   | Scattering angles   | -      | float  | deg.                  | -        | $n_2$ values                                    |
| $P(\theta)$  | 1 <sup>st</sup> Stokes parameter  | -      | float  | n.u.                  | -        | $n_2$ values                                    |
| $Q(\theta)$  | 2 <sup>nd</sup> Stokes parameter  | -      | float  | n.u.                  | -        | $n_2$ values                                    |
| $U(\theta)$  | 3 <sup>rd</sup> Stokes parameter  | -      | float  | n.u.                  | -        | $n_2$ values                                    |
| $V(\theta)$  | 4 <sup>th</sup> Stokes parameter  | -      | float  | n.u.                  | -        | $n_2$ values                                    |
| $\omega_{o,\lambda}, \omega_{o,\lambda_{ref}}$     | Single scattering albedos at wavelengths $\lambda$ and $\lambda_{ref}$              | -      | float  | n.u.                  | [0;1]    | -   |
| $\sigma_{e,\lambda}^*, \sigma_{e,\lambda_{ref}}^*$ | Normalized extinction coefficients at the wavelengths $\lambda$ and $\lambda_{ref}$ | -      | float  | n.u.                  | $\geq 0$ | Values normalized to $\sigma_{e,\lambda_{ref}}$ |
| $\sigma_{e,\lambda_{ref}}$                         | Extinction coefficient at the wavelength $\lambda_{ref}$                            | -      | float  | $\mu m^{-1}.pct^{-1}$ | $\geq 0$ | Values normalized to $\sigma_{e,\lambda_{ref}}$ |

*Nb:* Stoke parameters are normalized to  $4\pi$ .

## 10.1.2 Input/Output sample

### FUB MIE INPUT CARD

|                                       |     |                  |           |       |  |                                 |
|---------------------------------------|-----|------------------|-----------|-------|--|---------------------------------|
| 'sca_out:                             | '   | out_sc_test_12.s |           |       |  | scamat_out                      |
| 'wavelength:                          | '   | 443.00           |           |       |  | $\lambda$                       |
| 'ref. wavelength:                     | '   | 865.00           |           |       |  | $\lambda_{ref}$                 |
| 'number of angles (n2):               | '   | 171              |           |       |  | $n_2$                           |
| 'number of size distributions (N):    | '   | 3                |           |       |  | $N$                             |
| 'real, imag. refrac. index (m_i,k_i)  | 1:' | 1.530            | 0.500E-02 |       |  | $m_\lambda(1), k_\lambda(1)$    |
| 'ref. refractive index (m_r_i,k_r_i)  | 1:' | 1.520            | 0.121E-01 |       |  | $m_{ref}(1), k_{ref}(1)$        |
| 'min,max,step of particles (r0,rf,dr) | 1:' | 0.001            | 20.000    | 0.001 |  | $r_{min}(1), r_{max}(1), dr(1)$ |
| 'size distri. parameters (ind,a,b)    | 1:' | 2                | 0.005     | 2.99  |  | $ind(1), a(1), b(1)$            |
| 'volume percentages (n_i/n):          | 1:' | 0.93877          |           |       |  | $n(1) / n$                      |
| 'real, imag. refrac. index (m_i,k_i)  | 2:' | 1.530            | 0.800E-02 |       |  | $m_\lambda(2), k_\lambda(2)$    |
| 'ref. refractive index (m_r_i,k_r_i)  | 2:' | 1.520            | 0.800E-02 |       |  | $m_{ref}(2), k_{ref}(2)$        |
| 'min,max,step of particles (r0,rf,dr) | 2:' | 0.01             | 40.000    | 0.01  |  | $r_{min}(2), r_{max}(2), dr(2)$ |
| 'size distri. parameters (ind,a,b)    | 2:' | 2                | 0.5       | 2.99  |  | $ind(2), a(2), b(2)$            |
| 'volume percentages (n_i/n):          | 2:' | 2.27E-06         |           |       |  | $n(2) / n$                      |
| 'real, imag. refrac. index (m_i,k_i)  | 3:' | 1.750            | 0.455E-00 |       |  | $m_\lambda(3), k_\lambda(3)$    |
| 'ref. refractive index (m_r_i,k_r_i)  | 3:' | 1.750            | 0.430E-00 |       |  | $m_{ref}(3), k_{ref}(3)$        |
| 'min,max,step of particles (r0,rf,dr) | 3:' | 0.001            | 20.000    | 0.001 |  | $r_{min}(3), r_{max}(3), dr(3)$ |



|                                      |                   |                           |
|--------------------------------------|-------------------|---------------------------|
| 'size distri. parameters (ind,a,b)   | 3:' 2 0.0118 2.00 | <i>ind(3), a(3), b(3)</i> |
| 'volume percentages (n_i/n):         | 3:' 0.06123       | <i>n(3) / n</i>           |
| 'volume (1) and particle (2) ratio : | ' 2               | <i>ratio</i>              |

**FUB MIE OUTPUT FILE**

```
'Wavelength (nm):          ' 443.00
'Reference wavelength (nm): ' 865.00
'Number of scattering angles: ' 171
'Number of particle size distributions: ' 3
'Refractive index (Re,Im)    1:' 1.530 .500E-02
                             2:' 1.530 .800E-02
                             3:' 1.750 .455E+00
'Reference refractive index (Re,Im): 1:' 1.520 .121E-01
                                   2:' 1.520 .800E-02
                                   3:' 1.750 .430E+00
'Min,max,step of particle size (mic.) 1:' .0010 20.0000 .0010
                                       2:' .0100 40.0000 .0100
                                       3:' .0010 20.0000 .0010
'Size distrib. (ind) & param. (a,b)  1:' 2 .0050 2.9900
                                       2:' 2 .5000 2.9900
                                       3:' 2 .0118 2.0000
'Volume percentage           1:' .93877E+00
                             2:' .22700E-05
                             3:' .61230E-01
'Volume [1] or particle [2] ratio:  ' 2

*****
**** MIE/FUB - PHASE-FUNCTION ****
*****

'Medium = ' 1
'ScatType = ' 2
'NumAngles = ' 171
'NumLambda = ' 1

'wavelength [nm] = ' 443.00 'ex_norm=' .221548E+01 'w_o=' .905069E+00 ex_ref [mic^-1]=' .358230E-03
 1  0.0  .5551E+02  -.2090E-25  .5551E+02  -.3597E-26
 2  0.1  .5092E+02  .2658E-03  .5092E+02  -.1304E-01
 3  0.2  .4003E+02  .7814E-03  .4003E+02  -.3884E-01
 4  0.3  .2860E+02  .1085E-02  .2860E+02  -.5547E-01
 5  0.4  .2029E+02  .1074E-02  .2029E+02  -.5773E-01
 6  0.5  .1517E+02  .9437E-03  .1516E+02  -.5453E-01
 7  0.6  .1187E+02  .8218E-03  .1187E+02  -.5173E-01
 8  0.7  .9516E+01  .6948E-03  .9516E+01  -.4879E-01
 9  0.8  .7823E+01  .5547E-03  .7823E+01  -.4531E-01
10  0.9  .6587E+01  .4244E-03  .6587E+01  -.4217E-01
11  1.0  .5640E+01  .3061E-03  .5640E+01  -.3942E-01
12  1.2  .4327E+01  .8995E-04  .4327E+01  -.3427E-01
13  1.4  .3486E+01  -.8390E-04  .3486E+01  -.3016E-01
14  1.6  .2922E+01  -.2231E-03  .2921E+01  -.2679E-01
15  1.8  .2523E+01  -.3316E-03  .2523E+01  -.2403E-01
16  2.0  .2234E+01  -.4130E-03  .2234E+01  -.2183E-01
17  2.2  .2018E+01  -.4732E-03  .2017E+01  -.2002E-01
18  2.4  .1851E+01  -.5151E-03  .1850E+01  -.1857E-01
19  2.6  .1720E+01  -.5418E-03  .1720E+01  -.1740E-01
20  2.8  .1615E+01  -.5565E-03  .1614E+01  -.1646E-01
21  3.0  .1529E+01  -.5608E-03  .1528E+01  -.1571E-01
22  3.2  .1458E+01  -.5570E-03  .1457E+01  -.1512E-01
23  3.4  .1397E+01  -.5464E-03  .1397E+01  -.1466E-01
24  3.6  .1346E+01  -.5302E-03  .1345E+01  -.1432E-01
25  3.8  .1301E+01  -.5096E-03  .1300E+01  -.1407E-01
26  4.0  .1262E+01  -.4855E-03  .1261E+01  -.1390E-01
27  4.2  .1227E+01  -.4585E-03  .1226E+01  -.1379E-01
```

|    |       |           |            |           |            |
|----|-------|-----------|------------|-----------|------------|
| 28 | 4.4   | .1195E+01 | -.4295E-03 | .1195E+01 | -.1375E-01 |
| 29 | 4.6   | .1167E+01 | -.3987E-03 | .1167E+01 | -.1375E-01 |
| 30 | 4.8   | .1141E+01 | -.3667E-03 | .1141E+01 | -.1379E-01 |
| 31 | 5.0   | .1118E+01 | -.3339E-03 | .1117E+01 | -.1386E-01 |
| 32 | 6.0   | .1021E+01 | -.1675E-03 | .1020E+01 | -.1459E-01 |
| 33 | 7.0   | .9467E+00 | -.1316E-04 | .9459E+00 | -.1564E-01 |
| 34 | 8.0   | .8851E+00 | .1167E-03  | .8841E+00 | -.1680E-01 |
| 35 | 9.0   | .8316E+00 | .2165E-03  | .8304E+00 | -.1793E-01 |
| 36 | 10.0  | .7839E+00 | .2841E-03  | .7824E+00 | -.1900E-01 |
| 37 | 11.0  | .7405E+00 | .3188E-03  | .7388E+00 | -.1997E-01 |
| 38 | 12.0  | .7006E+00 | .3208E-03  | .6987E+00 | -.2081E-01 |
| 39 | 13.0  | .6637E+00 | .2903E-03  | .6615E+00 | -.2153E-01 |
| 40 | 14.0  | .6292E+00 | .2279E-03  | .6268E+00 | -.2213E-01 |
| 41 | 15.0  | .5970E+00 | .1346E-03  | .5944E+00 | -.2260E-01 |
| 42 | 16.0  | .5668E+00 | .1172E-04  | .5639E+00 | -.2297E-01 |
| 43 | 17.0  | .5383E+00 | -.1380E-03 | .5353E+00 | -.2323E-01 |
| 44 | 18.0  | .5114E+00 | -.3111E-03 | .5083E+00 | -.2340E-01 |
| 45 | 19.0  | .4860E+00 | -.5034E-03 | .4828E+00 | -.2348E-01 |
| 46 | 20.0  | .4620E+00 | -.7110E-03 | .4586E+00 | -.2349E-01 |
| 47 | 21.0  | .4392E+00 | -.9304E-03 | .4358E+00 | -.2344E-01 |
| 48 | 22.0  | .4177E+00 | -.1159E-02 | .4141E+00 | -.2332E-01 |
| 49 | 23.0  | .3972E+00 | -.1393E-02 | .3936E+00 | -.2315E-01 |
| 50 | 24.0  | .3779E+00 | -.1632E-02 | .3742E+00 | -.2294E-01 |
| 51 | 25.0  | .3595E+00 | -.1874E-02 | .3557E+00 | -.2268E-01 |
| 52 | 26.0  | .3420E+00 | -.2118E-02 | .3381E+00 | -.2239E-01 |
| 53 | 27.0  | .3254E+00 | -.2361E-02 | .3215E+00 | -.2206E-01 |
| 54 | 28.0  | .3097E+00 | -.2604E-02 | .3057E+00 | -.2170E-01 |
| 55 | 29.0  | .2947E+00 | -.2845E-02 | .2906E+00 | -.2132E-01 |
| 56 | 30.0  | .2805E+00 | -.3084E-02 | .2763E+00 | -.2091E-01 |
| 57 | 32.0  | .2542E+00 | -.3552E-02 | .2499E+00 | -.2004E-01 |
| 58 | 34.0  | .2305E+00 | -.4004E-02 | .2260E+00 | -.1911E-01 |
| 59 | 36.0  | .2091E+00 | -.4434E-02 | .2044E+00 | -.1814E-01 |
| 60 | 38.0  | .1898E+00 | -.4840E-02 | .1849E+00 | -.1715E-01 |
| 61 | 40.0  | .1723E+00 | -.5217E-02 | .1673E+00 | -.1615E-01 |
| 62 | 42.0  | .1566E+00 | -.5565E-02 | .1514E+00 | -.1516E-01 |
| 63 | 44.0  | .1425E+00 | -.5880E-02 | .1371E+00 | -.1418E-01 |
| 64 | 46.0  | .1297E+00 | -.6162E-02 | .1241E+00 | -.1322E-01 |
| 65 | 48.0  | .1181E+00 | -.6410E-02 | .1124E+00 | -.1229E-01 |
| 66 | 50.0  | .1077E+00 | -.6625E-02 | .1019E+00 | -.1140E-01 |
| 67 | 52.0  | .9834E-01 | -.6807E-02 | .9231E-01 | -.1053E-01 |
| 68 | 54.0  | .8987E-01 | -.6956E-02 | .8369E-01 | -.9707E-02 |
| 69 | 56.0  | .8223E-01 | -.7073E-02 | .7588E-01 | -.8919E-02 |
| 70 | 58.0  | .7533E-01 | -.7161E-02 | .6882E-01 | -.8168E-02 |
| 71 | 60.0  | .6909E-01 | -.7219E-02 | .6243E-01 | -.7455E-02 |
| 72 | 62.0  | .6346E-01 | -.7250E-02 | .5664E-01 | -.6779E-02 |
| 73 | 64.0  | .5837E-01 | -.7255E-02 | .5139E-01 | -.6140E-02 |
| 74 | 66.0  | .5377E-01 | -.7235E-02 | .4662E-01 | -.5535E-02 |
| 75 | 68.0  | .4961E-01 | -.7193E-02 | .4230E-01 | -.4964E-02 |
| 76 | 70.0  | .4585E-01 | -.7129E-02 | .3837E-01 | -.4424E-02 |
| 77 | 72.0  | .4245E-01 | -.7045E-02 | .3480E-01 | -.3915E-02 |
| 78 | 74.0  | .3937E-01 | -.6943E-02 | .3155E-01 | -.3435E-02 |
| 79 | 76.0  | .3658E-01 | -.6824E-02 | .2859E-01 | -.2982E-02 |
| 80 | 78.0  | .3406E-01 | -.6689E-02 | .2589E-01 | -.2554E-02 |
| 81 | 80.0  | .3177E-01 | -.6540E-02 | .2344E-01 | -.2150E-02 |
| 82 | 82.0  | .2971E-01 | -.6378E-02 | .2119E-01 | -.1769E-02 |
| 83 | 84.0  | .2784E-01 | -.6204E-02 | .1914E-01 | -.1408E-02 |
| 84 | 86.0  | .2615E-01 | -.6019E-02 | .1727E-01 | -.1066E-02 |
| 85 | 88.0  | .2462E-01 | -.5825E-02 | .1555E-01 | -.7419E-03 |
| 86 | 90.0  | .2325E-01 | -.5621E-02 | .1398E-01 | -.4344E-03 |
| 87 | 92.0  | .2200E-01 | -.5410E-02 | .1254E-01 | -.1421E-03 |
| 88 | 94.0  | .2089E-01 | -.5191E-02 | .1122E-01 | .1363E-03  |
| 89 | 96.0  | .1988E-01 | -.4965E-02 | .1000E-01 | .4017E-03  |
| 90 | 98.0  | .1898E-01 | -.4733E-02 | .8888E-02 | .6554E-03  |
| 91 | 100.0 | .1818E-01 | -.4495E-02 | .7859E-02 | .8984E-03  |
| 92 | 102.0 | .1746E-01 | -.4251E-02 | .6911E-02 | .1132E-02  |

|     |       |           |            |            |            |
|-----|-------|-----------|------------|------------|------------|
| 93  | 104.0 | .1683E-01 | -.4001E-02 | .6035E-02  | .1356E-02  |
| 94  | 106.0 | .1627E-01 | -.3746E-02 | .5225E-02  | .1572E-02  |
| 95  | 108.0 | .1578E-01 | -.3484E-02 | .4475E-02  | .1781E-02  |
| 96  | 110.0 | .1536E-01 | -.3217E-02 | .3778E-02  | .1984E-02  |
| 97  | 112.0 | .1500E-01 | -.2944E-02 | .3131E-02  | .2181E-02  |
| 98  | 114.0 | .1470E-01 | -.2664E-02 | .2527E-02  | .2373E-02  |
| 99  | 116.0 | .1445E-01 | -.2378E-02 | .1963E-02  | .2561E-02  |
| 100 | 118.0 | .1426E-01 | -.2084E-02 | .1433E-02  | .2745E-02  |
| 101 | 120.0 | .1411E-01 | -.1782E-02 | .9354E-03  | .2926E-02  |
| 102 | 122.0 | .1402E-01 | -.1471E-02 | .4650E-03  | .3104E-02  |
| 103 | 124.0 | .1397E-01 | -.1150E-02 | .1831E-04  | .3280E-02  |
| 104 | 126.0 | .1397E-01 | -.8187E-03 | -.4081E-03 | .3452E-02  |
| 105 | 128.0 | .1402E-01 | -.4755E-03 | -.8180E-03 | .3623E-02  |
| 106 | 130.0 | .1411E-01 | -.1193E-03 | -.1215E-02 | .3790E-02  |
| 107 | 132.0 | .1425E-01 | .2513E-03  | -.1603E-02 | .3954E-02  |
| 108 | 134.0 | .1444E-01 | .6376E-03  | -.1986E-02 | .4113E-02  |
| 109 | 136.0 | .1467E-01 | .1041E-02  | -.2369E-02 | .4266E-02  |
| 110 | 138.0 | .1494E-01 | .1462E-02  | -.2756E-02 | .4411E-02  |
| 111 | 140.0 | .1527E-01 | .1903E-02  | -.3155E-02 | .4543E-02  |
| 112 | 142.0 | .1564E-01 | .2363E-02  | -.3570E-02 | .4657E-02  |
| 113 | 144.0 | .1605E-01 | .2841E-02  | -.4012E-02 | .4748E-02  |
| 114 | 146.0 | .1651E-01 | .3335E-02  | -.4490E-02 | .4805E-02  |
| 115 | 148.0 | .1700E-01 | .3840E-02  | -.5018E-02 | .4816E-02  |
| 116 | 150.0 | .1752E-01 | .4347E-02  | -.5610E-02 | .4762E-02  |
| 117 | 151.0 | .1778E-01 | .4596E-02  | -.5936E-02 | .4705E-02  |
| 118 | 152.0 | .1805E-01 | .4841E-02  | -.6285E-02 | .4622E-02  |
| 119 | 153.0 | .1832E-01 | .5077E-02  | -.6660E-02 | .4511E-02  |
| 120 | 154.0 | .1859E-01 | .5301E-02  | -.7063E-02 | .4368E-02  |
| 121 | 155.0 | .1885E-01 | .5509E-02  | -.7498E-02 | .4189E-02  |
| 122 | 156.0 | .1910E-01 | .5696E-02  | -.7967E-02 | .3972E-02  |
| 123 | 157.0 | .1935E-01 | .5858E-02  | -.8473E-02 | .3712E-02  |
| 124 | 158.0 | .1959E-01 | .5987E-02  | -.9020E-02 | .3408E-02  |
| 125 | 159.0 | .1981E-01 | .6079E-02  | -.9611E-02 | .3059E-02  |
| 126 | 160.0 | .2003E-01 | .6126E-02  | -.1025E-01 | .2666E-02  |
| 127 | 161.0 | .2024E-01 | .6123E-02  | -.1093E-01 | .2230E-02  |
| 128 | 162.0 | .2044E-01 | .6065E-02  | -.1167E-01 | .1756E-02  |
| 129 | 163.0 | .2065E-01 | .5950E-02  | -.1246E-01 | .1255E-02  |
| 130 | 164.0 | .2089E-01 | .5776E-02  | -.1330E-01 | .7419E-03  |
| 131 | 165.0 | .2116E-01 | .5549E-02  | -.1419E-01 | .2392E-03  |
| 132 | 166.0 | .2149E-01 | .5273E-02  | -.1516E-01 | -.2294E-03 |
| 133 | 167.0 | .2190E-01 | .4955E-02  | -.1619E-01 | -.6445E-03 |
| 134 | 168.0 | .2241E-01 | .4600E-02  | -.1732E-01 | -.9917E-03 |
| 135 | 169.0 | .2302E-01 | .4212E-02  | -.1853E-01 | -.1261E-02 |
| 136 | 170.0 | .2374E-01 | .3796E-02  | -.1983E-01 | -.1445E-02 |
| 137 | 171.0 | .2456E-01 | .3355E-02  | -.2120E-01 | -.1542E-02 |
| 138 | 172.0 | .2548E-01 | .2896E-02  | -.2263E-01 | -.1552E-02 |
| 139 | 173.0 | .2646E-01 | .2426E-02  | -.2409E-01 | -.1480E-02 |
| 140 | 174.0 | .2749E-01 | .1956E-02  | -.2555E-01 | -.1336E-02 |
| 141 | 175.0 | .2852E-01 | .1497E-02  | -.2697E-01 | -.1135E-02 |
| 142 | 175.2 | .2872E-01 | .1408E-02  | -.2724E-01 | -.1090E-02 |
| 143 | 175.4 | .2892E-01 | .1320E-02  | -.2751E-01 | -.1043E-02 |
| 144 | 175.6 | .2911E-01 | .1233E-02  | -.2778E-01 | -.9954E-03 |
| 145 | 175.8 | .2930E-01 | .1148E-02  | -.2804E-01 | -.9467E-03 |
| 146 | 176.0 | .2949E-01 | .1064E-02  | -.2830E-01 | -.8973E-03 |
| 147 | 176.2 | .2967E-01 | .9822E-03  | -.2856E-01 | -.8474E-03 |
| 148 | 176.4 | .2984E-01 | .9019E-03  | -.2881E-01 | -.7970E-03 |
| 149 | 176.6 | .3001E-01 | .8236E-03  | -.2905E-01 | -.7465E-03 |
| 150 | 176.8 | .3017E-01 | .7473E-03  | -.2929E-01 | -.6959E-03 |
| 151 | 177.0 | .3033E-01 | .6733E-03  | -.2952E-01 | -.6453E-03 |
| 152 | 177.2 | .3047E-01 | .6015E-03  | -.2975E-01 | -.5948E-03 |
| 153 | 177.4 | .3061E-01 | .5322E-03  | -.2997E-01 | -.5444E-03 |
| 154 | 177.6 | .3074E-01 | .4656E-03  | -.3018E-01 | -.4942E-03 |
| 155 | 177.8 | .3086E-01 | .4017E-03  | -.3038E-01 | -.4439E-03 |
| 156 | 178.0 | .3097E-01 | .3410E-03  | -.3057E-01 | -.3937E-03 |
| 157 | 178.2 | .3107E-01 | .2835E-03  | -.3075E-01 | -.3433E-03 |

|     |       |           |           |            |            |
|-----|-------|-----------|-----------|------------|------------|
| 158 | 178.4 | .3116E-01 | .2298E-03 | -.3092E-01 | -.2927E-03 |
| 159 | 178.6 | .3124E-01 | .1802E-03 | -.3107E-01 | -.2423E-03 |
| 160 | 178.8 | .3132E-01 | .1353E-03 | -.3121E-01 | -.1924E-03 |
| 161 | 179.0 | .3138E-01 | .9579E-04 | -.3132E-01 | -.1440E-03 |
| 162 | 179.1 | .3142E-01 | .7824E-04 | -.3137E-01 | -.1208E-03 |
| 163 | 179.2 | .3144E-01 | .6228E-04 | -.3142E-01 | -.9875E-04 |
| 164 | 179.3 | .3147E-01 | .4799E-04 | -.3145E-01 | -.7800E-04 |
| 165 | 179.4 | .3150E-01 | .3545E-04 | -.3149E-01 | -.5896E-04 |
| 166 | 179.5 | .3152E-01 | .2473E-04 | -.3151E-01 | -.4199E-04 |
| 167 | 179.6 | .3154E-01 | .1589E-04 | -.3154E-01 | -.2745E-04 |
| 168 | 179.7 | .3155E-01 | .8962E-05 | -.3155E-01 | -.1571E-04 |
| 169 | 179.8 | .3156E-01 | .3991E-05 | -.3156E-01 | -.7068E-05 |
| 170 | 179.9 | .3157E-01 | .9988E-06 | -.3157E-01 | -.1780E-05 |
| 171 | 180.0 | .3157E-01 | .2090E-25 | -.3157E-01 | -.3429E-26 |

Note: Inputs used to generate the scattering phase function are given in the header. The output is formatted into 5 columns, respectively Theta, P(Theta), Q(Theta), U(Theta), V(Theta)

with Theta : scattering angle  
(P,Q,U,V): 4 Stokes parameters  
normalized to 4 Pi.

ex\_norm = extinct.(l) / extinct.(l\_ref)  
w\_o = single scatt. albedo at l  
ex\_ref = extinction coeff. at l\_ref  
[mic^-1]

Nb: Column values are respectively for  $n_2$ ,  $\theta$ ,  $P(\theta)$ ,  $Q(\theta)$ ,  $U(\theta)$ ,  $V(\theta)$ .

## 10.2 MOMO INPUT/OUTPUT DESCRIPTION

### RTC/FUB-MOMO Inputs

| <i>Input</i>     | <i>Descriptive name</i>  | <i>Source</i>                                  | <i>Format</i> | <i>Unit</i>   | <i>Range</i> | <i>Remarks</i>   |
|------------------|--|--|---------------|---------------|--------------|--|
| <i>out_file</i>  | Output filename  | -  | string        | <i>n.u.</i>   | -            | <i>MERIS radiances at TOA</i>  |
| <i>i_branch</i>  | Index to select the type of test case  | -  | int           | <i>n.u.</i>   | [1;4]        | 1-Land + Clear sky<br>2-Ocean + Clear sky<br>3-Land + Cloud sky<br>4-Land + Water vapor<br><u>Nb</u> : input not used in MOMO            |
| <i>n</i>         | MERIS band #   | -  | int           | <i>n.u.</i>   | [1;15]       | 15 MERIS spectral bands (not used)   |
| $U_{H_2O}$       | Total water vapor amount   | -  | float         | $g/cm^2$      | $\geq 0$     | See note 1   |
| $ESFT_{H_2O}$    | Auxiliary data file (atmospheric gaseous composition and ESFT coefficients for $H_2O$ transmittivity in the MERIS band $n$ ) | File provided by FUB institute                 | string        | <i>n.u.</i>   | -            | Coefficients $(a_i, k_i)$ for computing $H_2O$ transmittance above layer $i$<br>- Sample of filename:<br><i>'/sca_esft/H2O_01_bλ'</i>    |
| $U_{O_2}$        | Total oxygen vapor amount  | -  | float         | $g/cm^2$      | $\geq 0$     | See note 1   |
| $ESFT_{O_2}$     | Auxiliary data file (atmospheric gaseous composition and ESFT coefficients for $O_2$ transmittivity in the MERIS band $n$ )  | File provided by FUB institute                 | string        | <i>n.u.</i>   | -            | Coefficients $(a_i, k_i)$ for computing $O_2$ transmittance above layer $i$<br>- Example of filename:<br><i>'/sca_esft/O2a_01_bλ'</i>    |
| $U_{O_3}$        | Total ozone vapor amount   | -  | float         | <i>cm-atm</i> | $\geq 0$     | See note 1   |
| $ESFT_{O_3}$     | Auxiliary data file (atmospheric gaseous composition and ESFT coefficients for $O_3$ transmittivity in the MERIS band $n$ )  | File provided by FUB institute                 | string        | <i>n.u.</i>   | -            | Coefficients $(a_i, k_i)$ for computing $O_3$ transmittance above layer $i$<br>- Example of filename:<br><i>'/sca_esft/O3_01_bλ'</i>     |
| $P_s$            | Surface pressure   | -  | float         | <i>hPa</i>    | $\geq 194$   | -  |
| $\tau_\lambda^R$ | Rayleigh optical thickness (for $P_s \geq 1013.25$ hPa)  | Input value or output from <i>otc_rayleigh</i> | float         | <i>n.u.</i>   | [0;1[        | -  |
| <i>aerosol1</i>  | Scattering phase matrix for aerosol layer #1   | Output file from <i>mie36</i>                  | string        | <i>n.u.</i>   | -            | $\theta, P(\lambda, r, m, \theta), \omega_{o,\lambda}, \sigma_{e,\lambda}$<br>for the Legendre polyn. development of scatt. phase matrix |

| <i>Input</i>               | <i>Descriptive name</i>                         | <i>Source</i>                        | <i>Format</i> | <i>Unit</i> | <i>Range</i> | <i>Remarks</i>   |
|----------------------------|---|--------------------------------------|---------------|-------------|--------------|--|
| $\tau_{550}^a(1)$          | Aerosol optical thickness at 550nm for layer #1 | -                                    | float         | n.u.        | [0;10]       | Realistic values in [0;0.8].<br>(See note 2)   |
| <i>aerosol2</i>            | Scattering phase matrix for aerosol layer #2    | Output file from mie36               | string        | n.u.        | -            | $\theta, P(\lambda, r, m, \theta), \omega_{o,\lambda}, \sigma_{e,\lambda}$<br>for the Legendre polyn. development of scatt. phase matrix     |
| $\tau_{550}^a(2)$          | Aerosol optical thickness at 550nm for layer #2 | -                                    | float         | n.u.        | [0;10]       | Realistic values in [0;0.8].<br>(See note 2)   |
| <i>aerosol3</i>            | Scattering phase matrix for aerosol layer #3    | Output file from mie36               | string        | n.u.        | -            | $\theta, P(\lambda, r, m, \theta), \omega_{o,\lambda}, \sigma_{e,\lambda}$<br>for the Legendre polyn. development of scatt. phase matrix     |
| $\tau_{550}^a(3)$          | Aerosol optical thickness at 550nm for layer #3 | -                                    | float         | n.u.        | [0;10]       | Realistic values in [0;0.8].<br>(See note 2)   |
| <i>cloud1</i>              | Scattering phase matrix for cloud layer #1      | Output file from mie36               | string        | n.u.        | -            | $\theta, P(\lambda, r, m, \theta), \omega_{o,\lambda}, \sigma_{e,\lambda}$<br>for the Legendre polyn. development of scatt. phase matrix     |
| $\tau_{550}^c(1)$          | Cloud optical thickness at 550nm for layer #1   | -                                    | float         | n.u.        | [0;300]      | Realistic values in [0;300]  |
| <i>cloud2</i>              | Scattering phase matrix for cloud layer #2      | Output file from mie36               | string        | n.u.        | -            | $\theta, P(\lambda, r, m, \theta), \omega_{o,\lambda}, \sigma_{e,\lambda}$<br>for the Legendre polyn. development of scatt. phase matrix     |
| $\tau_{550}^c(2)$          | Cloud optical thickness at 550nm for layer #2   | -                                    | float         | n.u.        | [0;300]      | Realistic values in [0;300]  |
| <i>cloud3</i>              | Scattering phase matrix for cloud layer #3      | Output file from mie36               | string        | n.u.        | -            | $\theta, P(\lambda, r, m, \theta), \omega_{o,\lambda}, \sigma_{e,\lambda}$<br>for the Legendre polyn. development of scatt. phase matrix     |
| $\tau_{550}^c(3)$          | Cloud optical thickness at 550nm for layer #3   | -                                    | float         | n.u.        | [0;300]      | Realistic values in [0;300]  |
| <i>phyto</i>               | Scattering phase matrix for phytoplankton       | File provided by FUB (Petzold)       | string        | n.u.        | -            | $\theta, P(\lambda, r, m, \theta), \omega_{o,\lambda}, \sigma_{e,\lambda}$<br>for the Legendre polyn. development of scatt. phase matrix     |
| $\sigma_{e,\lambda}^p$     | Extinction coefficient for phytoplankton        | Input value or output from iop_water | float         | $m^{-1}$    | $\geq 0$     | To compute the contribution of oceanic layers to upwelling radiances at TOA  |
| $\omega_{o,\lambda}^p$     | Single scattering albedo for phytoplankton      | Input value or output from iop_water | float         | n.u.        | [0;1]        | To compute the contribution of oceanic layers to upwelling radiances at TOA  |
| <i>spm</i>                 | Scattering phase matrix for SPM                 | File provided by FUB (Petzold)       | string        | n.u.        | -            | $\theta, P(\lambda, r, m, \theta), \omega_{o,\lambda}, \sigma_{e,\lambda}$<br>for the legendre polynomial development of scatt. phase matrix |
| $\sigma_{e,\lambda}^{spm}$ | Extinction coefficient for SPM                  | Input value or output from iop_water | float         | $m^{-1}$    | $\geq 0$     | To compute the contribution of oceanic layers to upwelling radiances at TOA  |

| <i>Input</i>               | <i>Descriptive name</i>  | <i>Source</i>                               | <i>Format</i> | <i>Unit</i>   | <i>Range</i> | <i>Remarks</i>   |
|----------------------------|--|---|---------------|---------------|--------------|--|
| $\omega_{o,\lambda}^{spm}$ | Single scattering albedo for SPM   | Input value or output from <i>iop_water</i> | float         | <i>n.u.</i>   | [0;1]        | To compute the contribution of oceanic layers to upwelling radiances at TOA  |
| $\sigma_{a,\lambda}^{ys}$  | Absorption coefficient for yellow substance  | Input value or output from <i>iop_water</i> | float         | $m^{-1}$      | $\geq 0$     | To compute the contribution of oceanic layers to upwelling radiances at TOA  |
| <i>vertical</i>            | Vertical distribution of aerosols, cloud scatterers and oceanic components ( <i>phyto.</i> , <i>SPM</i> , <i>yellow subst.</i> ) | Output from <i>vip</i>                      | string        | <i>n.u.</i>   | -            | Vertical profile generated with respect to a defined model layer, the US-standard profile and a vertical distribution of constituents  |
| $I_s$                      | Maximum order of the Legendre polynomial decomposition ( <i>Fourier</i> )  | Optimal value after tests                   | int           | <i>n.u.</i>   | 70           | Not used.<br><u>Note:</u> This value is already defined in the ' <i>mom_in/mom_def</i> ' file  |
| $\rho_s$                   | Surface reflectance  | -   | float         | <i>n.u.</i>   | [0;1]        | Lambertian surface (for land and sea bottom)   |
| $E_o$                      | Solar constant at TOA  | -   | float         | $W/m^2/\mu m$ | $\geq 0$     | -  |
| $\sigma_{a,\lambda}^w$     | Absorption coefficient for pure oceanic water  | Output from <i>IOP_water</i>                | float         | $m^{-1}$      | $\geq 0$     | -  |
| $w_s$                      | Wind speed at 10m above sea level  | -   | float         | <i>m/s</i>    | $\geq 0$     | To compute multiple reflexions (sun glint) on the wind-roughened sea surface (see note 3)  |
| $n_s$                      | Number of SZAs   | -   | int           | <i>n.u.</i>   | [1;21]       | Not used (defined by the Gauss-Lobatto quadrature in MOMO)<br><u>Note:</u> The upper limit is given by the <i>MATDIMWINK</i> variable in the ' <i>input/param</i> ' include file |

Notes: (1) **Be careful:** Depending on the termination of ESFT filename selected for each atmospheric gas ( $H_2O$ ,  $O_2$ ,  $O_3$ ), the absorber amount  $U$  will be considered or not in the gaseous transmittivity computation. If the termination is '*\_b00*' then the gaseous transmittance will be 1 whatever the input value of  $U$ . In all the other cases, the gaseous transmittivity will be computed using either the input gaseous amount if  $U > 0$  or using the total absorber amount  $U$  from the atmospheric profile specified in the ESFT file for the case where  $U = 0$ . Note that for the oxygen ( $U_{O_2} > 0$ ), a vertical distribution of the oxygen vapor amount is computed in RTC/FUB using a pressure profile derived from the US-Standard62.

(2) A scattering phase matrix has to be always selected for each atmospheric or oceanic layer even if the optical thickness is nil for the layer.

(3) For a wind-roughened sea surface ( $W_s > 0$ ), RTC/MOMO needs a Cox-Munk ASCII file which contains the Fourier series terms of the Fresnel reflection and transmission matrices at the 'air-sea' interface. This ASCII file is provided by the FUB institute. Note that 2 current versions of RTC/MOMO are available to be run with 2 differents sets of 3 Cox-Munk files:

(a) Cox-Munk file for a wind-speed of 1.5 m/s ( $w_s < 2$ ), 3 m/s ( $2 \leq w_s < 5$ ), and 7.2 m/s ( $w_s \geq 5$ ).

(b) Cox-Munk file for a wind-speed of 1.5 m/s ( $w_s < 3.25$ ), 5 m/s ( $3.25 \leq w_s < 7.5$ ), and 10 m/s ( $w_s \geq 7.5$ ).

### RTC/FUB-MOMO Outputs

| Input                          | Descriptive name                                      | Source                   | Format | Unit      | Range    | Remarks   |
|--------------------------------|---|--------------------------|--------|-----------|----------|---|
| <i>input</i>                   | Input data card                                       | -                        | string | n.u.      | -        | -   |
| $\tau_{\lambda}$               | Total optical thickness                               | -                        | float  | n.u.      | $\geq 0$ | -   |
| $\tau_{\lambda}^R$             | Rayleigh optical thickness                            | -                        | float  | n.u.      | $\geq 0$ | -   |
| $V_{\lambda}$                  | Horizontal visibility                                 | -                        | float  | m         | $\geq 0$ | -   |
| $AT_{\lambda}$                 | Atmospheric turbidity                                 | -                        | float  | m         | $\geq 0$ | -   |
| $\mathcal{G}_s, \mathcal{G}_v$ | Sun / view zenith angles                              | Gauss-Lobatto quadrature | float  | deg.      | [0;90[   | 16 fixed values:<br>0; 6.97; 12.76; 18.51; 24.24; 29.96;<br>35.68; 41.40; 47.12; 52.84; 58.56; 64.28;<br>69.99; 75.71; 81.43; 87.14   |
| $\Delta\phi$                   | Relative azimuth angles between sun / view directions | -                        | float  | deg.      | [0;180]  | 25 fixed values:<br>0; 7.50; 15.00; 22.50; 30.00; 37.50;<br>45.00; 52.50; 60.00; 67.50; 75.00; 82.50;<br>90.00; 97.50; 105.00; 112.50; 120.00;<br>127.50; 135.00; 142.50; 150.00; 157.50;<br>165.00; 172.50; 180.00 |
| $L_{\lambda}^{\uparrow(TOA)}$  | MERIS normalized radiances (TOA)                      | -                        | float  | $sr^{-1}$ | $\geq 0$ | $(n_s \times n_v \times n_{\Delta\phi})$ values<br>(solar irradiance = $1 W m^{-2} \mu m^{-1}$ )  |

## 10.3 SOFTWARE TECHNICAL DESCRIPTION

The *Mie's* code ('*mie36.f*') and RTC/FUB ('*mom39.f*') are controlled by a common auxiliary file (namely, '*mom\_def*') which are read during the execution. The final results from the RTC/FUB are saved in a certain number of output files given in this auxiliary file. Moreover, an additional include file (namely '*param*') in which are specified the maximal size of arrays is required by the RTC/FUB.

### 10.3.1 Include file: '*param*'

This file contains data on the maximum size of the arrays used in the program. Computer memory can become a problem with the matrix-operator method as many three or four-dimensional arrays are used. It is therefore a good practice to keep the dimension of the matrices as small as possible. Six groups of parameters are included in this file:

- *Parameters 1:* Contains the number of zenith angles in the atmosphere and in the ocean.
  - ATMWINKEL: Number of zenithal angles in the atmosphere (default value: **17**)
  - ATMZUSATZ: Number of additional zenithal angles in the atmosphere (default value: **1**)
  - MATDIMWINK: Number of zenithal angles in the ocean (default value: **21**)
- *Parameters 2:* Contains the maximal number of layers and the maximal number of *Fourier* terms.
  - MAXAZIMUT: Max. number of azimuthal angles (default value: **48**)
  - MAXFOURIER: Max. number of *Fourier* terms (default value: **70**)



MAXSCHICHT: Max. number of layers for the coupled 'atmosphere-ocean' system (default value: **23**)

- *Parameters 3:* Contains the maximal number of wavelengths and the maximum number of coefficients used for the treatment of the gas absorption in the atmosphere.

MAXILAM: Max. number of wavelengths (fixed value: **1**)

MAXTERME: Max. number of terms used in the ESFT for  $H_2O$ ,  $O_2$  and  $O_3$  transmittivities (default value: **20**)

- *Parameters 4:* Contains the maximal number of atmospheric and oceanic constituents as well as additional information on the atmospheric and oceanic constituents with respect to storage order.

MAXZUTAT: Max. number of atmospheric (aerosols+clouds) and oceanic constituents (default value: **11**)

MAXGASART: Max. number of atmospheric gases (default value: **3**)

MAXSONST: Max. number of atmospheric (aerosols+clouds) and oceanic scatterers (default value: **10**)

LUFTRAY: Index for *Rayleigh* scattering in the atmosphere (default value: **1**)

AEROANF: Index for the first aerosol layer (default value: **2**)

AEROLE: Number of aerosol layers (default value: **3**)

WOLKANF: Index for the first cloud layer (default value: **5**)

WOLKEN: Number of cloud layers (default value: **3**)

H2OANF: Index for the first oceanic constituents (default value: **8**)

H2OINH: Number of oceanic constituents (default value: **3**)

H2ORAY: Index for *Rayleigh* scattering in the ocean (default value: **10**)

- *Parameters 5:* Contains some additional information (not special of interest to the user).

GASART: Number of atmospheric gases (default value: **3**)

MAXZMIT: Maximum dimension for Zmit table (default value: **5**)  
(not used in RTC/FUB)

- *Parameters 6:* Other parameters.

PHASTUETZ: Used in *PHA\_ENTW()* [expansion of phase function into *Fourier* series] (default value: **501**)

AKIMADIM: Used in *PHA\_Akima()* [Akima interpolation method] (default value: **PHASTUETZ+4**)

### 10.3.2 Auxiliary file: 'mom\_def'

This file contains I/O filenames, flags for additional output data and the definition of the 15 MERIS spectral bands.

#### 'mom\_def' file

| Input            | Descriptive name  | Format | Unit        | Value      | Code           |
|------------------|---|--------|-------------|------------|----------------|
| <i>RunOption</i> | Structure of the input card: [0] with full description of input data (used for MERISAT), [1] without comment (used for RTC/Intervalidation) | int    | <i>n.u.</i> | [0] or [1] | mie34<br>mom39 |
| <i>OutFile1</i>  | Additional file for simulated downwelling and upwelling fluxes  | string | <i>n.u.</i> | -          | mom39          |
| <i>OutFile2</i>  | Additional file for simulated downwelling and upwelling fluxes  | string | <i>n.u.</i> | -          | mom39          |

| <i>Input</i>            | <i>Descriptive name</i>   | <i>Format</i> | <i>Unit</i> | <i>Value</i> | <i>Code</i> |
|-------------------------|---|---------------|-------------|--------------|-------------|
| <i>OutFile3</i>         | Additional file for simulated downwelling and upwelling fluxes  | string        | <i>n.u.</i> | -            | mom39       |
| <i>OutFile4</i>         | Additional file for simulated downwelling and upwelling fluxes  | string        | <i>n.u.</i> | -            | mom39       |
| <i>OutFile5</i>         | Additional file for simulated downwelling and upwelling fluxes  | string        | <i>n.u.</i> | -            | mom39       |
| <i>Fluorescence</i>     | Flag for in-water fluorescence computation  | logical       | <i>n.u.</i> | -            | mom39       |
| <i>FluoFile</i>         | Additional file for fluorescence fluxes   | string        | <i>n.u.</i> | -            | mom39       |
| <i>PhaseDatei(1)</i>    | Atmospheric <i>Rayleigh</i> scattering phase function   | string        | <i>n.u.</i> | -            | mom39       |
| <i>PhaseDatei(10)</i>   | Oceanic <i>Rayleigh</i> scattering phase function   | string        | <i>n.u.</i> | -            | mom39       |
| <i>ZwischDatei_1</i>    | <i>Fresnel</i> reflexion and transmission matrices of a wind-roughened sea surface (1 <sup>st</sup> wind-speed) | string        | <i>n.u.</i> | -            | mom39       |
| <i>ZwischDatei_2</i>    | <i>Fresnel</i> reflexion and transmission matrices of a wind-roughened sea surface (2 <sup>nd</sup> wind-speed) | string        | <i>n.u.</i> | -            | mom39       |
| <i>ZwischDatei_3</i>    | <i>Fresnel</i> reflexion and transmission matrices of a wind-roughened sea surface (3 <sup>rd</sup> wind-speed) | string        | <i>n.u.</i> | -            | mom39       |
| <i>Aufgeloest</i>       | Flag to check the number of azimuthal angles  | logical       | <i>n.u.</i> | -            | mom39       |
| <i>MaxAzi</i>           | Number of azimuthal angles  | int           | <i>n.u.</i> | -            | mom39       |
| <i>MaxFou</i>           | Maximum order of the Fourier expansion  | int           | <i>n.u.</i> | -            | mom39       |
| <i>Flag Surface</i>     | Flag to test sea surface state  | logical       | <i>n.u.</i> | -            | mom39       |
| <i>Nb of bands</i>      | Number of MERIS spectral bands  | int           | <i>n.u.</i> | -            | mom39       |
| <i>MERIS band X</i>     | Nominal wavelength and FWHM for MERIS band X  | float         | <i>nm</i>   | -            | mom39       |
| <i>Output_structure</i> | Structure of the output file: [0] without header, [1] with header (list of 33 output flags; [0]/[1])            | int           | <i>n.u.</i> | [0] or [1]   | mom39       |

*Note: This 'mom\_def' file has to be created with an header of 4 lines. The last column indicates which codes from the RTC/FUB package use the inputs of 'mom\_def'. Note that the parameter 'Mtotal' is fixed to 1 in 'mom39'.*

### Sample of 'mom\_def' file

```
*****
*** RTC/FUB - I/O files - Flags - MERIS Bands ***
*****

'RunOption      = '      1
'OutFile1       = '      'mom_out/flux_test0'
'OutFile2       = '      'mom_out/ld_test0'
'OutFile3       = '      'mom_out/lu_0001'
'OutFile4       = '      'mom_out/lu_n_0001'
'OutFile5       = '      'mom_out/flu_0001'
'Fluorescence   = '      .FALSE.
```

```

'FluoFile           = '      'mom_in/flu_chL_00'
'PhaseDatei (1)    = '      'sca_out/sc_ray_a.s'
'PhaseDatei (10)   = '      'sca_out/sc_ray_o.s'
'ZwischDatei_1     = '      'sca_out/cm_s1721.w01'
'ZwischDatei_2     = '      'sca_out/cm_s1721.w03'
'ZwischDatei_3     = '      'sca_out/cm_s1721.w07'
'Aufgeloest        = '      .TRUE.
'MaxAzi            = '      48
'MaxFou           = '      70
'Flat Surface      = '      .TRUE.
'Nb of bands       = '      15
'MERIS band_01    = '      412.5      10.0
'      band_02    = '      442.5      10.0
'      band_03    = '      490.0      10.0
'      band_04    = '      510.0      10.0
'      band_05    = '      560.0      10.0
'      band_06    = '      620.0      10.0
'      band_07    = '      665.0      10.0
'      band_08    = '      681.25     7.5
'      band_09    = '      708.75     10.0
'      band_10    = '      753.75     7.5
'      band_11    = '      761.875    3.75
'      band_12    = '      778.75     15.0
'      band_13    = '      865.0      20.0
'      band_14    = '      885.0      10.0
'      band_15    = '      900.0      10.0
'Output_structure = '      ' 1
'Mtotal =         = '      ' 1
'CtrlString (1) - HEADER = '      ' 0
'CtrlString (2) - VERT. PROFILES = '      ' 1
'CtrlString (3) - DATA ON O1-FILE = '      ' 1
'CtrlString (4) - VECT. IRR. UP = '      ' 1
'CtrlString (5) - VECT. IRR. DOWN = '      ' 1
'CtrlString (6) - SCAL. IRR. UP = '      ' 0
'CtrlString (7) - SCAL. IRR. DOWN = '      ' 0
'CtrlString (8) - DIR. SOLAR IRR. = '      ' 1
'CtrlString (9) - REFL. SOL. IRR. = '      ' 1
'CtrlString (10) - REFLECTANCE = '      ' 1
'CtrlString (11) - NOT USED = '      ' 0
'CtrlString (12) - DATA ON O2-FILE = '      ' 1
'CtrlString (13) - RADIANCES DOWN = '      ' 1
'CtrlString (14) - NOT USED = '      ' 0
'CtrlString (15) - NOT USED = '      ' 0
'CtrlString (16) - DATA ON O3-FILE = '      ' 0
'CtrlString (17) - RADIANCES UP = '      ' 1
'CtrlString (18) - NOT USED = '      ' 0
'CtrlString (19) - NOT USED = '      ' 0
'CtrlString (20) - DATA ON O4-FILE = '      ' 0
'CtrlString (21) - NADIR RAD. UP = '      ' 0
'CtrlString (22) - NOT USED = '      ' 0
'CtrlString (23) - ESA_task-force = '      ' 0
'CtrlString (24) - NOT USED = '      ' 0
'CtrlString (25) - NOT USED = '      ' 0
'CtrlString (26) - NOT USED = '      ' 0
'CtrlString (27) - NOT USED = '      ' 0

```

```
'CtrlString (28) - NOT USED      ' 0
'CtrlString (29) - NOT USED      ' 0
'CtrlString (30) - ESA_L_0-      ' 0
'CtrlString (31) - ESA_L_0+      ' 0
'CtrlString (32) - ESA_L_top     ' 1
```

### 10.3.3 Input files to RTC/MOMO

Before running the RTC/MOMO (*i.e.*, *'mom39.f'*), several input files need to be firstly defined. The latters describe the vertical structure of the atmosphere and ocean (pressure, temperature, altitude, atmospheric gaseous and oceanic compositions), the wavelength dependent optical properties (extinction coefficient and single scattering albedo) and phase functions of the atmospheric and oceanic scatterers, the absorption of the atmospheric gases and the concentrations of the atmospheric and oceanic constituents.

Scattering and absorption properties of atmospheric and oceanic particles, such as aerosols, hydrosols and water constituents can be pre-computed using the *Mie's* code presented in [Section 8.1](#) or can be derived from in-situ measurements. In order to allow more flexibilities in the use of MERIS acquisitions (*i.e.*, for a large variety of atmospheric conditions), a procedure for computing optical characteristics of atmospheric and oceanic components (*i.e.*, spectral extinction and absorption coefficients) has been developed (*see* [\[AD-4\]](#) for more details).

Atmospheric gaseous absorption is estimated by an ESFT using the *correlated k-distribution* method (*see* [Sections 2.9 & 7.2.3](#)). The computation of exponential terms remains complex and needs different tools. First, for each relevant gases ( $H_2O, O_2$ ) a LBL code allows one to compute the absorption of each line, whereby the line has to be spectrally resolved. The absorption line parameters of these relevant gases are taken from the HITRAN-2000 database. The latters are used to simulate gaseous transmission functions which are finally approximated as a finite series of exponentials (ESFT). Due to the fact that the tools developed for retrieving these exponentials need to be carefully manipulated, it is highly recommended to use pre-computed exponents for all relevant MERIS bands. Moreover different sets of absorption and extinction coefficients have been established for taking into account eventual wavelength shifts within the MERIS band definition. This allows one to reduce the time-consuming of computation while the high performance is kept.

### 10.3.4 Tree directories

The main directory of MOMO (/RTC/FUB) which contains all the procedures to simulate the MERIS radiances/reflectances is separated into two major sections:

- 'Mie36' directory for the *MIE* computations, with the following sub-directories:

*/sca\_in, /sca\_out, and /src*

Contains the routine for computing optical properties (*i.e.*, scattering phase matrices and single scattering albedo and extinction coefficients) from the *Mie's* theory.

**mie36:** *Mie*-theory calculator: creates files in */sca\_out* directory;  
considers single type of scatter (*i.e.*, clouds) and creates aerosol models when different aerosol components are defined (*i.e.*, maritime aerosol).

- 'Mom39' directory for the radiative transfer computation, with the following sub-directories:

*/mom\_in, /mom\_out, /sca\_esft, /sca\_out, /sca\_vert, /src, /up\_in, /up\_out*

Contains all the routines for computing the multi-spectral radiances for all the MERIS acquisitions and the code to calculate the optical properties for the selected vertical layers with respect to a standard or given atmosphere. Pre-computed tables of the ESFT exponents are also included.

**/up\_in:** Contains files which specify the inputs of *mom39* for the simulation (in parallel with /mom\_in/mom\_def).

**/up\_out:** Contains the outputs of *mom39* which were specified by the input parameter file /up\_in.

**/mom\_in:** Contains the input files which specify various control flags needed in parallel with */up\_in* input file to run the simulation. The file '*mom\_def*' contains flags giving additional output data.

**/mom\_out:** Contains the output additional files which were specified by various control flags in '*mom\_in/mom\_def*' file.

**/sca\_out:** Contains the output files of *mie36*, which includes the scattering phase-matrix, the normalized extinction coefficient and the single scattering albedo. It contains as well as all the related files or the *Fourier* series, which are generated by *mom39*, when the files do not exist.

**/sca\_esft:** Contains files of the '*exponential sums*' to account for the absorption of atmospheric gases, in each MERIS band and for water vapour, oxygen or ozone. These data are the precomputed exponentials used as input files to *mom39*.

**/sca\_in:** Contains input data for *Mie* calculations. The input files contain parameters such as the wavelength, complex refractive index, type of size distribution, ratio and range of particle sizes for aerosols, hydrosols or water substances; all data used to compute the optical properties at a reference wavelength are also given.

Note: The *mie36* code computes the *Mie* scattering output files \*.s (for scattering). When the .s file is available, the phase function has to be expanded into *Fourier* coefficients. MOMO (*mom39*) produces an equivalent .d file of the output scattering file, containing angles, corresponding scattering functions, and series development. The .d file is only created when it does not exist; when MOMO program runs a second time, it reads the .d file instead of the .s file and does not need to re-compute the *Fourier* terms, so it is noticeably faster.

**WARNING: If the scattering output file .s need to be re-computed by mie36 with different optical properties, the corresponding \*.d file will have to be deleted before running MOMO.**

**/sca\_vert** Contains the routine *vtp* to generate the vertical profiles with respect to the defined model layers (*i.e.*, /dat\_scavtp.hsv\_12), the atmospheric profiles (*i.e.*, US-standard62) and the vertical distribution of the constituents (*i.e.*, /dat\_scavscat\_01.ein). The output file includes all information on the vertical distribution (height, pressure, temperature, [*H<sub>2</sub>O*], [*O<sub>2</sub>*] and aerosols, clouds, oceanic components profiles) usefull to run *mom39*.

**scpf\_2** Calculates the forward scattering proportion of a series of aerosol models. The list of aerosol models is given in the file '*scfp.ein*' and corresponds to the scamat output filenames obtained using **mie36**. The outputs derived from **scpf\_2** are stored in the '*ae\_fp.d*' file.

### 10.3.5 Vertical profile

Vertical profiles used as inputs to the RTC/MOMO are generated by the **vtp** code. The latter allows one to build a vertical structure thanks to several defined parameters from an input file placed in '*/dat\_vtp*' directory. These parameters comprise the height profile ('*vtp.hsv*' file), the types of scatterers ('*vtp.ein*' file), and the output file '*vtp1\_XXX.01*' where as an example **XXX** stands for cloud optical thickness and **01** is an index for the selected atmospheric profile. This output does not need to be recomputed as long as the atmosphere model structure remains the same. This input is very important mainly for atmospheric gases, like water vapour, which lines depend strongly on the pressure (line widths) whereas this is not the case for the aerosol scattering.

Sample of input card to the **vtp** code: */sca\_vert/dat\_vtp/vtp12.ein* defines the selected atmospheric profile.

```
Eingabefile fuer Berechnung von VTPn-Profilen aus AFGL-Daten
'AFGL - Profilnummer      : ' 2
'Radiosonden - Profil    : ' profil/profil_12.dat
'Hoehenschichtenverteilung : ' profil/vtp.hsv_23'
'Streuerbelegung        : ' dat_scat/scat_00.ein'
'Ausgabedatei1          : ' dat_vert/vtp1_12'
'Ausgabedatei2          : ' dat_vert/vtp2_12'

Bitte auf die ' achten !!!

AFGL-ATMOSPHAEREN-MODELL
TROPICAL                : 1
MIDLATITUDE SUMMER     : 2
MIDLATITUDE WINTER     : 3
SUBARCTIC SUMMER       : 4
SUBARCTIC WINTER       : 5
U.S. STANDARD           : 6
```

Sample of radiosonde profile: */sca\_vert/profil/profil\_12.dat* contains altitude (km), pressure (hPa), temperature (K), relative humidity (%) and ozone concentration ( $g/m^3$ ).

```
0.0000 1010.0000 276.1 59.9 4.708876E-05
0.2000 989.0000 279.2 49.1 4.862150E-05
0.4000 965.0000 280.3 45.0 5.003241E-05
0.6000 941.0000 279.1 47.5 5.107787E-05
0.8000 919.0000 277.4 51.2 5.198391E-05
1.0000 896.0000 275.5 55.7 5.296464E-05
1.3000 863.0000 273.0 62.0 5.439026E-05
1.6000 831.0000 271.1 65.0 5.590637E-05
2.0000 790.0000 268.9 66.3 5.862374E-05
2.5000 741.0000 266.1 65.6 6.288275E-05
3.0000 695.0000 262.7 67.3 6.727582E-05
3.5000 651.0000 259.0 70.8 7.193130E-05
4.0000 609.0000 255.1 73.3 7.696632E-05
5.0000 532.0000 247.5 75.2 8.814244E-05
7.0000 400.0000 232.1 73.5 1.249216E-04
```

|         |          |       |      |              |
|---------|----------|-------|------|--------------|
| 9.0000  | 296.0000 | 224.0 | 55.6 | 1.868254E-04 |
| 10.0000 | 254.0000 | 223.2 | 44.3 | 2.269797E-04 |
| 15.0000 | 116.0000 | 220.9 | 28.9 | 1.038565E-03 |
| 30.0000 | 12.1000  | 234.1 | 0.2  | 1.110821E-02 |
| 100.000 | 0.0003   | 210.0 | 0.01 | 8.639904E-05 |

Sample of height profile: `/sca_vert/profil/vtp.hsv_23` defines the distribution of the layers.

|                 |        |
|-----------------|--------|
| 'Testprofil'    |        |
| Atm. Ozean Ges. |        |
| 23              | 0 23   |
| 1               | 0.01   |
| 2               | 10.0   |
| 3               | 50.0   |
| 4               | 100.0  |
| 5               | 150.0  |
| 6               | 200.0  |
| 7               | 250.0  |
| 8               | 300.0  |
| 9               | 350.0  |
| 10              | 400.0  |
| 11              | 450.0  |
| 12              | 500.0  |
| 13              | 550.0  |
| 14              | 600.0  |
| 15              | 650.0  |
| 16              | 700.0  |
| 17              | 750.0  |
| 18              | 800.0  |
| 19              | 850.0  |
| 20              | 900.0  |
| 21              | 950.0  |
| 22              | 1000.0 |
| 23              | 1025.0 |

Sample of list of atmospheric and oceanic scatterers: `/sca_vert/dat_scat/scat_00.ein` contains altitude (*km*), pressure (*hPa*), temperature (*K*), relative humidity (%) and ozone concentration (*g/m<sup>3</sup>*).

| number | atmosphere | type | param 1 | param 2 |                 |
|--------|------------|------|---------|---------|-----------------|
| 1      | 1          | 4    | 0.0     | 1000.0  | 'maritim'       |
| 2      | 1          | 4    | 1000    | 12000.0 | 'background'    |
| 3      | 1          | 4    | 12000   | 30000.  | 'stratos'       |
| 4      | 1          | 4    | 0.0     | 1000.0  | 'continental'   |
| 5      | 1          | 5    | 2000    | 0.0     | 'pol mar'       |
| 6      | 1          | 5    | 12000   | 30000.  | 'stratospheric' |
| 7      | 0          | 1    | 1.0     | 0.0     | 'phytopl.'      |
| 8      | 0          | 1    | 1.0     | 0.0     | 'detr.'         |
| 9      | 0          | 1    | 1.0     | 0.0     | 'gelbst'        |

|        |                             |                          |                    |
|--------|-----------------------------|--------------------------|--------------------|
| Types: | 1 constant value not norm.  | param1: value            | param2: not used   |
|        | 2 exponential decrease      | param1: 90% height (m)   | param2: not used   |
|        | 3 Gaussian profile          | param1: mu in % of trop. | param2: sigma      |
|        | 4 constant value normalized | param1: start height (m) | param2: end height |

|               |                   |                      |
|---------------|-------------------|----------------------|
| 5 set to zero | param1: not used  | param2: not used     |
| 6 like 3, but | param1: mu in (m) | param2: sigma in (m) |

Sample of output vtp file: /sca\_vert/vtp1\_12

```

§-----*
§           'Testprofil'                               *
§-----*
'Total Levels      Ms=' 12
'Troposph. Levels Mg=' 11
'Stratosph. Levels Mo=' 3
'Ozoneloading [cm] =' .345
'O3 ratio strat / trop =' 8.320
'
'   Height      Pressure      Temp '
' 1' 90000.00    .18400E-02    186.900
' 2' 25000.00    .25490E+02    221.600
' 3' 12000.00    .19400E+03    216.700
' 4' 9000.00     .30800E+03    229.700
' 5' 7000.00     .41110E+03    242.700
' 6' 5000.00     .54050E+03    255.700
' 7' 4000.00     .61660E+03    262.200
' 8' 3000.00     .70120E+03    268.700
' 9' 2000.00     .79500E+03    275.200
'10' 1000.00     .89880E+03    281.700
'11' .00         .10130E+04    288.200
'12' -.01       .00000E+01    288.200
'
'           Press.[Pa]    Temp.[K]    Mol.[m^-3]    Ozone[m^-3]    H2O[m^-3]'
' Layer 1- 2' .26771E+03 .23151E+03 .83873E+23 .52255E+18 .39568E+18
' Layer 2- 3' .82762E+04 .21763E+03 .27634E+25 .37645E+19 .18219E+20
' Layer 3- 4' .24718E+05 .22110E+03 .80862E+25 .14033E+19 .53458E+21
' Layer 4- 5' .35741E+05 .23620E+03 .10957E+26 .70288E+18 .39793E+22
' Layer 5- 6' .47326E+05 .24920E+03 .13751E+26 .58038E+18 .13132E+23
' Layer 6- 7' .57771E+05 .25895E+03 .16165E+26 .57720E+18 .28397E+23
' Layer 7- 8' .65799E+05 .26545E+03 .17959E+26 .60229E+18 .47516E+23
' Layer 8- 9' .74712E+05 .27195E+03 .19908E+26 .65263E+18 .77114E+23
' Layer 9-10' .84584E+05 .27845E+03 .22017E+26 .67788E+18 .11736E+24
' Layer 10-11' .95476E+05 .28495E+03 .24286E+26 .67785E+18 .16727E+24
' Layer 11-12' .10130E+06 .28820E+03 .00000E+01 .00000E+01 .00000E+01
' Dummy-Layer' .10130E+06 .28820E+03 .00000E+01 .00000E+01 .00000E+01
'           Scatter1    Scatter2    Scatter3    Scatter4    Scatter5    Scatter6
' Layer 1- 2' .00000E+01 .00000E+01 .00000E+01 .00000E+01 .00000E+01 .00000E+01
' Layer 2- 3' .00000E+01 .00000E+01 .62500E-04 .00000E+01 .00000E+01 .00000E+01
' Layer 3- 4' .00000E+01 .00000E+01 .62500E-04 .00000E+01 .00000E+01 .20000E-03
' Layer 4- 5' .00000E+01 .00000E+01 .00000E+01 .00000E+01 .14286E-03 .20000E-03
' Layer 5- 6' .00000E+01 .20000E-03 .00000E+01 .00000E+01 .14286E-03 .00000E+01
' Layer 6- 7' .00000E+01 .20000E-03 .00000E+01 .00000E+01 .14286E-03 .00000E+01
' Layer 7- 8' .00000E+01 .20000E-03 .00000E+01 .00000E+01 .14286E-03 .00000E+01
' Layer 8- 9' .00000E+01 .20000E-03 .00000E+01 .00000E+01 .14286E-03 .00000E+01
' Layer 9-10' .50000E-03 .00000E+01 .00000E+01 .50000E-03 .00000E+01 .00000E+01
' Layer 10-11' .50000E-03 .00000E+01 .00000E+01 .50000E-03 .00000E+01 .00000E+01
' Layer 11-12' .00000E+01 .00000E+01 .00000E+01 .00000E+01 .00000E+01 .00000E+01
' Dummy-Layer' .00000E+01 .00000E+01 .00000E+01 .00000E+01 .00000E+01 .00000E+01
'           Scatter7    Scatter8    Scatter9
' Layer 1- 2' .00000E+01 .00000E+01 .00000E+01

```



|                 |            |            |            |            |            |            |
|-----------------|------------|------------|------------|------------|------------|------------|
| ' Layer 2- 3'   | .00000E+01 | .00000E+01 | .00000E+01 |            |            |            |
| ' Layer 3- 4'   | .00000E+01 | .00000E+01 | .00000E+01 |            |            |            |
| ' Layer 4- 5'   | .00000E+01 | .00000E+01 | .00000E+01 |            |            |            |
| ' Layer 5- 6'   | .00000E+01 | .00000E+01 | .00000E+01 |            |            |            |
| ' Layer 6- 7'   | .00000E+01 | .00000E+01 | .00000E+01 |            |            |            |
| ' Layer 7- 8'   | .00000E+01 | .00000E+01 | .00000E+01 |            |            |            |
| ' Layer 8- 9'   | .00000E+01 | .00000E+01 | .00000E+01 |            |            |            |
| ' Layer 9- 10'  | .00000E+01 | .00000E+01 | .00000E+01 |            |            |            |
| ' Layer 10- 11' | .00000E+01 | .00000E+01 | .00000E+01 |            |            |            |
| ' Layer 11- 12' | .10000E+01 | .10000E+01 | .10000E+01 |            |            |            |
| ' Dummy-Layer ' | .00000E+01 | .00000E+01 | .00000E+01 | .00000E+01 | .00000E+01 | .00000E+01 |

### 10.3.6 Forward scattering proportion computation

The *scfp\_2* code allows one to compute the forward scattering proportion using as input the results derived from *mie36* for different aerosol models. The latter are listed in '*scfp.ein*' file and the scattering proportion outputs are saved in '*ae\_fp.d*' file.

**'scfp.ein' file format:**

First line: number of wavelengths  $N_\lambda$  and number of aerosol models  $N_{aer}$

Second line and followings: aerosol scatmat output filenames

The total number of aerosol filenames must be equal to  $N_\lambda \times N_{aer}$

**'ae\_fp.d' file format:**

First column: scatmat aerosol output file from *mie36*

Second column: wavelength in nanometers

Third column: extinction coefficient

Fourth column: single scattering albedo

Fifth column: scattering forward proportion

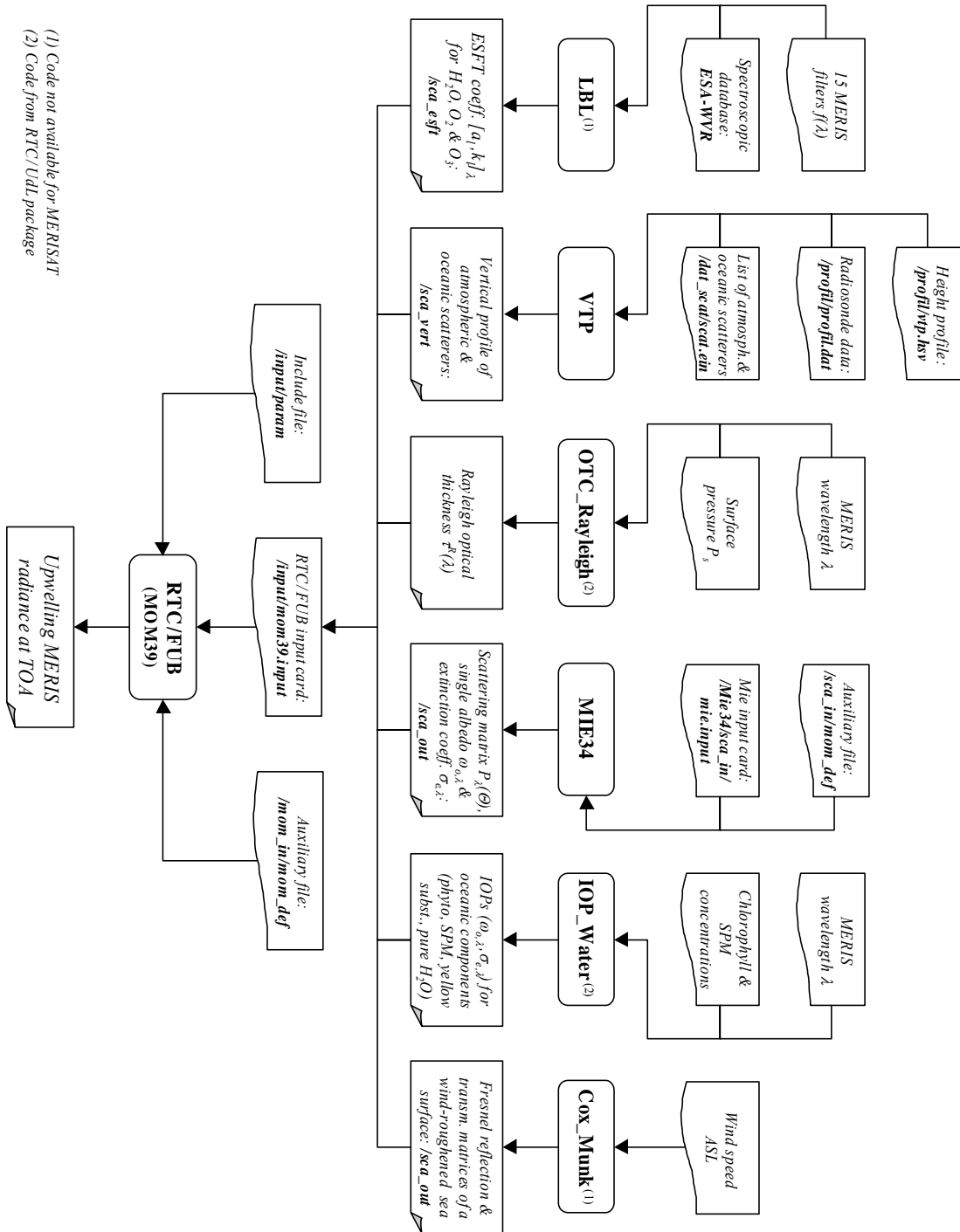


Figure 2: Overview of the RTC/FUB package

## 11. APPENDIX-3: SPECIFICATION OF RTC/MOS PACKAGE

The following tools are useful to generate 4 MERIS LUTs at the level-2 relying on the dense dark vegetation (DDV) parameters for the bidirectionality correction.

### 11.1 RTC/LUT\_ALB\_GDDV

#### Description:

This code allows one to generate the MERIS LUT-322, *i.e.* the ground DDV albedos ( $\rho_{DDV}$ ) at 4 MERIS wavelengths (412.5 nm, 442.5 nm, 490 nm and 665 nm) for each of 20 DDV models defined by the CESBIO (Centre d'Etudes Spatiales de la BIOSphère, Toulouse - FRANCE) institute. These 20 DDV models are represented by the *Hapke's* model parameters ( $\omega$ ,  $g$ ,  $S$  and  $h$ ).

#### Processing:

The MERIS LUT-322 is generated with the following steps:

- *Step1:* Extract the 4 *Hapke's* parameters ( $\omega$ ,  $g$ ,  $S$  and  $h$ ) for each DDV model ( $N_{DDV} = 20$ ) and each MERIS wavelength  $\lambda$  ( $N_{\lambda} = 4$ ), from an input *Hapke's* parameters file provided by the CESBIO institute.
- *Step2:* Compute ground DDV albedo  $\rho_{DDV}(ddv, \lambda)$  for each DDV and each  $\lambda$ , by an angular integration of the DDV BRDF,  $R_{DDV}(ddv, \lambda, \vartheta', \vartheta_v, \Delta\phi')$  (*Hapke's* model).

$$\rho_{DDV}(ddv, \lambda) = \frac{1}{2\pi} \cdot \int_0^{2\pi} \int_0^1 \int_0^1 R_{DDV}(ddv, \lambda, \vartheta', \vartheta_v, \Delta\phi') \cdot d\mu' \cdot d\mu_v \cdot d\Delta\phi'$$

This angular integration is numerically achieved with 3 *Gaussian* quadratures for  $\mu'$ ,  $\mu_v$  and  $\Delta\phi'$  (24  $\vartheta'$ ; 24  $\vartheta_v$ ; 48  $\Delta\phi'$ ).

#### Tool:

'lut\_alb\_gddv.f'

#### Input description:

#### RTC/lut\_alb\_gddv – Inputs

| Input       | Descriptive name   | Source | Format     | Unit        | Range | Remarks  |
|-------------|--|--------|------------|-------------|-------|--|
| param_Hapke | Hapke's parameters ( $\omega, g, S, h$ ) for all DDV BRDF models | CESBIO | ASCII file | <i>n.u.</i> | -     | - <i>Hapke's</i> parameters:<br>1-single scattering albedo ( $\omega$ )<br>2-assymmetry factor of phase function ( $g$ )<br>3-amplitude of the hot-spot ( $S$ )<br>4-width of the hot-spot ( $h$ ) |

Output description:

**RTC/lut\_alb\_gddv – Outputs**

| Output                 | Descriptive name   | Source | Format      | Unit        | Range | Remarks   |
|------------------------|--|--------|-------------|-------------|-------|---|
| <i>ddv_alb_lut</i>     | DDV albedos in 4 MERIS bands (412.5, 442.5, 490, 665 nm) | -      | ASCII file  | <i>n.u.</i> | [0;1] | $\Rightarrow (N_{DDV} \times N_{\lambda})$ values |
| <i>ddv_alb_lut.bin</i> | DDV albedos in 4 MERIS bands (412.5, 442.5, 490, 665 nm) | -      | Binary file | <i>n.u.</i> | [0;1] | $\Rightarrow (N_{DDV} \times N_{\lambda})$ values |

## 11.2 RTC/LUT\_RHOB\_AGDDV

Description:

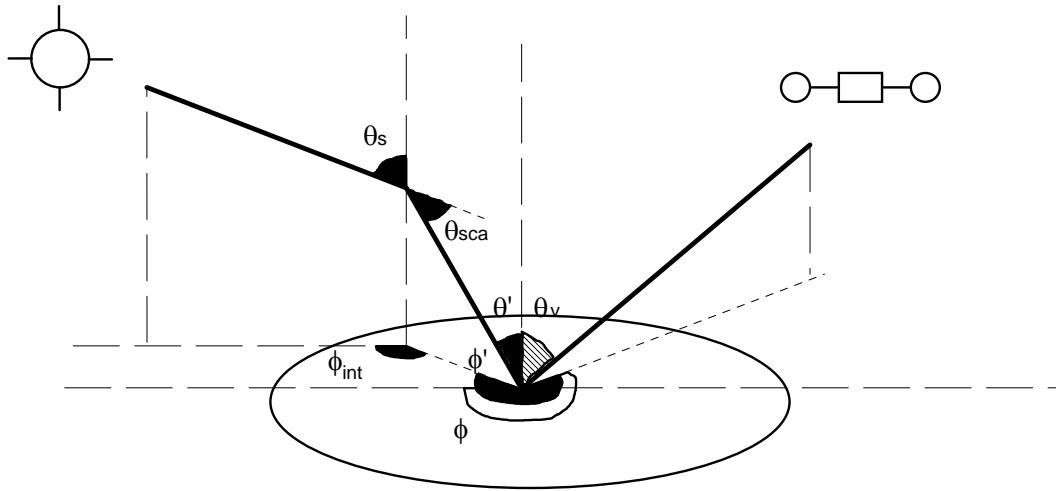
This code allows one to generate the 5 *Fourier* series coefficients  $(\bar{\rho}_{aG})^{(s)}$  of the aerosol-ground DDV coupling bidirectionality term  $(\bar{\rho}_{aG})$  at 4 MERIS wavelengths (412.5 nm, 442.5 nm, 490 nm and 665 nm) for each of 20 DDV models defined by the CESBIO institute. The latter are represented by the *Hapke's* model parameters ( $\omega$ ,  $g$ ,  $S$  and  $h$ ).

Processing:

The MERIS LUT-321 is generated with the following steps:

- *Step 1:* Compute DDV BRDF  $R_{DDV}(ddv, \lambda, \mathcal{G}', \mathcal{G}_v, \Delta\phi')$  using *Hapke's* parameters provided by the CESBIO institute, for each DDV model ( $N_{DDV} = 20$ ), for each MERIS wavelength  $\lambda$  ( $N_{\lambda} = 4$ ), and for each illumination and viewing configuration  $(\mathcal{G}', \mathcal{G}_v)$  and  $\Delta\phi'$  ( $N_{\mathcal{G}'} = 24$ ;  $N_{\mathcal{G}_v} = 12$ ;  $N_{\Delta\phi'} = 72$ ). Note that the zenithal angles  $(\mathcal{G}', \mathcal{G}_v)$  (within  $[0^\circ; 90^\circ]$ ) derive from *Gauss* quadratures and the relative azimuthal differences  $(\Delta\phi')$  (within  $[-180^\circ; 180^\circ]$ ) follow a parabolic distribution centred at  $0^\circ$ .
- *Step 2:* Set a table with pre-computed values of downward normalized aerosol phase function  $P(\theta, N_{aer})$  (or  $P(\mathcal{G}_s, \mathcal{G}', \Delta\phi, \Delta\phi', N_{aer})$  with  $N_{\mathcal{G}_s} = 12$ ,  $N_{\mathcal{G}'} = 24$ ,  $N_{\Delta\phi} = 30$ ,  $N_{\Delta\phi'} = 72$ ) for all the SAMs over land ( $N_{aer} = 78$ ) and all the scattering geometries ( $N_{\theta} = 83$ ). For each combination  $(\mathcal{G}_s, \mathcal{G}', \Delta\phi, \Delta\phi')$ , we compute:

- the scattering angle  $\theta_{sca}$  as follows:  
$$\cos(\theta_{sca}) = \cos(\mathcal{G}_s) \cos(\mathcal{G}') + \sin(\mathcal{G}_s) \cdot \sin(\mathcal{G}') \cdot \cos(\Delta\phi' - \Delta\phi)$$
- the aerosol phase function  $P(\theta_{sca}, i_{aer})$  for each aerosol model  $i_{aer}$  by interpolation from tabulated values of  $P(\theta, N_{aer})$  using a 5<sup>th</sup> degree polynomial.



Geometries: 12  $\vartheta_s$ , 24  $\vartheta_v$ , 30  $\Delta\phi$ , 72  $\Delta\phi'$

Compute downward  
scattering angle  $\theta_{sca}$

$\theta_{sca}(\vartheta_s, \vartheta_v, \Delta\phi, \Delta\phi')$

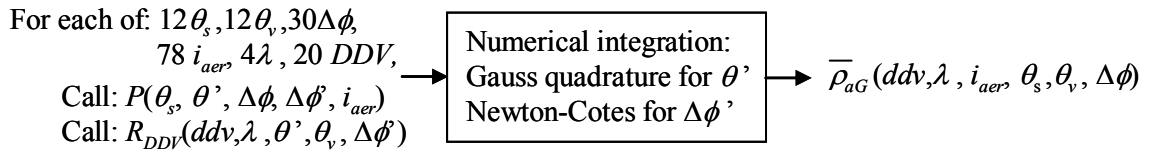
For each aerosol model  
 $i_{aer}$ , interpolate the  
aerosol phase function  
 $P(\theta, i_{aer})$  at  $\theta_{sca}$

$P(\vartheta_s, \vartheta_v, \Delta\phi, \Delta\phi', i_{aer})$

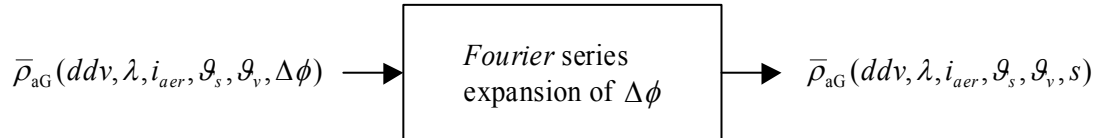
- Step 3: Compute the aerosol-ground DDV coupling bidirectionality term  $\bar{\rho}_{aG}(ddv, \lambda, i_{aer}, \vartheta_s, \vartheta_v, \Delta\phi)$  for each DDV, each  $\lambda$ , each SAM over land  $i_{aer}$  and each illumination and viewing configuration  $(\vartheta_s, \vartheta_v, \Delta\phi)$  (with  $N_{\vartheta_s} = 12$ ,  $N_{\vartheta_v} = 12$ ,  $N_{\Delta\phi} = 30$ ):

$$\bar{\rho}_{aG}(ddv, \lambda, i_{aer}, \vartheta_s, \vartheta_v, \Delta\phi) = \frac{\int_0^{2\pi} \int_0^1 R_{DDV}(ddv, \lambda, \vartheta_s, \vartheta_v, \Delta\phi') \cdot P(\vartheta_s, \vartheta_v, \Delta\phi, \Delta\phi', i_{aer}) \cdot d\mu' \cdot d\Delta\phi'}{\int_0^{2\pi} \int_0^1 P(\vartheta_s, \vartheta_v, \Delta\phi, \Delta\phi', i_{aer}) \cdot d\mu' \cdot d\Delta\phi'}$$

This angular integration is numerically performed using a *Gauss* quadrature for  $\mu'$  and the *Newton-Cotes* method for  $\Delta\phi'$ .



- Step4: Remove the azimuthal dependence  $\Delta\phi$  by expanding  $\bar{\rho}_{aG}$  into *Fourier* series at the 4<sup>th</sup> order:



Tool:

'lut\_rhob\_agddv.f'

Input description:


**RTC/lut\_rhob\_agddv – Inputs**

| Input       | Descriptive name   | Source | Format     | Unit | Range | Remarks   |
|-------------|--|--------|------------|------|-------|---|
| phase_aer78 | Scattering phase functions for 78 <i>Junge's</i> models (SAMs over land) | LISE   | ASCII file | n.u. | -     | $\Rightarrow (N_{scat} \times N_{aer})$ values  |
| param_Hapke | <i>Hapke's</i> parameters ( $\omega, g, S, h$ ) for all DDV BRDF models  | CESBIO | ASCII file | n.u. | -     | - <i>Hapke's</i> parameters:<br>1 - single scattering albedo ( $\omega$ )<br>2 - asymmetry factor of phase function ( $g$ )<br>3 - amplitude of the hot-spot ( $S$ )<br>4 - width of the hot-spot ( $h$ ) |

Output description:

**RTC/lut\_rhob\_agddv – Outputs**

| Output            | Descriptive name  | Source | Format      | Unit | Range | Remarks   |
|-------------------|---|--------|-------------|------|-------|---|
| rhob_aG_LUTXX     | LUTs with <i>Fourier</i> series coefficients (5) of $\bar{\rho}_{aG}$ computed at 412.5, 442.5, 490, 665 nm and for each of 12 <i>Gaussian</i> angles | -      | ASCII file  | n.u. | -     | XX stands for DDV model #<br>( $N_\lambda \times N_{aer} \times N_{\mu_s} \times N_{\mu_v} \times N_S$ ) values |
| rhob_aG_LUTXX.bin | LUTs with <i>Fourier</i> series coefficients (5) of $\bar{\rho}_{aG}$ computed at 412.5,  | -      | Binary file | n.u. | -     | XX stands for DDV model #<br>( $N_\lambda \times N_{aer} \times N_{\mu_s} \times N_{\mu_v} \times N_S$ )        |

|   |   |                           |
|---|---|---------------------------|
|  | <b>MERIS/ ENVISAT-1</b><br>Medium Resolution Imaging Spectrometer | Ref.: PO-RS-PAR-GS-0003   |
|   |   | Issue: 4 Rev.: A          |
|   |   | Date: 16-Dec-10 Page: 143 |

| Output | Descriptive name   | Source | Format | Unit | Range | Remarks |
|--------|--|--------|--------|------|-------|---------|
|        | 442.5, 490, 665 nm and for each of 12 <i>Gaussian</i> angles |        |        |      |       | values  |

### 11.3 RTC/LUT\_RHOB\_RGDDV

#### Description:

This code allows one to generate the *Rayleigh*-ground DDV coupling bidirectionality term ( $\bar{\rho}_{RG}$ ) at 4 MERIS wavelengths (412.5 nm, 442.5 nm, 490 nm and 665 nm) for each of 20 DDV models defined by the CESBIO institute. The latter are represented by the *Hapke's* model parameters.

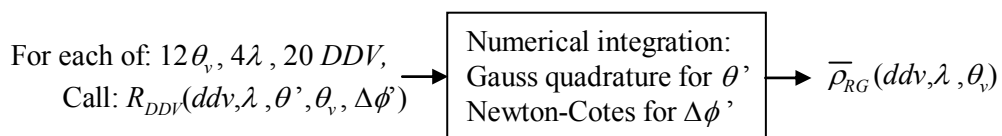
#### Processing:

The MERIS LUT-320 is generated with the following steps:

- *Step 1:* Compute DDV BRDF  $R_{DDV}(ddv, \lambda, \mathcal{G}', \mathcal{G}_v, \Delta\phi')$  using *Hapke's* parameters provided by the CESBIO institute, for each DDV model ( $N_{DDV} = 20$ ), for each MERIS wavelength  $\lambda$  ( $N_\lambda = 4$ ), and for each illumination and viewing configuration ( $\mathcal{G}', \mathcal{G}_v$ ) and  $\Delta\phi'$  ( $N_{\mathcal{G}'} = 24$ ;  $N_{\mathcal{G}_v} = 12$ ;  $N_{\Delta\phi'} = 72$ ). Note that the zenithal angles ( $\mathcal{G}', \mathcal{G}_v$ ) (within  $[0^\circ; 90^\circ]$ ) derive from *Gauss* quadratures and the relative azimuthal differences ( $\Delta\phi'$ ) (within  $[-180^\circ; 180^\circ]$ ) follow a parabolic distribution centred at  $0^\circ$ .
- *Step 2:* Compute the *Rayleigh*-ground DDV coupling bidirectionality term  $\bar{\rho}_{RG}(ddv, \lambda, \mathcal{G}_v)$  for each DDV, each  $\lambda$ , and each viewing angle  $\mathcal{G}_v$  ( $N_{\mathcal{G}_v} = 12$ ), using the numerical angular integration of  $R_{DDV}(ddv, \lambda, \mathcal{G}', \mathcal{G}_v, \Delta\phi')$  on  $\mu'$  and  $\Delta\phi'$ :

$$\bar{\rho}_{RG}(ddv, \lambda, \mathcal{G}_v) = \frac{1}{2\pi} \cdot \int_0^{2\pi} \int_0^{\pi} R_{DDV}(ddv, \lambda, \mathcal{G}', \mathcal{G}_v, \Delta\phi') \cdot d\mu' \cdot d\Delta\phi'$$

This angular integration on  $\mu'$  is performed using a *Gauss* quadrature whereas the azimuthal integration on  $\Delta\phi'$  is completed with the *Newton-Cotes* method.



#### Tool:

'lut\_rhob\_Rgddv.f'

#### Input description:

### RTC/lut\_rhob\_Rgddv – Inputs

| Input              | Descriptive name  | Source | Format     | Unit        | Range | Remarks   |
|--------------------|---|--------|------------|-------------|-------|---|
| <i>param_Hapke</i> | <i>Hapke's</i> parameters ( $\omega, g, S, h$ ) for all DDV BRDF models | CESBIO | ASCII file | <i>n.u.</i> | -     | - <i>Hapke's</i> parameters:<br>1 - single scattering albedo ( $\omega$ )<br>2 - asymmetry factor of phase function ( $g$ )<br>3 - amplitude of the hot-spot ( $S$ )<br>4 - width of the hot-spot ( $h$ ) |

#### Output description:

### RTC/lut\_rhob\_Rgddv – Outputs

| Output                   | Descriptive name  | Source | Format      | Unit        | Range | Remarks  |
|--------------------------|---|--------|-------------|-------------|-------|--|
| <i>rhob_RG_LUTXX</i>     | LUTs with $\bar{\rho}_{RG}$ computed at 412.5, 442.5, 490, 665 nm and for each of 12 <i>Gaussian</i> angles | -      | ASCII file  | <i>n.u.</i> | -     | <i>XX</i> stands for DDV model # ( $N_{\mu_v} \times N_{\lambda}$ ) values |
| <i>rhob_RG_LUTXX.bin</i> | LUTs with $\bar{\rho}_{RG}$ computed at 412.5, 442.5, 490, 665 nm and for each of 12 <i>Gaussian</i> angles | -      | Binary file | <i>n.u.</i> | -     | <i>XX</i> stands for DDV model # ( $N_{\mu_v} \times N_{\lambda}$ ) values |

## 11.4 RTC/LUT\_RHOB\_AR

#### Description:

This code allows one to generate the 4 polynomial coefficients fit  $k_i^{(s)}(i_{aer}, \mathcal{G}_s, \mathcal{G}_v)$  for the aerosol-molecule coupling bidirectionality term ( $\bar{\rho}_{ar}$ ) retrieval for 78 *Junge's* models (or 78 SAMs over land) and 12 *Gaussian* angles. These coefficients derived from a third order polynomial fit as function of the aerosol optical thickness ( $\tau^a$ ) applied to a set of  $\bar{\rho}_{ar}$  values.

#### Processing:

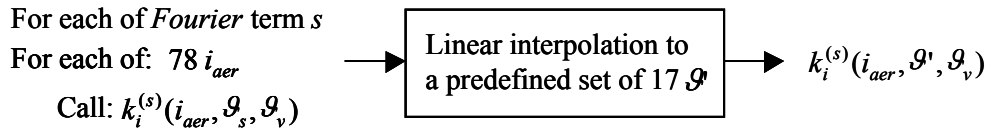
Based on the database derived from the MOS ground segment (see [Section 7.3.6](#) for more details), the MERIS LUT-324 is generated with the following steps:

- *Step 1:* Set a table with 4 pre-computed polynomial coefficients  $k_i^{(s)}(i_{aer}, \mathcal{G}_s, \mathcal{G}_v)$  ( $i = [1; 4]$ ) for each term  $s$  of the *Fourier* series decomposition ( $N_s = 6$ ) of the multiplicative aerosol scattering function  $f_a(\mathcal{G}_s, \mathcal{G}_v, \tau^a)$ , for each SAM over land  $i_{aer}$  ( $N_{aer} = 78$ ),



and each illumination and viewing geometries  $\mathcal{G}_s \times \mathcal{G}_v$  ( $N_{\mathcal{G}_s} = 12$ ;  $N_{\mathcal{G}_v} = 12$ ). These coefficients were determined for the MERIS ground segment and tabulated values were saved in several files for each of 78 SAMs over land. The latters were provided by the CESBIO institute.

- *Step 2:* Interpolate linearly the 4 pre-computed MERIS polynomial coefficients  $k_i^{(s)}(i_{aer}, \mathcal{G}_s, \mathcal{G}_v)$  for each *Fourier* term  $s$ , each aerosol model  $i_{aer}$ , and each viewing angle  $\mathcal{G}_v$ , to the predefined set of 17 *Gaussian* angles ( $\mathcal{G}'$ ) for the MERIS segment.



- *Step 3:* Generate the aerosol-molecule coupling bidirectionality term ( $\bar{\rho}_{aR}$ ) by recombination of the first 6 *Fourier* terms.
- *Step 4:* Determine the 3<sup>rd</sup> order polynomial fit as function of the aerosol optical thickness ( $\tau^a$ ) on the ( $\bar{\rho}_{aR}$ ) values in order to remove the explicit dependence on  $\tau^a$ .

$$f_a^{(s)}(i_{aer}, \tau^a, \mathcal{G}_s, \mathcal{G}_v) = \sum_{i=0}^3 k_i^{(s)}(i_{aer}, \mathcal{G}_s, \mathcal{G}_v) \cdot (\tau^a)^i$$

$$f_a(i_{aer}, \tau^a, \mathcal{G}_s, \mathcal{G}_v) = \sum_{s=0}^5 (2 - \delta_{0,s}) \cdot f_a^{(s)}(i_{aer}, \tau^a, \mathcal{G}_s, \mathcal{G}_v) \cdot \cos(s \cdot \Delta\phi)$$

$$\rho_{a,P}^{(s)}(i_{aer}, \tau^a, \mathcal{G}_s, \mathcal{G}_v) = P_a^{(s)}(\mathcal{G}_s, \mathcal{G}_v, \Delta\phi, i_{aer}) \cdot \frac{(1 - e^{-M \cdot \tau^a})}{4 \cdot (\cos \mathcal{G}_s + \cos \mathcal{G}_v)}$$

with  $M$  the airmass defined as:

$$M = \frac{1}{\cos \mathcal{G}_s} + \frac{1}{\cos \mathcal{G}_v}$$

$$\rho_a^{(s)}(i_{aer}, \tau^a, \mathcal{G}_s, \mathcal{G}_v) = \rho_{a,P}^{(s)}(i_{aer}, \tau^a, \mathcal{G}_s, \mathcal{G}_v) \cdot f_a^{(s)}(i_{aer}, \tau^a, \mathcal{G}_s, \mathcal{G}_v)$$

$$\bar{\rho}_{aR}(i_{aer}, \mathcal{G}_v, \tau^a) = \frac{\int_0^{2\pi} \int_0^{2\pi} R_{DDV}(i_{aer}, \tau^a, \mathcal{G}', \mathcal{G}_v, \Delta\phi') \cdot P(\mathcal{G}_s, \mathcal{G}', \Delta\phi, \Delta\phi', i_{aer}) \cdot d\mu' \cdot d\Delta\phi'}{\int_0^{2\pi} \int_0^{2\pi} P(\mathcal{G}_s, \mathcal{G}', \Delta\phi, \Delta\phi', i_{aer}) \cdot d\mu' \cdot d\Delta\phi'}$$

Tool:

'lut\_rhob\_AR.f'

Input description:

**RTC/lut\_rhob\_aR – Inputs**

| Input              | Descriptive name  | Source | Format     | Unit        | Range | Remarks  |
|--------------------|---|--------|------------|-------------|-------|--|
| <i>phase_aer78</i> | Scattering phase functions for 78 <i>Junge's</i> models (SAMs over land)  | LISE   | ASCII file | <i>n.u.</i> | -     | $\Rightarrow (N_{scat} \times N_{aer})$ values   |
| <i>fa_XX</i>       | 78 SAMs phase function files, with 4 polynomial coefficients fit for each of the first 6 <i>Fourier</i> series terms and for each of the 78 SZA-VZA geometries. | LISE   | ASCII file | <i>n.u.</i> | -     | <i>XX</i> stands for aerosol model #<br>$\Rightarrow (78 \times N_{coef} \times N_s)$ values |

Output description:

**RTC/lut\_rhob\_aR – Outputs**

| Output                 | Descriptive name   | Source | Format      | Unit        | Range | Remarks  |
|------------------------|--|--------|-------------|-------------|-------|--|
| <i>rhob_aR_LUT</i>     | LUTs with 4 polynomial coefficients fit for $\bar{\rho}_{aR}$ retrieval, computed for each aerosol model and each <i>Gaussian</i> angles | -      | ASCII file  | <i>n.u.</i> | -     | $\Rightarrow (N_{aer} \times N_{\mu_v} \times N_{coeff})$ values |
| <i>rhob_aR_LUT.bin</i> | LUTs with 4 polynomial coefficients fit for $\bar{\rho}_{aR}$ retrieval, computed for each aerosol model and each <i>Gaussian</i> angles | -      | Binary file | <i>n.u.</i> | -     | $\Rightarrow (N_{aer} \times N_{\mu_v} \times N_{coeff})$ values |

LUT\_file will contain polynomial coefficients fit  $(k_0, k_1, k_2, k_3)$  for  $\bar{\rho}_{aR}$  retrieval, given for each SAM and each Gauss angle

## 12. APPENDIX-4: SPECIFICATION OF TOOLS FOR MERISAT

The following algorithms are given as processing units included in MERISAT (see [AD-7] for more details) to be used in conjunction with the two RTCs (FUB & UdL) for the final assemblage of MERIS LUTs. Each algorithm is briefly described and I/O are listed in an associated table.

### 12.1 LINEAR FITTING

Description:

This function is used to determine the slope and the ordinate of a straight line through a set of data points. A general description is given here for the implementation of the algorithm which is independent of the type of data used as input.

Processing:

| Variable | Descriptive Name                               | I/O | Type  | Ranges / References / Remarks                   |
|----------|--|-----|-------|---|
| $N$      | Dimension of vectors to fit                    | I   | int   | No restriction on the size of $N$               |
| $x_i$    | Abscissa data values                           | I   | float | Could also be specified by $x_0$ and $\Delta x$ |
| $y_j$    | Ordinate data values                           | I   | float | -   |
| $m$      | Computed slope of the fitted line              | O   | float | -   |
| $b$      | Computed ordinate at origin of the fitted line | O   | float | -   |

One of the simplest implementation of the linear fitting is defined as follows:

$$y = m \cdot x + b$$

$$t = N \cdot \sum_{i=0}^{N-1} x_i^2 - \left( \sum_{i=0}^{N-1} x_i \right)^2$$

$$m = \frac{1}{t} \cdot \left[ N \cdot \sum_{i=0}^{N-1} x_i \cdot y_i - \sum_{i=0}^{N-1} x_i \cdot \sum_{i=0}^{N-1} y_i \right]$$

$$b = \frac{1}{t} \cdot \left[ \sum_{i=0}^{N-1} y_i \cdot \sum_{i=0}^{N-1} x_i^2 - \sum_{i=0}^{N-1} x_i \cdot \sum_{i=0}^{N-1} x_i \cdot y_i \right]$$

When the abscissa data is uniformly distributed at  $\Delta x$  intervals, the previous expression can be further simplified:

$$y = m \cdot x + b$$

$$\begin{aligned} x &= x_0, x_0 + \Delta x, x_0 + 2 \Delta x, \dots, x_0 + (N-1) \Delta x \\ &= x_0 + [0, 1, 2, \dots, (N-1)] \cdot \Delta x \end{aligned}$$

$$t_1 = \frac{6}{N(N+1) \Delta x} ,$$

$$t_2 = t_1 \cdot \sum_{i=0}^{N-1} y_i ,$$

$$t_3 = \frac{2 t_1}{N-1} \cdot \sum_{i=0}^{N-1} i \cdot y_i ,$$

$$m = t_3 - t_2 ,$$

$$b = t_2 \cdot \left( x_0 + \frac{2N-1}{3} \cdot \Delta x \right) - t_3 \cdot \left( x_0 + \frac{N-1}{2} \cdot \Delta x \right)$$

**Software:**Module name: ***LinearFit*****Validation:**

Pre-validation of algorithm with test data sets.

## 12.2 POLYNOMIAL FITTING

### Description:

This function computes coefficient of polynomial of order  $n$  passing through  $N$  points given in  $x_i$  and  $y_i$  vectors. If the order of the polynomial is 1, use linear fitting instead (see [Section 12.1](#)).

### Processing:

| Variable | Descriptive Name                 | I/O | Type  | Ranges / References / Remarks |
|----------|----------------------------------|-----|-------|-------------------------------|
| $N$      | Dimension of vectors to fit      | I   | int   | $i = 0..N-1$                  |
| $m$      | Order of the polynomial to fit   | I   | int   | $1 < m < N$                   |
| $x_i$    | Abscissa data values             | I   | float | -                             |
| $y_j$    | Ordinate data values             | I   | float | -                             |
| $c_j$    | Computed polynomial coefficients | O   | float | $j = 0..m$                    |

Proceeds by resolving the following system:

$$A \cdot X = B$$

using matrix inversion algorithm

$$\begin{bmatrix} N & \sum x_i & \sum x_i^2 & \dots & \sum x_i^m \\ \sum x_i & \sum x_i^2 & \dots & \dots & \sum x_i^{m+1} \\ \sum x_i^2 & \dots & \dots & \dots & \sum x_i^{m+2} \\ \dots & \dots & \dots & \dots & \dots \\ \sum x_i^m & \dots & \dots & \dots & \sum x_i^{2m} \end{bmatrix} \times \begin{bmatrix} c_0 \\ c_1 \\ c_2 \\ \vdots \\ c_m \end{bmatrix} = \begin{bmatrix} \sum_{i=0}^{N-1} y_i \\ \sum x_i y_i \\ \sum x_i^2 y_i \\ \vdots \\ \sum x_i^m y_i \end{bmatrix}$$

The polynomial is written as:

$$\sum_{j=0}^m c_j \cdot x^j$$

### Software:

Module name: **PolynomialFit**

### Validation:

Pre-validation of algorithm with test data sets.

## 12.3 LINEAR INTERPOLATION IN ONE DIMENSION

### Description:

This function is used to interpolate a value in a vector corresponding to a given abscissa value using a straight line model.

### Processing:

| <i>Variable</i> | <i>Descriptive Name</i>      | <i>I/O</i> | <i>Type</i> | <i>Ranges / References / Remarks</i>   |
|-----------------|------------------------------|------------|-------------|--|
| $N$             | Dimension of input vectors   | I          | int         | $k = 0..N-1$   |
| $x_k$           | Abscissa data values         | I          | float       | <i>Is specified by <math>x_0</math> and <math>\Delta x</math></i>  |
| $f(x_k)$        | Ordinate input data points   | I          | float       | -  |
| $x$             | Interpolation abscissa point | I          | float       | point at which interpolation is to be computed. Must be between input vector limits. Otherwise, extrapolation must be computed |
| $f(x)$          | Interpolated value           | O          | float       | -  |

The following description supposes an uniform points distribution:

For a given vector  $f(x_k)$  defined on  $N$  points, *linear* interpolation can be expressed as:

$$f(x) = f(x_k) + \delta[f(x_{k+1}) - f(x_k)]$$

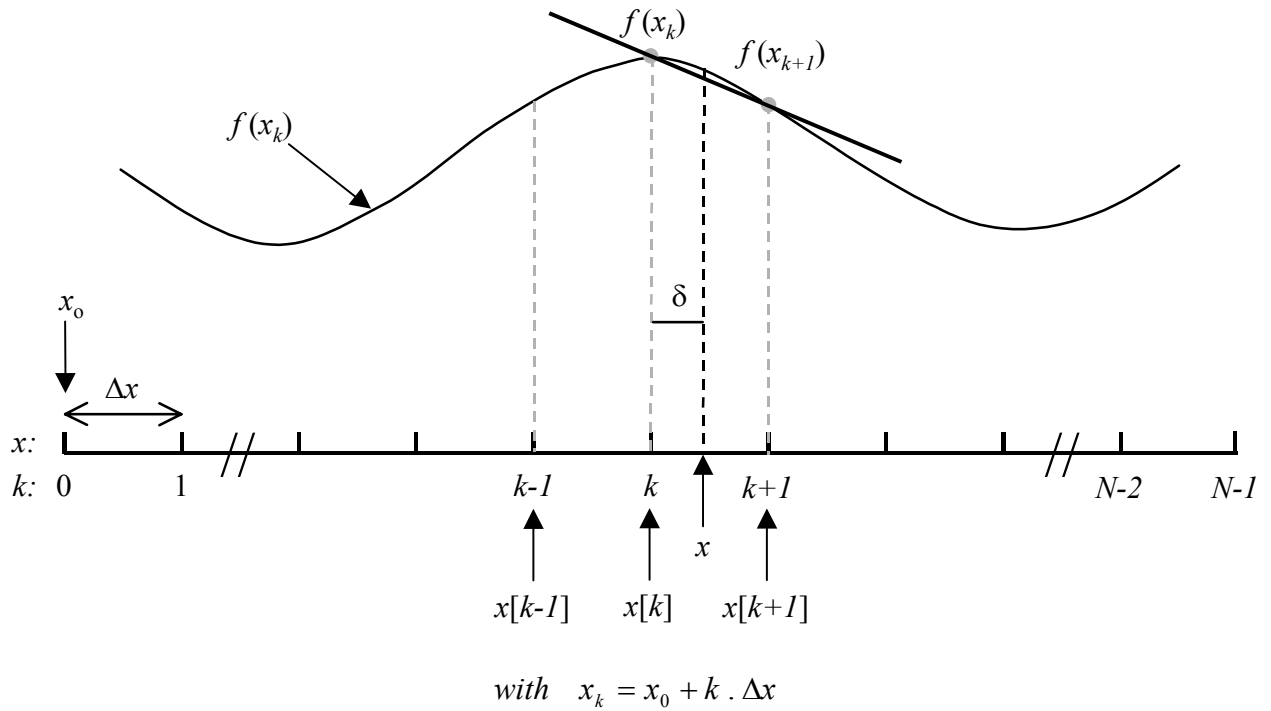
with the following definitions:

$$x \text{ is limited inside the vector: } x_0 \leq x \leq x_{N-1}$$

$$k \text{ is the interpolation coefficient index: } k = \text{Floor}\left\{\frac{x - x_0}{\Delta x}\right\}, 0 \leq k \leq N - 1$$

$$\delta \text{ is the offset between two discrete points: } \delta = \frac{x - x_k}{\Delta x}, 0 \leq \delta \leq 1$$

The values of the interpolation function at arbitrary positions within integer sampling positions, occur at fractional  $\delta$  values.



Software:

Module name: **LinearInterpolation**

Validation:

Pre-validation of algorithm with test data sets.

## 12.4 PARABOLIC INTERPOLATION IN ONE DIMENSION

### Description:

This function is used to interpolate a value in a vector corresponding to a given abscissa value using a parabolic fit model.

### Processing:

| <i>Variable</i> | <i>Descriptive Name</i>      | <i>I/O</i> | <i>Type</i> | <i>Ranges / References / Remarks</i>   |
|-----------------|------------------------------|------------|-------------|--|
| $N$             | Dimension of input vectors   | I          | int         | $k = 0..N-1$   |
| $x_k$           | Abscissa data values         | I          | float       | <i>Is specified by <math>x_0</math> and <math>\Delta x</math></i>  |
| $f(x_k)$        | Ordinate input data points   | I          | float       | -  |
| $x$             | Interpolation abscissa point | I          | float       | point at which interpolation is to be computed. Must be between input vector limits. Otherwise, extrapolation must be computed |
| $f(x)$          | Interpolated value           | O          | float       | -  |

The following description supposes an uniform points distribution:

For a given vector  $f(x_k)$  defined on  $N$  points, *parabolic* interpolation can be expressed as:

$$f(x) = A \cdot \delta^2 + B \cdot \delta + C$$

with the following definitions:

$x$  is limited inside the vector:  $x_0 \leq x \leq x_{N-1}$

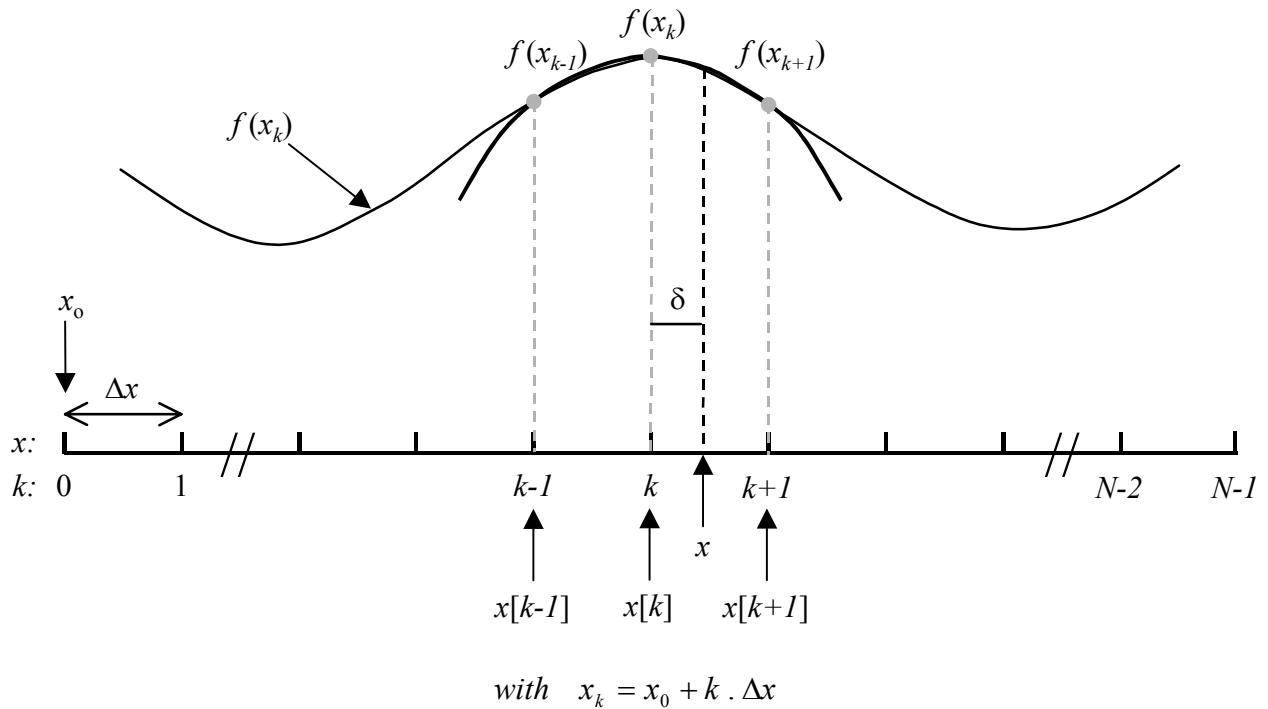
$k$  is the interpolation coefficient index:  $k = \text{Floor}\left\{\frac{x-x_0}{\Delta x}\right\}, 0 \leq k \leq N-1$

$\delta$  is the offset between two discrete points:  $\delta = \frac{x-x_k}{\Delta x}, 0 \leq \delta \leq 1$

$A, B$  and  $C$ , the parabolic coefficients: 
$$\begin{cases} A = 0.5 [f(x_{k-1}) - 2f(x_k) + f(x_{k+1})] \\ B = 0.5 [f(x_{k+1}) - f(x_{k-1})] \\ C = f(x_k) \end{cases} .$$

The values of the interpolation function at arbitrary positions within integer sampling positions, occur at fractional  $\delta$  values.





A special care must be taken at the extremities of the vector, where indication can exceed the numerical limits. In this case, a linear interpolation can be used at the extremity points, or a cyclic indication can be supposed with the use of modulus.

Software:

Module name: **ParabolicInterpolation**

Validation:

Pre-validation of algorithm with test data sets.

## 12.5 INTERPOLATION IN MULTI-DIMENSIONS

Multi-dimensions (linear) interpolation [RD-65] (for Section 9.4.3)

## 12.6 NUMERICAL INTEGRATION

### Description:

This function numerically integrates a distribution of points contained in tabulated vectors (containing abscissa and ordinate points) between specified limits.

When we talk about numerical integration (which is also called 'quadrature') we immediately think about *Simpson's* rule or *Trapezoidal* rule. The classical formulas for integrating a function for which values are known at equally spaced steps have a certain elegance about them, and they are redolent with historical association. But computing methods evolve and times change; with the exception of two of the most modest formulas ('*extended trapezoidal* rule' and '*extended midpoint* rule', see [RD-65] for more details), the classical formulas are almost entirely useless. They are museum pieces, but beautiful ones.

### • *Integration with Gaussian Quadratures*

*Gaussian* quadratures are among the most powerful methods for numerical integration [RD-66]. The theory behind these methods goes back to *Karl F. Gauss (1777-1885)*, who used in 1814 continued fractions to develop the subject. In 1826, *Karl G. Jacobi (1804-1851)* re-derived *Gauss* results by means of orthogonal polynomials. The systematic treatment of arbitrary weight functions  $W(x)$  using orthogonal polynomials is largely due to *Elwin B. Christoffel (1829-1900)* in 1877.

The basic idea of *Gaussian* quadratures is to give ourselves one more degree of freedom with respect to traditional methods by an enlightened choice of the location of the abscissa points at which the function is to be evaluated: these points will no longer be equally spaced.

Instead of studying the usual class of integrals of simple polynomial functions, we now study the class of integrands 'polynomial times some known function  $W(x)$ '. The function  $W(x)$  can then be chosen to remove integrable singularities from the desired integral. Given  $W(x)$ , in other words, and given an integer  $N$ , we can find a set of weights  $w_i$  and abscissas  $x_i$  such that the following approximation becomes exact if  $f(x)$  is a polynomial:

$$\int_a^b W(x).f(x) dx \approx \sum_{i=0}^{N-1} w_i . f(x_i)$$

The fundamental theorem behind  $N$ -point *Gaussian* quadratures comes from the fact that the abscissas of this equation together with the weighting function  $W(x)$  in the interval  $(a,b)$  are precisely the roots of an orthogonal polynomial  $P_N(x)$  for the same interval and weighting function. Without going into more mathematical details, let mention that many known quadratures exist for different forms of the  $W(x)$  function. The most general case where  $W(x)=1$  and with  $-1 < x < 1$ , implying *Legendre* polynomials  $P_N$ : these specific integrals are called *Gauss-Legendre quadratures*. This category is well suited for boundary conditioned physical problems like wave guides or resonators.

$$W(x)=1 \text{ and } -1 < x < 1$$

$$w_i = \frac{2}{(1-x_i^2) \cdot [P'_N(x_i)]^2}$$

• Legendre polynomial recurrence relation

$$(n + 1) \cdot P_{n+1} = (2n + 1) \cdot x P_n - n P_{n-1}$$

One important extension of the *Gaussian* quadrature is the case of 'preassigned nodes': Some points are required to be included in the set of abscissas, and the problem is to choose the weights and the remaining abscissas to maximize the degree of exactness of the quadrature rule. The most common cases are *Gauss-Radau* quadrature, where one of the nodes is an endpoint of the interval, either  $a$  or  $b$ , and *Gauss-Lobatto* quadrature, where both  $a$  and  $b$  are nodes. The *Gauss-Lobatto*  $x_i$  and  $w_i$  are defined as:

$$x_i = x_{i-1} - 1 \quad \text{zero of} \quad \frac{dP_{N-1}(x)}{dx}$$

where

$$\frac{dP_N(x)}{dx} = \frac{N \cdot P_{N-1}(x) - N \cdot x \cdot P_N}{(1 - x^2)}$$

$$w_i = \frac{2}{N(N-1) \cdot [P_{N-1}(x_i)]^2}$$

Definite algorithms give abscissa points and weighting function for these specific quadrature (see **GaussLegendre** and **GaussLobatto** functions). Because of the inherent central symmetry, only half of the distribution can be computed. Knowing these two series, one proceeds by the integration of a function  $f(x)$  by computing a simple summation of products as given by the first equation of this section.

As one can see, this method is time simple and elegant at the same from a theoretical and numerical point of view. It is difficult to imagine a more efficient method. Let us mention to finish that despite the various advantages of the integration method by *Gaussian* quadratures, they can not be easily applied in the presence of discontinuities, where we must resort to traditional methods.

Processing:

| Variable | Descriptive Name              | I/O | Type  | Ranges / References / Remarks   |
|----------|-------------------------------|-----|-------|---|
| $N$      | Dimension of input vectors    | I   | int   | $i = 0..N-1$  |
| $x_i$    | Abscissa vector data values   | I   | float | Is specified by $x_0$ and $\Delta x$                                  |
| $y_i$    | Ordinate vector data values   | I   | float | -   |
| $X_i$    | Quadrature abscissa values    | I   | float | defined for <i>Gauss-Legendre</i> or <i>Gauss-Lobatto</i> integration |
| $W_i$    | Quadrature weighting function | I   | float | -   |
| $a, b$   | Limits of integration         | I   | float | $x_0 \leq a \leq x_{N-1}, x_0 \leq b \leq x_{N-1}$ and $a < b$        |
| $I$      | Integral value                | O   | float | -   |

For tabulated data to be integrated with *Gauss-Legendre* quadrature between limits  $[a, b]$ , abscissa  $x_i$  and ordinate  $y_i$  points must be sampled according to the *Gauss-Legendre* decimation scheme. This will be true for most of the RTC raw output tables.

Another alternative method for uniform grid sampled data is integration by quadratic sub-intervals approximation. This is an excellent method for smooth and continuous data distributions, and can be applied on arbitrarily distributed data points.

### Software:

Module names: ***GaussLegendre***  
***GaussLobatto***  
***GaussIntegrate***  
***IntegrateData***

### Validation:

Pre-validation of algorithm with test data sets.

Validate the generated coefficients through the *Gauss-Legendre* or *Gauss-Lobatto* integration on theoretical data sets to check that the obtained precision is within expected limits.

## 12.7 SIMPLEX MINIMIZATION

### Description:

For the solution of arbitrary algebraic equations, it is often useful to use minimization algorithms. This strategy, based on a convergent minimization of residuals between the reference data and the fit, enables the resolution of complex equations that sometimes would be unsolvable.

Different algorithms can be used for the minimization of residuals between experimental points and a mathematical model according to a set of independent parameters. The most common alternatives for the search of a minimum are [\[RD-65\]](#), [\[RD-66\]](#), [\[RD-67\]](#) and [\[RD-68\]](#):

1 – *The stepwise descent strategy*

Easy to program and converges virtually all the time, but can be extremely slow to run.

2 – *The steepest descent methods*

Involve fewer iterations, but require knowledge or computation (by numerical differentiation) of the first derivative of the sum of square residuals.

3 – *The Newton-Raphson algorithm*

The most popular non-linear least-square fitting algorithm today; it is fast, but always prone to divergence (if started from inaccurate initial guesses).

4 – *The Marquart algorithm*

This algorithm and more recent methods (like *Powell's quadratically convergent method*) are mathematically equivalent to a mixture of methods 2 and 3. They avoid divergence problems of Newton-Raphson without unacceptable losses in speed. The amount and complexity of code generated can become substantial.

5 – *The simplex algorithm*

Proposed in 1965 [\[RD-69\]](#), this method has the following advantages.

- Divergence is impossible
- Response value needs to be computed only once or at most a few times for each iteration.

- No previously required knowledge of derivatives or numerical differentiation. This avoids rounding-off errors and allows the handling of non continuous functions.
- The number of data points and the number of parameters ( $\eta$ ) are only limited by the speed and memory limitations of the computer on which the program will be run.
- Very generally speaking, the simplex algorithm usually converges in less than  $20\eta^2$  iterations.

Note that even if the simplex never diverges, this does not guarantee that no problem will develop. Failure to converge and premature conclusion are usually the results of using the wrong input parameters (or with truncation/round-off errors in the computer arithmetic when working with single precision numbers). But with appropriate guesses, this should never happen.

Sometimes, the simplex gives results far from expected, but the fitted curve matches the experimental data excellently. This happens when a particular function can be equally satisfied with more than one set of parameters.

The big advantages of the simplex algorithm are its remarkable speed, the fact that the program can never diverge, and the compactness of its implementation. Implemented in a curve-fitting algorithm, it is capable of handling virtually any function, no matter how complex, with any number of variables and parameters. It is the chosen tool for the current task of spectral calibration and instrument line shape retrieval, because of its remarkable speed, simplicity, and reliability.

### Processing:

| <i>Variable</i> | <i>Descriptive Name</i>              | <i>I/O</i> | <i>Type</i> | <i>Ranges / References / Remarks</i>                                  |
|-----------------|--------------------------------------|------------|-------------|---|
| $N$             | Dimension of input vectors           | I          | int         | $i = 0..N-1$  |
| $Ncoeffs$       | Number of coefficients to fit        | I          | int         | $Ncoeffs < 10$  |
| $p_j$           | Initial values for coefficients      | I          | float       | -   |
| $x_i$           | Abscissa input data values           | I          | float       | -   |
| $y_i$           | Ordinate input data values           | I          | float       | -   |
| $E$             | Merit value                          | T          | float       | <i>Sum of squared residuals</i>                                       |
| $tol$           | Tolerance for convergence            | I          | float       | <i>Relative convergence definition;</i><br>$10^{-10} < tol < 10^{-3}$ |
| model_fit       | Residual minimization function       | I          | fonct       | <i>Sub-function computing SSR</i>                                     |
| $p_j$           | Fitted coefficients                  | O          | float       | $j: 0.. Ncoeffs-1$  |
| $ftol$          | Residual error of fit                | O          | float       | <i>information parameter</i>  |
| $iters$         | Number of iterations for convergence | O          | int         | <i>informs about the speed of convergence</i>                         |

The simplex method presumes the existence of a 'black-box' sub-algorithm, the role of which is to compute the merit value, or the amplitude of what one is trying to minimize. In our case, we want to lessen the sum of the squares of the differences ( $\delta$ ) between the fitted model and the reference data points. For random errors randomly distributed, this is the best criterion of all.

$$\delta = \sum_{i=0}^{N-1} [\text{model\_fit}(i, p_0, p_1, p_2, \dots) - y_i]^2$$

where  $p_1, p_2, \dots$  are a set of input parameters that characterize the theoretical model. For such an algorithm to work correctly, one must set initial values for these parameters. These initial values will be computed according to the physics of each specific problem.

By setting a suitable precision or a maximum number of iterations, the simplex algorithm will modify the parameters and compute a residual value for each set until a minimum residual (or least square) is produced, yielding to the optimum set of parameters for the considered case.

Software:

Module names: **SimplexFit**

Validation:

Pre-validation of algorithm with test data sets.

## 12.8 DETERMINATION OF THE GOODNESS OF FIT

### Description:

After a given fit has been computed, the standard deviation can be computed to evaluate the dispersion of the fit. The standard deviation is the root mean square of the deviations, and is associated with the *second moment* of the data about the mean [RD-70].

A goodness of fit indicator can also be computed between the reference points and the fit to determine with which validity they are similar. A useful operator used to evaluate the goodness of fit criteria is mathematically derived as follows:

$$r = \frac{\sum_{i=0}^{N-1} (f_i - \bar{f}) \cdot (y_i - \bar{y})}{\sqrt{\sum_{i=0}^{N-1} (f_i - \bar{f})^2} \cdot \sqrt{\sum_{i=0}^{N-1} (y_i - \bar{y})^2}} \quad \text{with } r \text{ in } [-1; 1]$$

where  $f_i$  is the fitted data, or the experimental spectrum

$y_i$  is the model data, or the reference spectrum

and  $\bar{f}$  and  $\bar{y}$  are the means of the vectors  $f$  and  $y$ .

#### • Correlation coefficient $r$

$r$  is the *linear-correlation* coefficient, also called the '*product-moment correlation coefficient*', or *Pearson's  $r$* . It indicates the strength of the association between the dependent and independent variables. The magnitude of the coefficient is not easy to interpret (see definition of determination coefficient), but the sign (+ or -) indicates the direction of the relationship. The correlation coefficient varies from -1 to +1, with -1, for example, indicating a reversed relationship (as one grows larger, the other grows smaller).

#### • Coefficient of determination $r^2$

$r^2$  measures the proportion of the variation of the dependent variable about its mean that is explained by the independent or predictor variable(s). The coefficient  $r^2$  can vary between 0 and 1. If the regression model is properly applied and estimated, higher is the  $r^2$  value greater is the explanatory power of the regression equation and better is the prediction of the criterion variable [RD-71]. It takes a value of 1, termed '*complete correlation*', when the model and the experimental points match one-by-one.

$r^2$  has the following properties:

$r^2 = 1$  when input functions (the model and the experimental points) match perfectly.

$r^2 = 0$  when input functions are completely uncorrelated.

When a correlation is known to be significant,  $r^2$  is one conventional way of summarizing its strength. In fact, the value of  $r^2$  can be translated into a statement about what residuals (root mean square deviations) are to be expected if the data are fitted to a straight line by the least-squares method. This value is always bounded, but it does not indicate when a fit starts linearly from the reference.

Another similar determination coefficient is  $R^2$ , that is closely related to the  $r^2$  criteria, and is defined as:

$$R^2 = 1 - \frac{\sum_{i=0}^{N-1} (f_i - \bar{f})^2}{\sum_{i=0}^{N-1} (y_i - \bar{y})^2}$$

$$R^2 = 1 - \frac{\text{unexplained variation}}{\text{total variation about the mean}} \quad [-\infty \dots 1]$$

$R^2$  has the following properties:

$R^2 = 1$  when input functions (the model and the experimental points) match perfectly.

$R^2 = 0$  when input functions are completely uncorrelated.

$R^2 = -\infty$  when input functions are completely anti-correlated.

An ill-conditioned case occurs when the model  $y$  is distributed around zero in a horizontal line: this causes both correlation factors to take small values even in the presence of good fits.

In summary,  $r$  and  $R$  are the correlation coefficients, while  $r^2$  and  $R^2$  are the determination factors. It is on the last two values that the present analysis is based. The squared values are used to simplify the understanding, and both  $r^2$  and  $R^2$  are used to get as much information as possible for the goodness of the fit. At the end of the study, maybe it will be judged that only one identifier is sufficient for a correct identification.

Further details regarding the correlation/determination coefficient can be found at the following references: [RD-65], [RD-70] and [RD-72].

Processing:

| <i>Variable</i> | <i>Descriptive Name</i>                  | <i>I/O</i> | <i>Type</i> | <i>Ranges / References / Remarks</i> |
|-----------------|--|------------|-------------|--------------------------------------|
| $N$             | Dimension of input vectors               | I          | int         | $i = 0..N-1$                         |
| $y_i$           | Ordinate values of reference data points | I          | float       | -                                    |
| $f_i$           | Ordinate values of fitted data           | I          | float       | -                                    |
| $s$             | Standard deviation                       | O          | float       | -                                    |
| $r^2$           | Determination coefficient                | O          | float       | $0 \leq r^2 \leq 1$                  |
| $R^2$           | Determination coefficient                | O          | float       | $-\infty < R^2 \leq 1$               |

The expression for the standard deviation  $s$  of the sample fit is given by:

$$s = \sqrt{\frac{1}{N-1} \cdot \sum_{i=0}^{N-1} (f_i - y_i)^2}$$

where  $f_i$  is the fitted data

$y_i$  is the model data, or the reference points



Software:

Module name:    ***ComputeStats***

Validation:

Pre-validation of algorithm with test data sets.

**- END OF DOCUMENT -**